KfK 4159
Dezember 1986

Annual Report on Nuclear Physics Activities

July 1, 1985 - June 30, 1986

Editors:
G. Büche, P. Doll, L. Friedrich
Institut für Kernphysik

Kernforschungszentrum Karlsruhe

KERNFORSCHUNGSZENTRUM KARLSRUHE

Institut für Kernphysik

KfK 4159

ANNUAL REPORT

on

NUCLEAR PHYSICS ACTIVITIES

July 1, 1985 - June 30, 1986

Editors:

G.Büche, P.Doll, L.Friedrich

Kernforschungszentrum Karlsruhe GmbH, Karlsruhe

Last Annual Reports:

1984/85: KfK 3969 (Oktober 1985)
1983/84: KfK 3815 (Oktober 1984)
1982/83: KfK 3621 (November 1983)
1981/82: KfK 3427 (November 1982)
1980/81: KfK 3280 (Februar 1982)

Als Manuskript vervielfältigt
Für diesen Bericht behalten wir uns alle Rechte vor

Kernforschungszentrum Karlsruhe GmbH
Postfach 3640, 7500 Karlsruhe 1

ISSN 0303-4003
ISSN 0176-1501

ABSTRACT

This report surveys the activities in basic research from July 1, 1985 to June 30, 1986 at the Institute for Nuclear Physics (IK) of the Kernforschungszentrum Karlsruhe. The research program of this institute comprises laser spectroscopy, nuclear reactions with light ions, neutron physics, neutrino physics and physics at medium and high energies.

ZUSAMMENFASSUNG

Der vorliegende Bericht gibt einen Überblick über die Arbeiten am Institut für Kernphysik (IK) des Kernforschungszentrums Karlsruhe im Zeitraum vom 1. Juli 1985 bis zum 30. Juni 1986. Das Forschungsprogramm umfaßt die Gebiete Laserspektroskopie, Kernreaktionen mit leichten Ionen, Neutronenphysik, Neutrinophysik, sowie Mittel- und Hochenergiephysik.

PREFACE

This is the sixth annual report on nuclear physics activities at the Kernforschungszentrum Karlsruhe. These activities are carried out in the Institute of Nuclear Research (IK), which consists of three sections (IK I, IK II, IK III). Each section specialises in different energy regions.

Three groups in Section IK I are engaged in work in various fields of nuclear physics and particle physics:

- Fast Neutron Physics: Scattering experiments on very light nuclei are carried out using the polarized neutron beam of the Karlsruhe Cyclotron (POLKA). The main goal is to determine precise phase shifts from experiments with polarized neutrons on unpolarized and also on polarized protons. Moreover, the internal structure and dynamics of the nuclei up to the A = 5 system are to be studied. The large-volume polarized proton target has been successfully used for scattering experiments with the polarized neutron beam in a number of experiments.

- High Energy Physics: This group runs the CELLO detector system at the e^+e^- storage ring, PETRA, in Hamburg within the framework of an international collaboration. The detector serves for experiments to study e^+e^- collisions at the highest energies at present attainable. CELLO, with its modern liquid-argon calorimeter, lends itself particularly well to studies of the electromagnetic component in these reactions. This allows, e.g., precise studies of quantum electrodynamics, detailed studies of quark and gluon jets and the search for new quarks. The upgraded detector is working satisfactorily and is strongly involved in the search for a new quark during the continuous energy increases in PETRA. This work, carried out in cooperation with Karlsruhe University, was partly supported by BMFT through the "Verbund Hochenergiephysik".

- Neutrino Physics: The newly founded working group is concerned with neutrino physics in the energy range between approximately 10 and 50 MeV, at the Spallation Neutron Source (ISIS) under construction at the Rutherford Appleton Laboratory (RAL) in England. This is a new field of work involving fundamental questions in the fields of elementary particle physics, nuclear physics and astrophysics. The project was proposed by KfK. In the meantime, a bilateral agreement has been signed between KfK and RAL. Working groups of the University of Oxford (Prof.Dr.N.E.Booth), Queen Mary College of London (Prof.Dr.J.A.Edgington), and University of Erlangen (Prof.Dr.E.Finckh) have meanwhile joined the project called KARMEN (Karlsruhe-Rutherford-Medium-Energy-Neutrinoexperiment). Detector system KARMEN 1 (60 to scintillator) is being developed at KfK. It will be installed in a massive blockhouse of steel designed and built by KfK at the Rutherford ISIS accelerator until spring of 1987. This work, carried out in cooperation with Karlsruhe University, was partly supported by BMFT through the "Verbund Mittelenergiephysik".

Section IK II is mostly working on medium energy physics at CERN and SIN:

- One group, continuing a long tradition in the field of exotic atoms at CERN, has concentrated its activities on the LEAR facility (Low-Energy Antiproton Ring). This instrument, the realization of which was backed very strongly by Karlsruhe, offers unique possibilities for work with slow antiprotons. Antiprotonic X-ray-spectra of selected elements were obtained. They contain new information on the strong interaction of antiproton-nucleon pairs, on the magnetic moment of the antiproton, and on the spin-orbit coupling for antiprotons. Another experiment makes use of the idea of the cyclotron trap proposed by Dr. L.M. Simons, which permits measurements at low gas pressure, where Stark mixing is small. In the antiproton-nucleon system in antiprotonic hydrogen and deuterium, it has confirmed theoretical predictions. Moreover, it was found unexpectedly that the cascading exotic particle (anti-proton at LEAR, negative myon at SIN) empties the electron shells almost completely at low pressures by Auger-effect. Karlsruhe is involved personally and financially also in a technical upgrading of LEAR, namely the use of electron cooling. The 4π detector for charged and neutral particles "crystal barrel" for future LEAR experiments, proposed by KfK and a number of University groups from Germany, Europe and U.S.A., was approved by CERN; its realization is in progress.

- The experiments at SIN focus on problems of pion interaction scattering and absorption) with simple systems consisting of few nucleons. Theoretical assumptions, especially those about the existence of dibaryon states, are verified on the basis of additional information that can be obtained by using polarized targets. The low-energy spectrometer LEPS designed by Karlsruhe, which came into operation in the fall of 1986, combines good resolution with high luminosity. It will mainly be used in studies of very simple systems at energies close to the pion threshold. Absorption measurements of pion in ^{3}He show an unexpected isospin-dependence of the basic two-nucleon-absorption process and an unexpectedly large contribution of three-pion-absorption. This reaction is of great theoretical significance.

Some of this work, carried out in cooperation with Karlsruhe University was supported by BMFT through the 'Verbund Mittelenergiephysik'.

Section IK III is mainly working in the following fields:

- Nuclear astrophysics: Capture cross sections of fast neutrons in the keV to MeV range are measured in order to understand in detail the build-up of heavy elements in stars. Work in this area concentrates on building a novel 4π-BaF_2 scintillation detector in order to improve the accuracy of such elements considerably.

- Nuclear reactions: Work in this field makes use of the 26 MeV nucleon ^{6}Li beam from the Karlsruhe Isochronous Cyclotron and of the magnetic spectrometer for investigating continuous spectra in break-up reactions. Theoretical studies have shown that Coulomb break-up should allow the determination of radiative capture cross sections between light nuclei at very low relative velocities. Such cross sections are of great importance in astrophysics. Experiments have been started in order to verify these considerations.

- Laser spectroscopy: This technique is applied to sub-ng amounts of radioactive atoms in order to determine hyperfine structure and isotopic shifts of atomic transitions. The results yield information on nuclear moments and on the change of nuclear charge radii due to varying neutron number. At present nuclides of strontium are studied, and a new experimental technique, spectroscopy of ions stored in electromagnetic fields, is developed.

- Applied gamma-ray spectroscopy: Here instruments are developed to determine concentration and isotopic composition of fissile materials. The instruments make use either of the intrinsic radioactivity or of X-ray absorption and fluorescence. Their main applications are in the safeguards of nuclear fuel and in process control during fabrication and reprocessing.

- Section IK III is also responsible for operating the three accelerators of our institute: The Karlsruhe Isochronous Cyclotron which is mainly used for fast neutron physics and nuclear reaction experiments; the 3.75 MV Van de Graaff accelerator which serves mainly as a source of keV neutrons for the nuclear astrophysics studies; and a compact cyclotron which is basically a commercial installation to produce radioactive isotopes for nuclear medicine and mechanical engineering.

(A. Citron) (B. Zeitnitz) (G. Schatz)

CONTENTS

Page

1. NUCLEAR PHYSICS

1.1 NUCLEAR ASTROPHYSICS (VdG)

1.1.1 An activation Measurement of the ^{22}Ne(n,γ) cross section 1
1.1.2 Destruction of ^{26}Al in explosive nucleosynthesis 1
1.1.3 Neutron capture in the 1.15 keV resonance of ^{56}Fe using Moxon-Rae detectors 2
1.1.4 The s-process branching at ^{79}Se 2
1.1.5 The β^--branch in the decay of ^{79}Se^m 3
1.1.6 keV-neutron capture cross sections of the krypton isotopes 5
1.1.7 The S-process branching at ^{85}Kr 5
1.1.8 The isomeric ratio of ^{85}Kr at a thermal energy of kT = 52 keV 5
1.1.9 s-process nucleosynthesis below A = 90 6
1.1.10 A measurement of the ^{139}La capture cross section and a study of the s-process at magic neutron number 82 7
1.1.11 ^{148,150}Sm: A test for s-process nucleosynthesis 7
1.1.12 Search for weak transitions linking ground state and Isomer in ^{176}Lu 7
1.1.13 The stellar capture cross section of ^{197}Au - an absolute measurement at kT = 25 keV 9
1.1.14 ^{198,199,200,201,202,204}Hg(n,γ) cross sections and the termination of s-process nucleosythesis 10
1.1.15 The production and survival of ^{205}Pb in stars and the ^{205}Pb - ^{205}Tl s-process chronometry 10
1.1.16 Neutron capture cross sections for s-process studies 11
1.1.17 Competition of neutron capture and beta decay at the ^{85}Kr and ^{151}Sm branchings, a means to estimate the s-process pulse condition 12
1.1.18 s-process nucleosynthesis - stellar aspects and the classical model 13
1.1.19 Explosive nucleosynthesis in carbon deflagration models of type I supernovae 13
1.1.20 s-process studies using single and pulsed neutron exposures 14

1.2 NEUTRON SCATTERING

1.2.1 The backward angle np cross section in the energy range from 22 to 50 MeV 17
1.2.2 The np analyzing power a_y at backward angles 18

Page

1.2.3 Results of the $\vec{n}\vec{p}$ spin correlation parameter A_{yy} 19

1.2.4 Status of np phase shift analyses for energies up to 50 MeV 21

1.3 NEUTRON INDUCED REACTIONS

1.3.1 Spin-spin cross section measurements of polarized neutrons on the polarized nuclei ^{27}Al and ^{93}Nb 22

1.3.2 Measurement of the analyzing power of the reactions ^{3}He($\vec{n}$,$\vec{p}$)t and ^{3}He($\vec{n}$,$\vec{d}$)d 23

1.3.3 Charge exchange reaction (n,p) on ^{12}C at 50 MeV 24

1.3.4 Preliminary neutron capture studies 25

1.4 NUCLEAR REACTIONS BY CHARGED PARTICLES

1.4.1 Resonant and non-resonant Coulomb break-up of ^{6}Li 27

1.4.2 Coulomb dissociation as a source of information on radiative capture processes of astrophysical interest 27

1.4.3 Inclusive energy spectra of break-up fragments and break-up cross sections at very forward emission angles in ^{6}Li induced nuclear reactions 29

1.4.4 Experimental features of particle-particle coincidence measurements at very forward emission angles using the magnetic spectrograph "Little John" 31

1.4.5 On the possibility to detect two coincident particles in narrow-angle geometry with the magnetic spectrograph "Little John" 33

1.4.6 Monte Carlo simulation of detector geometry effects in coincidence spectra of cluster-fragments from projectile break-up reactions 35

1.4.7 A half-shell treatment of the direct break-up of light ions 37

1.4.8 The nonelastic projectile break-up cross section from particle-gamma coincidence measurements for the ^{6}Li + ^{40}Ca reaction at 156 MeV 38

1.4.9 Intermediate mass fragments from the reaction ^{6}Li + ^{46}Ti, at E/A = 26 MeV 38

1.4.10 Intermediate mass fragments from the reactions ^{6}Li + ^{nat}Cu, and ^{6}Li + ^{nat}Ag, at E/A = 26 MeV 40

1.4.11 Fission barriers of light nuclei 41

1.4.12 Element distributions after binary fission of ^{44}Ti 42

1.4.13 α-particle scattering from Ni isotopes at E_α = 172.5 MeV 43

Page

1.4.14 Combined analysis of $\bar{p}$ - scattering by $^{16,18}O$ and of $^{16,18}O$ - $\bar{p}$ - atoms 43

1.4.15 Excitation and decay of isoscalar giant resonances in ^{90}Zr studied in ^{6}Li-scattering at extreme forward angles 45

1.4.16 Monopole strength in ^{12}C extracted from ^{6}Li small angle scattering 46

1.5 NUCLEAR FISSION

1.5.1 Cold fragmentation in thermal-neutron-induced fission of ^{233}U and ^{235}U 48

1.5.2 Mass yields of fission fragments as a function of kinetic energy in the reaction $^{249}Cf(n_{th},f)$ 48

1.5.3 Mass and charge distribution of fission fragments in $^{237}Np(2n,f)$ 49

1.5.4 Mass and charge distribution of fission fragments in $^{249}Cf(n,f)$ 50

1.5.5 A quantum model for nuclear fission 50

1.5.6 Fission fragment properties in fast-neutron-induced fission of $^{237}Np^{*}$ 51

1.6 THEORY

1.6.1 Breathing cluster model for two s-wave clusters 52

1.6.2 Unified microscopic description of the lightest nuclei 53

1.6.3 Neutron-proton cross sections in a simple interaction model 54

2. LASER SPECTROSCOPY

2.1 The odd-even staggering of the nuclear charge radii of Pb isotopes 56

2.2 Charge radii and moments of tin nuclei by laser spectroscopy 56

2.3 Laser spectroscopy of stable and radioactive Sr isotopes 57

2.4 Isotope shifts and hyperfine structure splitting in atomic transitions of ^{242m}Am by optogalvanic laserspectroscopy 61

2.5 Reevaluation of isotope shift data for a series of stable and radioactive lead isotopes 63

2.6 Laserspectroscopic investigations in an RF ion trap 64

2.7 Theoretical predictions on even parity energy levels in the Americium atom 66

2.8 Heterodyne frequency metrology for laser radiation 67

Page

3. NEUTRINO PHYSICS

3.1 STATUS OF THE PROJECT

3.1.1 Neutrino area 70
3.1.2 KARMEN 1 detector 71
3.1.3 Photomultiplier tests 72
3.1.4 Electronics 72
3.1.5 Data acquisition for KARMEN 1 74

3.2 PROTOTYPE III 75

3.3 MONTE-CARLO SIMULATION OF NEUTRINO EVENTS IN KARMEN 1 76

4. INTERMEDIATE ENERGY PHYSICS

4.1 PION-NUCLEUS INTERACTIONS

4.1.1 Investigation of the final state interaction in the $\pi^+d\to\pi^+pn$ cross section 79
4.1.2 Measurement of iT_{11} in the $\pi^+d\to\pi^+pn$ reaction at T_π = 134 MeV and 228 MeV 80
4.1.3 Tensor analyzing power t_{20} in πd elastic scattering at T_π = 134 MeV and 151 MeV 81
4.1.4 Direct Measurement of the tensor polarization of a polarized deuteron target 83
4.1.5 Measurement of T_{20} and "T_{21}" in πd elastic scattering 85
4.1.6 First measurements of the tensor analyzing power "T_{22}" in πd elastic scattering 86
4.1.7 Measurement of the $\pi d\to pp$ reaction at T_π = 65 MeV 87
4.1.8 First kinematically complete measurements of the $\pi^+d\to\pi^0pp$ charge exchange reaction 88
4.1.9 Measurement of three particles in coincidence following the interaction of positive pions with carbon 90
4.1.10 Investigation of the ^{6}Li (π,πd) reaction at T_π = 219 MeV 91
4.1.11 Measurement of the charge-exchange reaction in ^{3}He with stopped pions 92
4.1.12 Pion absorption in ^{3}He at 320 MeV/c 94
4.1.13 Observation of a three-nucleon pion-absorption mechanism in the (π+^{4}He)-interaction 95

Page

4.2 INTERACTION OF ANTIPROTONS AND ANTINEUTRONS

4.2.1 Strong interaction shifts and widths in antiprotonic helium isotopes 98
4.2.2 Pressure dependence of the antiprotonic cascade in Hydrogen 100
4.2.3 Strong interaction shifts and widths in antiprotonic hydrogen 102
4.2.4 On the production of highly ionized antiprotonic noble gas atoms 104
4.2.5 Investigations of antiprotonic atoms at LEAR 106
4.2.6 Particle spectroscopy after antiproton annihilation in light atoms 108
4.2.7 Critical absorption of a 70-Ge antiprotonic X-ray transition 110
4.2.8 Search for narrow lines in gamma spectra from proton-antiproton annihilations at rest 112
4.2.9 Measurement of the antineutron-proton cross section at very low energy 114
4.2.10 Feasibility study for antihydrogen production 116

4.3 THE CRYSTAL BARREL PROJECT AT LEAR

4.3.1 Status of the CB-project 119
4.3.2 Test of a modular CsI(Tl) prototype calorimeter with photodiode readout at 200 MeV/c 122
4.3.3 Read out of CsI-crystals with wave length shifters (WLS) 123
4.3.4 Monte Carlo studies of electromagnetic showers in the crystal barrel detector 125

4.4 THEORY

4.1.1 Applications of the πNN bound-state problem: The deuteron and the 4,4 resonance 127
4.4.2 Standard relativistic Faddeev theory of the πNN system with application to πd scattering 128
4.4.3 Nonexistence of Λnn or Σ^-nn bound states 130
4.4.4 Relativistic one-pion-exchange potentials 132

5. HIGH ENERGY PHYSICS

5.1 HARDWARE ACTIVITIES

5.1.1 CELLO operation 135
5.1.2 Calorimeter development 136
5.1.3 Optical fiber read-out for scintillator 138

Page

5.2 ANALYSIS OF HADRONIC FINAL STATES AND TEST OF QCD

5.2.1 Measurements of the total hadronic cross section in e^+e^- annihilation between center of mass energies of 14 and 47 GeV 139

5.2.2 Comparison of the lowest energy jet in three-jet events at 44 GeV with the average jet in two-jet events at 14 GeV 143

5.3 STUDY OF ELECTROWEAK INTERACTION

5.3.1 Study of inclusive leptons from b-Quark production in e^+e^- annihilations at energies above 43 GeV 146

5.4 SEARCH FOR NEW PARTICLES IN e^+e^- ANNIHILATION 149

5.4.1 Search for light leptoquark bosons 150

5.4.2 Search for excited quarks 152

5.4.3 Search for charged and neutral heavy leptons 155

5.4.4 Search for supersymmetric particles 158

6. DEVELOPMENTS AND INSTRUMENTATION

6.1 DETECTORS

6.1.1 Prototype crystals for the Karlsruhe 4π Barium Fluoride detector 170

6.1.2 Completion of the mechanical support for the 4π BaF_2 detector 170

6.1.3 Test measurements with the first six detector modules of the 4π BaF_2 detector 171

6.1.4 A gas ionization chamber for on-line heavy ion identification 173

6.1.5 A ten-fold coincidence pulse generator for the electronic set-up of the focal plane detector of the magnetic spectrograph 174

6.1.6 A liquid argon time projection chamber 175

6.1.7 Study of n-γ pulse-shape-discrimination (PSD) with a large NaI(Tl)-crystal 177

6.1.8 Detector developments for neutron flux measurements 178

6.1.9 Precise threshold determinations for absolute neutron counting 180

6.2 INSTRUMENTATION

6.2.1 A device production an ultrapure stopped muon beam of high intensity 182

6.2.2 Commissioning of the low energy pion spectrometer (LEPS) at SIN 183

6.2.3 An inexpensive temperature-compensated hall-probe device for monitoring the magnetic field of the spectrograph "Little John" 187

Page

6.2.4 A low temperature ^{3}He gas target system 187

6.2.5 A new CAMAC system for high rate, low dead time multi-parameter data acquisition 189

6.3 ACCELERATORS

6.3.1 Operation of the isochronous cyclotron (KIZ) 191

6.3.2 Operation of the Karlsruhe Compact H^--Cyclotron (KAZ) 194

6.3.3 Status of the external ion sources of the Karlsruhe Isocronous Cyclotron 194

6.3.4 An ECR ion source with a high ionization efficiency 197

6.3.5 Status of the electron cooling device under construction at CERN 199

6.3.6 General issues for the design of lattices for EHF 202

6.4 APPLICATIONS

6.4.1 Application of proton-induced X-ray emission (PIXE) to the determination of trace elements in biological samples 204

6.4.2 Proton microbeam study of calcium-phosphate complexes in human arteries 204

6.4.3 Elemental composition in ocular tissue of rat 205

6.4.4 Ca^{2+} analysis in arteries of spontaneously hypertensive rats by proton-induced X-ray emission 205

6.4.5 Trace element distributions in human livers determined with MICRO-PIXE 206

6.4.6 Localized changes of trace element concentration within diseased human liver lobules 206

6.4.7 Measurement of regional perfusion of the myocard by recording the distribution of ^{81}Rb-^{81m}Kr with a spect-system 207

6.4.8 Evaluation of severe coronary artery stenoses using tomographic ^{81}Rb^{81m}Kr myocardial images 207

6.4.9 Performance of plutonium isotopic analysis by gamma spectrometry in reprocessing product solutions 208

6.4.10 How to simplify the analytics for input-output accountability measurements in a reprocessing plant 210

6.4.11 Calibration of X-ray densitometers for the determination of Uranium and Plutonium concentrations in reprocessing input and product solutions 210

6.4.12 Performance evaluation of an X-ray spectrometer for uranium and plutonium elemental analysis in dissolved spent nuclear fuels 212

Page

6.4.13 KFKPU - A computer program for the evaluation of the plutonium isotopic composition from gamma spectra 214
6.4.14 Investigations of X-ray fluorescence for uranium monitoring in a reprocessing plant 216
6.4.15 Production of isotopes for medical applications 218
6.4.16 Blood flow measurement using ultra-pure Rb-81 220
6.4.17 Activation of machine parts for mechanical engineering 222

7. LIST OF PUBLICATIONS

7.1 PUBLICATIONS AND REPORTS 224

7.2 CONFERENCE CONTRIBUTIONS 229

8. PERSONELL 234

1. NUCLEAR PHYSICS

1.1 NUCLEAR ASTROPHYSICS (VdG)

1.1.1 AN ACTIVATION MEASUREMENT OF THE ^{22}Ne(n,γ) CROSS SECTION

H. Beer, F. Voss, F. Käppeler, G. Rupp, R.-D. Penzhorn[+]

The ^{22}Ne (α,n) reaction is one of the relevant neutron sources for the nucleosynthesis of heavy elements in stars. At the same time ^{22}Ne may also be a strong neutron poison due to its great abundance. Therefore, an accurate determination of its neutron capture rate is important, which is underway using the activation method. The short half-life of the product nucleus ^{23}Ne (28s) requires an experimental setup for cyclic activation at the Karlsruhe 3.75 MV pulsed Van de Graaff accelerator. The activity is counted via the 439 keV gamma-ray line of ^{23}Ne with a 154 ccm Ge(Li) detector. The sample consists of zeolite loaded with highly enriched ^{22}Ne. First test measurements showed that the sensitivity of the apparatus is sufficient to determine capture cross sections as small as 0.05 mb.

[+] Institut für Radiochemie, Kernforschungszentrum Karlsruhe.

1.1.2 DESTRUCTION OF ^{26}Al IN EXPLOSIVE NUCLEOSYNTHESIS

H.P. Trautvetter[+], H.W. Becker[+], U. Heinemann[+], L. Buchmann[+], C. Rolfs[+],
F. Käppeler, M. Baumann[++], H. Freiesleben[++], H.-J. Lütke-Stetzkamp[++],
P. Geltenbort[+++], F. Gönnenwein[+++],(1)

The ^{26}Al(n,p)^{26}Mg reaction has been studied using neutron spectra which closely resembled Maxwell-Boltzmann distributions with thermal energies of kT = 40 x 10^{-6}, 31 and 71 keV and also for $E_n = 310 \pm 40$ keV. These energies correspond to stellar temperatures $T_9 = 4.6 \times 10^{-7}$, 0.36, 0.82 and 3.6 $\pm$ 0.5, where T_9 is in units of 10^9 K. The partial cross sections for the p_o-(p_1-) transitions are found to equal 26 $\pm$ 10 (1850 $\pm$ 150), 14 $\pm$ 8 (145 $\pm$ 26), 16 $\pm$ 13 (84 $\pm$ 14) and 21 $\pm$ 8 (72 $\pm$ 17) mb for the above neutron spectra, respectively. The astrophysical reaction rate is determined for the combined p_o- and p_1-transitions to be $N_A\langle\sigma v\rangle$ = (0.324 $\pm$ 0.026, 20.5 $\pm$ 2.7, 22.6 $\pm$ 4.3 and 38.7 $\pm$ 11.7) x 10^6 cm^3 mole^{-1}s^{-1}. The results are compared with previous investigations and with statistical model calculations.

(1) Z. Phys. A 323 (1986) 1

[+] Institut für Kernphysik, Univ. Münster, Fed. Rep. of Germany
[++] Institut für Experimentalphysik, Ruhr-Univ. Bochum, Fed. Rep. of Germany
[+++] Institut Laue-Langevin, Grenoble, France

1.1.3 NEUTRON CAPTURE IN THE 1.15 keV RESONANCE OF ^{56}Fe USING MOXON-RAE DETECTORS

F. Corvi[+], C. Bastian[+], K. Wisshak, (1)

The capture area in the 1.15 keV neutron resonance of ^{56}Fe was measured with Moxon-Rae detectors with converters of bismuth, bismuth-graphite and graphite. The data were normalized to Au capture at 4.91 eV using the saturated resonance method. Two separate measurements were performed, the first with the detector axis at 120° with respect to the neutron beam direction, the second with the axis at 90°. The average of the results over the three detectors is:

$g\Gamma_n\Gamma_\gamma/\Gamma = (64.9 \pm 2.4)$ meV for the 120° run and
$g\Gamma_n\Gamma_\gamma/\Gamma = (63.5 \pm 2.1)$ meV for the 90° run.

These values are 14 to 16 % larger than the corresponding ones from transmission data. No reason is found for such a discrepancy.

(1) Nucl. Sci. Eng. 93 (1986) 348

+ CEC-JRC, Central Bureau for Nuclear Measurements, B-2440 Geel, Belgium

1.1.4 THE s-PROCESS BRANCHING AT ^{79}Se

G. Walter, H. Beer, F. Käppeler, G. Reffo[+], F. Fabbri[+], (1)

Neutron capture cross section measurements have been carried out for the isotopes ^{75}As, ^{79,81}Br, ^{71}Ga, and ^{74}Ge by the activation method and for ^{nat}Ga and ^{80}Se by the time-of-flight technique, and Maxwellian averaged capture cross sections were derived. The measurements were supplemented by capture cross section calculations with the statistical model especially for the radioactive nuclei ^{79}Se and ^{81,85}Kr. The analysis of the s-process branching at ^{79}Se with a two component model of exponential neutron exposures provided the last missing link for a determination of allowed ranges of s-process neutron densities and temperatures. The solar Kr abundance was determined in the frame of this analysis to be $N_\odot$ (Kr) = 50 ± 8 (Si = 10^6) and the solar abundances from A = 69 to 88 were decomposed into the s- and r-process contributions.

(1) Astron. Astrophys. (in print)

+ Laboratorio Dati Nucleari, E.N.E.A., Bologna, Italy

1.1.5 THE β^--BRANCH IN THE DECAY OF $^{79}Se^m$

N. Klay, F. Käppeler, G. Rupp, A. Hanser

The β^--branch in the decay of the 96 keV isomeric state in ^{79}Se is of special importance for nuclear astrophysics because it is this transition that can greatly enhance the total beta decay rate of ^{79}Se at the high temperature of ∿ $3 \cdot 10^8$ K prevailing during nucleosynthesis. Under such conditons, thermal equilibrium leads to a population of the excited states leaving about 1 % of the nuclei in the isomeric state. Contrary to the ground state, the isomer can decay to ^{79}Br by an allowed beta transition at a correspondingly faster rate. Log ft values of 5.4 (1) and 5.0 (2) were deduced for this decay from similar transitions in neighbouring isotopes but with uncertainties of ∿ 10 %.

We have measured this log ft value by determining the branching ratio between the 3.9 m ground state transition and the beta decay. Activation of an extremely clean sample - consisting of a thin carbon backing with an implanted layer of ^{78}Se - at the ILL high flux reactor in Grenoble provided the isomer $^{79}Se^m$. Beside the purity of the sample, the second problem of the experiment was the suppression of the conversion electrons from the ground state transition. This was achieved by means of a mini-orange spectrometer (3) made of samarium cobalt permanent magnets, which is shown schematically in Fig. 1. With this spectrometer inserted between sample and detector, the conversion electrons were sufficiently suppressed to record the electrons from beta decay for about 3 half

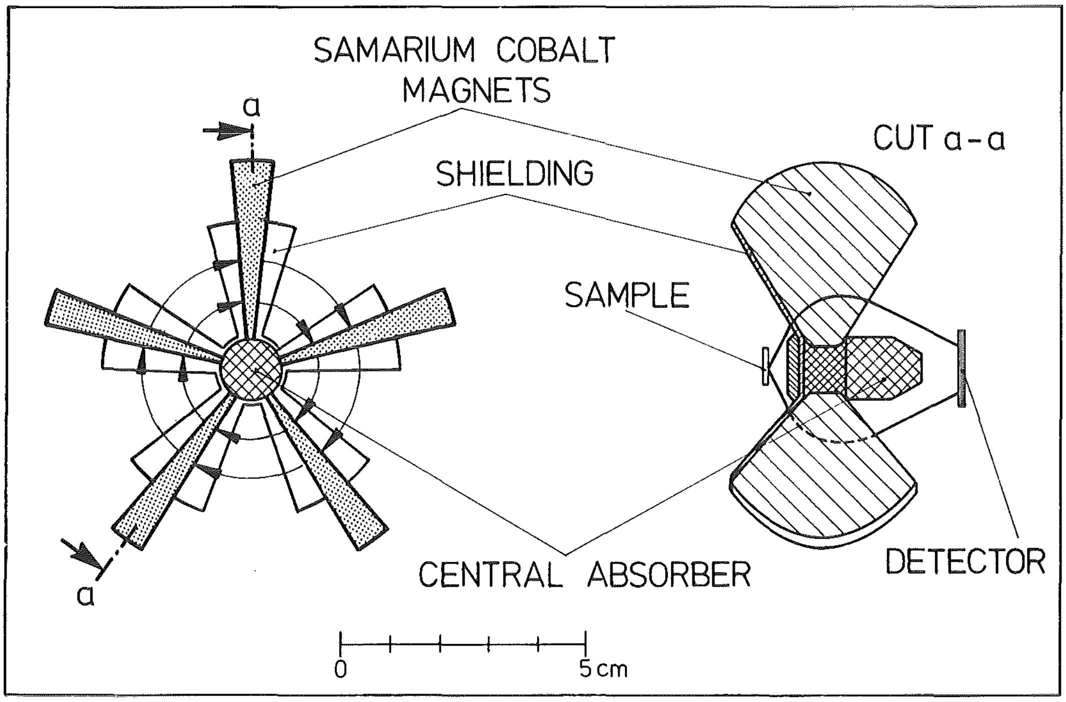

Fig. 1 Schematic setup of the mini-orange spectrometer for suppression of the conversion electron background from $^{79}Se^m \rightarrow {}^{79}Se^g$ transitions.

lives. Then, the mini-orange was removed and the much more intense ground state decay recorded for direct comparison. In this way, we have measured a branching ratio between ground state transition and beta decay of 1970 ± 350, corresponding to log ft = 4.80 ± 0.08 for the isomeric state.

With this value, the formalism of Yokoi and Takahashi (2) provides the temperature dependence of the ^{79}Se half-life plotted in Fig. 2.

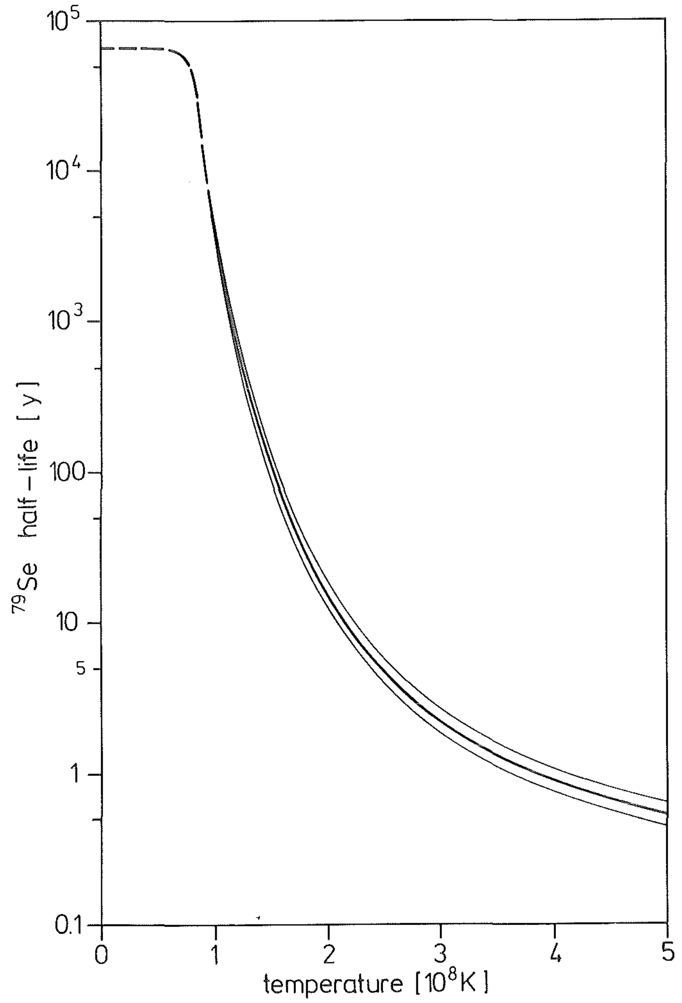

Fig. 2 The stellar beta half-life of ^{79}Se as a function of temperature. The error band reflects the uncertainty due to the measured log ft value.

The effective stellar half-life of ^{79}Se can be estimated from the s-process branching at $79 < A < 82$ to range between 2 and 13 y. Hence, one can read from Fig. 2 the respective range of s-process temperatures: $200 < T_s < 350$ million degrees.

(1) J.H. Conrad, PhD Thesis, University of Heidelberg (1976)
(2) K. Yokoi, K. Takahashi, Report KfK-3849, Kernforschungszentrum Karlsruhe 1985
(3) J. van Klinken, K. Wisshak, Nucl. Instr. Meth. 98 (1972) 1
J. van Klinken, S.J. Feenstra, G. Dumont, Nucl. Instr. Meth. 151 (1978) 433

1.1.6 keV-NEUTRON CAPTURE CROSS SECTIONS OF THE KRYPTON ISOTOPES

G. Walter, B. Leugers, F. Käppeler, Z.Y. Bao[+], G. Reffo[++], F. Fabbri[++], (1)

The neutron capture cross sections of the stable krypton isotopes were determined in the energy interval from 4 to 250 keV using a C_6D_6-detector system in conjunction with the time-of-flight technique. The energy resolution of the measurement was 4 % at 20 and 6 % at 100 keV, and the experimental uncertainties were typically 6 to 10 %. The measurements were complemented by statistical model calculations of all krypton isotopes in the mass range $78<A<86$ in order to obtain also reliable cross sections for the unstable nuclei ^{79,81,85}Kr. These calculations were based on local systematics for all relevant parameters, and the results were estimated to show uncertainties of 20 - 25 %. Maxwellian average cross sections were calculated for kT = 30 keV.

(1) Nucl. Sci. Eng. 93 (1986) 357

[+] On leave from the Institute of Atomic Energy, Academia Sinica, Beijing, Peoples Republic of China

[++] Laboratorio Dati Nucleari, E.N.E.A., Bologna, Italy

1.1.7 THE s-PROCESS BRANCHING AT ^{85}Kr

G. Walter, H. Beer, F. Käppeler, R.-D. Penzhorn[+], (1)

The Maxwellian average neutron capture cross sections of ^{86}Kr, ^{85}Rb and ^{87}Rb have been measured at kT = 25 keV by activation. These data together with recently published neutron capture cross sections of Kr and Sr isotopes allow for a determination of the neutron density of the weak s-process component in the framework of the classical s-process model with two independent fluence distributions. The s-process abundances from this study are compared with the pure s-process krypton discovered in primitive meteorites.

(1) Astron. Astrophys. 155 (1986) 247

[+] Kernforschungszentrum Karlsruhe, Institut für Radiochemie.

1.1.8 THE ISOMERIC RATIO OF ^{85}Kr AT A THERMAL ENERGY OF kT = 52 keV

F. Käppeler, A.A. Naqvi[+], M. Al-Ohali[+]

Studies of neutron capture nucleosynthesis in the s-process usually refer to a thermal energy of kT = 30 keV, corresponding to a temperature of $T = 3.5 \times 10^8$ K. This convention is justified as stellar neutron capture rates are in general not sensitive to temperature due to the approximate $E^{-1/2}$-dependence of most capture cross sections. One of the exceptions from this rule concerns the fractional population of the isomeric state in ^{85}Kr which strongly influences the s-process branching at this isotope. We have shown that activation measurements can be performed in a quasi stellar neutron spectrum using the ^{3}H(p,n) reaction. This was achieved for a proton energy of E_p = 1099 keV, 80 keV above the reaction threshold. Integration over the resulting neutron spectrum (kinematically collimated in a forward cone of 120 deg opening angle, E_n^{max} = 225 keV) yielded the histogram in Fig. 1 which approximates a Maxwell-Boltzmann spectrum of kT = 52 keV (solid line).

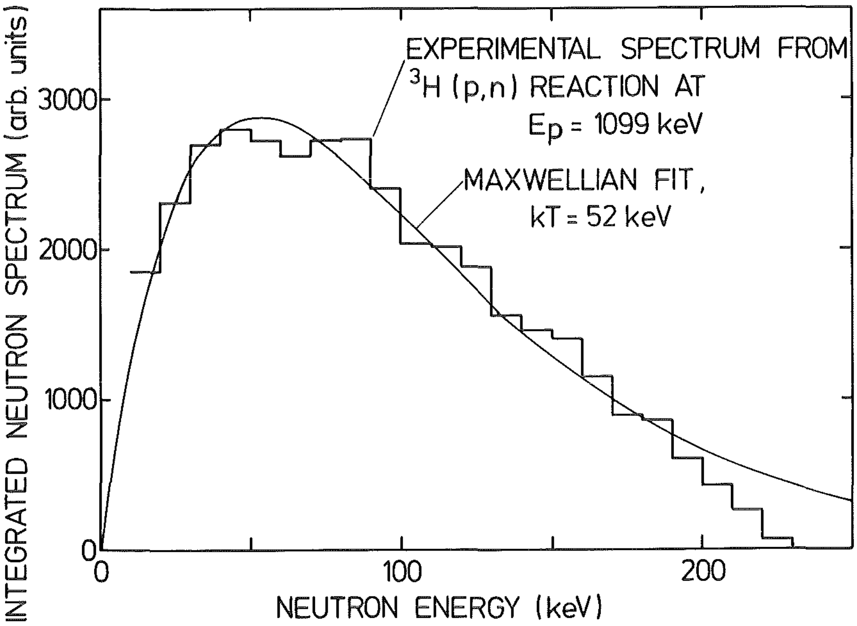

Fig. 1 Angle-integrated neutron spectrum from the ^{3}H(p,n) reaction at Ep = 1099 keV (histogram) fitted by a Maxwell-Boltzmann distribution for kT = 52 keV.

Activation measurements were performed with natural Kr samples in this spectrum for kT = 52 keV and in that for kT = 25 keV from the ^{7}Li(p,n) reaction (1). These results together with the total (n,γ) cross section of ^{84}Kr (2) indicate an almost constant isomeric ratio of ^{85}Kr between 25 and 52 keV.

(1) H. Beer, F. Käppeler, Phys. Rev. C 21 (1980) 534

(2) G. Walter, B. Leugers, F. Käppeler, G. Reffo, F. Fabbri, Z.Y. Bao, KfK-3969, Kernforschungszentrum Karlsruhe; Z.Y. Bao, F. Käppeler, Atomic Data and Nuclear Data Tables (in print)

+ University of Dhahran, Saudi Arabia

1.1.9 s-PROCESS NUCLEOSYNTHESIS BELOW A = 90

H. Beer, (1)

A complete s-process analysis of heavy elements is carried out in the frame of the classical model with three exponential neutron exposure distributions. Special emphasis is placed on the mass region below A = 90 where the main and weak s-process components are effective. The derived astrophysical parameters of this model are able to reproduce heavy s-process element abundances correctly and consistently with the other processes of nucleosynthesis.

(1) Nucleosynthesis and its Implications on Nuclear and Particle Physics, eds. J. Audouze, N. Mathieu, Dordrecht, D. Reidel Publ. Company, 1986, p. 263

1.1.10 A MEASUREMENT OF THE ^{139}La CAPTURE CROSS SECTION AND A STUDY OF THE s-PROCESS AT MAGIC NEUTRON NUMBER 82

H. Beer, (1)

The Maxwellian averaged neutron capture cross section of ^{139}La has been measured at $kT = 25$ keV to be 44.1 ± 2.9 mb by means of the activation technique. A study of the precipice of the $\sigma N(A)$ curve at magic neutron shell 82 using the new cross section was carried out. The average time-integrated neutron flux τ_o was found to be $\tau_o = (0.304 \pm 0.013)$ mb^{-1} at $kT = 30$ keV and an s-process abundance of ^{139}La of 0.33 ± 0.03 ($Si \equiv 10^6$) was calculated.

(1) Astron. Astrophys. 162 (1986) 330

1.1.11 ^{148,150}Sm: A TEST FOR s-PROCESS NUCLEOSYNTHESIS

R.R. Winters+, F. Käppeler, K. Wisshak, A. Mengoni, G. Reffo++, (1)

We have measured to a precision of ∿ 4.5 % the neutron capture cross sections of ^{148,149,150}Sm over the neutron energy range $4 < E < 250$ keV. These data, in conjunction with calculated cross sections for ^{147}Nd and ^{147,148}Pm, are used to establish a set of Maxwellian-averaged cross sections useful for investigation of branchings in the s-process of stellar nucleosynthesis. The ratio of the values of the s-process $\langle\sigma\rangle N_s$ (Maxwellian-averaged neutron cross section times s-process abundance) for the s-only isotopes ^{148,150}Sm is 0.91 ± 0.03 rather than unity as predicted by the local approximation. We interpret this result as due to an s-process branching which partly bypasses ^{148}Sm. Since the ß-decay rates at the branching points are expected to be almost independent of temperature, we are able to obtain an estimate of the s-process neutron density of $n_n = (1.0 \pm 0.4) \times 10^8$ cm^3. The new results have also served to considerably improve the $\langle\sigma\rangle N_s$-systematics in the mass region $A \approx 145$.

(1) Ap.J. 300 (1986) 41

+ Denison University, Granville, Ohio
++ Laboratorio Dati Nucleari, E.N.E.A., Bologna, Italy

1.1.12 SEARCH FOR WEAK TRANSITIONS LINKING GROUND STATE AND ISOMER IN ^{176}Lu

N. Klay, H. Beer, H. Börner+, F. Hoyler+, F. Käppeler, G. Schatz, K. Schreckenbach+

Among the nuclides produced by the s-process, ^{176}Lu has the following unique features: (i) there is no r-process contribution to this nuclide due to the existence of stable ^{176}Yb; (ii) it is beta unstable with a half-life of 3.6×10^{10} a. A detailed analysis of the s-process near ^{176}Lu should hence allow for a determination of the time which has elapsed since the s-process nuclides were formed. This problem has been studied in a number of papers (1-4) but the result has so far been inconclusive. This is due to insufficient knowledge of the excited states of ^{176}Lu and to the existence of an isomeric state at 126.3 keV which undergoes beta-decay to ^{176}Hf with a half-life of 3.7 h. Both the isomer and the ground state are produced by neutron capture. Since the s-process occurs in the hot interior of stars at a temperature of $2...3 \times 10^8$ K there is in addition the possibility of thermal excitation from the ground state to the isomer. This would lead to a substantial reduction of the effective ground state half-life. The mere existence of ^{176}Lu in the solar system today proves that thermal equilibrium between isomer and ground state cannot have been achieved during the s-process. On the other hand, inconsistent results are obtained if thermally induced transitions between the two states are neglected. In the intermediate case, the transition rate is governed by the γ-decay half-lives of excited states.

Excited states of ^{176}Lu have been mainly studied by thermal neutron capture (5) and by Coulomb excitation from the ground state (6,7). These studies have established two completely separate systems of nuclear states with no known transitions connecting them. This is not surprising since ground state and isomer belong to bands with $K = 7^-$ and 0^-, respectively. So far no low-lying states of intermediate K are known, except a recently discovered 5^- state (7).

Therefore, we set out to search for (presumably very weak) transitions between the two systems of excited states, using the outstanding spectrometers at the high flux reactor at the ILL Grenoble. In a first step, we have measured the gamma-ray spectrum emitted from ^{176}Lu following neutron capture in ^{175}Lu between E_γ = 30 and 1150 keV with optimal resolution. This measurement was repeated with reduced sensitivity for ^{176}Lu (n_{th},γ) in order to account for the 0.2 % isotopic impurity of ^{176}Lu in the ^{175}Lu sample. In total, we found 460 transitions in ^{176}Lu, which we analyzed according to energy, width and intensity. Many of the weaker transitions had not been detected before.

Next, a high resolution measurement of the conversion electron spectrum is planned to obtain complementary information on multipolarities. This should enable us to contruct a refined level scheme of ^{176}Lu which hopefully provides evidence for the thermal effects on the half-life of ^{176}Lu.

(1) H. Beer, F. Käppeler, Phys. Rev. C21 (1980) 534

(2) H. Beer, F. Käppeler, K. Wisshak, R. Ward, Ap. J. Suppl. Series 46 (1981) 295

(3) H. Beer, Ap. J. 262 (1982) 739

(4) H. Beer, G. Walter, R.L. Macklin, P.J. Patchett, Phys. Rev. C30 (1984) 464

(5) M.K. Balodis, J.J. Tambergs, K.J. Alksnis, P.T. Prokofjev, W.G. Vonach, H.K. Vonach, H.R. Koch, U. Gruber, B.P.K. Maier, O.W.B. Schult, Nucl. Phys. A194 (1972) 305

(6) J. Gerl, K. Ronge, K. Venkata Ramaniah, Th. W. Elze, A. Hanser, L.D.Tolsma, Z. Phys. A310 (1983) 349

(7) Th. W. Elze, priv. communication

+ Institut Laue-Langevin, Grenoble, France.

1.1.13 THE STELLAR CAPTURE CROSS SECTION OF ^{197}Au - AN ABSOLUTE MEASUREMENT AT kT = 25 keV

W. Ratynski+, F. Käppeler

Gold has become an important standard for neutron cross section measurements in the keV energy range, because direct neutron flux determination is very difficult in this energy domain. The advantageous features of gold are:

- only one stable isotope;
- reasonably large cross section;
- easily available with high purity;
- chemically stable;
- can be used in activation measurements.

However, the absolute magnitude of this cross section is still not sufficiently well known, various recent measurements show discrepancies of ∿ 7 % for the stellar cross section at kT = 30 keV (1).

Therefore, we have started a new measurement, using the ^{7}Li(p,n)^{7}Be reaction for neutron production. This reaction does not only provide the time-integrated neutron flux via the ^{7}Be activity of the target, but also allows for the simulation of a Maxwellian energy spectrum at kT = 25 keV. As this spectrum is emitted in a forward cone of 120° opening angle (2), the cross section can be measured in good geometry and independent of any other standard (3,4). Then, the extrapolation to kT = 30 keV can be made reliably as the relative energy dependence of the cross section is well known.

So far, we have started with a series of activations to systematically study the required corrections (e.g. for neutron scattering or ^{7}Be losses from the target) and the associated uncertainties. In the final results we aim for a precision of 2 %.

(1) Z.Y. Bao, F. Käppeler, Atomic Data and Nuclear Data Tables (in print)
(2) H. Beer, F. Käppeler, Phys. Rev. C21 (1980) 534
(3) W.P. Poenitz, J. Nucl. Energy 20 (1966) 825
(4) S. Zhu, S. Jiang, Y. Chen, D. Luo, Chin. J. Nucl. Phys. 6 (1984) 23

+ On leave from Institute for Nuclear Studies, Swierk, Poland.

1.1.14 $^{198,199,200,201,202,204}Hg(n,\gamma)$ CROSS SECTIONS AND THE TERMINATION OF s-PROCESS NUCLEOSYNTHESIS

H. Beer, R.L. Macklin[+], (1)

The neutron capture cross sections of $^{198,199,200,201,202,204}Hg(n,\gamma)$ were measured in the energy range 2.6 to 500 keV. The average capture cross sections were calculated and fitted in terms of strength functions. Resonance parameters for the observed resonances were determined by a shape analysis. Maxwellian averaged capture cross sections were computed for thermal energies kT between 5 and 100 keV. The solar mercury abundance was determined to be 0.34 ± 0.04 relative to Si $\equiv 10^6$. The termination of s-process nucleosynthesis at lead and bismuth was investigated. The abundances of $^{206,207,208}Pb$ were reproduced introducing a strong fluence component of the s-process in addition to normal s- and r-process nucleosynthesis. The radiogenic ^{207}Pb abundance was determined and the r-process age was calculated via ^{235}U. Using Fowler's exponential model, an age $T = 4.6$ Gyr $+ \Delta =$ 17.2 ± 2.6 Gyr was obtained.

(1) Phys. Rev. C 32 (1985) 738

[+] Oak Ridge National Laboratory, Oak Ridge, Tennessee 37830

1.1.15 THE PRODUCTION AND SURVIVAL OF ^{205}Pb IN STARS AND THE ^{205}Pb - ^{205}Tl s-PROCESS CHRONOMETRY

K. Yokoi, K. Takahashi[+], M. Arnould[++], (1)

The s-process production ratio of ^{204}Pb and ^{205}Pb, which is of importance for the ^{205}Pb-^{205}Tl chronometry, is calculated in two schematic s-process models. Special emphasis is put on the role of the bound-state β^--decay of ^{205}Tl which has been totally overlooked in previous studies. It is shown that the ^{205}Pb production under certain s-process conditions might be large enough for making worthwhile a renewed search for extinct ^{205}Pb in meteorites. The influence of uncertainties in the input quantities (electron capture Q-values and ft values) on the results is also discussed.

(1) Astron. Astrophys. 145 (1985) 339

[+] Lawrence Livermore National Laboratory, Univ. of California, Livermore, California

[++] Univ. Libre de Bruxelles, Brussels, Belgium

1.1.16 NEUTRON CAPTURE CROSS SECTIONS FOR s-PROCESS STUDIES

Z.Y. Bao^{+}, F. Käppeler, (1)

The existing information on experimental and calculated neutron capture cross sections in the keV energy range was surveyed, properly renormalized if necessary, and converted into Maxwellian averages over stellar neutron spectra characterized by thermal energies between 10 and 50 keV. This compilation includes all isotopes involved in the slow neutron capture process (s-process) of nucleosynthesis between ^{12}C and ^{209}Bi as well as the longer-lived actinide isotopes which might have been modified by the s-process. Gaps in the experimental data were covered with calculated cross sections, which are particularly important in case of radioactive nuclei and for estimating the effect of thermally populated excited states. From the entire body of evaluated data a present best set of cross sections is recommended for use in s-process studies.

Of the 240 considered isotopes on or near the s-process path, Fig. 1 shows

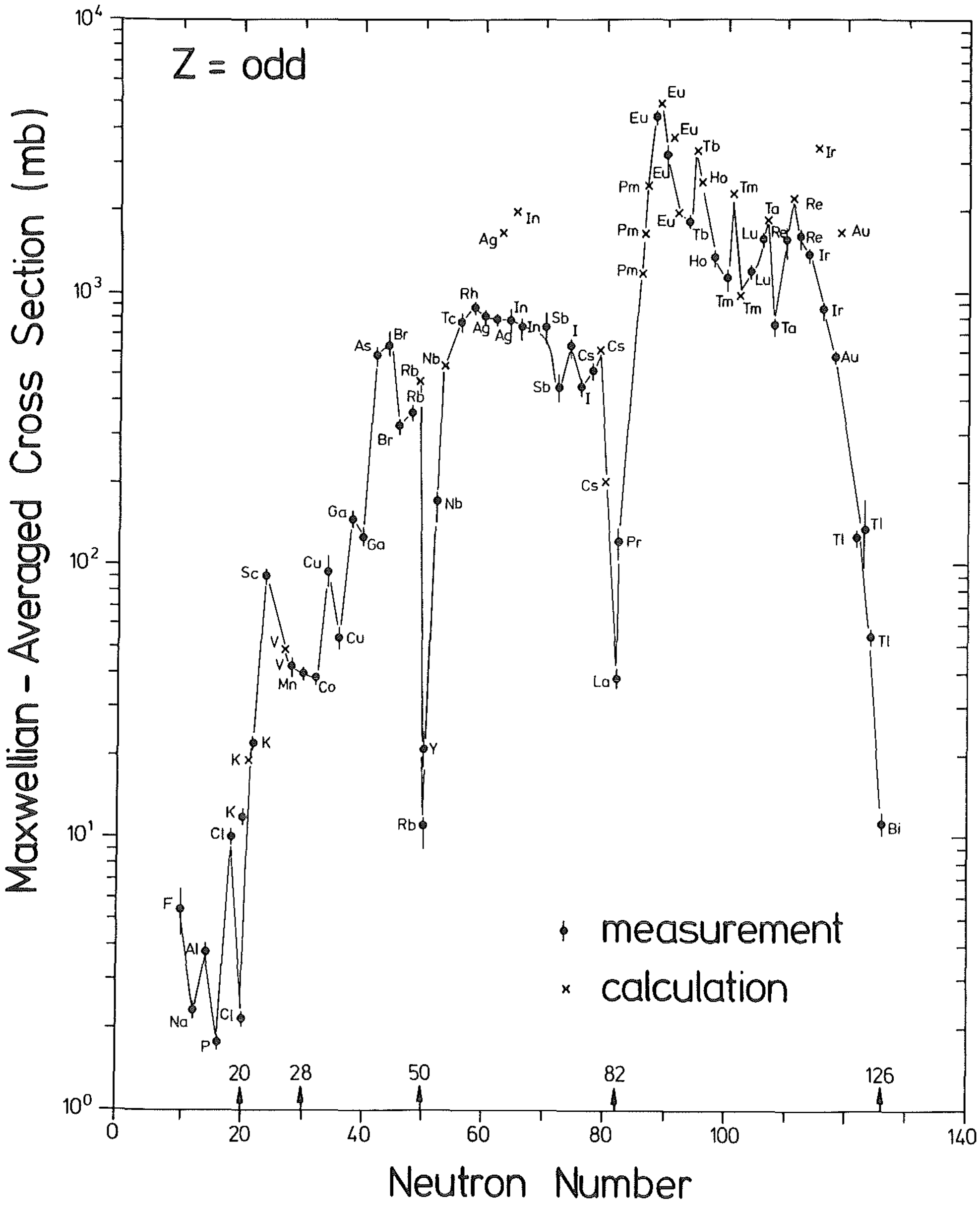

Fig. 1
Maxwellian averaged cross sections for kT = 30 keV (odd Z isotopes)

the cross sections of the odd Z nuclei. Note that most of the small cross sections near magic neutron numbers are meanwhile measured with reasonable accuracy.

(1) Atomic Data and Nuclear Data Tables (in print)

+ On leave from the Institute of Atomic Energy, Academia Sinica, Beijing, Peoples Rep. of China

1.1.17 COMPETITION OF NEUTRON CAPTURE AND BETA DECAY AT THE ^{85}Kr and ^{151}Sm BRANCHINGS, A MEANS TO ESTIMATE THE s-PROCESS PULSE CONDITION

H. Beer, (1)

s-Process abundances of heavy elements are successfully reproduced using an exponential distribution of neutron exposures (1,2). This behaviour has been explained as the result of a pulsed irradiation of s-process seed material in the He-shell of red giant stars (3). A possibility to ascertain the pulsed nature of the s-process is offered by the analysis of branchings in the synthesis path. A branching results from competition between neutron capture and beta decay in case of a radioactive isotope situated on the path. The pulsed nature of the s-process can show up due to the interpulse decay of the radioactive branch point nucleus and the necessary reformation of its abundance during the next pulse.

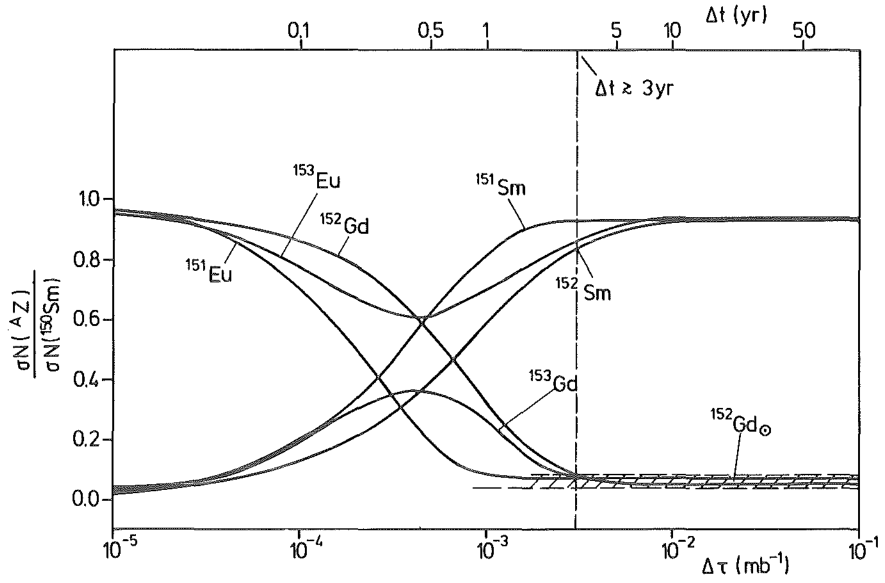

Fig. 1 The analysis of the isotopes located in the ^{151}Sm branching is shown. The σN (capture cross section times s-process abundance) values normalized to ^{150}Sm are plotted as a function of the exposure . For ^{152}Gd an empirical value can be given (hatched area). The intercept of the theoretical curve with the empirical value yields $\Delta t \geq 3$ yr. Note that a sufficiently small Δτ practically cancels the branch to ^{152}Sm.

In this work it was found that the branchings at ^{85}Kr and ^{151}Sm are especially sensitive to the pulse conditions. While ^{151}Sm provided a lower bound for the pulse duration, ^{85}Kr gave an upper limit. For the analysis, the pulsed s-process model of Ward and Newman (4) assuming a constant irradiation during the pulse was used. The classical s-process appears as a limiting case for very large pulse durations ($\Delta t \to \infty$). In Fig. 1 the analysis of the ^{151}Sm branching is shown. Comparison of the solar ^{152}Gd abundance with the calculation exhibits that a pulse duration $\Delta t \geq 3$ yr is required. A similar calculation on the ^{85}Kr branching yields an upper limit $\Delta t \leq 50$ yr.

(1) F. Käppeler, H. Beer, K. Wisshak, D.D. Clayton, R.A. Ward, Ap. J. 257 (1982) 821
(2) H. Beer, Nucleosynthesis and its Implications on Nuclear and Particle Physics, eds. J. Audouze, N. Mathieu, Dordrecht, P. Reidel Publishing Company, 1986, p. 263
(3) K. Cosner, I. Iben jr., J.W. Truran, Ap. J. 238 (1980) L91
(4) R.A. Ward, M.J. Newman, Ap. J. 219 (1978) 195

+ Int. Symp. on Weak and Electromagnetic Interactions in Nuclei, Heidelberg, 1.-5. July 1986

1.1.18 s-PROCESS NUCLEOSYNTHESIS - STELLAR ASPECTS AND THE CLASSICAL MODEL

F. Käppeler, (1)

The sensitivity and the limits of s-process analyses with the classical model are discussed with respect to the interpretation of abundance patterns in the atmosphere of red giant stars. In particular, the effects of neutron capture cross sections, mean neutron exposure, and neutron density on the resulting s-process overabundances are considered.

(1) Nucleosynthesis and its Implications on Nuclear and Particle Physics, eds. J. Audouze, N. Mathieu, Dordrecht, P. Reidel Publishing Company, 1986, p. 253

1.1.19 EXPLOSIVE NUCLEOSYNTHESIS IN CARBON DEFLAGRATION MODELS OF TYPE I SUPERNOVAE

F.-K. Thielemann^{+}, K. Nomoto^{++}, K. Yokoi, (1)

There is increasing evidence that type I supernovae (SN 1) are the main producers of iron-peak elements in the Galaxy. In addition observations of SN1 also indicate the existence of appreciable amounts of intermediate elements like O, Mg, Si, S and Ca in the outer layers of the exploding star. In an earlier paper we have shown that such an abundance pattern can be produced by carbon deflagration models of accreting carbon oxygen white dwarfs in binary systems or stars on the asymptotic giant branch which ignite central carbon burning explosively. In the present study explosive nucleosynthesis results of these carbon deflagration supernovae are presented in detail. Special emphasis is given to the discussion of burning conditions and corresponding nucleosynthesis products, and the nuclear uncertainties which govern the amount of electron captures in the central part of the core. The latter gives constraints on the isotopic composition of the iron peak elements. The overproduction of ^{54}Fe + ^{58}Ni is still existing. Assuming that SN1 which contributed to the abundances in the solar system, originated from white dwarfs with a metallicity range $0.1 < Z/Z_0 < 1$, might remove this overproduction. This would allow for SN1 to be the major contributors of Fe-group nuclei in galactic nucleosynthesis.

(1) Astron. Astrophys. 158 (1986) 17

+ Univ. of Illinois, Urbana, Illinois

++ College of Arts and Science, Univ. of Tokyo, Tokyo, Japan

1.1.20 s-PROCESS STUDIES USING SINGLE AND PULSED NEUTRON EXPOSURES

H. Beer

The aim of this work is the search for an improved phenomenological description of the solar s-process abundances from ^{56}Fe to ^{209}Bi. Problems in reproducing the abundances exist at the beginning and termination of the s-process path. Previous work (1,2,3) tried to meet these problems using an s-process with a superposition of three exponential exposure distributions.

On the basis of a series of new improved capture cross sections modifications of this concept are necessary. This is illustrated in Fig. 1 (above) where a fit of the empirical data in the frame of the current three component s-process model using exponential exposure distributions is shown. The bulk of nuclei from A = 90 - 200 is described by the so called main component. Below A = 90 the weak component and above A = 200 the strong component is added. Fig. 1 (above) shows for these regions the course of the main s-process and the composite curve of main+weak and main+strong, respectively. The discrepancies between calculation and empirical data are obvious at ^{70}Ge and ^{76}Se, two s-only isotopes which are underproduced and at the ^{85}Kr branching where ^{87}Rb is overproduced by the calculation. This overproduction is still more aggravating if we bear in mind that the empirical ^{87}Rb point contains a significant r-process contribution. The underproduction of the two s-only isotopes cannot be removed in the frame of the current model by varying the free parameters, the iron seed abundance N(56) and the average time integrated neutron flux τ_0. An increase of N(56) to match ^{70}Ge and ^{76}Se signifies an overall shift of the curve (Fig. 1) (above) with corresponding over-

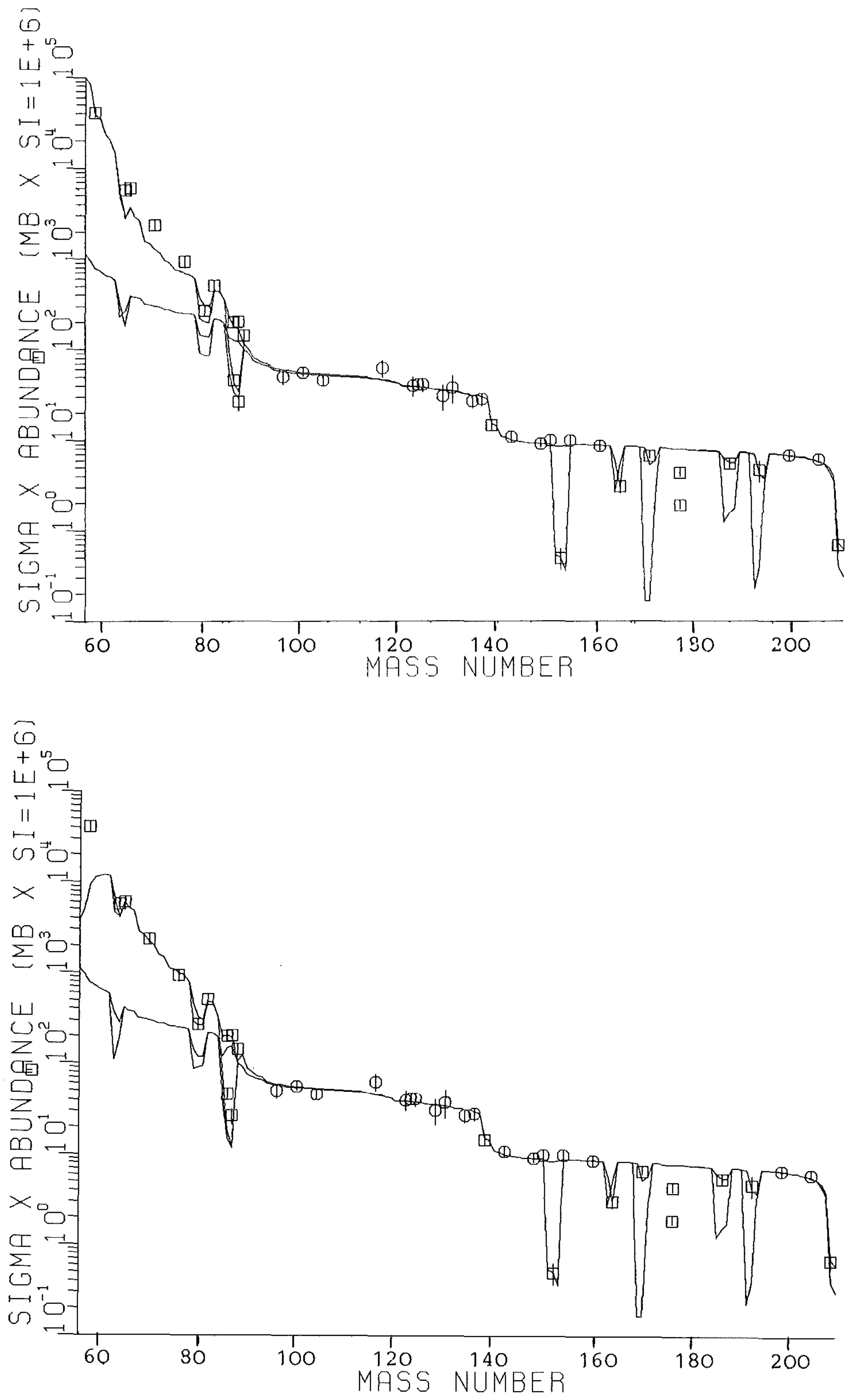

Fig. 1 The product σN (capture cross section times abundance) as a function of mass number. The symbols correspond to empirical data. Significant branchings were identified due to low empirical values on one of the branches. Note that the ^{86}Kr and ^{87}Rb data located in the ^{85}Kr branching are not corrected for r-process contributions. Therefore, the theoretical calculations (solid lines) must remain below the empirical values to avoid

overproduction. Below A $\approx$ 86 the weak component and above A = 205 the strong component is significant. For these mass ranges additional to the composite curve, the course of the main s-process component is plotted, too. In the upper part the previous s-process analysis is shown. In the lower part the result of the new calculation is given using a single flux s-process for the weak and the strong component and a pulsed s-process (pulse duration 10 a) for the main component.

productions at ^{58}Fe and the isotopes of Zr. A variation of τ_0 leads to a steeper or flatter course of the curve with similar problems. It is shown in this work that these problems can be solved if the weak component is modeled as a single flux exposure s-process and the main component as a pulsed s-process. The treatament of the strong component as a single flux s-process is also considered.

In Fig. 1 (below) the new overall calculation of the s-process from ^{56}Fe to ^{209}Bi is displayed using single flux exposure s-process components for the beginning and termination of the synthesis path and a pulsed s-process for the bulk of nuclei. The pulse duration was found to lie between 3 and 50 a.

This new analysis of the s-process showed that neutron density and temperature derived from the continuous s-process calculation is still valid. ^{58}Fe is now no dominant s-process isotope anymore. The overproduction of ^{87}Rb in the s-process is avoided.

The analysis with the chosen single flux s-process for the strong component is equivalent to the corresponding analysis with an s-process using an exponential exposure distribution. An advantage of the single flux exposure s-process might be that its contribution outside the terminal cycle is extremely small. E.g., the abundance contribution of the strong component at A = 160 is 0.05 % for a single flux s-process, but 1.3 % for an s-process with an exponential exposure distribution.

(1) R.A. Ward, M.J. Newman Ap. J. 219 (1978) 195

(2) F. Käppeler, H. Beer, K. Wisshak, D.D. Clayton, R.A. Ward, Ap, J. 257 (1982) 821

(3) H. Beer, Nucleosynthesis and its Implications on Nuclear and Particle Physics, eds. J. Audouze, N. Mathieu, Dordrecht, P. Reidel Publishing Company, 1986, p. 263.

1.2 NEUTRON SCATTERING

1.2.1 THE BACKWARD ANGLE np CROSS SECTION IN THE ENERGY RANGE FROM 22 TO 50 MeV

G.Fink, P.Doll, W.Heeringa, H.O.Klages, H.Krupp*

Final results for the np differential cross section in the backward angle range are presented. The experimental setup, the measurement, and the off-line data analysis have been described in the last years annual report (1).

The first results contain precise information on the shape of the angular distributions only. The absolute normalization for each energy was found in two steps. Firstly, at each energy the data points at 120° were set to the values predicted by the Paris potential (2). In this way a preliminary normalization was found for the angular distribution at each energy. These "preliminary data" were used as additional input in a series of phase shift analyses together with all available np scattering data in the energy range from 16 to 54 MeV, including analyzing power data and spin correlation parameters. In these analyses the normalization factors of our new data sets were used as free parameters. The resulting factors turned out to be stable within 2% for any reasonable change in the data base or in phase parameter constraints in various independent analyses. Taking this uncertainties as a measure for the accuracy of the scale, we were able to derive absolute values for the np differential cross section, shown in figure 1.

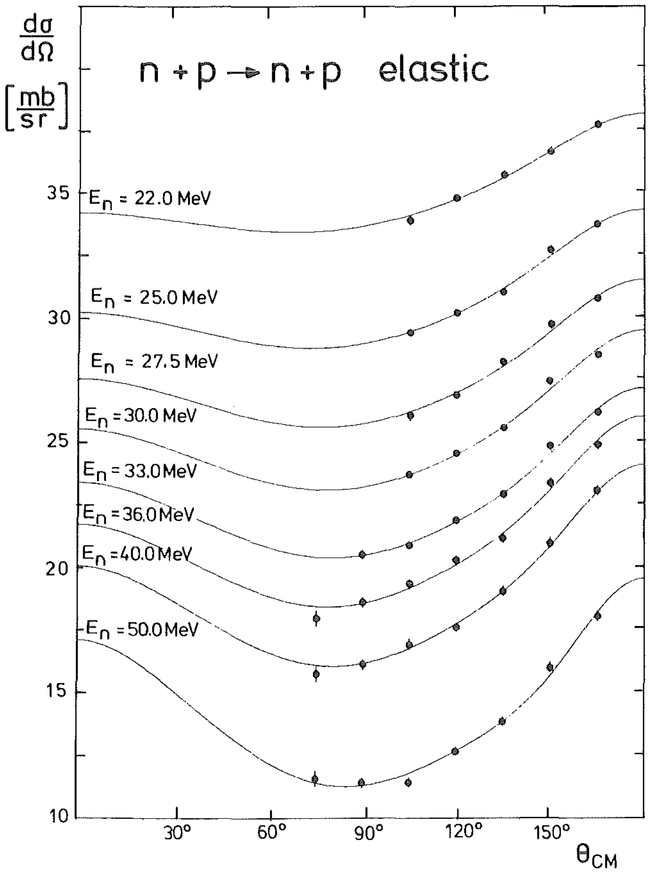

Fig.1: Results for the np differential cross sections. Solid lines: new phase shift analyses.

The results are in very good agreement with the precise data from U.C. Davis at 50 MeV (3). At the other energies the accuracy has been considerably improved compared to previous data. The precise knowledge of the backward angle shape of the differential cross section enables the determination of the $^1P_1$ phase shift in np phase shift analysis, as shown in contribution 1.2.4.

(1) P.Doll et al., KfK report 3969 (1985 22
(2) M.Lacombe et al., Phys.Rev. C21 (1980) 861
(3) T.C.Montgomery et al., Phys.Rev.C16 (1977) 499

* now at Siemens AG München

1.2.2 THE np ANALYZING POWER A_y AT BACKWARD ANGLES

V.Eberhard, P.Doll, G.Fink, R.W.Finlay*, T.D.Ford,
W.Heeringa, H.O.Klages, H.Krupp**

In the last few years, several groups (1) have contributed high accuracy data of the np analyzing power in the energy range up to 50 MeV. Phase shift analyses and sensitivity calculations reveal, that these data have strong impact on the ^3D_J- and on the np ^3P_J-phase shifts .

Especially the backward angle results for A_y have gained new attention due to severe disagreements between some data sets (3). Neutron detection seems to bear serious experimental problems at far backward angles. The detection of the recoil protons with ΔE/E telescopes at forward angles yields much cleaner spectra and more reliable results.

We have used a set of four such telescopes at small angles as flux monitors for polarized neutrons in several experiments. Simultaneously, the statistical accuracy of the backward angle analyzing power A_y was improved, see fig.1.

In a recent experiment, these telescopes were used at $\Theta_{lab} = \pm 10^o$ and $\pm 17.5^o$. At the same time, a setup of 4 symmetric pairs of proton telescopes in an evacuated scattering chamber was used to measure the same quantity at 10°, 17.5^o, 25° and 32.5^o in the lab. system. For details of the experimental setup see ref.4. The targets used in the experiment were 3 mm polyethylene (PE) for the monitor telescopes and 2 mm PE for the chamber experiment.

This measurement was carried out using the continuous energy neutron beam from POLKA (5). Therefore, the results will cover the angular range from 115° c.m. to 160° c.m. for neutron energies from 20 to 50 MeV.

Data are presently being analyzed. The estimated accuracy will enable us to put sharper constraints on the ^3D_J phase shifts.

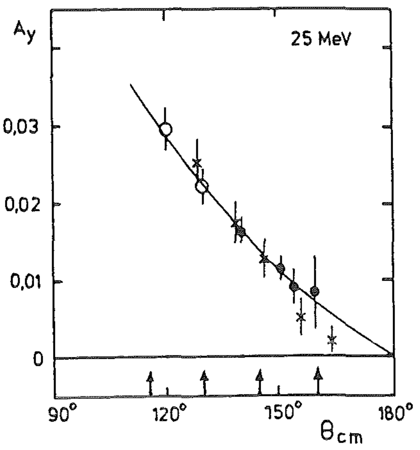

Fig.1:The backward angle distribution of the np analyzing power A_y at 25 MeV. Recent Karlsruhe data (full dots) compared to the results of the Madison group (3). Circles: neutrons detected, crosses: protons detected. Solid line: phase shift analysis. The arrows indicate the new measurements.

(1) J.Wilczynski et al., Nucl.Phys. A425 (1984) 458
W.Tornow et al., Nucl.Phys. A340 (1980) 34
M.D.Barker et al., Proc.Few Body X, Karlsruhe (1983) IIp.31
(2) H.Krupp, Ph.D.thesis, Univ. Karlsruhe (1986)
(3) J.Sromicki et al., Proc.Few Body XI, Sendai (1986) IIp.394
(4) P.Doll et al., Nucl.Instr.Meth. A250 (1986) 526
(5) H.O.Klages et al., Nucl.Instr.Meth. 219 (1984) 269

* Ohio State University, Athens, USA

** now at Siemens AG, München

1.2.3 RESULTS OF THE $\vec{n}\vec{p}$ SPIN CORRELATION PARAMETER A_{yy}

H.Krupp*, P.Doll, V.Eberhard, G.Fink, W.Heeringa, K.Hofmann**, H.O.Klages, Chr.Wölfl

At the Karlsruhe cyclotron the $\vec{n}\vec{p}$ spin correlation parameter A_{yy} has been determined for the energy range 17 to 50 MeV. The experiment has been described in some detail in the 1984/85 annual report (1). Briefly, polarized neutrons with a continuous energy distribution were scattered by polarized protons in a TiH_2 sample.

The target polarization was achieved in the facility KRYPTA (2) by cooling the sample to ~ 11 mK in a field of 9 T. An effective polarization of the protons of 0.66 was reached.

Five symmetric pairs of detectors were used for the scattered neutrons. Light pulses from thermally stabilized LEDs were used for gain monitoring (3). The background of neutrons scattered from Ti was determined in extensive measurements using a Ti sample instead of the TiH_2 probe. Samples were exchanged at full field and low temperature. The incident neutron flux was monitored by a set of four recoil proton telescopes (4).

In the off-line analysis, e.g. the spin-dependent flux attenuation in the TiH_2 sample had to be considered. In extensive Monte Carlo calculations the effects of the sample thickness, of the finite geometry and of multiple scattering were investigated (5).

The final results were obtained by subtracting the normalized Ti events from the TiH_2 events. This method is applicable for all scattering angles where the n-p and the n-Ti cross sections are of the same magnitude. At forward angles the n-Ti cross section dominates considerably. Therefore, the np scattering results suffer from large statistical uncertainties at 10° and 15°.

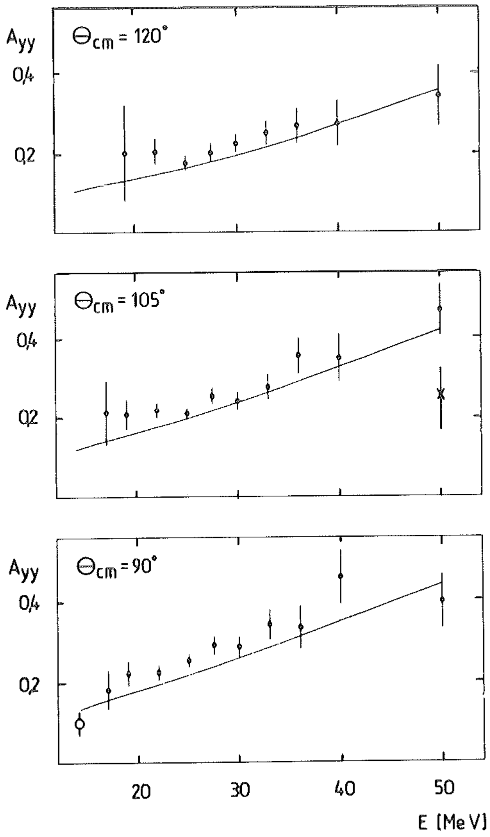

Fig.1: Results for the np spin correlation parameter A_{yy} compared to Paris potential predictions (solid line)

In figure 1 the new A_{yy} data at the three backward angles are shown together with the predictions from the Paris potential (6).

The experiment will be continued to cover also the angular range from 45° to 90° (c.m.). These data are still needed to put sharper constraints on the $^3S_1$ - $^3D_1$ mixing parameter ε_1 in np phase shift analyses.

(1) P.Doll et al., KfK report 3969 (1985) 21
(2) R.Aures et al., Nucl.Instr.Meth. 224 (1984) 347
(3) V.Eberhard et al., KfK report 3969 (1985) 157
(4) P.Doll et al., Nucl.Instr.Meth. A250 (1986) 526

(5) H.Krupp, Ph.D.thesis, Univ. Karlsruhe (1986)
(6) M.Lacombe et al., Phys.Rev. C21 (1980) 861

* Now at Siemens AG, München

** Now at Bosch AG, Bühlertal

1.2.4 STATUS OF np PHASE SHIFT ANALYSES FOR ENERGIES UP TO 50 MeV

H.O.Klages, G.Fink, H.Krupp, P.Doll, W.Heeringa

The parametrization of the low energy NN interaction in terms of phase shifts has been improved considerably in the last few years by the inclusion of new high quality data in the analyses.

In the pp-channel, only T = 1 phase shifts can contribute, corresponding to ~ 5 free parameters in the energy range up to 50 MeV. However, there is still need for very precise data on the pp analyzing power A_y to determine the ^3P_J phase shifts. These experiments are presently under way at SIN. For the np-channel, in addition, all T = 0 phase shifts contribute, adding at least 6 parameters.

If charge symmetry is assumed for the NN interaction, the T = 1 parameters can be taken from pp analyses. This has been done by most authors up to now. On the other hand, theoretical predictions exist (1) of differences in the ^3P_J phase shifts from pp and from np interaction based on the charge symmetry breaking effect of up/down quark mass differences.

Therefore, we used all available experimental information on np scattering, including the new Karlsruhe data presented above, to perform a series of phase shift analyses for the np system in the energy range 20 to 50 MeV in energy bins of ± 4 MeV width.

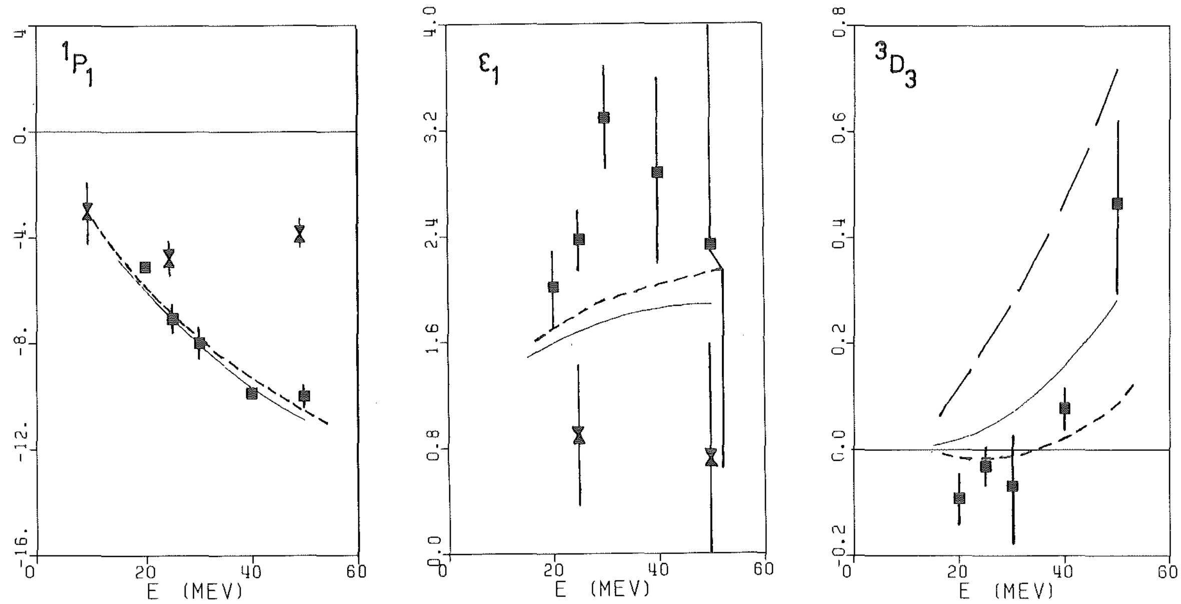

Fig.1: T = 0 phase shifts from new np phase shift analyses (squares) compared to the results of ref.2 (triangles and long dashed curve). Solid line: Paris potential (3), short dashed line: Bonn potential (4).

The first result of these analyses is that the np data base is not sufficient to determine the np ^3P phase shifts with uncertainties smaller than the predicted differences to the pp ^3P phase shifts. Especially the $\vec{n}p$ analyzing power data still have too large errors, both from statistics and sytematics.

On the other hand, some T = 0 phase shifts could be determined much better with the inclusion of the new data. The long standing problem of the $^1P_1$ phase shift, which did not agree with potential model predictions in older analyses (2), could be solved.

The ^3D phase shifts differ considerably in the predictions from various models like the Paris (3) or the Bonn potential (4). In our analyses the agreement with the Bonn potential is surprisingly good.

The $^3S_1$ - $^3D_1$ mixing parameter ε_1 is still not very well determined, in spite of 30 new data points for the spin correlation parameter A_{yy}. More precise experiments are necessary to solve this "last" problem in the T = 0 phase shifts at low energies.

(1) P.Langacker, D.A.Sparrow, Phys.Rev. C25 (1982) 1194
(2) R.A.Arndt, private communication (1983)
(3) M.Lacombe et al., Phys.Rev. C21 (1980) 861
(4) R.Machleidt, private communication (1986)

1.3 NEUTRON INDUCED REACTIONS

1.3.1 SPIN-SPIN CROSS SECTION MEASUREMENTS OF POLARIZED NEUTRONS ON THE POLARIZED NUCLEI ^{27}Al AND ^{93}Nb

Chr.Wölfl, D.Reppenhagen, P.Doll, R.W.Finlay*, W.Heeringa,
H.O.Klages, H.Skacel

Spin-spin cross section measurements have been carried out at the polarized neutron beam POLKA of the Karlsruhe cyclotron for the nuclides ^{27}Al and ^{93}Nb. The target samples were 40 mm long and had a diameter of about 30 mm. They were polarized in the cryostat KRYPTA by a 9 T magnetic field at temperatures around 10 - 15 mK. During the measurements the average polarization of the samples was 45% for aluminium and 55% for niobium.

For the neutron flux measurement in front of and behind the target three different types of detectors were employed: thin scintillation detectors, converter-ΔE-Δ arrangements and converter-ΔE-ΔE arrays. The properties of these flux detectors are discussed in contribution 6.1.9.

The measured effects are of the order of 10^{-3} corresponding to spin-spin cross sections of about 10 mb. Systematic uncertainties appear to be of the same size, however. They show up by analyzing measurements carried out with unpolarized beam or unpolarized target. It is not yet clear whether they are inherent in the data or are originated by the way in which the data are analyzed. This problem is being investigated thoroughly at present.

* Ohio State University, Athens, USA

1.3.2 MEASUREMENT OF THE ANALYZING POWER OF THE REACTIONS $^3He(\vec{n},p)t$ AND $^3He(\vec{n},d)d$

A.Vollmer, P.Doll, G.Fink, R.W.Finlay*, T.D.Ford, W.Heeringa, H.O.Klages

The A = 4 system has gained new interest recently as the improvements of theoretical methods and computer power have led to a number of promising approaches to the microscopic description of the "lightest real nuclear system" (1). Observables are calculated by R-matrix codes, by resonating group methods and by solving Faddeev type equations using effective interactions. In most cases the inclusion of the Coulomb interaction is possible in an approximative way only. Therefore, the Karlsruhe group has started a systematic study of the n+^{3}He entrance channel. In this framework the analyzing power of the reactions $\vec{n}+^3He \rightarrow p+t$ and $\vec{n}+^3He \rightarrow d+d$ has been measured in the energy range from 20 to 50 MeV.

The experiment was carried out using the polarized continuous energy neutron beam from POLKA (2), a ^{3}He gas target and 8 $\Delta E/E$ telescopes (3) in an evacuated scattering chamber for the charged reaction products. An angular range from 12.5° to 77.5° (lab.) was covered.

At forward angles, also tritons are detected to avoid the detection of protons at far backward angles. Therefore, the gas target foils and the ΔE detectors have to be rather thin. We decided to use a cold (18 K) gas target at a pressure of 2 - 3 bar. This device is described in contribution 6.2.2 of this report. For the $\Delta E/E$ telescopes at forward angles 150 μm Si detectors and 1" thick NaJ scintillators were used.

At the larger angles, where only protons are detected, the thickness of the ΔE detectors was 500 μm. The design of the telescopes is described in detail in ref.3. Data were taken for about 250 h of beam time including extensive background measurements with empty target. The raw data are presently being analyzed.

(1) Proceedings Few Body XI, Sendai (1986), to be published in Nucl.Phys.A
(2) H.O.Klages et al., Nucl.Instr.Meth. 219 (1984) 269
(3) P.Doll et al., Nucl.Instr.Meth. A250 (1986) 526

* Ohio Univ. Athens, Ohio, USA

1.3.3 CHARGE EXCHANGE REACTION (n,p) on ^{12}C at 50 MeV

P.Doll, T.D.Ford, R.Garrett*, H.O.Klages, H.Krupp**

As reported in the 1985 annual report (1) a large solid angle detector system consisting of multiwire-proportional chambers and plastic ΔE and E scintillation detectors has been set up (2) to investigate neutron induced reactions on nuclei leading to charged particles in the excit channel. The wire chambers allow reconstruction of trajectories for the charged particles from the reaction target, since one chamber was operated directly behind the target in the neutron beam. Scattering angles between 0° and 35° were measured simultaneously.

The pilot experiment was to study the feasibility of neutron induced reactions with the polarized white neutron beam from POLKA (3). These type of studies are important to investigate so far widely unknown neutron induced reaction cross sections especially the (n,p) reaction leading to spin and isospin (Gamov-Teller) excitations in the residual nucleus. The inverse reaction (p,n), intensively studied at higher energies (4), suffers from various possible isospin transitions while energies below 100 MeV involve strong spin excitations which we hope to attack with a polarized beam.

We analyzed the data in 2 degree wide angle bins for protons identified by the plastic ΔE-E detectors. Since the measurements were carried out with a 0.5 mm polyethylene target, good statistics was achieved for neutron-proton scattering which was used to normalize the $^{12}C(n,p)^{12}B$ cross section. By calculating the trajectory of the protons back onto the beam axis, for forward angles the contributions from the aluminium window of the scattering chamber and the air outside the chamber could be discriminated.

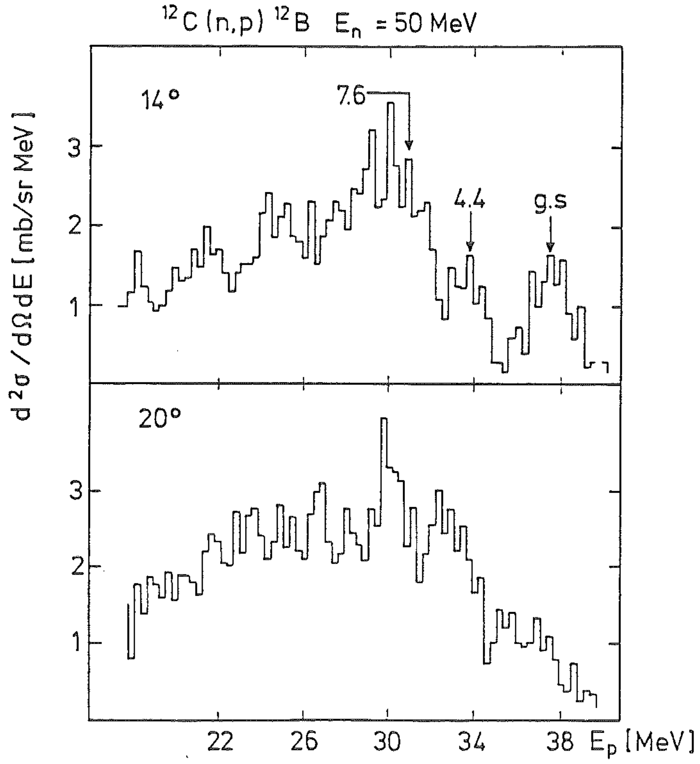

Fig.1: Proton energy spectra for E_n = 50 ± 2 MeV, evaluated in two angular bins.

Fig.1 shows proton energy spectra from the $^{12}C(n,p)^{12}B$ reaction for an incident energy of 50 MeV at 14° ± 1° and 20° ± 1° in the laboratory system. The spectra exhibit the ground-state transition, the 4.4 MeV and the 7.6 MeV Gamov Teller resonance in ^{12}B. Evaluation of energy spectra for lower incident neutron energies still suffers from energy loss straggling of the protons in the air gap between the target and the E detector.

(1) P.Doll et al., KfK report 3969 (1985) p.155
(2) P.Doll et al., to be published
(3) H.O.Klages et al., NIM 219 (1984) 269
(4) T.N.Taddeucci et al., Phys.Rev. 25 (1981) 1094

* University of Auckland, New Zealand

** Now at Siemens AG, München

1.3.4 PRELIMINARY NEUTRON CAPTURE STUDIES

P.Doll, G.Fink, R.W.Finlay**, M.Haupenthal, H.O.Klages,
B.Kasten*, F.Smend*, J.Wicke*

Many capture studies have been carried out with high flux proton beams (1) so far but only few results are reported on neutron capture expecially with energies of several tens of MeV. It is generally believed that fast neutron capture presents the advantage that effective charge effects (2) in exciting higher multipols of high isospin are much reduced and the strong interaction dominates. Many open questions even in light nuclear systems are waiting for the complementary neutron capture studies. In collaboration with a group from Göttingen University we started to use the polarized "white" neutron beam from POLKA (3) to study the capture rates on ^{12}C. A large NaI crystal was shielded passively and actively as described in 6.1.8 and set at 90° in the laboratory system. Even at this scattering angle elastically and inelastically scattered neutrons are about 2000 times more intense than the capture γ rays at these high neutron energies. Therefore, n-γ discrimination techniques had to be employed (see 6.1.8).

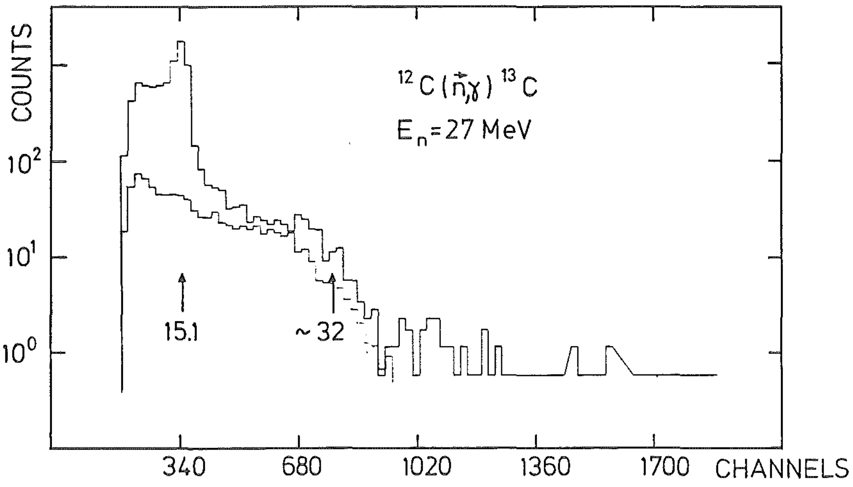

Fig.1: Pulse-height spectrum of the NaI crystal from the capture reaction $^{12}C(n,\gamma)^{13}C$ at a neutron energy of 27 MeV. The inserted curve represents the background distribution.

Fig.1 shows a pulse height spectrum of the NaI detector for gammas separated in the pulse shape parameter. The incident neutron energy bin was choosen to be 27 MeV ± 1 MeV. The energy threshold for the NaI was set to about 9 MeV. We see a strong deexcitation of the 15.11 MeV state in ^{12}C populated by inelastic neutron scattering. In ^{13}C γ-transitions with maximum ground-state transition energies of about 32 MeV are expected and an edge is indicated at about this pulse height. Structures for lower transition energies are not pronounced. The background taken without carbon sample is inserted in the figure with a preliminary normalization.

It is not yet fully understood what the few very high pulse heights are due to. Similar pulse height spectra were obtained simultaneously between 17 and 50 MeV incident neutron energy. The statistical uncertaintis are too large to divide the data further into both spin orientations for the incident neutron beam. However, this first test experiment has proven the feasibility of fast neutron capture experiments at the continuous energy neutron beams of POLKA.

(1) H.Ejiri et al., AIP Conf.Proc. 125 (1984) 582
(2) G.Longo and F.Saporetti, Nuovo Cimento B61 (1969) 167
and K.A.Snover et al., Phys.Rev.Lett. 23 (1974) 317
(3) H.O.Klages et al., NIM 219 (1984) 269

* Universität Göttingen, W.-Germany
** Ohio State University, Athens, USA

1.4 NUCLEAR REACTIONS BY CHARGED PARTICLES

1.4.1 RESONANT AND NON-RESONANT COULOMB BREAK-UP OF ^{6}Li

D.K. Srivastava$^+$ and H. Rebel, (1)

The resonant and non-resonant cross sections for the break-up of ^{6}Li in the Coulomb field of a heavy nucleus are studied theoretically on the basis of a DWBA approach and analysed with a view to possible experimental measurements of the electromagnetic transition-matrix elements between the ground state of the projectile and the α + d continuum states at small relative energies. The calculations uses explicitly some of the simplifications that appear in the particular case of the quadrupole transitions which dominate the case considered here. The things the cross sections are sensitive to are also discussed.

(1) KfK-Report 3985; Journ. Phys. G: Nucl. Phys. 12 (1986) 717

+ On leave from VEC Centre, Calcutta, India

1.4.2 COULOMB DISSOCIATION AS A SOURCE OF INFORMATION ON RADIATIVE CAPTURE PROCESSES OF ASTROPHYSICAL INTEREST

G. Baur$^+$, C.A. Bertulani$^+$, and H. Rebel

The cross sections for radiative capture of α-particles, deuterons and protons by light nuclei at very low relative energies are of particular importance for the understanding of the nucleosynthesis of chemical elements and for determinating the relative elemental abundances in stellar burning processes at various astrophysical sites. As example we quote the reactions $\alpha+d\rightarrow{}^6\text{Li}+\gamma$, $\alpha+{}^3\text{He}\rightarrow{}^7\text{Be}+\gamma$, or $\alpha+{}^{12}\text{C}\rightarrow{}^{16}\text{O}+\gamma$. As an alternative to the direct experimental study of these processes we consider (1,2) the inverse process, the photodisintegration, by means of the virtual photons provided by a nuclear Coulomb field. The radiative capture processes $b+c\rightarrow a+\gamma$ is related to the inverse process, the photodisintegration $\gamma+a\ b+c$ by the detailed balance theorem. Except for the extreme case very close to the threshold the phase space favours the photodisintegration cross section as compared to the radiative capture. The disintegration by means of the virtual photons in a Coulomb collision

$$Z + a \rightarrow Z + b + c \qquad (1)$$

makes use of the high virtual photon number and also of possible kinematical advantages. The fragments b and c have high energies in the lab system and can be conveniently detected. From the kinematics the relative energy E_{bc} can be accurately deduced (see Ref. 2). Care will have to be taken for "post-acceleration" effects, possibly more serious for fragments with different charge to mass ratios.

The double differential cross section for the excitation of the projectile into the continuum with excitation energy E_γ and angle Θ of the c.m. of the broken up pair is given by

$$\frac{d^2\sigma}{d\Omega dE_\gamma} = \frac{1}{E_\gamma} \sum_\lambda \frac{dn_{E\lambda}}{d\Omega} \sigma^{photo}_{E\lambda} \tag{2}$$

where $\sigma^{photo}_{E\lambda}$ denotes the photodisintegration cross section of multipolarity $E\lambda$ (magnetic excitations are neglected). The virtual photon numbers for the multipolarity $E\lambda$ are denoted by $dn_{E\lambda}/d\Omega$ and are calculated from the kinematics of the process. We are especially interested in the case where the scattering angle is small, $\Theta \ll 1$, i.e. $\varepsilon = \frac{1}{\sin\Theta/2} \gg 1$. In this case we have

$$\frac{dn_{E1}}{d\Omega} = \frac{Z^2}{4\pi^2} \alpha \varepsilon^2 (\frac{c}{v})^2 x^2 \{K_o^2(x) + K_1^2(x)\}^2 = \frac{Z^2}{4\pi^2} \alpha \varepsilon^2 (\frac{c}{v})^2 \phi_1(x) \tag{3}$$

where $x = \frac{\omega b}{v}$ is the adiabaticity parameter. The impact parameter is given by b, v is the velocity of the projectile and $E_\gamma = \hbar\omega$. Corrections due to Coulomb repulsion depend on $\xi = \frac{\omega a}{v}$, where a is half the distance of closest approach in a head on collision; they are small and easily evaluated. For the important E2 case we obtain

$$\frac{dn_{E2}}{d\Omega} = \frac{Z^2\alpha}{\pi^2} \frac{1}{\xi^2} (\frac{c}{v})^4 \cdot \phi_2(x) \tag{4}$$

where

$$\phi_2(x) = x^2\{K_1^2 + x^2 (K_1^2 + x_o^2) + xK_oK_1\} \tag{5}$$

The functions ϕ_1 and ϕ_2 are given in Fig. 1.

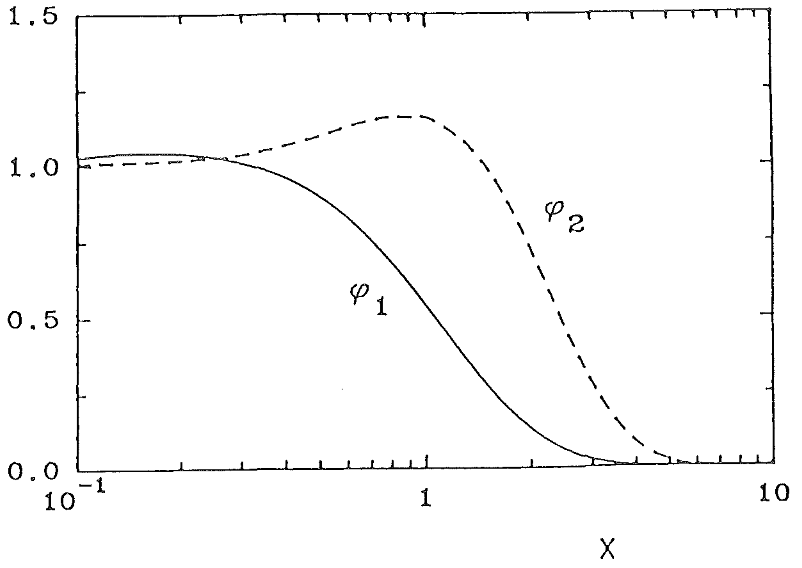

Fig. 1 The shape of the virtual photon spectrum as a function of the adiabaticity parameter x for the multipolarities E1 and E2

It can be seen that the E2 virtual photon numbers are in many interesting cases much larger than the corresponding E1 ones. From various experimental conditions with different relative E1 and E2 virtual photon numbers the quantity $\sigma^{\mathrm{photo}}_{E\lambda}$ can be individually determined. In coincidence studies of reaction (1) interference effects between different multipoles will show up in general, which can in principle help to disentangle the various multipole contributions. A selective population of magnetic substates of the system b+c is expected, it can be directly calculated from the theory of Coulomb excitation.

From the virtual photon numbers (3), (4) and (5) and the estimated cross sections $\sigma^{\mathrm{photo}}_{E\lambda}$ (from the astrophysical S-factor measured at higher relative energies) it is concluded that dedicated experiments asre feasible in the astrophysically relevant region. It is especially noticeable that even at modest energies ($\sim$ 60 MeV/A) the severe adiabaticity condition in the $^{16}O \rightarrow \alpha + {}^{12}C$ dissociation ($Q = -7.162$ MeV) and $^{20}Ne \rightarrow \alpha + {}^{16}O$ ($Q = -4.73$ MeV) can be overcome.

(1) H. Rebel: Proc. Workshop on Nuclear Reaction Cross Sections of Astrophysical Interest, unpublished report, Kernforschungszentrum Karlsruhe, February 1985.

(2) G. Baur, C.A. Bertulani, and H. Rebel: Preprint KfK, December 1985, Nucl. Phys. A, in press.

+ Inst. für Kernphysik, KFA Jülich, D-5170 Jülich.

1.4.3 INCLUSIVE ENERGY SPECTRA OF BREAK-UP FRAGMENTS AND BREAK-UP CROSS SECTIONS AT VERY FORWARD EMISSION ANGLES IN ^{6}Li INDUCED NUCLEAR REACTIONS

H. Jelitto, J. Buschmann, H.J. Gils, N. Heide, J. Kiener, H. Rebel, S. Zagromski

The inclusive charged particle spectra from collisions of 156 MeV ^{6}Li ions with ^{12}C and ^{208}Pb have been previously measured by B. Neumann et al. (1) at emission angles $\Theta_{\mathrm{Lab}} \geq 10°$, and an exponential increase of the yield from projectile break-up processes has been observed with decreasing emission angles. We have extended these measurements to very forward angles up to 0° by use of the magnetic spectrometer "Little John" in order to determine the zero-degree-limit of the inclusive break-up cross section. Fig. 1 displays some α-particle spectra in the energy region around the beam-velocity. The gaps in the centers of the bumps originate from suppressing the elastic ^{6}Li scattering by a properly positioned graphite block in front of the focal plane. Due to the relatively high intensity of the elastically scattered ^{6}Li particles the usual ΔE-E electronic discrimination between ^{6}Li, α and d is not sufficient and leads to difficulties for higher currents of the primary beam.

As Fig. 2 indicates a change in the slope of the integrated yields of the break up bumps when the elastic scattering changes from nuclear to Coulomb scat-

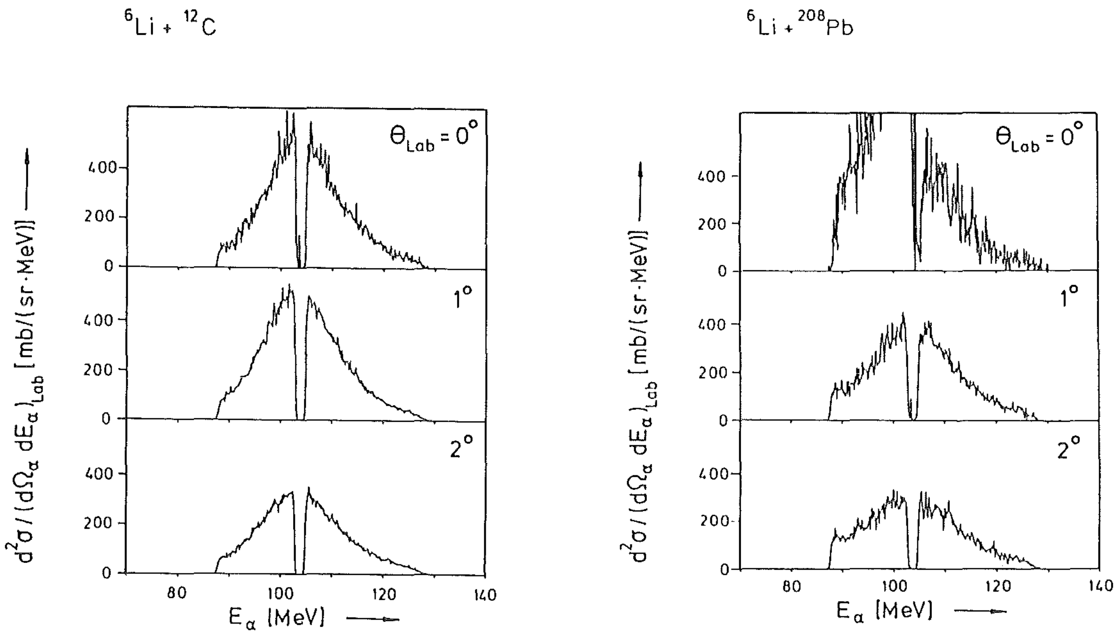

Fig. 1 Inclusive alpha-particle spectra from the reaction 156 MeV ^{6}Li + ^{12}C and ^{6}Li + ^{208}Pb at very forward emission angles. The strong increase on the low energy side of the break-up bump (^{6}Li+^{208}Pb,0°) originates from slit scattering.

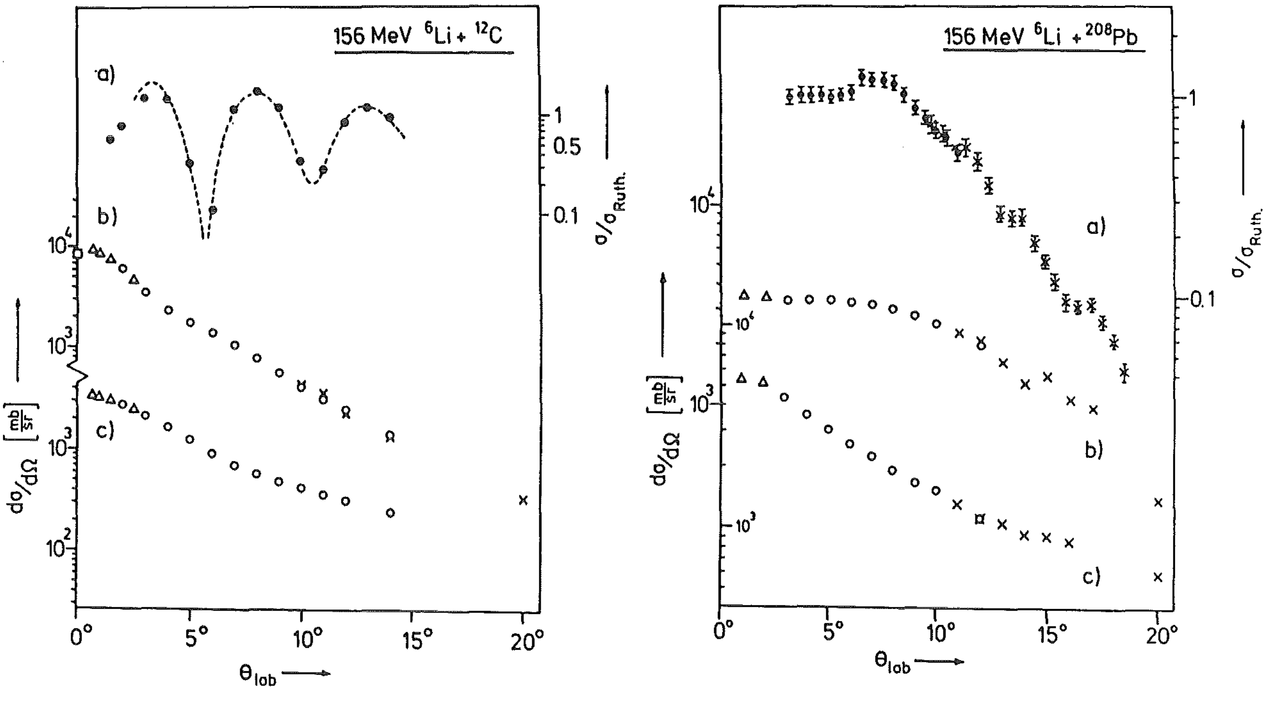

Fig. 2 Differential cross section for elastic scattering of 156 MeV ^{6}Li from ^{12}C and ^{208}Pb and energy integrated yields of α particles (b) and deuterons (c) from projectile break-up (the symbols 0, Δ and represent different experimental runs, x data taken from Neumann et al. (1).

tering (where $\sigma_{el}/\sigma_{Ruth} \approx 1$). The angular distribution can be parametrized for $\Theta = 0°$ to $10°$ by

$$d\sigma/d\Omega \; = \; C\, e^{-\xi\,\Theta}$$

with $C_\alpha = 3.7$ b and $\zeta_\alpha = 1.55\ \mathrm{rad}^{-1}$ for ^{208}Pb, and $C_\alpha = 9.5$ b and $\xi_\alpha = 17.8\ \mathrm{rad}^{-1}$ ($C_d = 3.8$ b $\xi_d = 12.8\ \mathrm{rad}^{-1}$) for ^{12}C. It turns out that the angular distribution for the α-particle data with ^{208}Pb at $\Theta_{Lab} > 12°$ is less steep than found for $\Theta_{Lab} > 12°$ by Neumann et al. (1).

(1) B. Neumann, H. Rebel, H.J. Gils, R. PLaneta, J. Buschmann, H. Klewe-Nebenius, S. Zagromski, R. Shyan and H. Machner, Nucl. Phys. A382 (1982) 296; B. Neumann, H. Rebel, J. Buschmann, H.J. Gils, H. Klewe-Nebenius, S. Zagromski, Z. Phys. A296 (1980) 113

1.4.4 EXPERIMENTAL FEATURES OF PARTICLE-PARTICLE COINCIDENCE MEASUREMENTS AT VERY FORWARD EMISSION ANGLES USING THE MAGNETIC SPECTROGRAPH "LITTLE JOHN"

H. Jelitto, J. Kiener, S. Zagromski, H.J. Gils, H. Rebel

The direct (nonresonant) break up of light ion projectiles in the Coulomb field of a target nucleus has so far not been experimentally identified in a unique way (may be with the exception of ^{7}Li (1)), in contrast to several interesting aspects of this type of nuclear reactions. The experimental observation requires

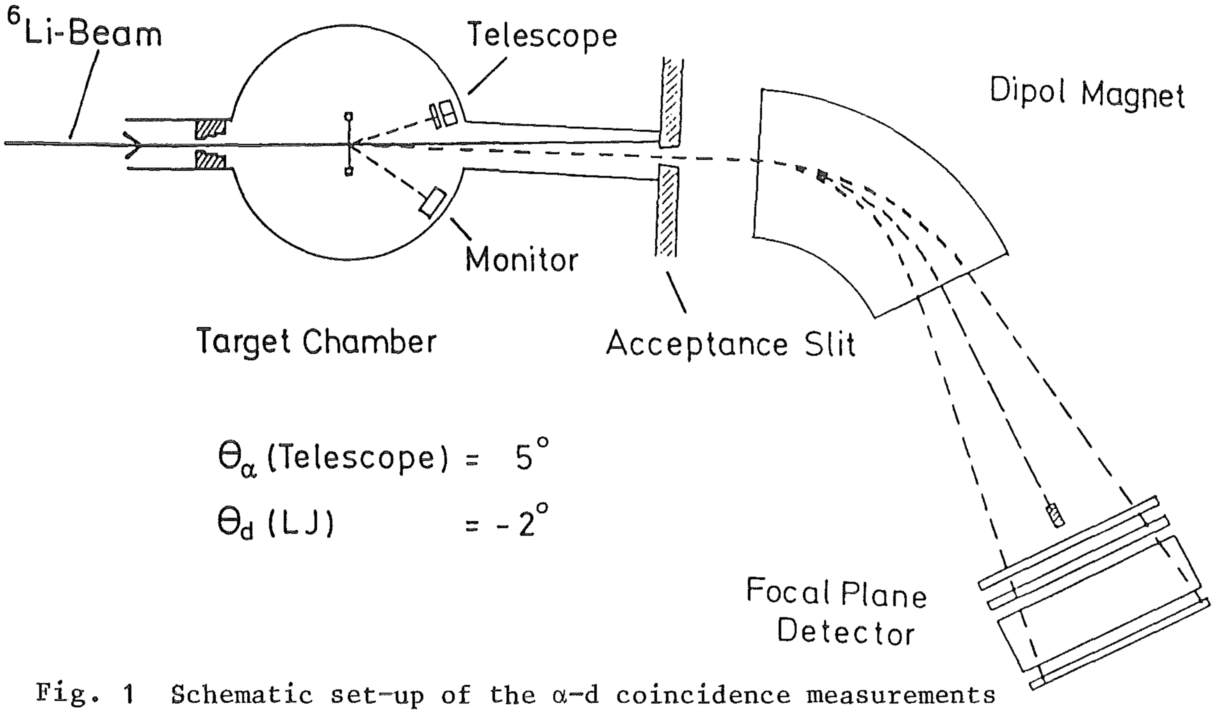

Fig. 1 Schematic set-up of the α-d coincidence measurements

the coincident detection of the break-up fragments emitted with small relative energies (in a narrow angular geometry) to very forward angles i.e. with large impact parameters. In order to explore the experimental implications of investigations of the Coulomb break-up, we have started some experiments with 156 MeV ^{6}Li projectiles and looked for the elastic break-up ^{6}Li + ^{208}Pb$\to\alpha$+d+^{208}Pb$_{gs}$. The experimental set up using the magnetic spectrograph "Little John" is shown in Fig. 1. The spectrograph was positioned at Θ_{Lab} = -2° detecting the break-up deuteron (with energies around the beam velocity energy). A semiconductor telescope consisting of a 2 mm surface barrier detector and a 5 mm thick lithium drifted Si detector measured the energy spectra of the α-particles at Θ_{Lab}= 5°. The detector positions fix the emission angle of the centre of mass of the (α+d) system

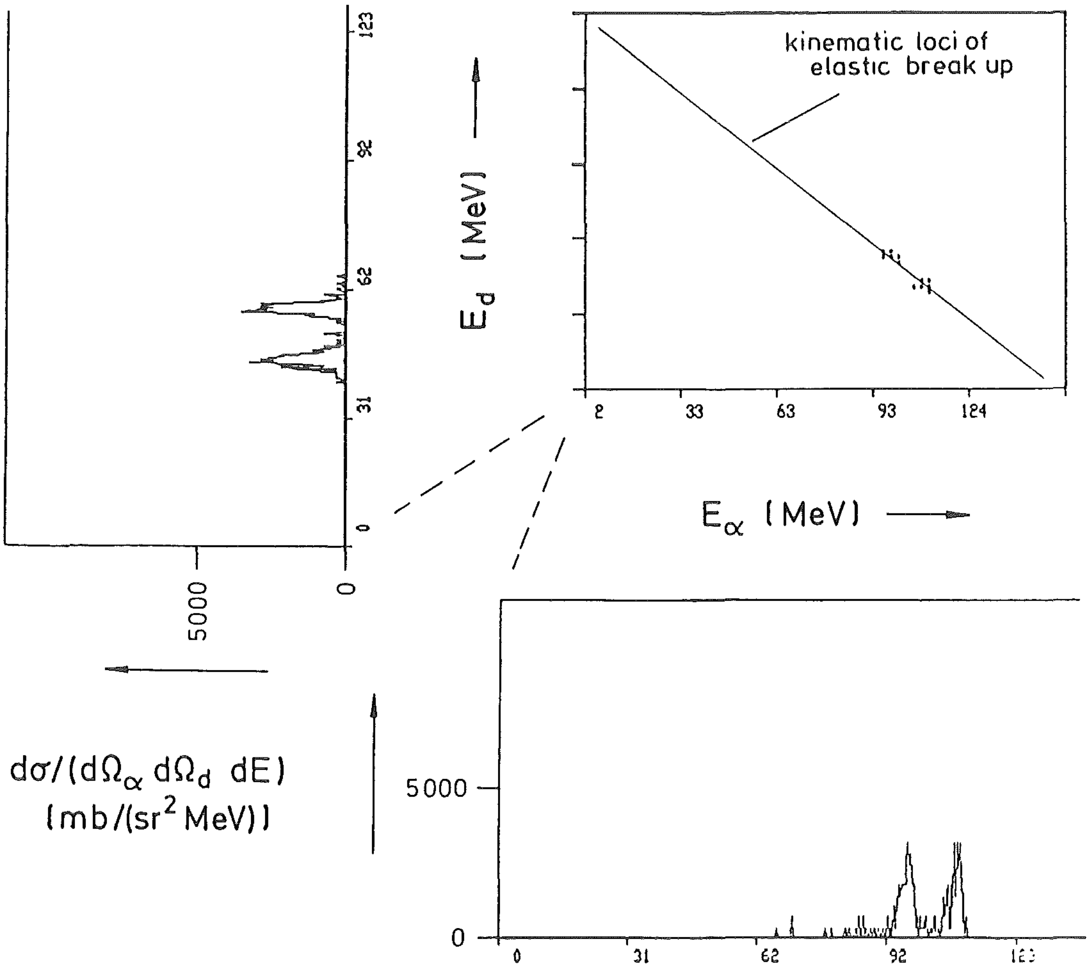

Fig. 2 Coincidence energy spectra of the reaction ^{208}Pb(^{6}Li,αd) with Θ_α = 5° and Θ_α = -2°.

to ca. 2.6° which is considerably smaller than the grazing angle (6°) thus guaranteeing pure Coulomb effects. The comparatively high elastic scattering intensity causes severe problems. In order to reduce the effects (random coincidences, insufficient particle separation) elastically scattered ^{6}Li particles were stopped on a properly placed graphite block in front of the focal plane detector. The high counting rate (from elastic scattering) in the semiconductor telescope, however, limits the beam current to $I_{Li} \approx 100$ pA. With the described set up ca. 200 α-d coincidence events were registered in 70 hours. The result is displayed in Fig. 2. The two peaks correspond to the sequential (resonant) break-up via the first excited state of ^{6}Li ($E_{\alpha d} = 0.71$ MeV). The lines are broadened by an insufficient energy resolution of the semiconductor telescope and due to the chosen width of the acceptance slits (angular resolution). The effects can be reproduced by Monte Carlo simulation. The experimental experiences are the basis for detailed consideretions and proposals for an improved detection system.

The value of the resonance cross section ($\Theta = 5°$, $\Theta_\alpha = -2°$) is $d^2\sigma/d\Omega_\alpha d\Omega_d = 5.5 \pm 1.5$ b/sr², the upper limit for the nonresonant part centered around $E_{\alpha d} = 0.5$ MeV is $d^2\sigma/dE_\alpha d\Omega_\alpha d\Omega_d \approx 6$ mb / sr²·MeV.

(1) A. Shotter, V. Rapp, T. Davinson, D. Branford, N.E. Sanderson and M.A. Nagarajan, Phys. Rev. Lett. 53 (1984) 1539

1.4.5 ON THE POSSIBILITY TO DETECT TWO COINCIDENT PARTICLES IN NARROW-ANGLE GEOMETRY WITH THE MAGNETIC SPECTROGRAPH "LITTLE JOHN"

H.J. Gils, J. Kiener, S. Zagromski, H. Rebel

The break-up of ^{6}Li → α + d in the Coulomb field of a heavy target nucleus may be interpreted as time reversed reaction of the α + d fusion reaction, which is of particular astrophysical interest. This interpretation requires the simultaneous detection of the two fragments under a relative angle around 1° and a mean reaction angle (with respect to the ^{6}Li-beam) of less than 5°. For fragments near beam velocity this reaction geometry corresponds to a relative energy of the fragments down to ∿ 10 keV.

Geometrical limitations due to the detector housings and high counting rates due to the dominating ^{6}Li elastic scattering excludes the use of semiconductor or scintillation-detector telescopes for such measurments. Therefore, it is considered, to detect both break-up fragments in coincidence using the magnetic spectrograph "Little John". The general advantage of the use of the spectrograph is demonstrated in Fig. 1. The elastically scattered ^{6}Li-particles (in case of a reaction angle of $\Theta_R = 0°$ also the beam particles) are focussed on a Faraday cup in front of the focal plane of the spectrograph. Due to the three-body kinematics and due to the momentum dispersion of the magnet system, the two fragments of the elastic ^{6}Li → α + d break-up reaction pass the focal plane of the spectrograph on either side of the Faraday cup. Therefore, a coincident detection of the fragments is possible when having a focal plane detector system consisting of two nearly identical parts as shown in Fig. 1. In this set-up the undesired events of elastically scattered ^{6}Li-particles are completely suppressed.

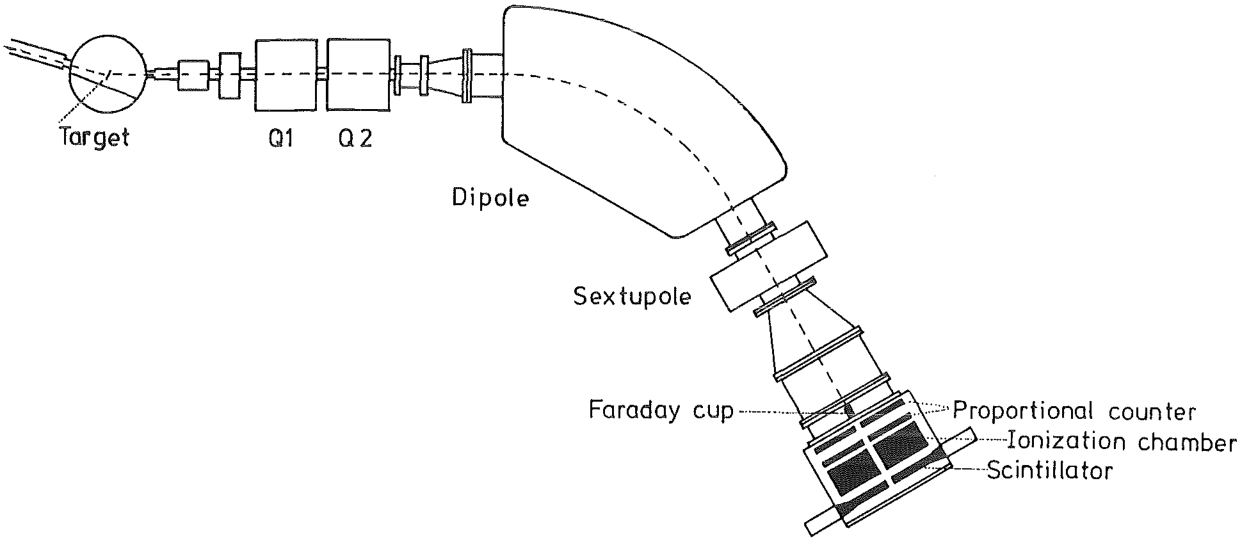

Fig. 1 Magnetic spectrograph "Little John" with focal plane detector

A detector system according to these requirements has been designed. Each focal plane detector consists of two position sensitive proportional counters followed by an ionization chamber and a plastic scientillator. The horizontal position of the particle, determining its energy, is calculated by the charge division method. The vertical information is given by the drift time of the electrons to the anode the scintillator pulse serving as start signal. Thus energy and trajectory angle at the focal plane of two particles are determined by four proportional counters. Particle identification is provided by the ionization chamber and the scintillator.

All housings of the new detector are the same as already used in the standard focal plane detector (2) with the modification that the scintillator and the anode wires in the drift chambers and the ionization chamber have to be divided and separated electrically. The position resolution should reach 0.5 mm FWHM for α-particles and deuterons. This allows an energy resolution of 80 keV - 40 keV for 104 MeV α-particles, respectively 40 keV - 20 keV for 52 MeV deuterons, depending on the momentum dispersion. Several calculations with different focussing conditions showed, that a satisfactory determination of the relative emission angle ($\Delta\phi \sim 2$ mrad) between the fragments can be achieved with this special focal plane detector, giving a resolution of the relative energy between the fragments of better than 10 keV.

For a redundant determination of the relative emission angle the set-up of a two-fold two-dimensional position-sensitive entrance detector is also planned.

(1) G. Baur, C.A. Bertulani, and H. Rebel, KfK 4032 (1986) Nucl. Phys. A in press
(2) S. Zagromski, unpublished report, KfK Karlsruhe, 1980.

1.4.6 MONTE CARLO SIMULATION OF DETECTOR GEOMETRY EFFECTS IN COINCIDENCE SPECTRA OF CLUSTER-FRAGMENTS FROM PROJECTILE BREAK-UP REACTIONS

N. Heide, H.J. Gils, H. Rebel, S. Zagromski, V. Corcalciuc$^+$

Coincidence spectra of cluster-fragments from direct projectile break-up reactions can provide information on the cluster structure of the incident projectile. The purpose of the present study is to estimate by Monte-Carlo calculations the influence of the detector geometry on the shape of the coincidence spectra for the direct break-up reaction ^{208}Pb(^{6}Li,αd)^{208}Pb at $E_{^6Li}$ = 156 MeV within the assumptions of the Serber-model (1).

According to this model the c.m. cross-section for the break-up reaction is proportional to the absolute square of the Fourier transform of the α-d relative motion wave-function. Two alternative descriptions have been used for the α-d relative motion wave function to estimate the sensitivity of the coincidence spectra to the details of the internal momentum distribution. The calculations started with a Yukawa-type function which is implicitly adopted by the post-form DWBA calculations of Baur (2).

An alternative and probably more realistic approach of the (α+d) bound state wave-function is obtained when generating it in a Woods-Saxon potential well. The WS momentum distribution has a singularity at $k \sim 0.75$ fm^{-1} in contrast to the Lorentzian shape corresponding to the Yukawa-type function. Fig. 1 shows the Monte-Carlo simulated coincidence spectra for α-particles for two pairs of scattering angles.

The singularity of the WS momentum distribution leads to two minima in the coincidence spectrum. Due to the particular three-body kinematics it is possible - by choosing appropriate scattering angles - to shift both of the minima in such a way that they overlap each other. The Yukawa-type spectra, of course, do not show these minima. The Monte-Carlo calculations take into account

- finite size of the detector solid angles,
- finite size of the beamspot on the target
- energy width of the incident ^{6}Li-beam
- energy resolution of the detectors.

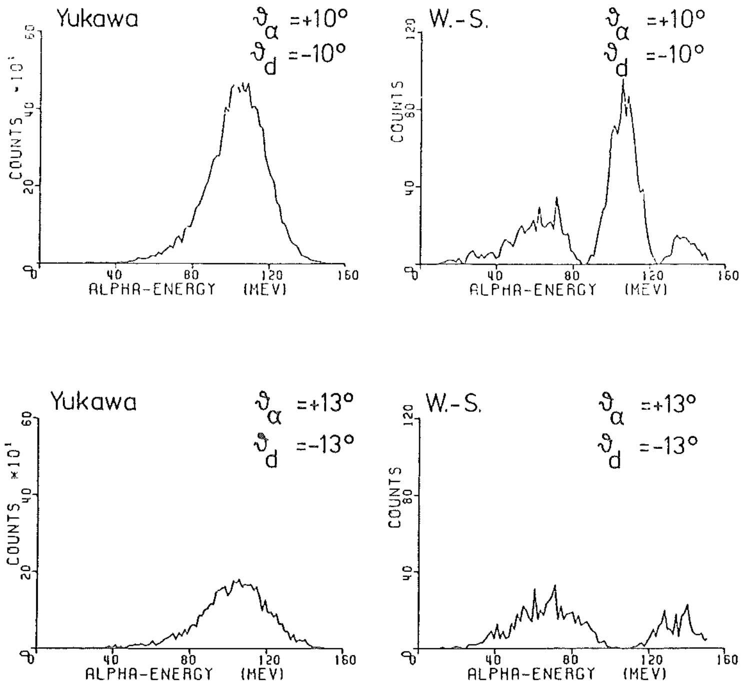

Fig. 1 Monte-Carlo simulated coincidence spectra for the direct reaction $^{208}Pb(^{6}Li,\alpha d)^{208}Pb$ at $E_{^{6}Li}$ = 156 MeV.

It turned out that the angular resolution of the detector is the most important quantity for observing the minima expected in the spectra. Due to the very low coincidence count-rate it is desirable to have the solid angles of the detectors as large as possible but without washing out the minima. The optimum conditions for the solid angles of the detectors can be selected by using the results of the MC calculations.

(1) R. Serber, Phys. Rev. 72 (1947) 1008
(2) G. Baur, F. Rösel, D. Trautmann, R. Shyam, Phys. Rep. 111 (1984) 333

+ Central Institute of Physics, Bucharest, Romania

1.4.7 A HALF-SHELL TREATMENT OF THE DIRECT BREAK-UP OF LIGHT IONS

D.K. Srivastava^{+}, H. Rebel, and R.K. Bhowmik^{++}

The recently proposed transition matrix for the direct elastic break-up process given by (1)

$$T = \int e^{-i\vec{k}_f \cdot \vec{R}} \langle \phi_k^{(-)}(\vec{r})\, | V_{bA}(\vec{r}_b) + V_{cA}(\vec{r}_c) |\, \phi_a(\vec{r}) \rangle\, \chi_a^{(+)}(\vec{k}_i,\vec{R})\; d\vec{R}$$

with

$$\vec{r}_b = \vec{R} + \frac{m_c}{m_a}\vec{r} \quad \text{and} \quad \vec{r}_c = \vec{R} - \frac{m_b}{m_a}\vec{r}$$

is shown to be easily amenable to an evaluation in terms of the half-shell cross-section for the scattering of the projectile from the target. Using

$$\chi_a^{(+)}\ (\vec{k}_i, \vec{R}+\vec{\Delta}) \underset{-}{\sim} \chi_a^{(+)}(\vec{k}_i, \vec{R})\ e^{i\vec{k}_i \cdot \Delta}$$

which is expected to be a good approximation at high incident energies and for forward-angle emission of the break-up fragments, the above T-matrix reduces to

$$T = T_a(\vec{Q}, \vec{k}_i) \cdot \Phi(\vec{Q}, \vec{k})$$

with

$$\vec{Q} = \vec{k}_f - \vec{k}_i \quad \text{and} \quad \vec{k} = \frac{m_b}{m_a}\vec{k}_i - \frac{m_c}{m_a}\vec{k}_b$$

In the above expression, T_a is the half-shell T-matrix for the scattering of the projectile ($k_f \neq k_i$)

$$T_a = \int e^{i\vec{k}_f \cdot \vec{R}}\ V_{aA}(\vec{R})\ \chi_a^{(+)}(\vec{k}_i, \vec{R})\ d\vec{R}$$

and

$$\Phi = \int \phi_k^{(-)*}(\vec{r}) \left[\frac{m_b}{m_a} \exp(i\frac{m_c}{m_a}\vec{Q}\cdot\vec{r}) + \frac{m_c}{m_a}\exp(-i\frac{m_b}{m_a}\vec{Q}\cdot\vec{r}) \right] \phi_a(\vec{r})\ d\vec{r}$$

It is interesting to note that in the case that the continuum state $\phi_k(\vec{r})$ may be represented by a plane wave $e^{-i\vec{k}r}$(i.e. $V_{bc} = 0$), the nuclear structure quantity Φ reduces just to the Fourier transform of the ground state wave function $\phi_a(\vec{r})$. The a heavy target the triple differential cross-section can be approximately written by

$$\frac{d^3\sigma}{dE_b d\Omega_b d\Omega_c} \cong \frac{m_b m_c (2\pi\mu)^3}{(2\pi\hbar)^{10}}\ \frac{k_b k_c}{k_a}\ |\Phi|^2\ \frac{d\sigma}{d\Omega}\Bigg|_{(a,A)}^{\text{half-sh.}}$$

The half-shell T-matrix is related to the half-shell cross section through

$$\frac{d\sigma}{d\Omega}\Bigg|_{(a,A)}^{\text{half-sh.}} = \left[\frac{\mu_a}{2\pi\hbar^2}\right]^{-2} \left|T_a(\vec{Q}, \vec{k}_i)\right|^2$$

Further approximating (2) the half-shell cross section to the corresponding on-shell cross section for the same momentum transfer, the expression for the theoretical cross section can be easily evaluated.

Exploratory applications to the break-up of 56 MeV deuterons yield reasonable agreement with experimental data (3) whereas the application to the (α+d)-break-up of ^{6}Li shows an appreciable dependence on the potential $V_{\alpha d}$ generating Φ_k. The results of the studies seem to require a state-dependent interaction $V_{\alpha d}$ (see ref. 4) generating a consistent set of $[\phi_a, \phi_k]$ for the calculation of Φ.

(1) D.K. Srivastava and H. Rebel, Phys. Rev. C33 (1986) 1221
(2) L.P. Kok and H. van Haeringen, Phys. Rev. Lett. 46 (1981) 1257
(3) N. Matsuoka, M. Kondo, K. Hatanaka, T. Saito, T. Itahashi, K. Hosomo, A. Shimizu, F. Ohtani and O. Cynski, Nucl. Phys. A 391 (1982) 357
(4) D.M. Boal and J.C. Shillcock, Phys. Rev. C33 (1986) 549

+ Variable Energy Cyclotron Centre, Calcutta, India
++ Tata Institute of Fundamental Research, VECC, Calcutta, India.

1.4.8 THE NONELASTIC PROJECTILE BREAK-UP CROSS SECTION FROM PARTICLE-GAMMA COINCIDENCE MEASUREMENTS FOR THE ^{6}Li + ^{40}Ca REACTION AST 156 MeV

R. Planeta$^+$, H. Klewe-Nebenius^{++}, J. Buschmann, H.J. Gils, H. Rebel and S. Zagromski; T. Kozik$^+$, L. Freindl$^+$, and K. Grotowski$^+$, (1)

The cross sections for nonelastic break up modes have been studied for the ^{6}Li + ^{40}Ca reaction at E_{Li} = 156 MeV. Gamma-ray spectra from target-like residual nuclei were measured in coincidence with beam velocity projectile fragments and a value for the nonelastic break-up cross section $\sigma^{b.u}_{non}$ = 582 ± 110 mb has been found. Together with results of inclusive charged particle measurements we infer for the total break-up cross section $\sigma^{b.u}_{tot}$ = 930 ± 115 mb comprising about 50 % of the total reaction cross section. The nonelastic contribution of the break-up reaction appears to be less than predicted by the DWBA break up theory. This result is directly evident from the differential cross sections by comparing inclusive and exclusive results.

(1) Nucl. Phys. A448 (1986) 110

+ Institute of Physics, Jagellonian University and Institute of Nuclear Physics, Cracow, Poland
++ Institut für Radiochemie, Kernforschungszentrum Karlsruhe GmbH, Karlsruhe

1.4.9 INTERMEDIATE MASS FRAGMENTS FROM THE REACTION ^{6}Li + ^{46}Ti, AT E/A = 26 MeV

T. Kozik, J. Buschmann, A.J. Cole$^+$, H.J. Gils, K. Grotowski, N. Heide, J. Kiener, H. Klewe-Nebenius^{++}, H. Rebel, and S. Zagromski

Energy spectra and angular distributions of fragments heavier than the projectile have been measured for the reaction ^{6}Li + ^{46}Ti at incident energy 156 MeV. Gas-Si ΔE-E telescopes were used for Z identification. Significant cross-sections have been measured for the pick-up of up to 20 nucleons. A deep inelastic collision explanation of such a phenomenon is rather unlikely at 26 MeV/A. It reminds rather of an intermediate mass fragment emission observed recently by Kwiatkowski et al.

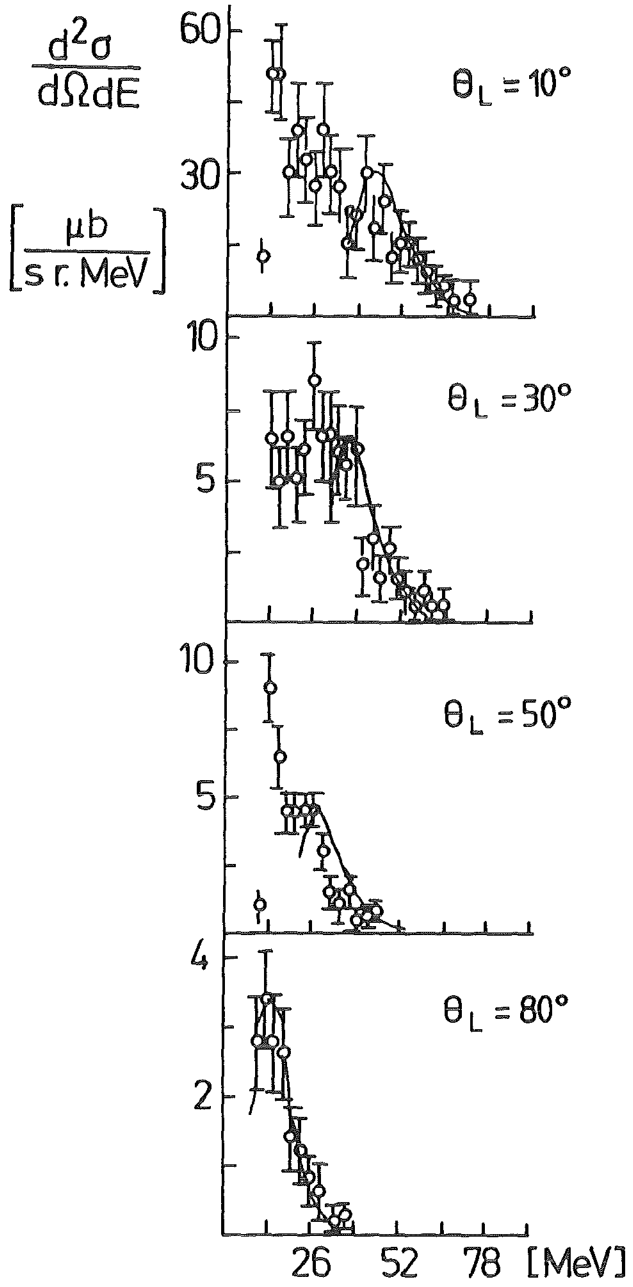

Fig. 1 Energy spectra of ^{16}O ejectiles for different LAB angles. Solid line corresponds to the binary decay of ^{52}Mn.

(1) K. Kwiatkowski, Phys. Lett. B 171 (1986) 41

+ I.S.N. Grenoble

++ Institut für Radiochemie

Kernforschungszentrum Karlsruhe

(1) in the ^3He+Ag reaction at 198.5 MeV. The back-angle data were in that case consistent with evaporation from the compound nucleus, while forward angles required an intermediate velocity source to explain energy spectra and angular distributions.

Element distributions observed in this work are similar to those measured by Kwiatkowski et al. (1) but our energy spectra and angular distributions suggest a somewhat different reaction mechanism. As an example Fig. 1 presents energy spectra of ^{16}O ejectiles at 10°, 30°, 50°, and 80° (LAB). The solid line represents the prediction of a simple model assuming a binary decay of the ^{52}Mn compound nucleus, and a Maxwellian CM energy distribution of ^{16}O emitted from the top of the Coulomb barrier with a $\frac{1}{\sin\Theta_{CM}}$ angular distribution. As one can see compound nucleus binary decay events are located at the higher energy part of all spectra in Fig. 1. At forward angles a second component is seen at lower energies.

In order to explain this second component we propose a multistep evaporation picture. In our case, the excitation energy, 159 MeV, of the compound nucleus $^{52}Mn^*$ is high enough to allow consecutive evaporations. Particles evaporated from $^{52}Mn^*$ gain a large part of their energy from acceleration in the Coulomb field. This Coulomb energy is considerably reduced in consecutive steps of the evaporation cascade. Further calculations are in progress.

1.4.10 INTERMEDIATE MASS FRAGMENTS FROM THE REACTIONS $^6Li + {}^{nat}Cu$, AND $^6Li + {}^{nat}Ag$, AT E/A = 26 MeV

K. Grotowski, J. Brzychczyk$^+$, A.J. Cole^{++}, H.J. Gils, N. Heide, H. Jelitto, J. Kiener, T. Kozik$^+$, Z. Majka$^+$, H. Rebel, Z. Sosin$^+$, and S. Zagromski

We have measured energy spectra and angular distributions of fragments heavier than projectile using the same ΔE-E identification method as mentioned in the previous contribution. A typical ΔE vs E map for products from the reaction $^6Li + {}^{nat}Ag$, $\Theta_L = 33°$ is shown in Fig. 1. An energy projection of the ΔE vs E map is presented in Fig. 2 for the same reaction but for a much larger angle Θ_L=120°. A well separated group of events is seen at both angles. Their energy approximates predictions of the binary fission systematics. The nuclear charges represented in this group extend up to the upper limit of the identification range, $Z \sim 18$. This binary fission group dominates at large angles but at small angles is outnumbered by a low energy group which is populated by events with $Z \leq 14$. The energy distribution of the latter group is very broad and for smaller Z probably overlaps with the former one. As in the case of ^{46}Ti target (see previous contribution) the low energy group originates probably from the multistep evaporation. A detailed analysis of data is in progress.

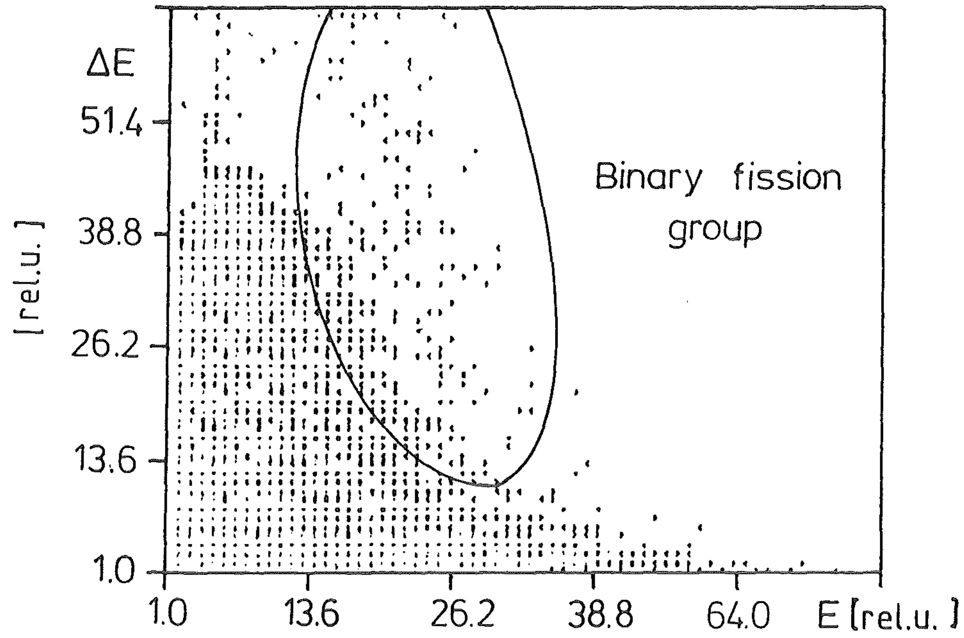

Fig. 1 The ΔE vs E map of events from $^6Li + {}^{nat}Ag$, at $\Theta_L = 33°$

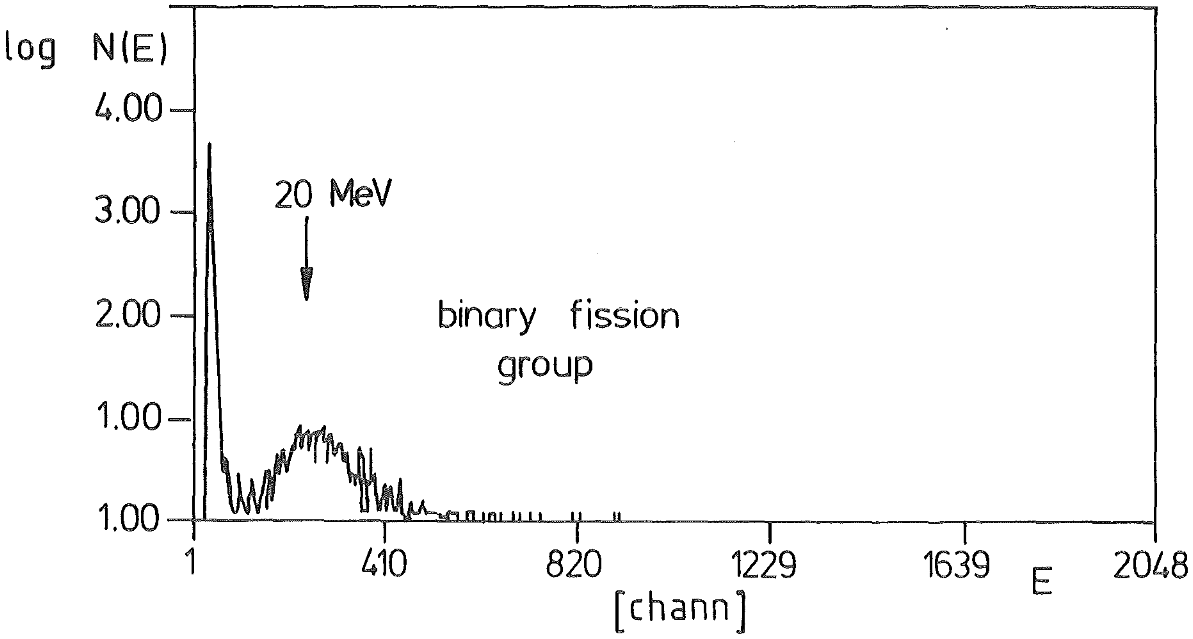

Fig. 2 Energy projection of the ΔE vs E map of events from ^{6}Li + ^{nat}Ag, at Θ_L = 120°

+ Institute of Physics, Jagellonian University, Institute of Nuclear Physics, Cracow, Poland

++ I.S.N. Grenoble

1.4.11 FISSION BARRIERS OF LIGHT NUCLEI

M. Blann+, K. Grotowski, and R. Płaneta++

In the present work we analyze fission-like yields from nearly symmetric decay of light composite systems $^{52}_{26}Fe^*$, $^{49}_{24}Cr^*$, $^{46}_{23}V^*$, and $^{44}_{22}Ti^*$ 1) in order to test several models of fission barriers of light nuclei at moderately high angular momenta.

For a long period of time the only set of fission barrier calculations for nuclei under rotation resulted from the rotating liquid drop model (RLDM) of Cohen, Plasil, and Swiatecki 2). Statistical model analyses of fission excitation functions for systems of mass 100 - 200 suggested that the RLDM barriers were somewhat higher than experimentally deduced results 3). A hint that such a conclusion should not be unexpected came from the early finite range barrier calculations of Krappe, Nix, and Sierk 4) performed for non-rotating systems. This model differed from the sharp surface liquid drop one in that an attractive force of finite range was permitted between nascent fragments at the fission saddle point. It was demonstrated that this effect could reproduce the angular momentum dependent barrier decrements from RLDM by modelling the static finite range effect to rotating systems. The explicit finite range rotating liquid drop model (RFRM) calculations were done by Mustafa, Baisden, and Chandra [5]. These models were shown to give good agreement with experimentally deduced barriers for systems formed in heavy ion bombardements with $A \lesssim 160$.

We wish to see if the conclusions stated above are valid in the much lower mass systems ($A \leq 52$) for which results were presented in refs. 1. In that mass range experimental determination of fission-like yields is much more difficult than for heavier nuclei for two principal reasons: the fission-like cross sections are much smaller, and the cahrge separation between target and projectile is much lower, rendering division between deep inelastic and fission-like products more difficult and ambiguous. In order to get reasonable fission yields one has to use here higher bombarding energies than those satisfactory for heavier, more fissile systems, what introduces additional complication in interpretation due to secondary evaporation from fission fragments, and due to incomplete fusion contributions to the reaction cross sections.

In our investigations we use the statistical codes ALERT I and ALERT II of the Hauser-Feshbach-type, with the Bohr-Wheeler model for estimating the angular momentum dependent fission excitation functions, in order to predict the fission cross sections expected from the experiments and based on RLDM and RFRM barriers. We also explore the sensitivity of calculated yields to transmission coefficients which depend on nuclear deformation. Calculations are in progress.

(1) K. Grotowski et al., Phys. Rev. C30, 1240 (1984);
R. Planeta et al., accepted for publication in Phys. Rev. C.
(2) S. Cohen et al., Ann. Phys. (N.Y.) 82, 557 (1974)
(3) M. Blann and T.A. Komoto, UCRL-87112 (1982)
(4) H.J. Krappe et al., Phys. Rev. C20, 992 (1979)
(5) M.G. Mustafa et al., Phys. Rev. C25, 2524 (1982)

+ Lawrence Livermore National Laboratory
++ Institute of Physics, Jagellonian University, Cracow, Poland

1.4.12 ELEMENT DISTRIBUTIONS AFTER BINARY FISSION OF ^{44}Ti

R. Płaneta[+], P. Belery[++], J. Brzychczyk[+], P. Cohilis[++], Y. El Masri[++], Gh. Grégoire[++], K. Grotowski, Z. Majka[+], S. Micek[+], M. Szczodrak[+], A. Wieloch[+], J. Albiński[+], (1)

Inclusive and coincidence measurements have been performed to study symmetric fragmentation of ^{44}Ti binary decay from the ^{32}S + ^{12}C reaction at 280 MeV incident energy. Element distributions after binary decay were measured. Angular distributions and fragment correlations are presented. Total CM kinetic energy for the symmetric products is extracted from our data and from Monte-Carlo model calculations including Q-value fluctuations. This result was compared to liquid drop model calculations and standard fission systematics. Comparison between the experimental value of TKE and the RLDM predictions locates the angular momentum window for symmetric splitting of ^{44}Ti between 33 and 38 h. It also showed that 50 % of the corresponding rotational energy contributes to the TKE values. The dominant reaction mechanism was found to be symmetric splitting followed by evaporation.

(1) Phys. Rev. C 34 (1986) 512

+ Institute of Physics, Jagellonian University, Institute of Nuclear Physics, Cracow, Poland

++ Institute of Nuclear Physics, Université Catholique de Louvain, B-1348 Louvain-la-Neuve, Belgium

1.4.13 α-PARTICLE SCATTERING FROM Ni ISOTOPES AT E_α = 172.5 MeV

J. Albinski[+], A. Budzanowski[+], H. Dabrowski[+], Z. Rogalska[+], and S. Wiktor[+]; H. Rebel and D.K. Srivastava; C. Alderliesten[++], J. Bojowald[++], W. Oelert[++], C. Mayer-Böricke and P. Turek[++], (1)

Differential cross sections have been measured for the elastic and inelastic scattering of 172.5 MeV alpha particles from ^{58,60,62,64}Ni nuclei. The analysis of the experimental data of elastic scattering in terms of optical potentials indicates an increasing neutron skin thickness in the isotopic sequence from ^{58}Ni to ^{64}Ni. Coupled channel analyses based on the anharmonic vibrational model approach determine the values of the dynamic deformation parameters for the most strongly excited states rather precisely and reveal enhanced hexadecapole ($0^+ \rightarrow 4^+_1$) transitions. Using an implicit folding-model procedure with a correction for the density-dependence of the effective α-nucleon interaction isoscalar transition rates are extracted and compared to electromagnetic results.

(1) Nucl. Physics A 445 (1985) 477

+ Institute of Nuclear Physics, 30-117 Krakow, Poland

++ Institut für Kernphysik, KFA Jülich, D-5170 Jülich

1.4.14 COMBINED ANALYSIS OF $\bar{p}$ - SCATTERING BY ^{16,18}O AND OF ^{16,18}O - $\bar{p}$ - ATOMS.

C. J. Batty[+], E. Friedman[++], and H.J. Gils

Recently, experimental data of high quality for the elastic scattering of antiprotons by ^{16,18}O and for strong interaction level shifts and widths of ^{16,18}O-antiprotonic atoms became available (1,2) from the LEAR facility. The analysis of both kinds of experiments involves a complex optical potential for the $\bar{p}$-nucleus interaction. This potential may either be obtained phenomenologically (3) or may be microscopically derived from the target nuclear density distribution and an effective $\bar{p}$-nucleon interaction e.g. within a folding model. Such analyses have been performed for the scattering problem determining the strength and range of a Gaussian $\bar{p}$-nucleon interaction (3,4).

In the case of the antiprotonic atoms, however, there are only two experimental numbers available, the strong interaction shift ε and width Γ, which makes a search on potential parameters - as in the scattering case - impossible. On the other hand, the atomic problem may determined the interaction potential at a *particular radius* quite well due to the localization of the $\bar{p}$-atomic orbitals the transition between which was observed. Therefore, a combined anlysis of both types of experiments may be useful as previoulsy applied (5) to the elastic scattering of alpha-particles and pionic atoms.

The first attempts of such a combined analysis showed that the two experiments are reasonably coupled so that the atomic problem acts as a constraint on the scattering experiment. In fact, a twofold ambiguity observed with the range of the real $\bar{p}$-nucleon effective interaction (Gaussian form) when analyzing the scattering only (^{18}O) is definitely excluded in the combined analysis. In Table 1 results of separate and combined analyses using a Gaussian folding model are compared indicating an improvement in the parameter errors from combined analyses.

The combined analysis of $\bar{p}$-scattering and $\bar{p}$-atomic X-ray measurements seems to be a promising tool for studying the $\bar{p}$-nucleus interaction. However, due to the small values of the strong interaction shifts and widths in $\bar{p}$-atoms of oxygen, the constraints are not sufficient to greatly affect analysis of $\bar{p}$-scattering and one must await results for heavier nuclei.

Table 1 Results for real and imaginary optical potentials from Gaussian folding model analyses of $\bar{p}$ - ^{16}O scattering and $\bar{p}$ - ^{16}O atoms from scattering only and combined analyses. Numbers in brackets are the errors of the last decimal digits.

	Real Volume (MeV fm³)	Real Range (fm)	Imaginary Volume (MeV fm³)	Imaginary Range (fm)	χ^2/F Scatt.	χ^2_ε	χ^2_Γ
Scatt.	281.(40.)	1.53(33)	902.(55.)	.964(36)	1.6	-	-
Comb.	299.(33.)	1.34(26)	872.(45.)	.981(29)	1.6	0.4	0.01

(1) D. Garetta et al. Phys. Lett. 135 B (1984) 266 ibid. 149 B (1984) 64, 151 B (1985) 473
(2) T. Köhler et al., CERN-preprint EP/86-02 (1986)
(3) C.J. Batty, E. Friedman and R. Lichtenstadt, Nucl. Phys. A 436 (1985) 621
(4) E. Friedman and J. Lichtenstadt, Nucl. Phys. A 455 (1986) 573
(5) H.J. Gils and E. Friedman, J. Phys. G 11 (1985) 85

+ Rutherford Appleton Laboratory, Chilton, Didcot, UK
++ Racah Institute of Physics, Hebrew University, Jerusalem, Israel

1.4.15 EXCITATION AND DECAY OF ISOSCALAR GIANT RESONANCES IN ^{90}Zr STUDIED IN ^{6}Li-SCATTERING AT EXTREME FORWARD ANGLES

H. Schlösser$^+$, W. Eyrich$^+$, A. Hofmann$^+$, A. Lehmann$^+$, B. Mühldorfer$^+$,
H. Wirt$^+$, H.J. Gils, H. Rebel, S. Zagromski

Decay experiments and small angle scattering are powerful tools for studying giant resonances. Combining both methods, we investigated the excitation and the neutron decay of the isoscalar E2 and E0 giant resonances (GR) in ^{90}Zr with the 156 MeV ^{6}Li beam of the Karlsruhe Isochronous Cyclotron. The main advantage of using ^{6}Li particles is the relatively low background in the (^{6}Li, ^{6}Li')-reaction, due to the low binding energy of the ^{6}Li-projectiles.

The scattered ^{6}Li particles were detected by the magnetic spectrograph "Little John" in an angular region between 1.5° and 4.5°. The single spectrum taken at 2°, shown in Fig. 1, demonstrates the favourable resonance to background ratio. In contradiction to α-spectra, taken under similar conditions, the continuum of the ^{6}Li-spectrum decreases towards higher excitation energies. The excited resonances marked with their multipolarities can be clearly identified. The extracted parameters of the different resonances are in good agreement with our results from (α,α') scattering (1).

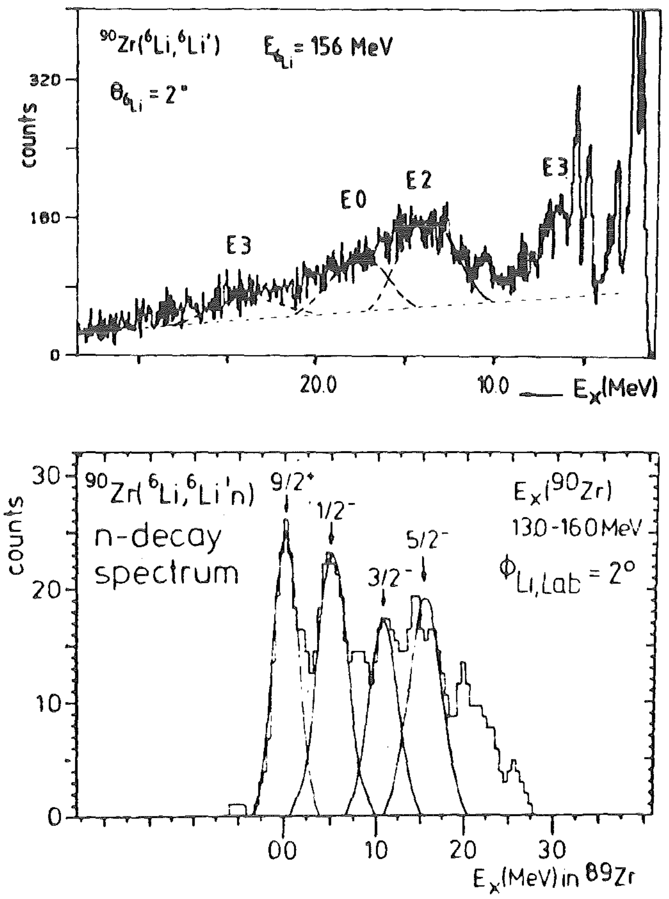

Fig. 1 Spectra of ^{90}Zr(^{6}Li,^{6}Li') u.p. and ^{90}Zr(^{6}Li,^{6}Li'n) l.p. taken at a scattering angle of 2°.

To investigate the decay of the E2 and E0 giant resonance regions we used an equipment consisting of four large scintillation detectors. The spectroscopy of the neutrons was performed using time of flight technique, similar as described in Ref. 1. The scattered ^{6}Li particles were detected at 2° by the magnetic spectrograph and, in addition, around 13° by surface barrier detectors. For the decay of the E2 GR region, we found a dominant statistical decay, and additionally the excitation of considerable strength with multipolarities $L \geq 4$, which can be deduced from the strong population of the $9/2^{+}$ "high spin" ground state in ^{89}Zr (cf. Fig. 1, lower part). This confirms the results of our ($\alpha,\alpha'n$) measurements (1) at larger scattering angles. For the E0 GR region we identified in addition of a dominant statistical decay, a direct component of 14 ± 3 % and a preequilibrium decay in the order of 5 %.

(1) K. Fuchs et al., Phys. Rev. C32 (1985) 418.

+ Physikalisches Institut der Universität Erlangen-Nürnberg

1.4.16 MONOPOLE STRENGTH IN ^{12}C EXTRACTED FROM ^{6}Li SMALL ANGLE SCATTERING

W. Eyrich^{+}, A. Hofmann^{+}, A. Lehmann^{+}, B. Mühldorfer^{+}, H. Schlösser^{+},
H. Wirth^{+}, H.J. Gils, H. Rebel and S. Zagromski

In light nuclei there is only few information concerning the giant monopole resonance (GMR). Especially in ^{12}C the situation with regard to the E0-strength distribution is still unclear. Besides the well known 0^{+} state at E_x = 7.65 MeV exhausting about 10 % of the energy weighted sumrule (EWSR), there is only confusing information about additional E0 strength. In a ^{3}He scattering experiment (1) monopole strength of about 2.1 % EWSR around 9.15 MeV excitation energy was reported, which could not be confirmed in a previous experiment of our group (2).

To clarify the situation, we studied ^{6}Li-scattering at extreme forward angles where the monopole assignment should be unambiguous. The experiment was carried out at the 156 MeV beam of the Karlsruhe Isochronous Cyclotron using the magnetic spectrograph "Little John".

In the upper part of Fig.1 an excitation spectrum taken at 2.5° is shown. At this angle, the monopole strength is only weakly excited, as can be seen from the 7.65 MeV state. At 1.5° (middle part), the relative intensities have already changed, and at 0° (lower part), the E0 strength has its maximum. In addition to the 0^{+} state at 7.65 MeV, a broad bump around 10.2 MeV arises in the 1.5° and 0° spectra. The angular distribution shown in Fig. 2 allows a distinct monopole assignment. A DWBA-calculation yields a strength of 5 % ± 1 % EWSR. In addition, we found monopole strength with 5 % ± 2 % EWSR in the region between 19.1 MeV and 21.4 MeV (compare Fig. 2). For this energy region, E0 strength was also reported in Ref. 1.

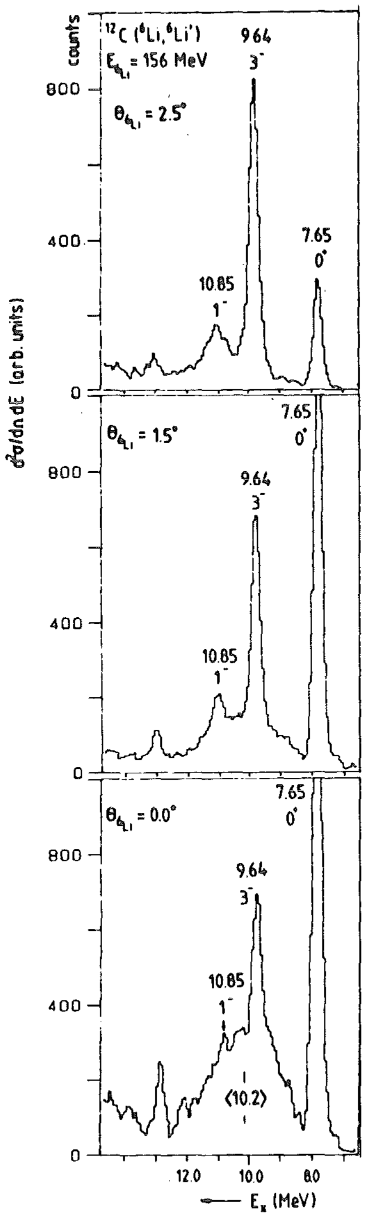

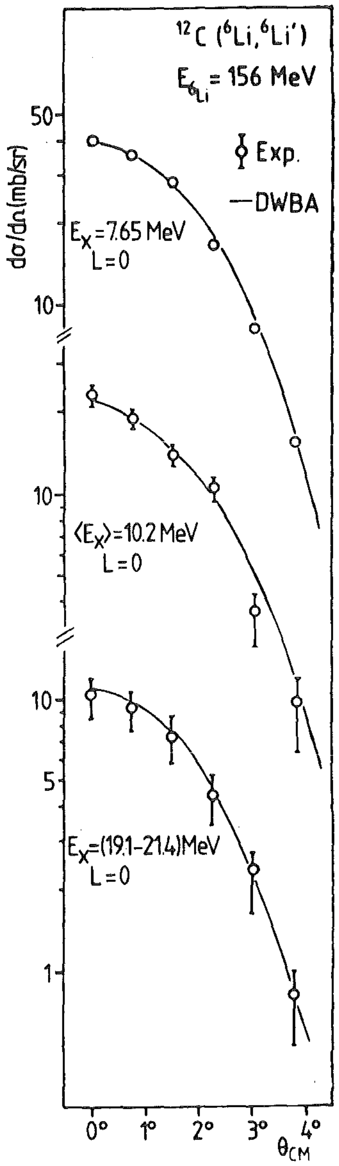

Fig. 1 (^{6}Li, ^{6}Li')-spectra from ^{12}C taken at 0°, 1.5° and 2.5°.

Fig. 2 Angular distributions of the extracted monopole strength in ^{12}C.

(1) D. Lebrun et al., Phys. Lett. B97 (1980) 358
(2) W. Eyrich et al., Phys. Rev. C24 (1981) 2720.
+ Physikalisches Institut der Universität Erlangen-Nürnberg

1.5 NUCLEAR FISSION

1.5.1 COLD FRAGMENTATION IN THERMAL-NEUTRON-INDUCED FISSION OF ^{233}U AND ^{235}U

H.-G. Clerc[+], W. Lang[+], M. Mutterer[+], C. Schmitt[+], J.P. Theobald[+], U. Quade[++], K. Rudolph[++], P. Armbruster[+++], F. Gönnenwein[++++], H. Schrader[++++], D. Engelhardt (1)

The experiments were performed at the ILL in Grenoble by measuring with the mass spectrometer Lohengrin fission fragment yields as a function of the kinetic energy of the fragments up to 115 MeV for the reactions ^{233}U(n,f) and ^{235}U(n,f). Fragments were detected in a mass range $80 \leq A \leq 107$. Cold fragmentation was observed, its definition being a fission process without evaporation of neutrons. The influence of the fission-fragment ground-state deformations on the yield in cold fragmentation could not be detected unambiguously. The kinetic energies corresponding to a common fixed yield level for each isobar reflect the influence of the proton pairing energy, but not of the neutron pairing energy. By using calculated Q-values for the different mass splits, mass distributions at fixed total kinetic energy are deduced from the data. At a fixed total excitation energy of 7 MeV, the yield increases from very asymmetric mass splits ($A_L \approx 80$) to more symmetric mass splits ($A_L \approx 105$) by more than two orders of magnitude. This strong dependence on the mass split seems to be correlated with the decreasing surface-to-surface distance of the unaccelerated fission fragments in this range of mass splits, as calculated under the assumption that the total Q-value is represented by the mutual Coulomb repulsion of the two fragments.

(1) dito, Nucl. Phys. A452(1986)277-295

[+] Institut für Kernphysik, Technische Hochschule Darmstadt
[++] Sektion Physik, Universität München
[+++] GSI, Darmstadt
[++++] Institut Laue-Langevin, Grenoble

1.5.2 MASS YIELDS OF FISSION FRAGMENTS AS A FUNCTION OF KINETIC ENERGY IN THE REACTION ^{249}Cf(n_{th},f)

E. Aker, D. Engelhardt, R. Brissot[+], P. Geltenbort[++], F. Gönnenwein[++], A. Oed[++], J. Gindler[+++], B. Wilkins[+++](1)

This experiment was performed at the "Cosi-fan-tutte" time-of-flight spectrometer at the ILL in Grenoble (2). Data evaluation was performed and results and their interpretation of mass and energy distributions of fission fragments were discussed by E. Aker (3,4). 97.2% of light fission fragment yields lies between fragment masses 85 to 123 amu, the most probable mass being m = 108. An average kinetic energy of light fragments is 105 MeV for m = 91, 100 MeV for m = 119 and 90 MeV for m = 123 amu. Energy spectra were calibrated using a $^{233}U(n_{th},f)$-run, whose fragment kinetic energy distribution is well-known from literature. For the highest fragment energies above 123 MeV (cold fragmentation) the mass distribution of fission fragments of $^{239}Cf(n_{th},f)$ shows only weak structure, contrary to fission fragments of $^{233}U(n_{th},f)$. Mass 116 amu is dominant. The heavy mass 134 amu is correlated to mass 116 in $^{249}Cf(n_{th},f)$; mass 134 amu shows also up strongly in the reaction $^{233}U(n_{th},f)$. The kinetic energy distribution does not correspond to a pure Gaussian shape, but shows an asymmetric tail to lower energies.

(1) dito, Verhandlungen DPB, Group Report, 1986
(2) A. Oed, P. Geltenbort, R. Brissot, F. Gönnenwein, P. Persin, E. Aker, D. Engelhardt, Nucl. Instr. Meth. 219(1984)569-574
(3) E. Aker, R. Brissot, D. Engelhardt, P. Geltenbort, J. Gindler, F. Gönnenwein, A. Oed, B. Wilkins, Int. Conf. on Nucl. Data for Basic and Appl. Science, May 13-17, Santa Fe (1985)
(4) E. Aker, Thesis (1986)

+ Université de Grenoble
++ Institut Laue-Langevin, Grenoble
+++ Argonne National Laboratory

1.5.3 MASS AND CHARGE DISTRIBUTION OF FISSION FRAGMENTS IN $^{237}Np(2n,f)$

R. Brissot+, G. Barreau++, G. Martinez++, EL-Samman+, D. Engelhardt (1,2,3)

The fissile isotope ^{238}Np was produced in situ at the Lohengrin mass separator target inside the High Flux Reactor of the ILL by neutron capture. As the counting rate is a function of the square of the neutron flux, this experiment was only feasible at the High Flux Reactor. For the first time it was thus possible to study mass and charge distributions as a function of kinetic energy of an isotope with odd nuclear charge. Fission of ^{239}Np leads to a distribution of nuclear charge, where one fragment has even and the other one odd charge. Nuclear charge was determined by residual energy measurement following dE/d in a solid absorber in an ionization chamber. The results shows a regular isotopic distribution. There is a similar shape of mass and kinetic energy distribution in the fission of ^{239}Np and ^{240}Pu (4). The experimental results were interpreted in the framework of the Wilkins model (5,6).

(1) dito, R. Brissot et al., to be published
(2) G. Martinez, Thesis, Bordeaux (1986)
(3) EL-Samman, Thesis, Grenoble (1986)
(4) C. Schmitt, A. Guessons, J.P. Boquet, H.-G. Clerc, R. Brissot, D. Engelhardt, H.R. Faust, F. Gönnenwein, M. Mutterer, H. Niefenecker, J. Pannicke, Ch. Ristori, J.P. Theobald, Nucl. Phys. A430(1984)21-60
(5) B.D. Wilkins, E.P. Steinberg, R.R. Chasman, Phys. Rev. C5(1976)1832

(6) B.D. Wilkins, J.E. Gindler, private communication (1986)

+ Université de Grenoble

++ CEN Bordeaux-Gradignan

1.5.4 MASS AND CHARGE DISTRIBUTION OF FISSION FRAGMENTS IN ^{249}Cf(n,f)

E. Aker, D. Engelhardt (1)

This experiment was recently performed at the Lohengrin mass separator at the ILL as an extension of an previous experiment on ^{249}Cf at the "Cosi Fan Tutte" time-of-flight spectrometer (2). A new target technique developped recently allowed us to use the ^{249}Cf targets for up to 1 week in the High Flux Reactor before nuclear burn-up had used the fissile isotope. The partial measurement of mass distribution as a function of kinetic energy is in good agreement with a complete set of data acquired at the "Cosi Fan Tutte" spectrometer previously (2). Nuclear charge was determined by measurement of residual energy following dE/dx in a solid absorber in an ionization chamber. A rather comprehensive distribution of nuclear charge as a function of mass and kinetic energy was obtained, except for cold fragmentation. There is evidence for at least three new isotopes, ^{115}Rh, ^{111}Tc and ^{109}Mo, which can only be produced in fission of very heavy nuclei. A further investigation is scheduled at both fission fragment spectrometers at the ILL before the end of 1986.

(1) E. Aker, D. Engelhardt et al., to be publsihed

(2) E. Aker, Thesis (1986)

1.5.5 A QUANTUM MODEL FOR NUCLEAR FISSION

E. Aker, R.W. Hasse^{+} (1,2)

A comparison of mass yields and kinetic energy distributions of fission fragments from ^{250}Cf fission experiments with static fission models (3) presently often used to interprete experimental results of fission studies show considerable discrepancies between experiment and theory. Static models do not take into account the dynamic evolution of the fission process through the various degrees of freedom of deformation until fission takes place nor do they include statistical or quantum fluctuations. Therefore dynamical model calculations were performed, which are based on an adiabatic quantum fission model (4). In this model the fission process is described by the propagation of a quantum mechanical wave packet in the potential of the deformed nucleus including their inertias. As parameters quadrupole and hexadecapole like deformatins (elongation and constriction) are employed and the evolution of the wave packet as solution of the time-dependent Schroedinger equation has been investigated between the saddle point and the scission line. From these calculations one gains information on the velocity of the separation as well as on the configuration of the fragments at scission. With these quantities the final kinetic energy distribution of the fragments is obtained. Our calculations are particularly interesting for the case of cold fragmentation.

(1) dito, to be published
(2) E. Aker, Thesis (1986)
(3) B.D. Wilkins, Phys. Rev. C14(1976)1832
(4) R.W. Hasse, Nucl. Phys. A128(1969)609

+ IK III, presently at GSI, Darmstadt

1.5.6 FISSION FRAGMENT PROPERTIES IN FAST-NEUTRON-INDUCED FISSION OF ^{237}Np*

A.A. Naqvi[+], F. Käppeler, F. Dickmann, R. Müller[++]

We have performed a complete (2E,2v) experiment of the kinetic energies E and velocities v of correlated fragments from fast-neutron-induced fission of ^{237}Np. The influence of excitation energy on the important fragment properties such as mass, kinetic energy and prompt neutron emission have been investigated experimentally at 0.80 and 5.55 MeV neutron energy. Our results include mean values of fragment properties before and after neutron evaporation, e.g. of fragment velocities and masses, total kinetic energies, and the respective variances. Also given are the distributions of fragment mass, of $E_{k,tot}$, the variance of $E_{k,tot}$ as well as the number of prompt fission neutrons as a function of fragment mass. These results show that shell effects are strong near threshold at E_n = 0.80 MeV, but decrease significantly at the higher excitation energy, in qualitative agreement with the model of Wilkins, Chasman and Steinberg (1). However, the observed increase in the number of prompt fission neutrons, which appears only in the heavy fragments, cannot be explained by this model.

(1) B.D. Wilkins, E.P. Steinberg, R.R. Chasman, Phys. Rev. C14 (1976) 1832

* Phys. Rev. C34 (1986) 218

+ University of Dhahran, Dhahran, Saudi-Arabia

++ Now at Siemens AG, D-8000 München, Fed. Rep. of Germany

1.6 THEORY

1.6.1 BREATHING CLUSTER MODEL FOR TWO s-WAVE CLUSTERS

A.T. Kruppa$^+$, R.G. Lovas$^+$, R. Beck and F. Dickmann, (1)

The nuclei with mass number $5 \leq A \leq 9$ may be concieved to consist of a α cluster and a cluster composed of the rest of the nucleons. The two clusters may distort each other, so the wave function must contain a combination of several states of the free clusters. In this work we described these nuclei microscopically by including the g.s.'s and breathing excitations of the clusters. One of our effective N-N interactions fitted to reproduce the measured energies and radii of the free clusters and the energy of ^{6}Li or ^{7}Li predicts the two-cluster energies as follows:

Potential	E(^{5}He)	E(^{6}Li)	E*(^{6}Li,L=2)	E/^{7}Li)	E(^{7}Be)	E(^{8}Be)
For ^{6}Li	-26.64	-31.99	3.76	-38.16		-55.79
For ^{7}Li	-26.81	-32.85		-39.24	-37.68	-56.49
Experiment	-26.08	-31.99	3.59	-39.09	-37.46	-56.50

The calculated squared monopole charge form factor $F^2(q)$ and αd fragmentation strength $G^2(q)$, shown below, improve on previous cluster-model calculations. It is argued that even the diffraction dip of $F^2(q)$ and the slope of $G^2(q)$ could be reproduced by explicitly including short-range N-N correlation in the wave function.

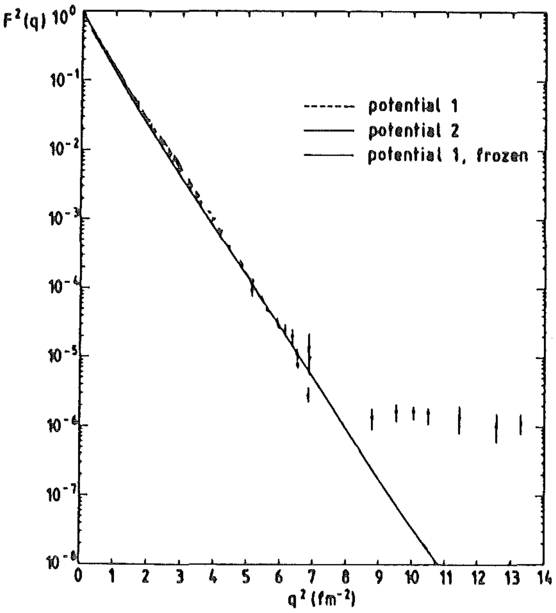

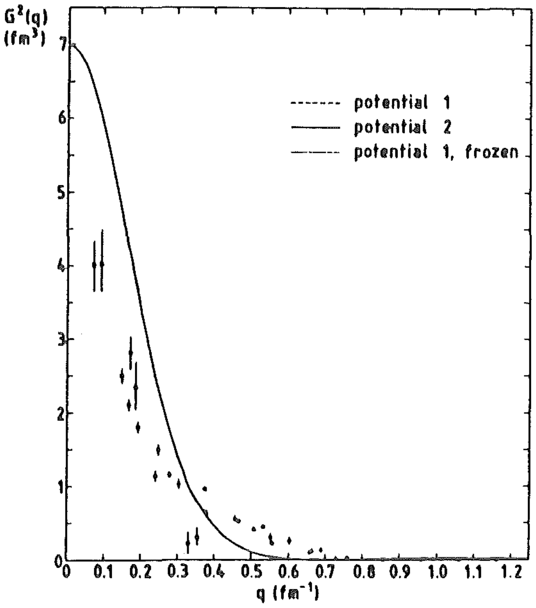

(1) Submitted to Phys. Lett. B

$+$ Institute of Nuclear Research, Debrecen, Hungary

1.6.2 UNIFIED MICROSCOPIC DESCRIPTION OF THE LIGHTEST NUCLEI

R.G. Lovas[+], A. T. Kruppa[+], R. Beck and F. Dickmann

The aim of this work was to describe the nuclei with $A \leq 8$ in a common microscopic framework (1). We built up the nuclei $2 \leq A \leq 4$ and $5 \leq A \leq 8$ from one and two 0s clusters, respectively. An n-nucleon ($n \leq 4$) cluster wave function was taken to be a superposition of N_n $(0s)^n$ oscillator states ($N_n \leq 5$) of different sizes, and the two-cluster nuclei were assumed to be superpositions of similar α + n-nucleon-cluster states. All wave funcitons were exactly antisymmetrized. The oscillator sizes as well as the $N_\alpha x N_d$ relative wave functions were determined variationally. A central nucleon-nucleon interaction was constructed by fitting to the energies and sizes of d, t, ^{3}He and α. The g.s. energies of ^{5}He, ^{6}Li, ^{7}Li, ^{7}Be and ^{8}Be were then determined, and a detailed analysis of the fragmentation and electromagnetic properties of ^{6}Li was performed.

The energies and rms charge radii of the single-cluster nuclei were obtained to be correct within 1 keV and 0.1 fm, respectively. With the exchange mixture of the force fixed appropriately, the g.s. energies of all two-cluster nuclei were then reproduced with an accuracy of 1 MeV. The excitation energy of the L = 2 triplet of ^{6}Li was predicted with an accuracy of 0.2 MeV. Although the energy of ^{6}Li is deeper in this model by as much as 2 MeV than in conventional α+d cluster models, yet the weight of the (g.s.) +d(g.s.) component (2) remains as high as 0.92. The conventional spectroscopic factors of the α+d and t+^{3}He fragmentations were obtained to be 0.93 and 0.58, respectively. These are somewhat larger than the average of the experimental estimates.

The charge rms radius and the B(E2, $3^+ \rightarrow 1^+$) transition strength agree with the data within the experimental errors. The calculated monopole charge form factor is excellent up to 7 fm^{-2}, but fails to show the diffraction minimum flund experimentally at 8 fm^{-2}. (The measured and calculated charge form factors of the α particle compare similarly.) The elastic magnetic dipole form factor is somewhat less accurate due to the lack of a tensor force. The inelastic quadrupole charge form factor is in almost perfect agreement with experiment.

In conclusion, the model gives a surprisingly coherent description of the $A \leq 8$ nuclei. What it fails to reproduce is the high-momentum behaviour of the wave function, in which strong short-range correlations or the effects of the non-nucleonic degrees of freedom are expected to be large.

(1) R. Beck, F. Dickmann and A.T. Kruppa, Phys. Rev. C30 (1984) 1044
(2) R. Beck, F. Dickmann and R.G. Lovas, Nucl. Phys. A446(1985) 703.

[+] Institute of Nuclear Research, Debrecen, Hungary

1.6.3 NEUTRON-PROTON CROSS SECTIONS IN A SIMPLE INTERACTION MODEL

P.Doll

There are very precise neutron-proton scattering data available (see 1.2.1) in an energy range which is known to be covered by the kinetic energy of nucleons in nuclei. These data represent a testing ground to be understood in an nucleon-nucleon interaction model. To find the components of the interaction which determine our precise nucleon-nucleon scattering data in the energy range between 20 and 50 MeV we investigated a simple Yukawa type interaction in the $M^{S'}_{m_S',m_S}$-matrix formalisme to calculate differential cross sections to start with. The $M^{S'}_{m_S',m_S}$ elements are decomposed into partial waves up to $l = 2$ and in the n-p system both amplitudes for isospin $t = 0$ and $t = 1$ contribute. It is assumed that at low energies the two nucleons feel only the nuclear interaction which is of short range ($\mu = 0.7\ \mathrm{fm}^{-1}$) and a small number of angular momentum states is justified.

When the scattered particle is detected in the scattering plane with $\phi = 0$ the $M^{S'}_{m_S',m_S}$ elements exhibit simple symmetries (1). The $M^{S'}_{m_S',m_S}$ elements contain the $T_{l',s\,ls}$ elements which are taken (2) in first Born approximation by

$$T_l = \frac{V_o}{2qq'} \times Q_l\left(\frac{q^2+q'^2+\mu^2}{2qq'}\right)$$

where Q_l is the Legendre function of the second kind. Q_o to Q_2 were used in the present calculation presenting a measure of the partial wave interaction strength. The M-matrix elements are taken between momentum and spin-eigen states, which can be decomposed into states of good angular momentum. The Wolfenstein (1) parameters which determine the observables are derived from the M-matrix elements.

Fig. 1
Comparison between experimental (1.2.1) and theoretical differential cross sections for neutron-proton scattering

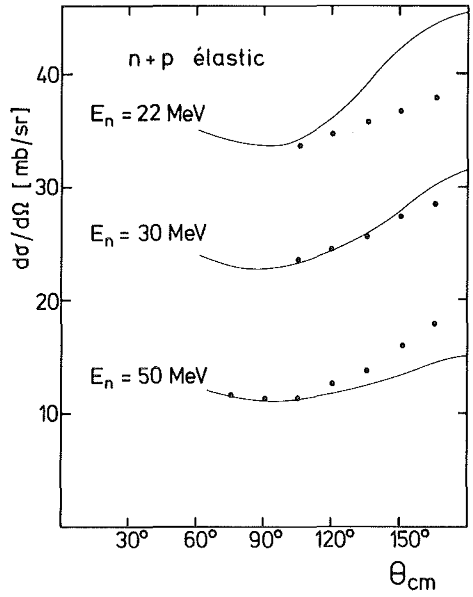

The figure shows our preliminary calculation in comparison with data at 22 MeV, 30 MeV and 50 MeV. The calculations are above the data a low energies, which may be due to the poor justification of the Born approximation and the missing tensor force and at higher energies below the data due to the absence of higher partial wave. These shortcomings should be removed in the future.

(1) N.Hoshizaki, Suppl.Progr.Theor.Phys. 42 (1968) 107
(2) G.Brown, Nucleon-Nucleon interaction (1975) North Holland Publishing Company

2. LASER SPECTROSCOPY

2.1 THE ODD-EVEN STAGGERING OF THE NUCLEAR CHARGE RADII OF Pb ISOTOPES

M. Anselment, W. Faubel$^+$, S. Göring, A. Hanser, G. Meisel, H. Rebel, and G. Schatz, (1)

Previous laserspectroscopic studies of the hyperfine structure splittings and isotope shifts of the ($6p^2\ ^3P_o$ - $6p7s\ ^3P_1$; 283.3 nm) Pb I resonance line have been extended to further radioactive Pb nuclides: ^{196,197,197m,211,214}Pb. Using an improved theoretical result about the specific mass shift, we recalibrate the isotope shifts of the full series (A = 196-214) of measured isotope shifts in terms of the nuclear parameter and determine the odd-even staggering parameters. The variation of the nuclear charge radii of the Pb nuclides exhibits distinct shell effects, and the odd-even staggering shows a conspicuous trend, being more pronounced for neutron deficient Pb isotopes.

(1) Nuclear Physics A451 (1986) 471

$+$ Institut für Radiochemie, Kernforschungszentrum Karlsruhe GmbH, Karlsruhe

2.2 CHARGE RADII AND MOMENTS OF TIN NUCLEI BY LASER SPECTROSCOPY

M. Anselment$^+$, K. Bekk, A. Hanser, H. Hoeffgen^{++}, G. Meisel, S. Göring, H. Rebel, and G. Schatz, (1)

The isotope shift and hyperfine structure of the optical Sn I resonance transition $5p^2\ ^3P_0 \rightarrow 5p6s\ ^3P_1$ at λ = 286.3 nm have been studied for 18 Sn nuclei including 2 isomers. Laser induced resonance fluorescence from a collimated atomic beam of tin was observed using a tunable cw dye laser with frequency doubler. The electromagnetic nuclear moments and changes of the mean square charge radii of the nuclear charge distributions were determined. The results are discussed with respect to the information they provide on the nuclear structure of the nuclei investigated; they are compared with various theoretical models.

(1) KfK-Report 4071 (1986) - Phys. Rev. C (in press)

$+$ Present address: Dep. of Physics and Astronomy, Louisiana State Univ., Baton Rouge, Louisiana, USA

$++$ Present address: Batelle-Institut e.V., D-6000 Frankfurt 90, Fed. Rep. of Germany

2.3 LASER SPECTROSCOPY OF STABLE AND RADIOACTIVE Sr ISOTOPES

M. Anselment, K. Bekk, S. Chongkum, S. Göring, A. Hanser, G. Meisel, and H. Rebel

Theoretical predictions (1) and gamma ray spectroscopic results (2) both come to the conclusion that neutron deficient strontium isotopes are strongly deformed as neutrons are removed from A = 80 on and below. This deformation has a corresponding effect on the mean square charge radii the isotopic variation of which can be deduced from optical isotope shift measurements. We therefore have extended our measurements of the hyperfine structure of the atomic transition $5s^2 \rightarrow {}^1S_o$ $5s6p$ ${}^1P_1^o$ at $\lambda = 293.2$ nm beyond the already known range (3) to lighter isotopes. Preliminary results were obtained for ^{85m}Sr and ^{87m}Sr, too.

The method applied is laser induced fluorescence in an atomic beam as described before (3). In order to increase the sensitivity, the ADA temperature tuned doubling crystal was replaced by a lithium iodate crystal that is angle tuned at room temperature. The UV output power thus obtained is about 3 mW instead of only 1 mW which leads to a corresponding increase of the fluorescence rate. The high UV power obtained it due to the fact that the Li-iodate crystal is used at an angle of zero degree with respect to the optical axis since the wavelength required for Sr happens the coincide precisely with the cutoff wavelength of this crystals; thus it is used at optimum efficiency with vanishing walkoff losses. To improve sample preparation, the Kr gas target (4) used for Kr (α,xn) production of Sr isotopes was altered to withstand 50 bar gas pressure instead of only 10 bar by replacing the foil window by the 3 mm thick beryllium discs used to match the incident α energy to the desired reaction.

The results are summarized in table 1. The experimental raw data are the component positions. For the odd isotopes the center of mass with respect to the ^{88}Sr position ("isotope shift") was deduced. From the isotope shifts the mean square charge radius changes $\delta\langle r^2\rangle$ were determined in the usual way by a King plot procedure. For calibration the following three $\delta\langle r^2\rangle$ (5) were used as independent input data:

$$\langle r^2\rangle^{86} - \langle r^2\rangle^{88} = +\,0.047(6)\ \mathrm{fm}^2$$
$$\langle r^2\rangle^{86} - \langle r^2\rangle^{87} = +\,0.040(4)\ \mathrm{fm}^2$$
$$\langle r^2\rangle^{84} - \langle r^2\rangle^{86} = +\,0.063(7)\ \mathrm{fm}^2 .$$

The $\delta\langle r^2\rangle$ results are plotted in Fig. 1. The plot shows as usually a steep increase for $\langle r^2\rangle$ above the closed shell at A = 88 due to the volume expansion upon addition of neutrons. For A < 88, however, the shrinking of the volume is overcompensated by an increase of $\langle r^2\rangle$ with decreasing neutron number due to nuclear deformation; this deformation increases rather steadily from A = 88 down to A = 80. It seems as if the sudden deformation jump predicted (1) below A = 80 is smeared out over many isotopes. Unfortunately, the measurements could not be ex-

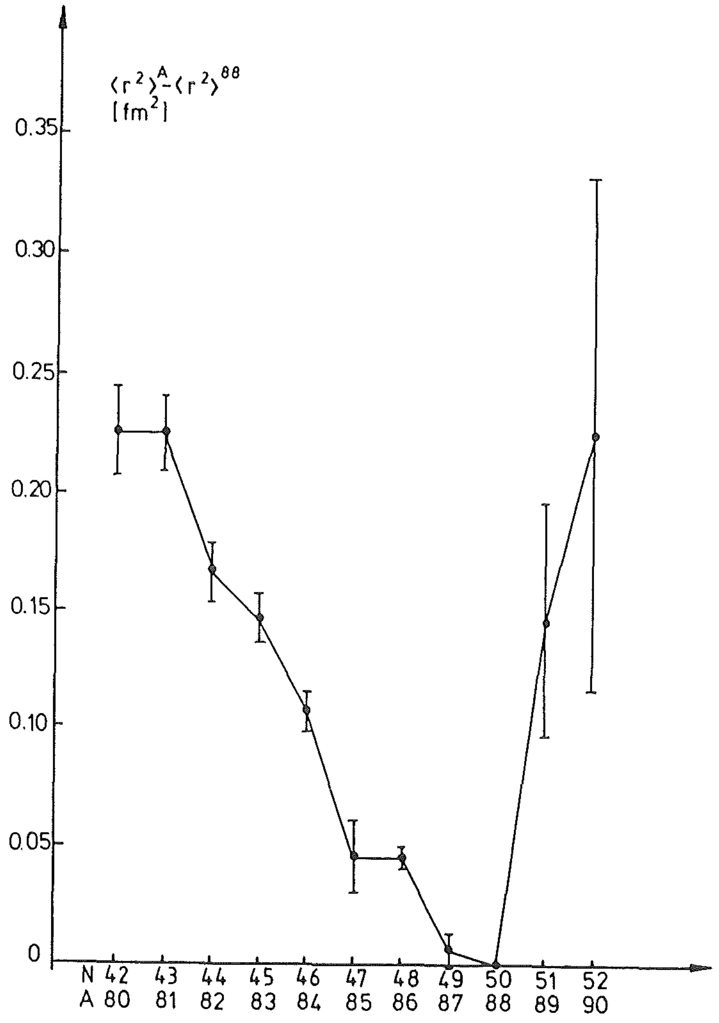

Fig. 1 Plot of the m.s. charge radius changes $<r^2>^A - <r^2>^{88}$ with the mass number A.

tended to A = 78 because of the short lifetime $T_{1/2}$ = 2.5(0.3) min (6) of this isotope.

The hyperfine splitting for the odd isotopes was converted into magnetic dipole and electric quadrupole interaction constants A and B, respectively (cf. Table 2). The μ_I values were determined from the A's by scaling, taking as reference $\mu_I(^{87}Sr) = -1.0924(7)$ nm (7,8); the derived μ_I values are given with a 2 % uncertainty throughout to account for a possible hyperfine anomaly that is ignored by the scaling procedure. The relation between the B factor and the quadrupole moment given in Table 2 has been taken from (8). Since the value given there is corrected for Sternheimer type polarization effects our scaled Q values can be considered as corrected, too. The increasing intrinsic deformation with decreasing neutron number as is obvious from the $<r^2>$ data (cf. Fig. 1) does not lead to correspondingly large spectroscopic quadrupole moments because of the rotational behaviour of these nuclei.

Table 1 Hyperfine structure results for Sr isotopes. For the calibration of the deduced data see text. The data for ^{85m}Sr and ^{87m}Sr are preliminary only.

Mass Number A	Nucl. Spin I	F Quant. Number	Component position $\nu_F^A - \nu^{88}$ [MHz]	Isotope Shift $\nu^A - \nu^{88}$ [MHz]	m.s. charge radius change $\langle r^2\rangle^A - \langle r^2\rangle^{88}$ [fm²]
80	0	1	-992(5)	-992(5)	0.227(19)
81	1/2	3/2	-1121(5)	-890(20)	0.227(20)
		1/2	-225(60)		
82	0	1	-728.4(5)	-728.4(5)	0.169(13)
83	7/2	9/2	-81.4(3)	-610.85(25)	0.149(11)
		7/2	-782.5(5)		
		5/2	-1264.45(30)		
84	0	1	-474.06(5)	-474.06(5)	0.110(9)
85	9/2	11/2	+317.2(3)	-314.8(2)	0.047(16)
		9/2	-462.8(2)		
		7/2	-1077.7(2)		
85m	1/2	3/2	-730(60)	-350(45)	0.08(4)
		1/2	+406(60)		
86	0	1	-224.73(5)	-224.73(5)	0.047(5)
87	9/2	11/2	+596.97(10)	-93.62(6)	0.007(8)
		9/2	-254.95(10)		
		7/2	-927.85(10)		
87m	1/2	3/2	-430(60)	-100(45)	0.013(40)
		1/2	+560(60)		
88	0	1	0	0	0
89	5/2	7/2	+692.8(1.0)	-25.8(5)	0.10(5)
		5/2	-304.8(4)		
		3/2	-1044.5(5)		
90	0	1	-79.7(3)	-79.7(3)	0.23(11)

Table 2 Hyperfine splitting data for the odd Sr isotopes. The μ_I value for ^{87}Sr was taken from (7,8). The quadrupole moments were calculated using Q/B = 0.0260(16) barn/MHz which follows from the value Q(^{87}Sr) = +0.335(20) barn given by Heider and Brink (8). It is meant to include Sternheimer corrections.

Mass number A	Nucl. Spin I	Magnetic Dipole Hyperfine Constant A [MHz]	Magnetic Dipole Moment μ_I [nm]	Electric Quadrupole Hyperfine Constant B [MHz]	Electric Quadrupole Moment Q [barn]
81	1/2	-660(40)	+0.524(30)	0	0
83	7/2	+149.0(2)	-0.829(17)	+31.6(5)	+0.823(60)
85	9/2	+139.75(6)	-1.000(20)	+12.4(3)	+0.323(20)
85m	1/2	-757(57)	+0.60(5)	0	0
87	9/2	+152.75(3)	-1.0924(7)	+12.87(12)	+0.335(20)
87m	1/2	-660(57)	+0.52(5)	0	0
89	5/2	+288.7(3)	-1.147(30)	-12.1(5)	-0.315(25)

(1) K. Heyde, J. Moreau, and M. Waroguier, Phys. Rev. C 29 (1984) 1859

(2) C.J. Lister, B.J. Varley, H.G. Prince, and J.W. Olness, Phys. Rev. Lett. 49 (1982) 308

(3) M. Anselment, S. Chongkum, S. Göring, A. Hanser, G. Meisel, H. Rebel, and G. Schatz, KfK-Report 3969 (1985) 63

(4) B. Feurer and A. Hanser, KfK internal report

(5) D. Bender, H. Brand, and V. Pfeufer, Z. Phys. A 318 (1984) 291

(6) C.F. Liang, P. Paris, D. Bucurescu, S. Della Negra, J. Obert, and J.C. Putaux, Z. Phys. A 309 (1982) 185

(7) L. Olschewski, Z. Phys. 249 (1972) 205

(8) S.M. Heider and G.O. Brink, Phys. Rev. A 16 (1977) 1371.

2.4 ISOTOPE SHIFTS AND HYPERFINE STRUCTURE SPLITTING IN ATOMIC TRANSITIONS OF ^{242m}Am BY OPTOGALVANIC LASERSPECTROSCOPY

W. Liewehr[+], K. Bekk, W. Kälber, G. Meisel, H. Rebel, and A. Ali Sameh[++]

Previous laserspectroscopic measurements of the isotope shift and hyperfine structure splitting of several atomic transitions of ^{241,243}Am (1) have been extended, and results for the long-lived isomer ^{242m}Am have been obtained for the first time. The experimental method was optogalvanic laserspectroscopy in a hollow cathode lamp with a neon gas discharge containing the Am sample. When tuning the laser light to an electronic transition of Am, a small change of the operating voltage of the discharge signals the resonance. The ^{242m}Am was from a ^{241}Am sample which has been irradiated for several months by the thermal neutron flux of a reactor, about 15 years ago, thus containing ca.1% ^{242m}Am and ca. 1% ^{243}Am. The sample has been radiochemically purified, but an isotope separation by a mass separator has not been performed. Due to the presence of the dominating ^{241}Am (98 %), many weak hyperfine components of the ^{242m}Am transitions could not be observed, since they are hidden within the wings of the ^{241}Am lines. Nevertheless several ^{242m}Am components of Am I ground state transitions (λ = 6405 Å and λ = 6054 Å) could be identified (Fig.1), two faint components of the λ = 5424 Å transitions are indicated. The identification and assignments are corroborated by the results obtained with pure ^{241,243}Am samples. Tab. 1 gives the results for two transitions.

Table 1 Values of the hyperfine structure constants and the ^{242m}Am - ^{241}Am isotope shifts (IS) observed in two Am I transitions.

λ(Å)	Term	A(MHz)	B(MHz)	IS (MHz)
6405	$5f^7 7s7p\ ^{10}P_{9/2}$	+444.3(2.4)	+1683(120)	-2510(50)
6054	$5f^7 7s7p\ ^{10}P_{7/2}$	+536 (9)	-5818(120)	-2490(75)

With the value μ = +1.58(3) nm of the magnetic moment of ^{241}Am (2), a value μ = +0.98(5) nm can be deduced for ^{242m}Am, and using the value Q_s = 4.29(3) eb of the spectroscopic quadrupole moment of ^{243}Am (3), the value Q_s = +6.8 eb is derived for ^{242}Am.

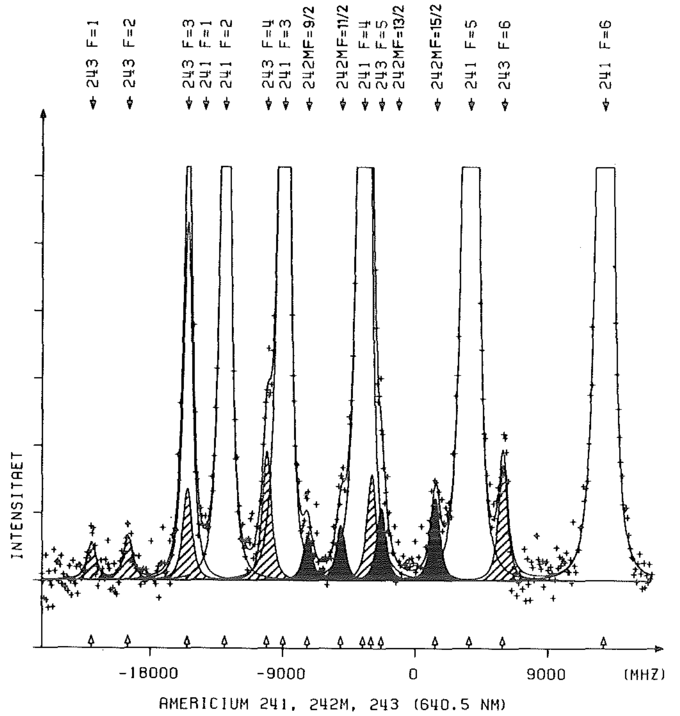

Fig. 1

Spectra of ^{242m}Am at 6405 Å and 6404 Å with ^{241}Am and ^{243}Am as impurities. The lines belonging to ^{242m}Am are marked.

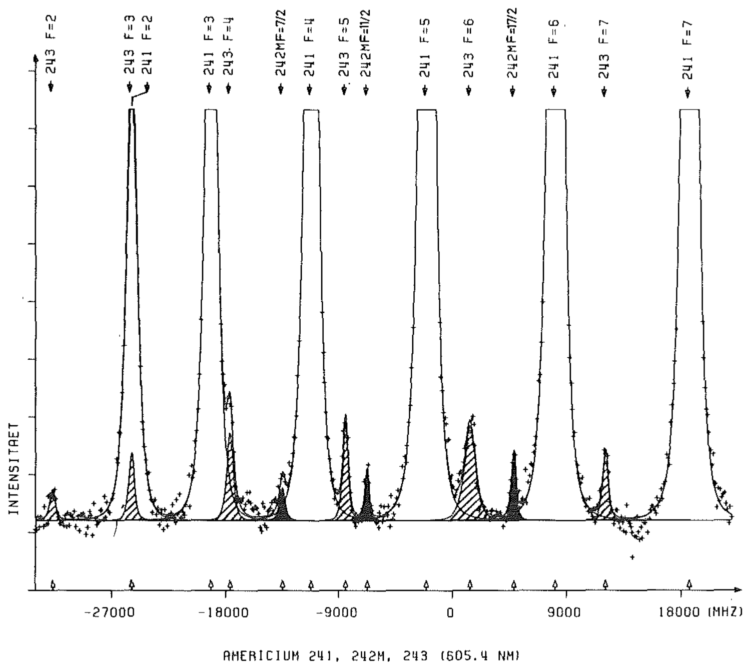

(1) W. Liewehr, K. Bekk, W. Kälber, G. Meisel, and H. Rebel, Annual Report on Nuclear Physics Activities, KfK 3969 (1985) 68

(2) L. Armstrong Jr., R. Marrus, Phys. Rev. 144 (1965) 3

(3) C.E. Bemis Jr., F.K. McGowan, J.L.C. Ford Jr., W.T. Milner, R.L. Robinson, and P.H. Stelson, Phys. Rev. C24 (1981) 2723

+ Forschungsgesellschaft für Angewandte Naturwissenschaften e.V. (FGAN) 5307 Wachtberg-Werthoven

++ Institut für Radiochemie des Kernforschungszentrums Karlsruhe.

2.5 REEVALUATION OF ISOTOPE SHIFT DATA FOR A SERIES OF STABLE AND RADIOACTIVE LEAD ISOTOPES

M. Anselment, K. Bekk, G. Meisel, H. Rebel, G. Schatz, and R. Thompson[+]

In two previous papers (1,2) isotope shift results were given for a series of lead isotopes; they were converted into changes of the mean square charge radius ($\delta\langle r^2\rangle$) with the neutron number. The conversion was performed in the usual way by means of a so called King plot (3). The following input data (4) were used in (1) to find the King line:

$$\lambda^{204} - \lambda^{208} = -0.2072(.0061)\ \mathrm{fm}^2$$
$$\lambda^{206} - \lambda^{208} = -0.1115(.0061)\ \mathrm{fm}^2$$
$$\lambda^{207} - \lambda^{208} = -0.0664(.0061)\ \mathrm{fm}^2$$

where it was assumed that $\lambda = 0.93\ \delta\langle r^2\rangle$. In (2) as an additional information we used a narrow limit on the total mass shift (5) as additional information which considerably reduced the spread of the King lines compatible with the uncertainties of the calibrating input data.

As in both cases procedures have been applied which had to incorrect results in the specific case considered, we give a corrected list with properly calculated errors as Tab. 1. The input data are an extended set of results given in ref. 2.

Table 1 Corrected list of $\delta\langle r^2\rangle$ values for the Pb-isotopes

Isotope Pb	$\delta\langle r^2\rangle$ (fm²) (previous)	$\delta\langle r^2\rangle$ (fm²) (corrected)
196	-0.6057(52)	-0.606(15)
197	-0.6038(50)	-0.604(15)
197m	-0.5739(47)	-0.573(14)
198	-0.5214(49)	-0.521(13)
199	-0.5163(42)	-0.516(13)
200	-0.4286(35)	-0.429(11)
201	-0.4093(34)	-0.409(10)
202	-0.3280(27)	-0.328(8)
202m	-0.3299(27)	-0.330(8)
203	-0.3045(25)	-0.305(8)
204	-0.2231(18)	-0.223(6)
205	-0.1967(16)	-0.197(5)
206	-0.1179(10)	-0.118(3)
207	-0.0737(6)	-0.074(2)
208	0.0	0.0
209	0.0937(9)	+0.096(2)
210	0.2107(18)	+0.211(5)
211	0.2995(25)	+0.299(8)
212	0.4144(38)	+0.414(11)
214	0.6099(52)	+0.610(16)

(1) R.C. Thompson, M. Anselment, K. Bekk, S. Göring, A. Hanser, G. Meisel, H. Rebel, G. Schatz, and B.A. Brown, J. Phys. G: Nucl. Phys. 9 (1983) 443
(2) M. Anselment, W. Faubel, S. Göring, A. Hanser, G. Meisel, H. Rebel, and G. Schatz, Nuclear Physics A 451 (1986) 471
(3) H.G. Kuhn, Atomic Spectra, 2nd. edn. London: Longmans, Grun and Co. (1969)
(4) G. Fricke, H. Miska, and D. Rychel, private communication, 1981
(5) W.H. King and M. Wilson, J. Phys. G: Nucl. Phys. 11 (1985) L43

+ National Physical Laboratory, Div. Mech. Optic. Metrology, Teddington, U.K.

2.6 LASERSPECTROSCOPIC INVESTIGATIONS IN AN RF ION TRAP

W. Kälber, K. Bekk, G. Meisel

An ion trap confines charged particles in a small area by means of radiofrequency (rf) and static electric quadrupole fields (1,2). Laserspectroscopy with an ion trap has been shown to be highly sensitive, since the storage times can be up to several days, and spectroscopy with even a single ion has been demonstrated (3). This method appears to be well suited for the study of radioactive atomic ions in the actinide region.

Fig. 1 gives a set-up for laserspectroscopy with the use of an ion trap. The ion trap electrodes are made of three hyperboloids of revolution to which an rf and a dc voltage are supplied, generating inside the trap structure electric quadrupole fields by which ions are confined. Atoms of interest are evaporated

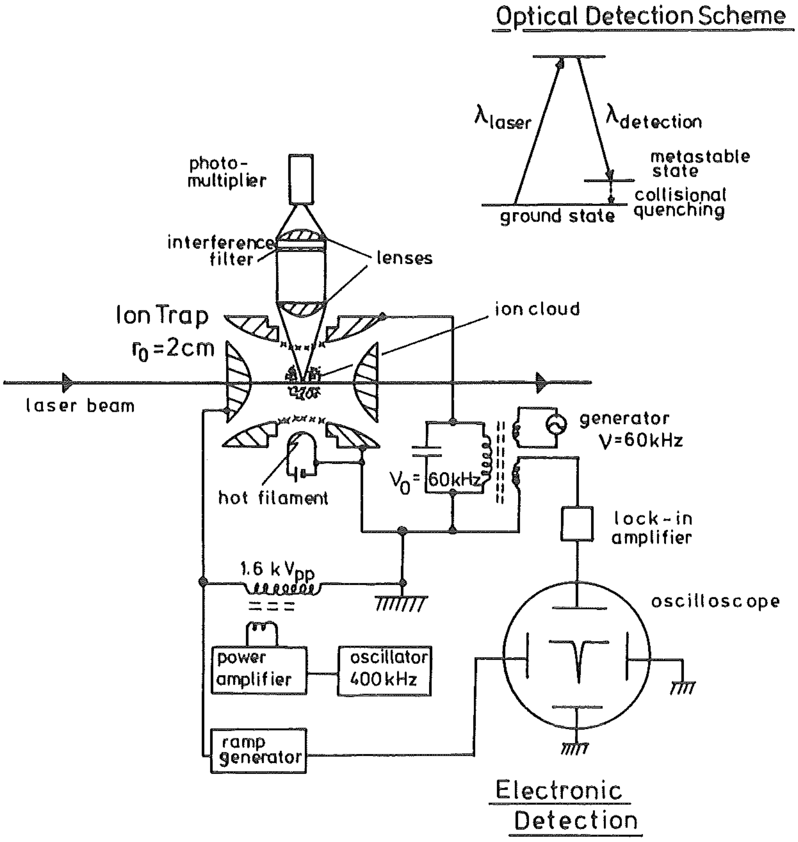
Optical Detection Scheme
λ_{laser}
$\lambda_{detection}$
metastable state
collisional quenching
ground state
photo-multiplier
interference filter
lenses
Ion Trap
r_0=2cm
ion cloud
laser beam
generator
V=60kHz
hot filament
V_0=
60kHz
lock-in amplifier
1.6 kV$_{pp}$
oscilloscope
power amplifier
oscillator 400kHz
ramp generator
Electronic Detection

Fig. 1 Set-up for laser spectroscopy with an ion trap

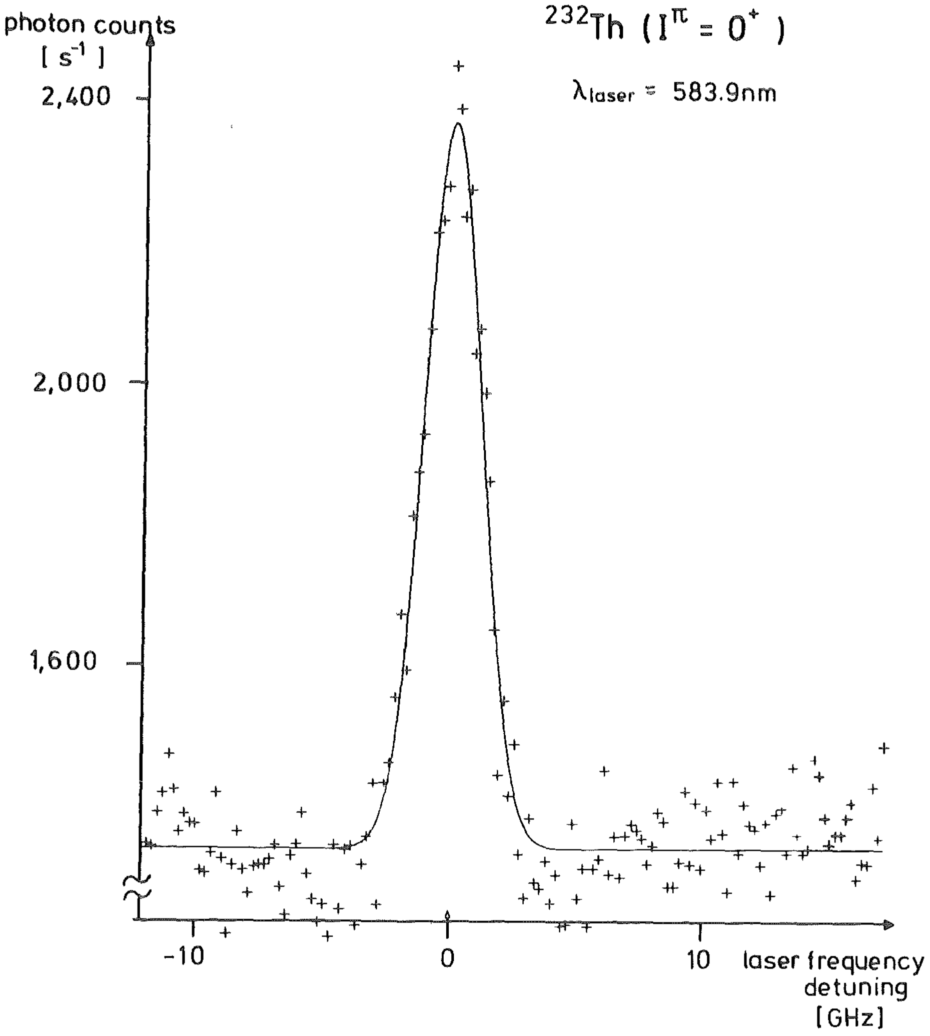

Fig. 2 Record of the 583.9 nm Th II transition of natural ^{232}Th with ∿ 10^6 ions confined.

from a hot filament (e.g. tungsten wire) and ionized inside the trap by electron impact. A light buffer gas (H_2 or He) at 10^{-7} to 10^{-3} mbar is used to increase the storage time (4). For electronic detection of the ions on outer LC resonance circuit is used. The fundamental frequency of motion of the ions is tuned to the resonance frequency of this circuit by a ramp voltage applied to the electrodes. In the case of resonance, energy is transfered from the circuit to the ions, and thus the forced amplitude of the circuit is damped. For hyperfine structure and isotope shift measurements a resonance transition of the ions is excited by laser irradiation. To reduce problems due to scattered laser light, the fluorescence is monitored by a transition into a metastable state which is subsequently quenched back into the ground state by collisions with the buffer gas.

In our first experiments we have observed the La II transition at 580.8 nm. The photon countrate was 15 kHz at the 632.0 nm detection wavelength with some 10^6 ions confined. The laser power was 10 mW and the buffer gas was 5 x 10^{-5} mbar of molecular hydrogen.

As the next step the measurement of the hyperfine structure and isotope shift of a Th II transition is planned in order to get information on the nuclear moments and the variation of the mean square charge radii in a chain of thorium isotopes. A spectrum of the 593.9 nm Th II transition of natural ^{232}Th is shown in Fig. 2. The detection wavelength was 640.9 nm; the fluorescence rate was 8 kHz with ∿ 10^6 ions confined at 3 mW laser power and 1 x 10^{-5} mbar H_2 buffer gas pressure.

(1) E. Fischer, Z. Phys. 156 (1959) 1
(2) G. Werth, Progr. At. Spectr. Part C (H.J. Beyer and H. Kleinpoppen Ed.) (1984) 151
(3) P.E. Toschek, W. Neuhauser, Phys. Bl. 36 (Nr. 7) (1980) 198
(4) H. Schaof, U. Schmeling, and G. Werth, Appl. Phys. 25 (1981) 249.

2.7 THEORETICAL PREDICTIONS ON EVEN PARITY ENERGY LEVELS IN THE AMERICIUM ATOM

J. Dembczyński$^+$, M. Elantkowska$^+$, K. Bekk, and H. Rebel

A preliminary term analysis of Am I spectrum was performed many years ago by Fred and Tomkins (1). However, the spectroscopic description of the electronic levels is not sufficient. It is limited to the quantum numbers J and SL's designation for several electronic levels. Recently Liewehr et al. (2) have studied hfs of some spectral lines of americium, providing new information concerning values of quantum number J, of values of hfs splittings and isotope shifts, useful for energy scheme construction. For the analysis of the isotope shifts and hfs splittings observed for the lines with 542.4 and 559.8 nm (2) we have assumed that the levels at 17858 cm^{-1} and 18429 cm^{-1} belong to different configurations and interact with each other. Therefore, if the level at 17858 cm^{-1} is assigned to configuration $5f^6 6d7s^2$, it should belong to term P.

The further calculation are based on the assumption that the level at 17858 cm^{-1} is a $^8P_{5/2}$ level of the configuration $(5f^6)^7F6d7s^2$. Positions of other levels have been determined in relation to this one. Fig. 1 indicates the results of predicted positions of electronic levels belonging to the system $[(5f^7)^8S, (7p7s)S_1L_1]$ SL + $[(5f^6)^7F,(7s^2)^1S\ 6d]$ SL. Only the transitions from levels with J = 5/2, 7/2, 9/2 to the ground level with J = 7/2 are possible.

The values of Slater integrals for the calculations have been taken from the monograph Fraga et al. (3), while the values of electrostatic integrals have been normalized by factor 0.6.

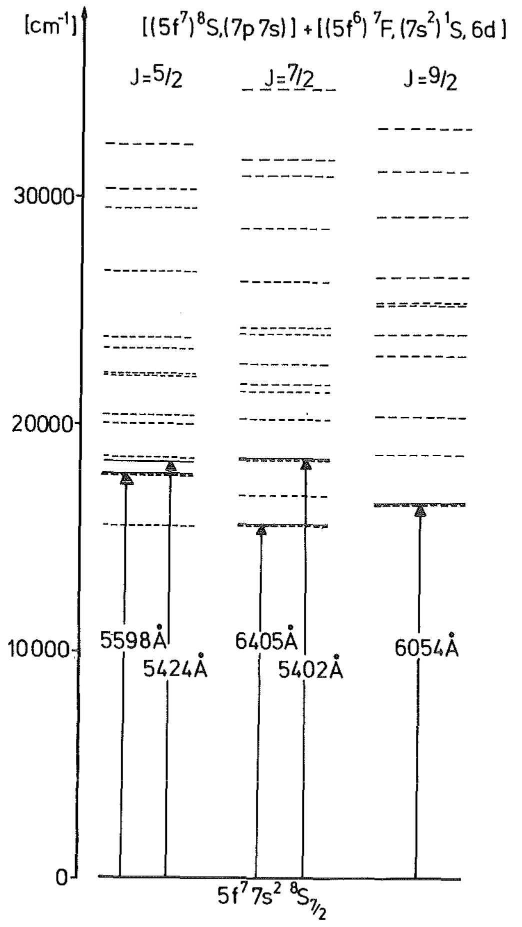
[cm^{-1}]
[(5f^7)^{8}S,(7p 7s)] + [(5f^6) ^{7}F,(7s^2)^{1}S, 6d]
J=5/2
J=7/2
J=9/2
30000
20000
10000
0
5598Å
5424Å
6405Å
5402Å
6054Å
5f^{7}7s^2 ^{8}S$_{7/2}$

Fig. 1 Energy level schheme of Am I (dashed lines: calculated levels, solid lines: measured levels).

(1) M. Fred, F.S. Tomkins, J. Opt. Soc. Am. 47 (1957) 1076

(2) W. Liewehr, K. Bekk, W. Kälber, G. Meisel, and H. Rebel, Annual Report, Kernforschungszentrum Karlsruhe, KfK 3969 (1985) 68

(3) S. Fraga, J. Karwowski, and K.M. Saxena, Atomic Energy Levels (Elsevier Scientific Publiching Company, Amsterdam - Oxford - New York 1979).

+ Politechnika Poznańska, Instytut Fizyki, ul. Piotrowo 3, 60-965 Poznán, Poland.

2.8 HETERODYNE FRAQUENCY METROLOGY FOR LASER RADIATION

K. Bekk, M. Eichenlaub, D. Knauß, and G. Meisel

During the past few years lasers were considerably improved with respect to their frequency stability and reproducibility. This is particularly true for cw dye lasers which are a very useful tool since they can be tuned to any frequency within the visible region and beyond (1). The frequency fluctuations for such lasers have been reduced down to 100 Hz (2,3) approaching the quality of a phase locked oscillator. The relative frequency stability of such laser is of order 10^{-13} indicating a great potential for precision measurements.

Oscillators used for high precision measurements require a correspondingly good frequency measuring technique. This in turn requires reference oscillators of high quality to compare the frequency of the laser in question with. Several oscillators as required are presently available, namely at 632.8, 612.0 and 514.7 nm (4,5,6,7). The comparison typically is performed interferometrically; therefore the two laser beams must be very well controlled geometrically, of particular importance is their parallelism. The error is of order cosα where α is the non-zero angle between the beams. For 10^{-10} accuracy, e.g. $\alpha < 10^{-5} \approx 2$ arc sec is necessary; this corresponds to a non-parallelism of 1 mm over a 100 m distance which is difficult to control since the beams must be made of wide aperture to reduce diffraction problems. The diffraction corrections are a further source of error that have lead to inconsistent results (8,9,10,11).

To overcome the limitations of interferometric frequency measurements, frequency related methods are to be applied that are not subject to geometrical problems. A scheme has been developed that is based on the heterodyne technique. The difficulty is to bridge the gap between one arbitrarily chosen optical frequency and the nearest reference oscillator since this gap can be many THz wide. A beat frequency of this size cannot be determined directly since present microwave technology is limited to several hundred GHz. The concept for a solution followed here is to cut the wide gap into many intervals of 80 GHz width. Two cw dye lasers are used as interpolating oscillators that are tuned to the intermediate frequencies 80 GHz apart. Thus the wide gap is determined as the sum of many difference frequencies (12,13).

For this purpose two cw ring dye lasers of special disign (14) are being set up. They are to operate with Rhodamine B between 612 and 633 nm since it is planned to compare the two iodine stabilized HeNe lasers operating at these wavelengths; this experiment will test the interferometric comparison of these two secondary standards on a 10^{-9} to 10^{-10} level. In addition a frequenvy stabilization for each of them that is designed to allow difference frequency determinations to within 1 kHz or better (15) is being constructed and tested. It uses an electro-optical phase modulator for peak lock to a reference etalon resonance by fast phase sensitive detection. Its feedback system is designed for 1 MHz cutoff frequency to reduce the fast frequency jitter of the dye laser.

The rf system has been rebuilt; it contains a phase locked gunn oscillator operating at 80 GHz which is used as local oscillator. The 3 E-band mixers required were supplied with Schottky diodes (16) and tested.

(1) G. Meisel, Laser and Optoelectronik 15 (1983) 105 and 245
(2) T.W. Hänsch, B. Couillard, Opt. Comm. 35 (1980) 441
(3) J.L. Hall, L. Hollberg, Ma Long-schen, T. Baer, and H.G. Robinson, J. de Physique 42 (1981) C8-59
(4) F. Bayer-Helms (ed.), PTB-Bericht Me-17 (1977)

(5) K.G. Dschao, J. Helmcke, G. Reim, PTB-Jahresbericht (1979) 132
(6) F. Spieweck, IEEE Trans. IM-27 (1978) 398
(7) F. Spieweck, G. Camy, and P. Gill, Appl. Phys. 22 (1980) 111
(8) S.R. Amin, C.D. Caldwell, and W. Lichten, Phys. Rev. Lett. 47 (1981) 1234
(9) J.R.M. Barr, J.M. Girkin, A.I. Ferguson, G.P. Barwood, P. Gill, W.R.C. Rowley, and R.C. Thomson, Opt. Comm. 59 (1985) 217
(10) E.A. Hildum, M. Boesl, D.H. McIntyre, R.G. Beausoleil, and T.W. Hänsch, Phys. Rev. Lett. 56 (1986) 576
(11) J.C. Garreau, F. Biraben, L. Julien, and B. Cagnac, Abstracts of the 18th EGAS Conference, Marburg (1986)
(12) B. Burghardt, H. Hoeffgen, H. Kriz, and G. Meisel, in: PTB report PTB-E-18 (1981) 171
(13) B. Burghardt, H. Hoeffgen, G. Meisel, W. Reinert, and B. Vowinkel, in: Precision Measurement and Fundamental Constants II, eds. B.N. Taylor and W.D. Phillips; Natl. Bur. Stand. (U.S.), Spec. Publ. 617 (1984) p.49
(14) H. Kriz, Diplomarbeit, Bonn 1980 (unpublished)
(15) H. Hoeffgen, Dissertation, Bonn 1982 (unpublished)
(16) B. Burghardt, H. Hoeffgen, G. Meisel, W. Reinert, and B. Vohwinkel, Appl. Phys. Lett. 35 (1979) 498.

3. NEUTRINO PHYSICS

Karlsruhe Rutherford Medium Energy Neutrino Experiment KARMEN

G.Drexlin, H.Gemmeke, G.Giorginis, W.Grandegger, A.Grimm,
R.Gumbsheimer, J.Hesselbarth, H.Hucker, L.Husson,
J.Kleinfeller, D.Mann, R.Maschuw, M.Momayezi, K.H.Ottmann,
P.Plischke, F.Raupp, M.Reuscher, F.K.Schmidt,
G.Spohrer, P.Wild, S.Wölfle, J.Wochele, B.Zeitnitz
Kernforschungszentrum Karlsruhe, IK I and University of
Karlsruhe
E.Finckh, W.Kretschmer, K.Stauber, D.Vötisch, J.Böttcher
University of Erlangen
N.E.Booth
Oxford University
J.A.Edgington, G.Marinos, A.Ryan, J.M.Lafontaine
Queen Mary College, London
A.Dodd, Rutherford Appleton Laboratory, Chilton

KARMEN denotes a programme of neutrino physics to be performed at the pulsed spallation neutron source ISIS at the Rutherford Appleton Laboratory (RAL). Its main purpose is to contribute to the questions of neutrino oscillations, neutrino nuclear excitation and neutrino electron scattering in the energy range from 5 to 50 MeV (1,2). The feasibility of these experiments is closely related to the distinct time structure of the ISIS neutrino source providing ν_μ as well as ν_e and $\bar{\nu}_\mu$ from π^+-decay at rest.

Two detectors are intended to be employed. A first 60 t scintillation calorimeter being currently assembled is scheduled to operate early in 1987.

3.1 STATUS OF THE PROJECT

3.1.1 NEUTRINO AREA

The KARMEN experimental area at RAL is now completed. Its most significant part is a 6000 t shielding bunker (inner dimensions 10 x 4 x 7 m^3) with 2 m thick steel walls and a 3 m thick steel roof. A 500 t sliding door opens into a 200 m^2 large experimental hall for detector assembly and service and for housing of the electronics.

3.1.2 KARMEN 1 DETECTOR

KARMEN 1 is a 60 t. liquid scintillation calorimeter dedicated to detect neutrino reactions on ^{1}H- and ^{12}C-nuclei with high precision. Time resolution will be about 1 nsec in order to make use of the time structure of the ν-beam. Energy resolution is designed to be 10% FWHM at 10 MeV absorbed energy.

The mineral oil based scintillator is contained in one single tank with dimensions 3.2 x 3.5 x 6 m^3. A totally reflecting lucite structure divides the central detector into 512 optically isolated modules (18 x 18 x 350 cm^3) each viewed by two 3" phototubes XP 3462 from either end.

Despite some difficulties with the manufacturer the detector vessel finally arrived at RAL. We completed the tank to be ready now for component assembly.

The phototubes have been mounted to form a complete phototube unit with PVC support, μ-metal screen, optical fibre guide pipes, bleeder, signal- and high voltage connections. Matched to pairs they are now being inserted into Al-sleeves with glass windows, already mounted to the detector head walls allowing to look into the scintillator volume, see fig.1.

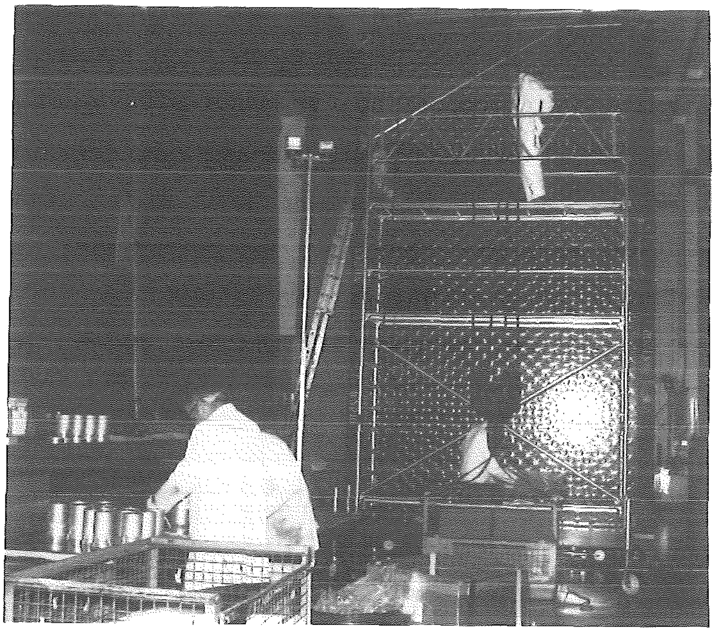

Fig.1: View of detectors head wall.

Two thirds of 1800 lucite double sheets needed to form the optical structure have been manufactured at KfK. Further mass production will continue now that some problems occuring during the prototyp III operation at KfK have been overcome.

With the exception of the optical structure which will be installed in subsequent stages, mechanical assembly of the detector is scheduled to be finished at the end of 1986. This includes cabling as well as parts of the anticounter system currently manufactured at Erlangen.

Thus we expect the first subunit being operational at the beginning of 1987. At that time the electronics trailer, the data handling system as well as the UV-laser calibration system will be linked to the detector to perform first cosmic ray calibration experiments.

The ISIS proton accelerator currently runs at 550 MeV with approx. 30 µA intensity. Meanwhile two more cavities have been installed and beam improvements are continously going on to push the accelerator to its design values of 800 MeV and 200 µA.

3.1.3 PHOTOMULTIPLIER TESTS

Each scintillator module of the main detector will be viewed by two 3" photomultipliers (PM) on both sides of the detector. The outputs of the two PM of one scintillator module end are connected by "Wired Or" within a specially designed junction box. Using the same high voltage supply for both PM it is necessary to match the PM-parameters to pairs to guarantee optimal energy and time resolution and stable operation for several years. The specifications of all of the 2500 PM of type XP 3462/PA were tested at the RAL test facilities, i.e. linearity, gain, single electron resolution, noise and ^{57}Co-resolution with a NaJ. The PM are matched to pairs by a computer program. The fabrication of the photomultiplier mounting units (see fig.3) designed to give save containment and magnetic shielding is almost finished. The PM are now completely tested at prototype III at KfK. At the end of September first units will be mounted at KARMEN 1. In the meantime some new results from prototype I with these photomultiplier pairs give projected resolutions for KARMEN 1 of $\sigma_E/E = 14.5\%/\sqrt{E}$ and $\sigma_t = .7$ ns or $\sigma_x = 5$ cm respectively (latter values at $E = 25$ MeV).

3.1.4 ELECTRONICS

In October 1985 we decided on the construction of an air-pad movable electronic platform (trailer). The trailer should contain the distribution of the cables for the 2512 PM of KARMEN 1, the front-end electronics, the computer controlled high-voltage system and cable distribution, timing and neutrino-trigger logic, Camac data conversion and control system with computers, laser calibration and distribution system. Mechanical construction started at the beginning of 1986 and installation of cables and electronics will be mostly finished within this year with the exception of the external cooling system for the electronics and 80% of the front-end-cards which will be delivered in line with installation of the optical structure of the detector.

Right now the bus system for the front-end cards and the first version of the software controlled event pattern (SCEPTU) unit are tested simultaneously. These new units introduce some changes in the interfacing of the different levels of the data-taking system, especially on the front-end card ASTERIX (analogue signal & time range integrator & multiplexer) and the ADC-interface. Fig.2 shows the last working version of ASTERIX which will go to mass production (200 cards) in October 1986. The card consists of control and interface logic for four scintillation modules, 8 gated charge integrators, fast leading edge discriminators, time-amplitude converters (TAC) and test-pulse generators. The layout of the very compact multilayer board reflects the symmetry of this design. The linearity of integrators and TAC's is better than two least significant bits measured in a 10 bit range.

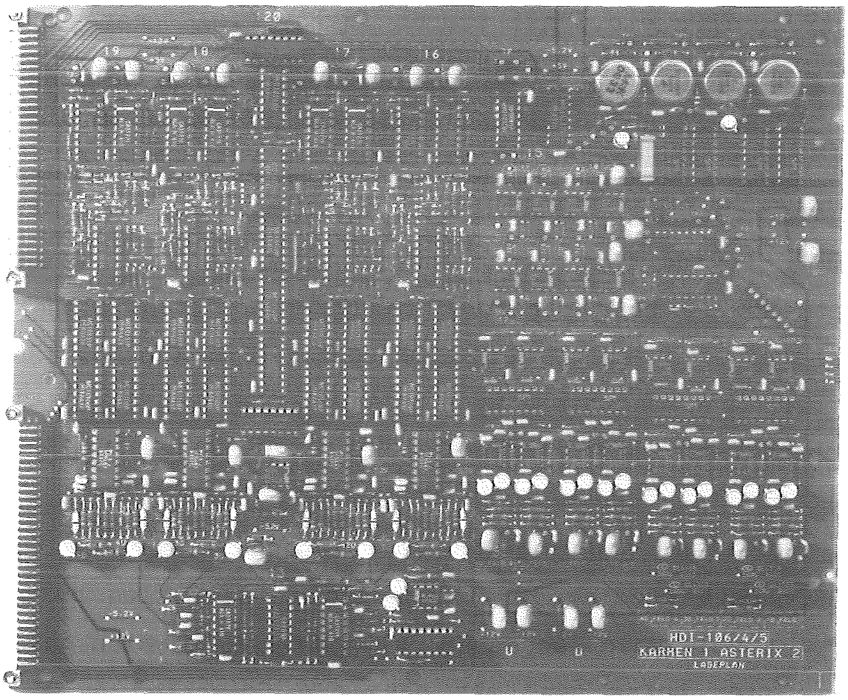

Fig.2: Front-end card ASTERIX

Results from precise n-background measurements at RAL and Monte-Carlo simulations of cosmics allow a better design of the trigger logic. Prototyp III at KfK is a very realistic playground for testing these triggers and the growing electronics. So we have the opportunity to test the electronics at this detector before the trailer is shipped to RAL at the end of January 1987.

3.1.5 DATA ACQUISITION FOR KARMEN 1

Within the 20 ms period of the ISIS beam, only the first few microseconds during beam-on and shortly after yield neutrino-induced events. The signature of some reactions includes a subsequent γ or β-decay with half-lives of up to 11 ms. Thus event data of one beam period are logically related. Only the first 16 ms of each period are utilized for measuring. Up to 8 events may be acquired during this time. The remaining 4 ms serve for reading the data from CAMAC units (ADCs, TDCs etc.) all housed in one CAMAC crate. Reading must be done within this time or otherwise neutrino events from the next beam pulse will be lost. Data include digitized time and energy from the detector modules, event time relative to the beam pulse, and some status and normalization information.

A CAMAC housed fast front-end processor (ACC 2180 auxiliary crate controller with DEC J-11 processor) is operated stand-alone in order to guarantee the required speed of real-time operations. The low 128 kByte of its fast static memory are accessible by a host computer via CAMAC. The host loads the RSX-11S operating system including all application tasks into the ACC memory. A "control" task keeps track of the experimental status, performs all time-critical operations and includes the interrupt service for data to be read from CAMAC. Data reading in a fast cycle is enabled by a special high speed read CAMAC module which accesses only those ADCs which have data for the current event. After being read the data are formatted by a separate task during the next 16 ms of measuring time and stored in a buffer of 8 kByte size. When a buffer is filled, it is read out by the host computer. Communication between ACC and host in both directions is initialized by an interrupt and synchronized by flags in the dual-ported ACC memory.

The host computer is a standard LSI-11/73 system operating under RSX-11M. It controls the conditions and all activities of the experiment including data handling, HV supplies, laser calibration, SCEPTU test pulsing system, temperature and voltage monitoring etc. For testing and monitoring, a second CAMAC crate is used. For command input and display of information graphic terminals, touch panel displays, and a printer are available. A variety of tasks operate in the host computer at different software priorities. Communication between and synchronization of the tasks is achieved by send data / receive data requests, and by event flags.

The experiment data are finally written to magnetic tape and/or transferred to a VAX-11/750 computer for further processing. Programming for the ACC has been done by HDI and is nearly finished. Programming for the host computer is going on.

3.2 PROTOTYPE III

Prototype III is the final test facility for KARMEN 1 design and electronics. It contains 8 tons of PMP loaded liquid scintillator with 35 central scintillator modules having same dimensions and features as the KARMEN 1 modules. All mounting facilities, Al-sleeves for PM-units and PM-units (as shown in fig.3) are the same as for KARMEN 1. In the course of painful testing and handling procedures we learned to correct the final assembly tools and parts. More difficulties arise from leakage tightness and assembly of optical segmentation, see fig. 4. Final tests are scheduled for October 1986.

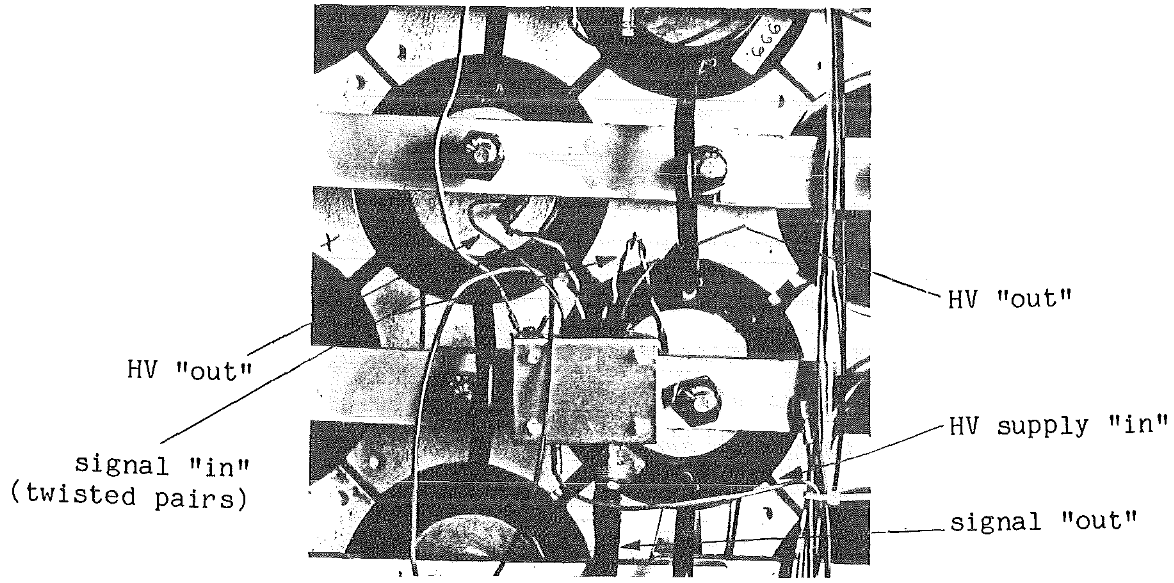

Fig.3: PM unit with distributor box.

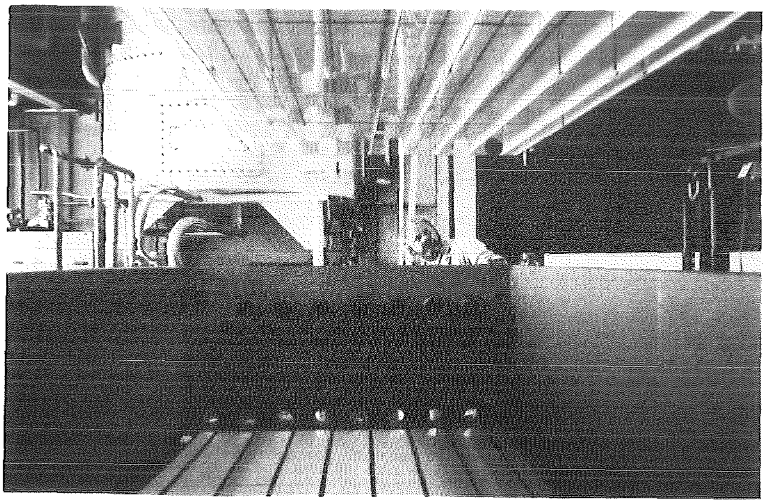

Fig.4: Installation of optical segmentation into prototype III vessel.

Prototype III was set up to get the exact position dependent light output curves, time, spatial and energy resolution. These calibrations are necessary to fix the parameters for ν-detection-efficiency of KARMEN 1 described in the next section. In order to track the cosmic events with high precision (1 cm position resolution) multiwire proportional chambers have been installed on top and bottom of the detector. This procedure is not possible with KARMEN 1.

Furthermore the coupling of the optical fibres to the detector modules for laser calibration was tested with satisfactory results. First data obtained with cosmics and laser both indicate an energy resolution that is better by 20% than in prototype I.

3.3 MONTE-CARLO SIMULATION OF NEUTRINO EVENTS IN KARMEN 1

A Monte Carlo program was developed to evaluate the efficiency of KARMEN 1 to detect neutrino induced reactions. The program simulates the transport of particles emitted in a neutrino reaction as well as the detector response in three steps:

1. Using the geometry of the neutrino source relative to the detector, the energy distribution of the ν-source at RAL, the modular structure of detector, the energy dependent differential cross sections, and also applying relativistic kinematics the position of a reaction, energy and momenta of emitted particles are determined randomly within the detector.
2. Particles are transported by the standard codes EGS and MORSE yielding the energy loss and particle tracks inside the different materials of the detector.
3. In the third step the energy loss in the scintillator is converted to light and the position dependent light output L(x,y,z) is calculated. L(x,y,z) is determined by calibration measurements and a special light transport Monte Carlo. Taking into account the photomultiplier parameters the simulation produces the number of photoelectrons per event in each scintillator module.

Calculations have been performed for the reactions $\bar{\nu}_e + p \rightarrow n + e^+$ and $\nu_e + {}^{12}C \rightarrow {}^{12}N + e^-$ which will be used to detect neutrino oscillations and $\nu + {}^{12}C \rightarrow {}^{12}C^* + \nu$ to detect inelastic neutrino-nucleus scattering.

In the following the results of the inelastic ν-${}^{12}C$ scattering will be described. The trigger for this reaction is the decay of the excited ${}^{12}C^*$ nucleus to the groundstate by the emission of a 15 MeV gamma. In fig.5 an example of such an event is shown.

The detection efficiency ε of the 15 MeV gammas is correlated to the starting point within the detector. ε amounts to 82% for events starting in the inner modules and decreases e.g. to 40% at 10 cm from the detector corners. The efficiency is not strongly dependent on the energy threshold because of the good energy resolution of the detector. Increasing the threshold from 10 to 100 photoelectrons the efficiency changes only from 82% to 79%.

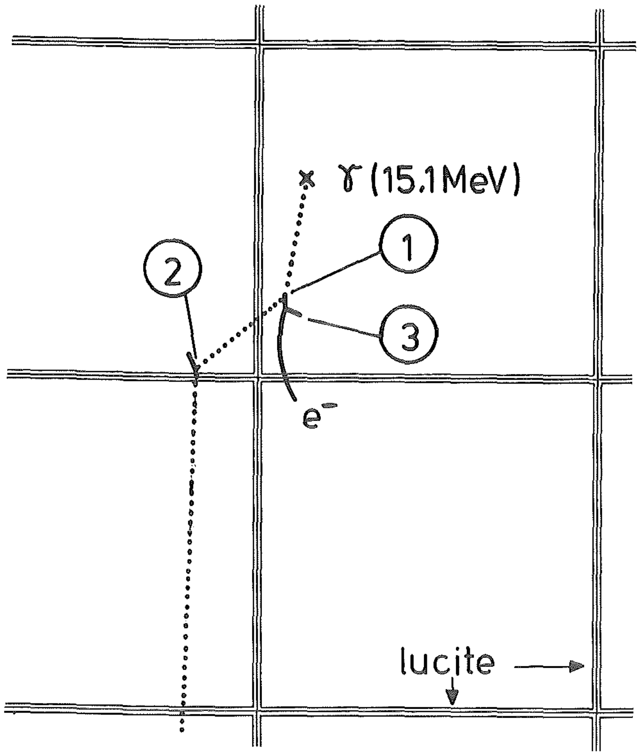

Fig.5: Example of a 15 MeV γ-event in KARMEN 1.
① compton scattering of a 13.2 MeV electron. ② compton scattering of a 1.4 MeV electron. ③ Møller scattering: delta-electron of 1.8 MeV emitted.

A fast on-line trigger should reject background events by inspection of sum-energy and multiplicity of triggered scintillator modules. Cosmic background has a mean energy loss of about $\sum E \sim 500$ MeV and multiplicities of about $\bar{m} \approx 25$ in KARMEN 1, while low energy background is dominantly distributed at sum-energies below 5 MeV. The simulated "on-line" energy distribution is smeared out because of the position dependence of the light output. The Monte-Carlo simulations show that "on-line" the inelastic neutrino scattering has a very distinct pattern in sum-energy and multiplicity (fig.6) yielding a very efficient trigger for these events and a good rejection ratio against background.

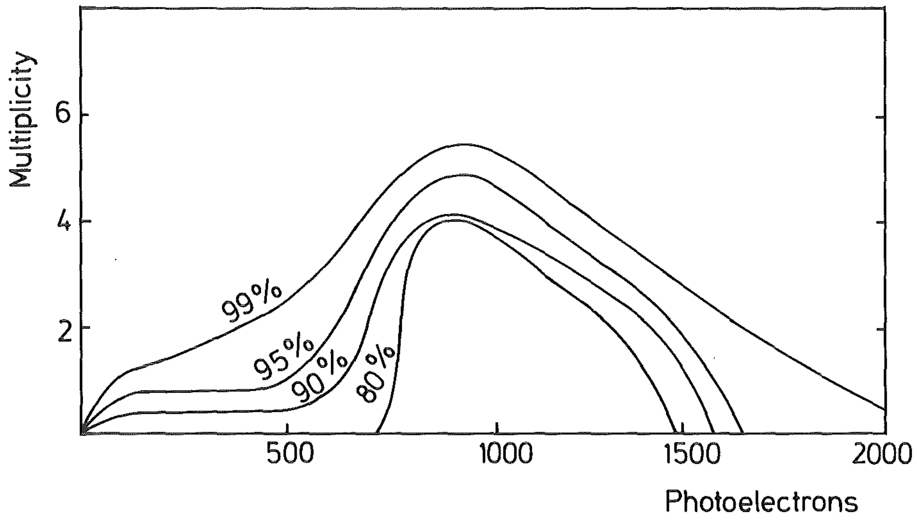

Fig.6: Distribution of 15 MeV γ-events as a function of the number of photoelectrons and multiplicity. 80% of the events are distributed within the inner contour line. The outer line includes 99% of all events.

In the "off-line" data simulation the energy resolution will be enhanced by correction for the position dependency of the light output. The "on-line" uncorrected sum-energy yields an energy resolution of 16.7% while the corrected "off-line" energy resolution for E_γ = 15 MeV is 15%.

(1) R.Maschuw, B.Zeitnitz, KfK 3362 (Juni 1982)
(2) B.Zeitnitz, Progress in Particle and Nuclear Physics 13 (1985) 445

4. INTERMEDIATE ENERGY PHYSICS

4.1 PION-NUCLEUS INTERACTIONS

4.1.1 INVESTIGATION OF THE FINAL STATE INTERACTION IN THE $\pi^+ d \rightarrow \pi^+ pn$ CROSS SECTION

W. List, E.T. Boschitz, H. Garcilazo, R.R. Johnson[+], C.R. Ottermann, R. Tacik, M. Weßler, U. Wiedner

The πd break up reaction has been investigated extensively by our group in earlier experiments [1,2,3]. In one of these experiments the triple differential cross section $\frac{d^3\sigma}{d\Omega_\pi d\Omega_p dP_p}$ has been measured as a function of the proton momentum for many pion proton angle pairs at 228 MeV and 294 MeV incident pion energy. The comparison with predictions from the relativistic Faddeev theory of Garcilazo showed an impressive overall agreement with the large data set. In these measurements a CD_2-target has been used. The background reaction from Carbon in CD_2 was measured in a separate experiment and properly subtracted. The off line analysis showed, however, that in the region of very small cross sections (it varies by 5 orders of magnitude in the kinematical range investigated) the statistical accuracy of the data was marginal for a detailed comparison with the final interaction effects predicted from Garcilazo's theory.

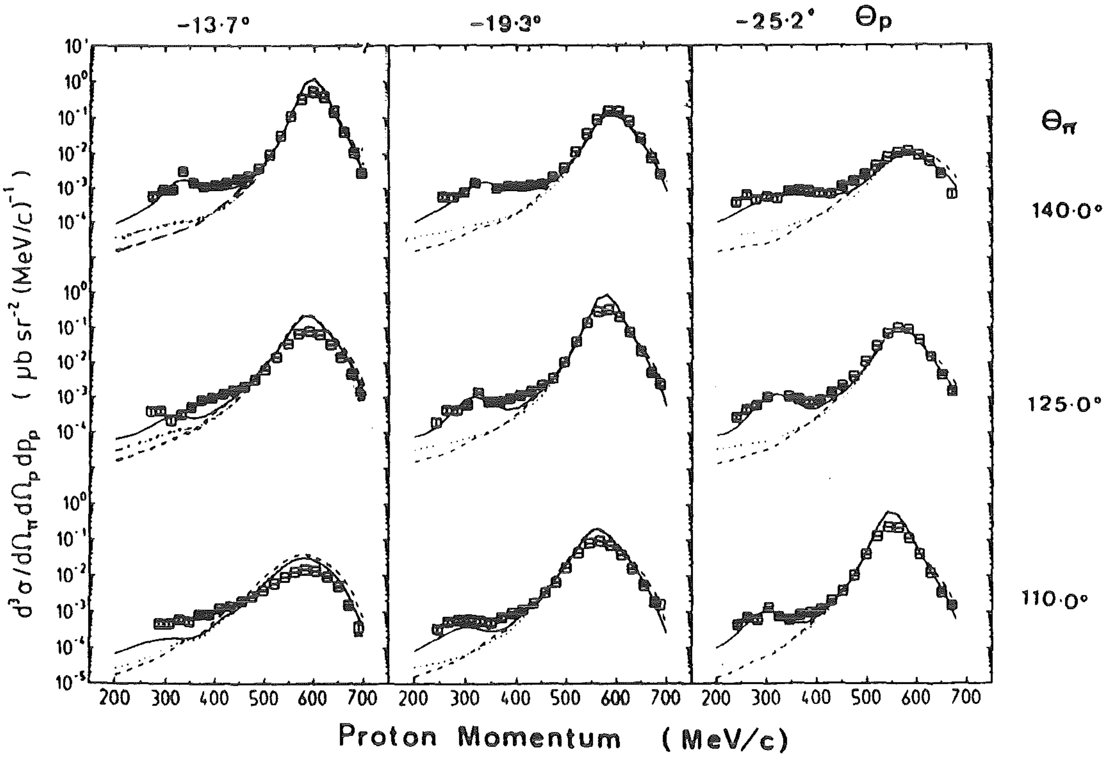

Fig. 1 Comparison of preliminary data of the πd break up cross section with predictions from the relativistic Faddeev theory of Garcilazo (see text). The incident pion energy was 294 MeV.

For this reason in March 1986 a liquid deuterium target cell with very thin Mylar windows was built and brought in operation. In order to see the final state interaction most pronounced we chose T_π = 294 MeV, and the kinematical region of small proton and large pion angles. While the pion detectors were the same as in the earlier experiments the proton detectors consisted of large $\Delta E - E$ scintillator arrangements (thick counter 20 x 70 cm^2 in area and 20 cm thick). The data analysis has not been completed yet, in particular, some corrections (like unfolding the momentum resolution and calibrating the time-of-flight measurements) still have to be applied. Preliminary data are shown in Fig. 1 together with the predictions from Garcilazo. The solid line corresponds to the full Faddeev calculations (with final state interaction included), the dashed line to the Faddeev calculation without the final state interaction, and the dotted line corresponds to the impulse approximation. The comparison shows that the full Faddeev calculation reproduces most of the data in the final state interaction region extremely well.

(1) E.L. Mathie et al., Phys. Lett. 154B(1985)28
(2) W. Gyles et al., Phys. Rev. C33(1986)583
(3) W. Gyles et al., Phys. Rev. C33(1986)595

+ TRIUMF and University of British Columbia, Vancouver, B.C., Canada

4.1.2 MEASUREMENT OF iT_{11} IN THE $\pi^+d \rightarrow \pi^+pn$ REACTION AT T_π = 134 MeV and 228 MeV

W. List, E.T. Boschitz, H. Garcilazo, W. Gyles, J.A. Konter[+], S. Mango[+], C.R. Ottermann, G.R. Smith[++], B. van den Brandt[++]

In order to provide new data for iT_{11} in the πd break-up reaction at an incident pion energy below the $\Delta(3,3)$ resonance, and to extend the existing data set at one energy into an extreme kinematical region (very small proton, very large pion angles) data have been taken at T_π = 134 MeV and 228 MeV. The experimental set up has been the same as in the earlier experiment$^{1)}$. The vector polarized target consisted of a ^{3}He cryostat and deuterated butanol for the target material. The target polarization has been rather low in this particular experiment, namely P^- = 0,153 ± 0.010 and P^+ = 0,145 ± 0,012. Only a quarter of the data is shown in Fig. 1. The data are compared with predictions from the relativistic Faddeev theory of Garcilazo. Similar to the results found in the earlier experiment at T_π = 180, 228 and 294 MeV, also at 134 MeV the agreement between theory and experiment is quite good within the statistical accuracy.

(1) W. Gyles et al., Phys. Rev. C33(1986)595

+ SIN, Villigen, Switzerland
++ TRIUMF, Vancouver, B.C., Canada

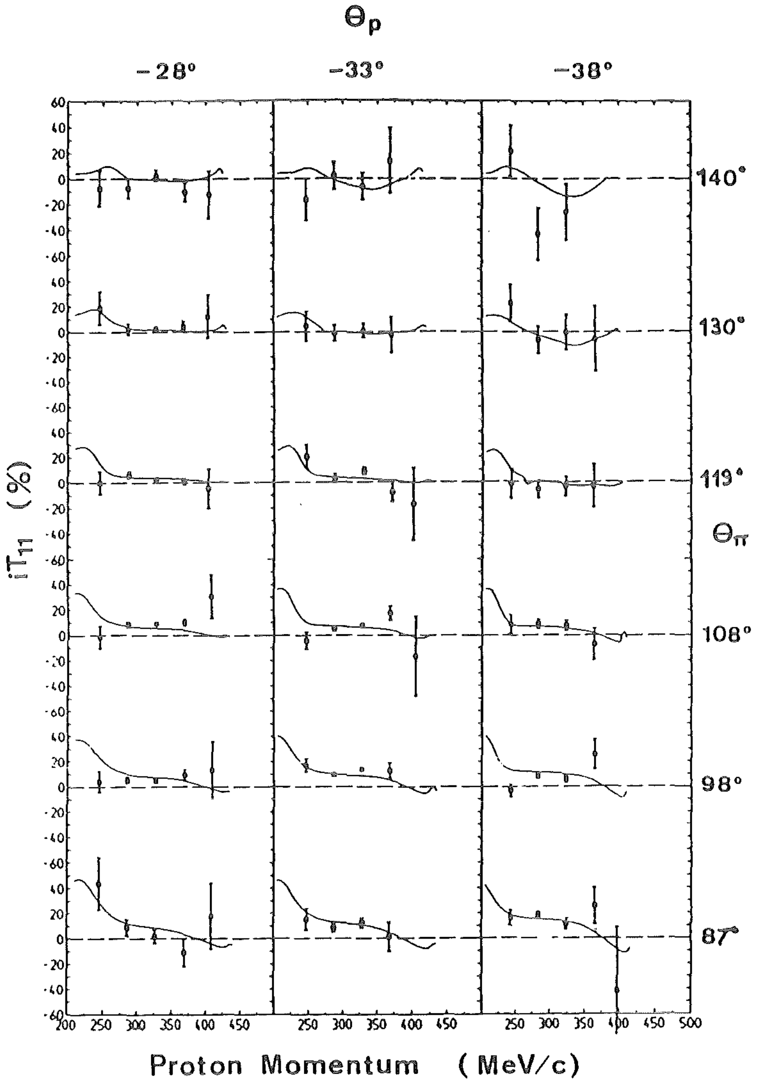

Fig. 1 Comparison of the vector analyzing power iT_{11} in the πd breakup reaction at T_π = 134 MeV with predictions from the relativistic Faddeev theory of Garcilazo.

4.1.3 TENSOR ANALYZING POWER t_{20} IN πd ELASTIC SCATTERING AT T_π = 134 MeV AND 151 MeV

G.R. Smith[+], A. Altman[+], P. Delheij[+], D.R. Gill[+], D. Healey[+], R.R. Johnson[+], G. Jones[+], D. Ottewell[+], F.M. Rozon[+], M.E. Sevior[+], F. Tervisidis[+], R.P. Trelle[+], G.D. Wait[+], P. Walden[+], G.J. Lolos[++], E.L. Mathie[++], S.I.H. Nagni[++], E.T. Boschitz, C.R. Ottermann, G.S. Kyle[+++], P.A. Amandruz[++++].

For the past several years, one of the most intriguing questions in intermediate energy pion physics has revolved around two sets of conflicting measurements of the tensor polarization, t_{20}, in πd elastic scattering. One set of measurements by an ETHZ group at SIN indicated that t_{20} is mostly positive, with striking, oscillatory angular distribution at T_π = 134 MeV; and a rapid energy dependence at θ_π = 150°. These data were considered evidence for the existence of a dibaryon resonance. Independent measurements at T_π = 142 MeV made by a group at LAMPF revealed a flat angular distribution of negative t_{20} values, and a smooth energy dependence. Both experiments employed the same technique for t_{20}, namely, recoil deuterons from πd elastic scattering events were analyzed in a second scattering within a ^{3}He cell polarimeter via the ^{3}He (d,p) reaction. Recently, an independent measurement of t_{20} was carried out at TRIUMF which used the same double scattering technique as both the ETHZ and LAMPF experiments. The TRIUMF data agreed with the LAMPF results. Although this experiment appeared to have resolved the discrepancy, doubts remained because the technique and geometry of the TRIUMF polarimeter was rather similar to the one used at LAMPF.

In order to provide an independent test the tensor analyzing power, T_{20}, for πd elastic scattering has been measured with a tensor polarized deuteron target in a single scattering experiment. The experiment was performed at the M_{11} beam line at TRIUMF. The magnetic field of the polarized deuteron target (the spin alignment axis) was oriented longitudinally with respect to the incident pion beam. For this orientation there is a simple relationship between the tensor analyzing power, T_{20}, the target tensor polarization (alignment), P_{zz}, and the cross sections measured with the target being polarized or unpolarized, σ_{pol} and σ_{unpol}, namely

$$T_{20} = \frac{\sqrt{2}}{P_{zz}} \left(\frac{\sigma_{pol}}{\sigma_{unpol}} - 1 \right)$$

The cross sections were measured with a multi counter time-of-flight set up similar to the one used for a series of iT_{11} measurements by our group at SIN.

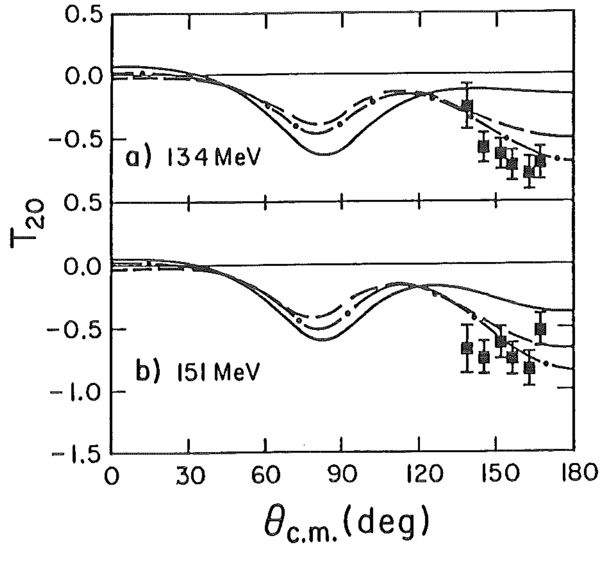

Fig. 1
The tensor analyzing power T_{20}^{cm} data obtained in this experiment are compared to calculations at T_π = 134 MeV (a) and 151 MeV (b). The solid curve (full calculation) and dash-dot curve (no P_{11} rescattering and no absorption) are from Blankleider and Afnan. The dashed curves are from Garcilazo

Data were taken of two energies, T_π = 134 and 151 MeV for 6 scattering angles between 135° and 170°. The target alignment P_{zz} was calculated from the expression $P_{zz} = 2 - \sqrt{4 - 3P_z^2}$, where P_z is the target vector polarization. P_z was determined from standard NMR techniques. In addition, P_{zz} was measured directly by utilizing the known tensor analyzing power at 90° c.m. in the $\pi d \rightarrow 2p$ reaction. This measurement is described in the following contribution.

The results are shown in Fig. 1 in comparison with different theoretical predictions (see figure caption). In order to help decide which of the t_{20} measurements are the correct ones, one must remember that t_{20}^{lab} is a linear combination of T_{20}^{cm}, T_{21}^{cm} and T_{22}^{cm}, while the quantity measured in this experiment, $T_{20}^{lab} = T_{20}^{cm}$. For a model independent comparison we utilized the maximum theoretically possible bounds on T_{21} and T_{22}, namely $\pm \frac{\sqrt{3}}{2}$. From our T_{20}^{cm} data and these limits on T_{21} and T_{22} the allowable band for t_{20}^{lab} is entirely negative in contrast to the ETHZ data at SIN which reach positive value as high as + 0.6.

+ TRIUMF, Vancouver, B.C., Canada
++ University of Regina, Regina, Sask, Canada
+++ New Mexico State University, Las Cinces, N.M., USA
++++ SIN, Villigen, Switzerland

4.1.4 DIRECT MEASUREMENT OF THE TENSOR POLARIZATION OF A POLARIZED DEUTERON TARGET

G.R. Smith$^+$, D.R. Gill$^+$, D. Healey$^+$, R.R. Johnson$^+$, G. Jones$^+$, D. Ottewell$^+$, M. Rozon$^+$, M. Sevior$^+$, F. Tervisidis$^+$, R.P. Trelle$^+$, P. Walden$^+$, E.L. Mathie^{++}, S.I.H. Naqvi^{++}, G.J. Lolos^{++}, E.T. Boschitz, C.R. Ottermann, G.S. Kyle^{+++}, P.A. Amandruz^{++++}

Tensor polarized deuteron targets have been employed in nuclear reaction studies only very recently[1,2]. For these experiments the reliable determination of the tensor polarization (alignment) P_{zz} of the target is important. The standard way to obtain this quantity is to utilize the relationship between vector and tensor polarization, i.e. $P_{zz} = 2 - \sqrt{4 - 3P_z^2}$. This relationship is valid under the assumption that the relative population of the magnetic substates of the deuteron are given by a Boltzmann distribution, and that the effects of the deuteron quadrupole moment are negligible. Both assumptions are generally considered reasonable. P_z is then determined from standard NMR techniques, i.e. measuring the area enhancement of the dynamical signal over the thermal equilibrium signal (the polarization of the latter can be calculated) or measuring the asymmetry of the doubly peaked dynamical signal. Both techniques contain inherent problems: the accurate measurement of the very small thermal equilibrium signal, and the reliable determination of the shape of the NMR signal which depends on the target material, solid state effects in the target and the characteristics of the NMR readout system.

For this reason it seemed appropriate to look for an independent method of determining P_{zz}. This can be achieved by measuring with the tensor polarized target a reaction for which the tensor analyzing power is well known. Such a reaction is the pion absorption on the deuteron at 90° c.m. Due to the dominance of the reaction amplitude a_2, and the cancellation of other amplitudes at 90° c.m. in the $\pi d \rightarrow 2p$ reaction, $T_{20}(90°) \approx -\sqrt{2}$, almost independent of incident pion energy. The exact value of $T_{20}(90°)$ at a particular energy can be obtained in three different ways, (1) from theoretical predictions, (2) from predictions of partial wave analyses, and (3) from existing experimental data of A_{yy} utilizing the relationship at 90°: $T_{20} = \frac{\sqrt{2}}{4}(3A_{yy} - 1)$. The values found in this way for $T_\pi = 80$ MeV were close to each other, the average being $T_{20} = -1,28 \pm 0,03$. The pion energy of 80 MeV was chosen for geometrical reasons (the protons should be emitted close to ± 90° to pass the gap of the polarized target magnet). The magnetic axis of the tensor polarized target was oriented parallel to the incident pion beam. For this orientation the tensor analyzing power simplifies to $T_{20} = \frac{2}{P_{zz}}\left(\frac{\sigma_{pol}}{\sigma_{unpol}} - 1\right)$ where σ_{pol} and σ_{unpol} are the differential cross sections with the target being polarized or unpolarized. The incident pion beam was counted directly with scintillation counters; the two outgoing protons were detected in coincidence by scintillator telescopes and delay line readout wire chambers. The cross sections σ_{pol} and σ_{unpol} were determined utilizing coplanarity or time-of-flight information. From these data and the "known" T_{20} value P_{zz} was calculated to be $P_{zz} = 0,098 \pm 0,024$ (coplanarity) and correspondingly by $P_{zz} = 0,100 \pm 0,022$ (time-of-flight). These values can be compared with those from the NMR signal "area" analysis, $P_{zz} = 0,083 \pm 0,008$ and the NMR signal "asymmetry" analysis $P_{zz} = 0,095 \pm 0,008$. The larger uncertainty associated with the present measurement arize from the statistical uncertainty of the measured cross section after background subtraction.

(1) W. Meyer, Helv. Phys. Acta 59(1986)728
(2) G.R. Smith et al., Phys. Rev. Lett. 57(1986)803

+ TRIUMF, Vancouver, B.C. Canada
++ University of Regina, Sask., Canada
+++ SIN, Villigen, Switzerland
++++ New Mexico State Univ., Las Cruces, N.M.,USA

4.1.5 MEASUREMENT OF T_{20} AND "T_{21}" IN πd ELASTIC SCATTERING

G.R. Smith[+], D.R. Gill[+], D. Healey[+], R.R. Johnson[+], G. Jones[+], D. Ottewell[+], M. Rozon[+], M. Sevior[+], R.P. Trelle[+], G. Wait[+], P. Walden[+], E.L. Mathie[++], S.I.H. Naqvi[++], G.J. Lolos[++], W. Gyles, C.R. Ottermann, G.S. Kyle[+++]

As a continuation of T_{20} mesaurements in πd elastic scattering at TRIUMPF in December 1985 T_{20} has been measured this spring at three more pion energies (T_π = 180, 219 and 256 MeV) at large angles. As in the previous measurement the tensor polarization of the deuteron target amounted to $P_{zz} = 0{,}08$. The data are presently being analyzed.

In the course of this experiment the set up has been changed to allow for the measurement of other tensor observables. While for the T_{20} measurement the spin alignment axis of the polarized target has been parallel to the incident pion beam, for the new measurement the target has been at 45° to the incident beam; but still in the scattering plane. In this geometry a linear combination of the three tensor observables T_{20}, T_{21}, T_{22} is measured, according to the expression:

$$"T_{21}" \equiv \frac{1}{2} \left(\frac{T_{20}}{\sqrt{6}} + T_{22} \right) + T_{21} = \frac{1}{2\sqrt{3}} \cdot \frac{1}{P_{zz}} \left(\frac{\sigma_{pol}}{\sigma_{unpol}} - 1 \right)$$

where P_{zz} is the target tensor polarization and σ_{pol} and σ_{unpol} are the differential cross sections for the target being polarized or unpolarized, respectively. The experimental problem for this set up arises from the fact that due to the "skewed" magnetic field of the superconducting Helmholtz coils of the polarized target the trajectories of incident as well as scattered particles are no longer in the scattering plane. Therefore the detectors have to be placed out of the scattering plane, different for each pion and deuteron scattering angle. The "effective" scattering plane is also different for each pion angle. In order to minimize these effects the polarized target was operated in the "frozen spin" mode with the magnetic field lowered to half of its normal value (26 kG). The data were taken for 180 MeV incident pion energy. The data analysis is in progress.

+ TRIUMF, Vancouver, B.C., Canada
++ University of Regina, Regina, Sask., Canada
+++ New Mexico State University, Las Cruces, N.M. USA

4.1.6 FIRST MEASUREMENTS OF THE TENSOR ANALYZING POWER "T_{22}" IN πd ELASTIC SCATTERING

C.R. Ottermann, E.T. Boschitz, W. Gyles, W. List, J.A. Konter, S. Mango,
E.L. Mathie[+], R. Tacik, B. van den Brand, M. Weßler

In Spring 1986 a new dilution refrigerator for polarized targets has been brought in operation at SIN. The lowest temperature achieved was 60 mK and a cooling power of 4 m Watt around 200 mK, where the target material is polarized. Utilizing this refrigerator and deuterated propandiol as target material vector polarizations around $P_z = 0.40$ have been obtained. This results in a tensor polarization of about $P_{zz} = 0.12$ which is 50% larger than the corresponding value achieved at TRIUMF. With this target and the higher pion fluxes at SIN more accurate polarization measurements can now be carried out in the πd reactions.

In an extended beam period in June/July 1986 we have measured for the first time "T_{22}" as defined by the expression:

$$"T_{22}" \equiv \left(\frac{T_{20}}{\sqrt{6}} + T_{22} \right) = \frac{2}{\sqrt{3}} \cdot \frac{1}{P_{zz}} \left(1 - \frac{\sigma^+ + \sigma^-}{2\sigma_{unpol}} \right), \text{ where}$$

σ^+, σ^-, and σ_{unpol} are the differential cross sections for positive, negative and zero vector polarization. The quantization axis for the polarized target has been perpendicular to the scattering plane. As an additional bonus we also obtain highly accurate iT_{11} data according to:

$$iT_{11} = \frac{1}{\sqrt{3}\,P_z} \cdot \frac{\sigma^+ - \sigma^-}{\sigma^+ P^- + \sigma^- P^+}$$

The data allow to check our earlier iT_{11} measurements obtained with less than half of the present target polarization. On line results already indicate very good agreement with our earlier data[1].

The tensor polarization "T_{22}" has been measured at five pion energies (T_π = 134, 180, 219, 256 and 294 MeV) in the angular range between 80° and 170°. The scattering angles were chosen largely in such a way as to match the angles for the T_{20} and "T_{21}" measurements at TRIUMF. The data are presently being analyzed.

(1) G.R. Smith et al., Phys. Rev. C29(1984)2206

[+] University of Regina, Sask., Canada

4.1.7 MEASUREMENT OF THE πd → pp REACTION AT T_π = 65 MeV

C.R. Ottermann, E.T.Boschitz, W. Gyles, J.A. Konter[+], W. List, S. Mango[+],
G.R. Smith[++], R. Tacik, B.van den Brandt

Recently, there has been considerable experimental and theoretical progress on the fundamental $\pi^+d \rightarrow pp$ reaction. Our group has previously measured the vector analyzing power iT_{11} in this reaction in order to test theoretical calculations, and moreover to provide crucial data for partial wave analyses1). The importance of such data has been pointed out by Weddigen2) and Foroughi3), and indeed, the most recent partial wave analysis by Bugg4) showed that these data substantial improved the determination of the πd → pp amplitudes. However, Bugg also pointed out that there is still a lack of iT_{11} data at very low energies.

Therefore, in a new measurement we have attempted to produce such data at a low pion energy. For technical reasons we had to use the πM1 channel at SIN, the advantage of which is the efficient proton rejection with an electrostatic seperator and the small beam spot on the target. On the other hand, the length of the channel and the resulting low rate of 65 MeV pions presented a considerable draw back. In order to achieve a rate of 4×10^5 pions per second, the full momentum acceptance of the channel (≈ 3%) had to be used. The experimental set-up was similiar to the previous one1).

The experimental results are presented in Fig. 1. They are compared with a coupled channel calculation from Niskanen4), a Faddeev calculation of the Lyon group5) and with predictions from the relativistic perturbation theory of Locher and Svarc6). Within the statistical accuracy the best agreement is with the prediction from the Lyon group.

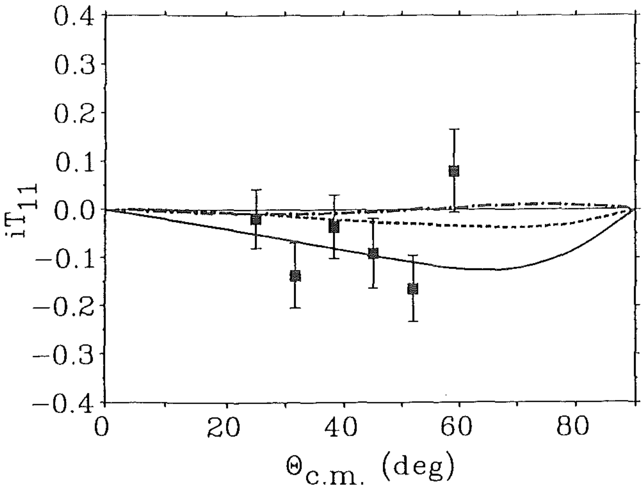

Fig. 1
The vector anlyzing power iT_{11} for the pion deuteron absorption reaction at T_π = 65 MeV compared with theoretical predictions. The solid curve is from the three body calculation of the Lyon group (Ref. 5), the dashed one from the calculation of Locher and Svarc (Ref. 6) and the dot-dashed one from Niskanen (Ref. 4)

(1) G.R. Smith et al., Phys. Rev. C30(1984)980
(2) Ch. Weddigen, Nucl. Phys. A312((1978)330
(3) F. Foroughi, J. Phys. G10(1984)617
(4) J.A. Niskanen, Phys. Lett. 141B(1984)301
(5) C. Fayard, private commication
(6) M.P. Locher and A. Svarc, J. Phys. G11(1985)183

[+] SIN, Villigen, Switzerland [++]
[++] TRIUMF, Vancouver, B.C., Canada

4.1.8 FIRST KINEMATICALLY COMPLETE MEASUREMENTS OF THE $\pi^+d \rightarrow \pi^o pp$ CHARGE EXCHANGE REACTION

W. Gyles, E.T. Boschitz, H. Garcilazo, R.R. Johnson[+], W. List,
C.R. Ottermann, R. Tacik, U. Wiedner, M. Weßler

The most important reaction channels for the πd interactions are in the order of decreasing cross sections

$$\pi^{\pm} d \rightarrow \pi^{\pm} NN \quad \text{(break-up)} \qquad (1)$$
$$\pi^{\pm} d \rightarrow \pi^{\pm} d \quad \text{(elastic scattering)} \qquad (2)$$
$$\pi^{\pm} d \rightarrow \pi^{o} NN \quad \text{(charge exchange)} \qquad (3)$$
$$\pi^{\pm} d \rightarrow NN \quad \text{(absorption)} \qquad (4)$$

The reactions (1), (2) and (4) have been studied fairly extensively in the past, but very little data exist for the charge exchange reaction. Except for earlier work with cloud and bubble chambers [1,2,3] the only more recent measurement is the one of the double differential cross section of the $\pi^- d \rightarrow \pi^o nn$ reaction with the LAMPF π^o spectrometer, but the data have not yet appeared in the literature.

In order to provide an additional test of relativistic Faddeev theories we have measured for the first time the triple differential cross section $\frac{d^3\sigma}{d\Omega_p\, d\Omega_p\, d\,P_p}$ in a kinematically complete experiment over a large kinematical range. The data have been taken at the πM1 channel at SIN using the time-of-flight method for measuring the momenta of the two protons in the final state of the $\pi^+d \rightarrow \pi^o pp$ reaction. Large two-element plastic scintillator telescopes (20 x 70 cm² in area) were used to detect the protons at 2 m distance. The timing resolution was 1 ns. The detectors were placed at angles of 45°, 60° and 120° on one side of the incident pion beam and at 20°, 45°, and 60° on the other side. Each counter on one side was placed in hardware coincidence with each counter on the other side. For the deuteron target a 10,4 cm diameter liquid deuterium target cell was used. The target thickness could be changed from 5 to 25 mm in a few minutes and back to 5 mm or empty in about 4 hours. Measurements were taken with both target thicknesses and with the empty target cell. Pion beam energies of 228 MeV and 294 MeV were used, and sufficient counts were recorded to give a 10%

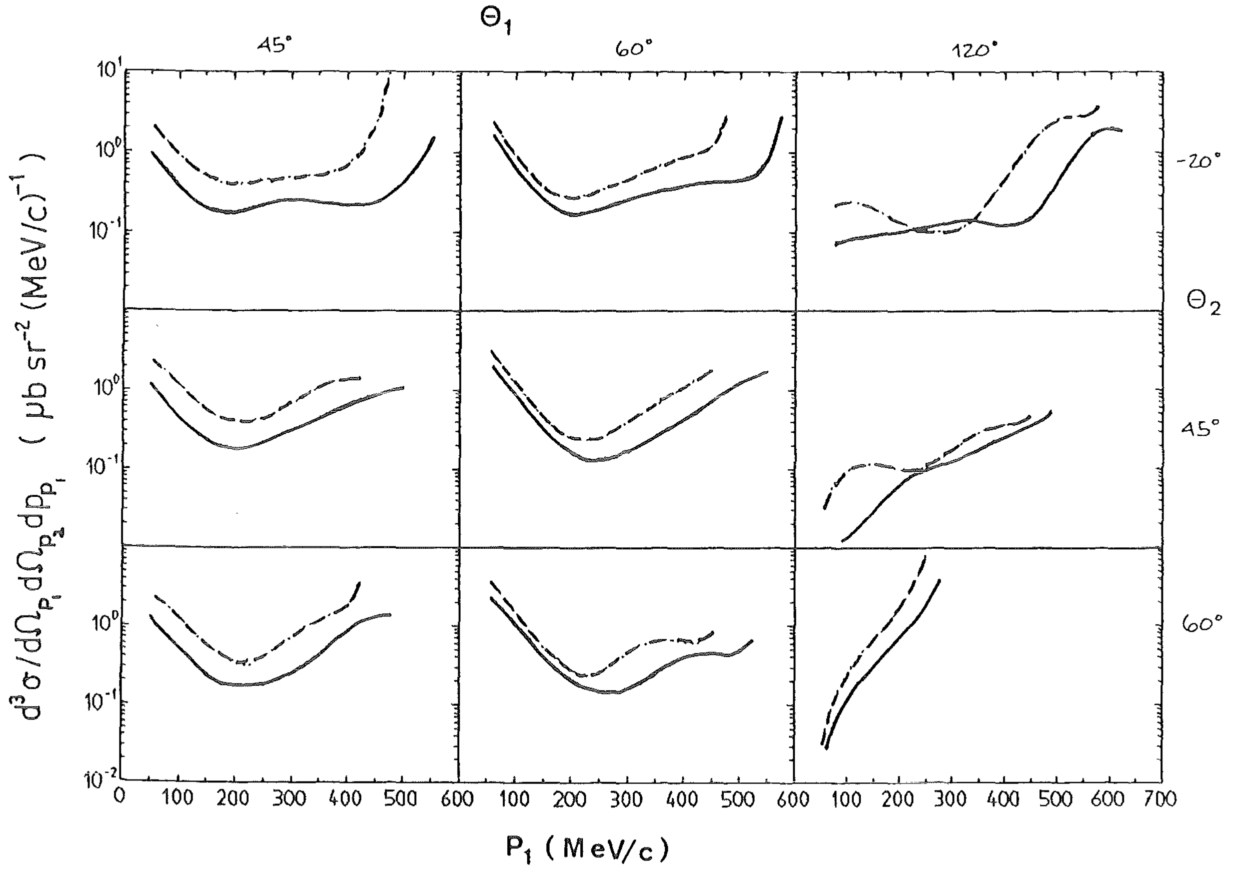

Fig. 1 Predictions for the $\pi^+d \rightarrow \pi^0pp$ reaction at 228 MeV (dashed line) and 294 MeV (solid line) from the relativistic Faddeev theory of Garcilazo

statistical uncertainty at the theoretically predicted minimum cross section of 0,1 $\frac{\mu b}{s^2 \cdot Mev/c}$, with a momentum byte of 20 MeV/c per data point. The background measured on line was typically 20-30%, but it is expected that much of it can be removed in off line analyses. The data are presently being analyzed. The charge exchange reaction has been calculated within the rélativistic Faddeev theory of Garcilazo for our specific kinematics. The predictions are shown in Fig. 1.

(1) K.C. Rogers and L.M. Ledermann, Phys. Rev. 105(1957)247
(2) E.G. Pewitt et al., Phys. Rev. 131(1963)1826
(3) J.H. Norem, Nucl. Phys. B33(1971)512

+ TRIUMF and University of British Columbia, Vancouver, B.C., Canada

4.1.9 MEASUREMENT OF THREE PARTICLES IN COINCIDENCE FOLLOWING THE INTERACTION OF POSITIVE PIONS WITH CARBON

R. Tacik, E.T. Boschitz, B. Gyles, W. List, C. Ottermann, M. Weßler, U. Wiedner, R.R. Johnson$^+$

Some time ago we performed an experiment in which we detected three protons in coincidence following the interaction of 228 MeV positive pions with carbon$^{1)}$. The experiment was performed with twelve plastic scintillator telescopes. Events were recorded in which one proton was detected at 30°, and the other two were detected in coincidence by the remaining 11 conters. Five of these were on one side of the beamline, and six on the other, giving rise to 30 possible combinations.

We found that several models could describe either the relatively narrow (60° FWHM) angular distribution in any individual counter; but no model we considered at the time could do both simultaneously. We speculated that a process involving the pion scattering several times before finally being absorbed on a nucleon pair would be consistent with our observations. Now, with a new more extensive data set, and our own cascade calculation, we have definite evidence that the process suggested above is in agreement both with our data, and that from the simpler (π,pp) experiments.

The new experiment was performed at the πM1 channel at SIN during March 1986, at incident pion energies of 130, 180, and 228 MeV. Again, twelve plastic scintillator telescopes were employed. This time, however, events were recorded in which any three of the counters were in coincidence. This leads to 220 possibilities for the detection of three protons. Also, six of the counters used in the previous experiment were replaced by much larger ones (20 x 20 x 70 cm^3), positioned 2 m away from the scattering target. These counters were suitable for neutron detection, which means that we have data on the (π,ppn) process as well, but which have not yet been analysed. For charged particle detection, the main advantage of these larger counters was in particle identification. We can now clearly separate (π,ppd) events. We can also distinguish between pions which pass through the counters ($T_\pi \geq 65$ MeV), and those which stop ($T_\pi \leq 65$ MeV). There are a surprisingly large number of the latter.

By looking at the sum of the energies of the two protons detected in coincidence with a pion, we can separate background events from those involving a genuine two proton knockout (π, pp). Since only two of the three particles in the final state of this reaction are indistinguishable, we have data on all 660 possible combinations. By looking at the angular correlation of the two protons detected in coincidence with a pion at a specified angle, we note that there are many events in angular regions kinematically forbidden for the (π,πpp) process.

This is evidence for further pion scatterings, that is, the (π,πppp) or (π,πppn) reactions.

The (π,ppp) data taken in the new experiment at 228 MeV confirm our previous measurement. Its more extensive nature enables a wider comparison with the results of our cascade calculation, and thus provides a firmer basis for the satisfactory agreement obtained. The main features of the measured angular distributions do not change substantially at 180 or 130 MeV. The integrated (π,ppp) count rate however decreases in a ratio of 5.0:3.6:1.0 with decreasing energy. The integrated count rate for the (π,πpp) measurement decreases more rapidly.

Our data for the two- and three-proton-knockout reactions are clearly consistent with our proposed picture for pion absorption. It remains to be seen whether a more detailed comparison of our data with our cascade model calculation still leaves room for more exotic absorption processes. At the moment it is clear that the process of a pion scattering several times before being absorbed on a nucleon pair provides a good description of the bulk of the data.

(1) R. Tacik et al., PRC 32(1985)1335

+ TRIUMF and University of British Columbia, Vancouver, B.C., Canada

4.1.10 INVESTIGATION OF THE ^{6}Li (π,πd) REACTION AT T_π = 219 MeV

R. Tacik, E.T. Boschitz, W. Gyles, W. List, C.R. Ottermann, K. Junker[+]

We have measured triple differential cross sections $d^3\sigma/d\Omega_\pi d\Omega_d dp_d$ for the inclusive Li(π,πd) X reaction. The experiment was performed on the πM3 beamline at SIN. The pion and deuteron were detected in coincidence with essentially the same apparatus used previously by our group in measurements of the d(π,π)d and d(π,πp)n reactions. Indeed one of the purposes of the present experiment was to see whether any new insights into the free π-d system could be obtained by studying what is essentially π-d elastic scattering from a bound (and thus "off-shell") deuteron.

Pions were detected at angles of 87.5°, 102.5°, 117.5°, 132.5°, 147.5° and 162.5°. The deuteron detectors were positioned at the "conjugate" angles corresponding to free πd → πd kinematics; namely, 41.2°, 33.9°, 26.9°, 20.2°, 13.7°, and 7.3°. The deuteron detectors consisted of one plastic scintillator (10 x 40 x 0.5 cm³) at 1.3 m from the target, through which the deuterons passed; followed by an absorber, chosen in thickness to stop all deuterons; which was in turn followed by another plastic scintillator (10 x 42 x 0.5 cm³) at 1.34 m from the target, which was used to veto out protons coming from the target. This arrangement eliminated most of the proton background, originating from quasielastic πp scattering. The exception was the low energy protons which also stopped in the absorber between the two scintillators, and thus were not vetoed out. The background due to these low energy protons extended into the region where deuterons were observed in the time-of-flight spectra recorded for the deuteron counters. Thus, some peak fitting was necessary in order to separate the real deuteron events. These were then transformed from time-of-flight distributions into momentum distributions with the use of a Monte-Carlo program which accounted for such things as deuteron energy loss in the target and air, and our experimental time resolution.

Thus far, the data have been compared with an impulse approximation calculation using the three body wave function of Kukulin et al.$^{1)}$, which exhibits the proper asymptotic behavior, and has been used successfully in describing deuteron knockout data with other probes. The calculation describes our data well at the conjugate angles near the momenta corresponding quasifree kinematics, but does worse as one goes to larger momentum transfers. Generally the width of the calculated momentum distributions is narrower than the experimental one. This can be explained by the fact that the calculation assumes the exclusive ^{6}Li(π,πd)α reaction while we measured the inclusive reaction ^{6}Li(π,πd)X. Similar behavior has been observed the proton induced ^{6}Li breakup reaction$^{2)}$.

(1) Kukulin et al., NP 417A(1984)128
(2) Kitching et al., PRC 11(1975)420

+ SIN, 5234 Villigen, Switzerland

4.1.11 MEASUREMENT OF THE CHARGE-EXCHANGE REACTION IN ^{3}He WITH STOPPED PIONS

G. Backenstoss$^+$, S. Cierjacks, M. Izycki$^+$, W. Kowald$^+$, S. Ljungfelt, U. Mankin, G. Schmidt, H. Ullrich, P. Weber$^+$, H.J. Weyer$^+$

^{3}He is the only nucleus (besides H) where the charge-exchange reaction is already possible for pions at rest. For this nucleus this reaction contributes in fact with an appreciable amount, which cannot be neglected in the total rates, nor in more global considerations of the absorption process. Nevertheless not much experimental information is available. As an example, up to now data about the charge-exchange contribution to S-wave absorption were missing completely.

Our experiment was performed with a gaseous ^{3}He target cooled down to 5K. Two gammas from the π^0 decay were detected in coincidence by two large NaI detectors 27.5 cm and 21 cm in diameter, 28 cm thick and positioned at 1 m distance from the target. The relative angle between the two counters was close to the minimum angle of 153°. Distributions measured by the counters are shown in

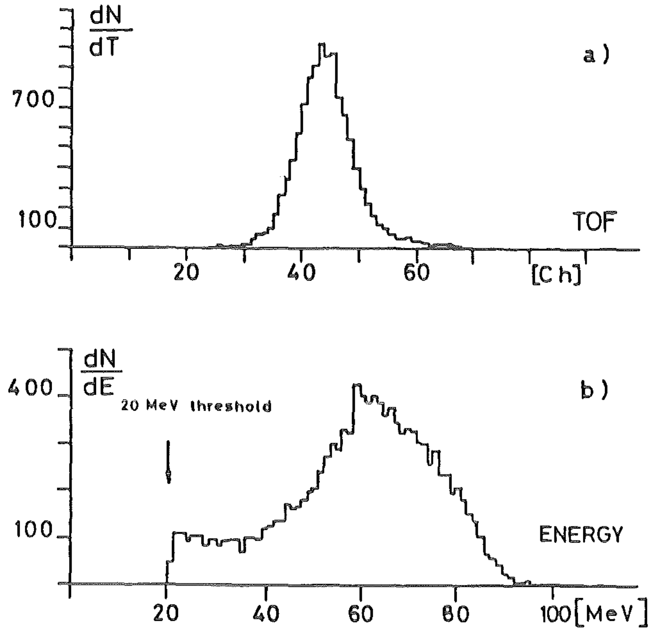

Fig. 1 a: Time spectrum of the γ's from the $\pi^o \rightarrow 2\gamma$ decay as registered by one of the two large NaI-detectors.

b: Energy spectrum of coincident γ-rays from π^o decay measured in the same counter.

Table I Branching ratios (per stopped pion) for different reaction channels

channel	S+P absorption (%)	1 S-absorption (%)
n_{dn}	11.7 ± 1.8	5.5 ± 0.9 ≙ (0.58 ± 0.1) x 10^{-15} s^{-1}
n_{pnn}	60.8 ± 4.0	17.6 ± 2.7 ≙ (1.86 ± 0.28)x 10^{-15} s^{-1}
n_{π^o}	13.5	4.7 ± 0.9 ≙ (0.50 ± 0.10)x 10^{-15} s^{-1}

Figure 1. A Monte Carlo programme[1)] was used to calculate acceptance and efficiency for π^o detection. In order to detect pionic X-rays four thin NaI detectors with 4,5 cm active diameter each were placed 12 cm below the target. This additional X-ray detection was used to identify S-wave charge-exchange reactions by their coincidence with an X-ray of the pionic K-series.

The results of the present measurement together with our results for other reaction channels[2)] make possible a consistent set of data containing all absorption channels for stopped pions[3)]. Some numbers are given in Table 1.

(1) R.L. Ford, W.R. Nelson, SLAC (1978)
(2) D. Gotta et al., Phys. Lett. 112B(1982)129
G. Backenstoss et al., Phys. Lett. 115B(1982)445
I. Schwanner et al., Nucl. Phys. A412(1984)253
(3) G. Backenstoss et al., Nucl. Phys. A448(1986)567

+ Physikinstitut der Universität Basel, Basel/Switzerland

4.1.12 PION ABSORPTION IN ^{3}He AT 320 MeV/c

G. Backenstoss[+], S. Cierjacks, M. Furic[++], A. Hoffart, M. Izycki[+],
T. Petkovic[++], B. Rzehorz, P. Salvisberg[+], N. Šimičević[++], M. Steinacher[++],
H. Ullrich, P. Weber[+], H.J. Weyer[+]

The dependence of pion absorption reactions on the pion energy should lead us to a better understanding of the reaction mechanisms. In ^{3}He the dominant reactions are a) the quasifree absorption on an isospin T = 0 nucleon pair; b) the quasifree absorption on a T = 1 pair; and c) the three-nucleon absorption. So far information about these reactions exists only below and around the top of the Δ-resonance. In this region all cross sections increase with increasing energy. The open question is, however, whether or not the cross sections decrease above the resonance.

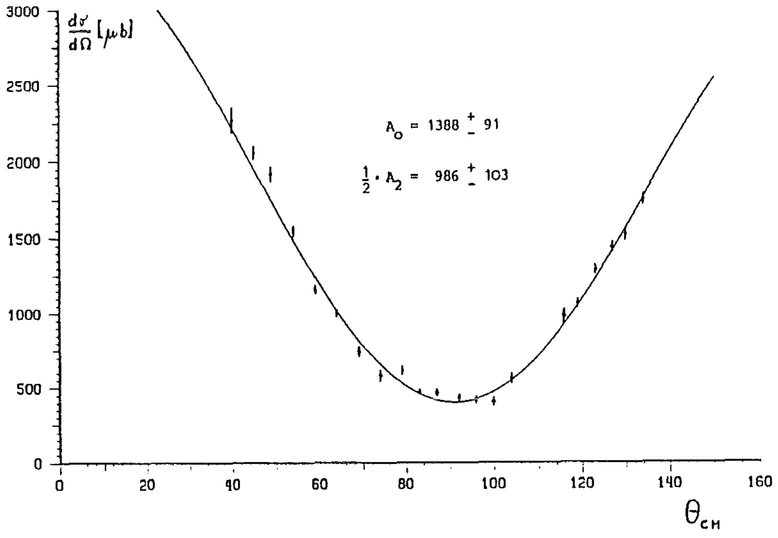

Fig. 1
Angular distribution of the quasifree absorption reaction ^{3}He(π^+,pp)p for 320 MeV/c pions. The solid line is a Legendre fit with the coefficients given in the insert.

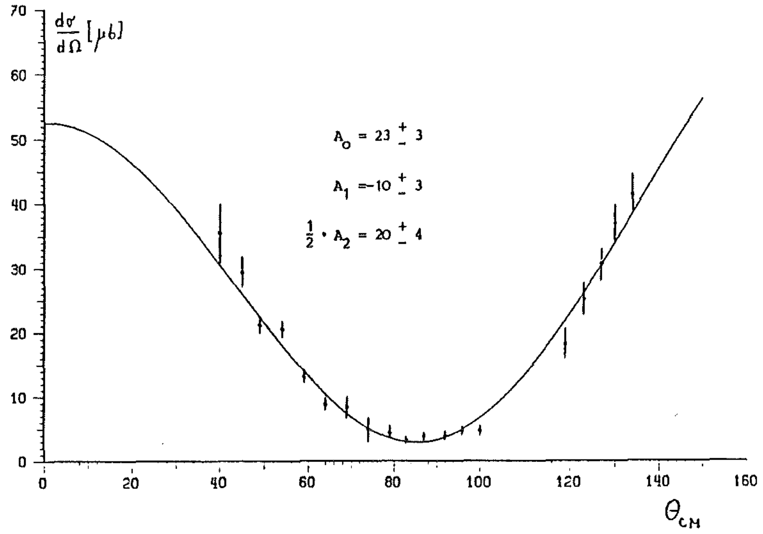

Fig. 2
Same as Fig. 1 for ^{3}He(π^-,np)n

To answer this question we have made measurements on the reactions ^{3}He (π^+,pp)p and ^{3}He(π^-,pn)n with pions of 320 MeV/c. The apparatus has been described elsewhere$^{1)}$. Figures 1 and 2 show angular distributions for the quasifree absorption on T = 0 and T = 1 pairs, respectively. For each angle, integration over the entire quasifree peak has been made and corrections have been applied for the finite acceptance of the counters. The ordinate gives cross sections in absolute units. The curves are Legendre fits with the parameters given in the figures.

Comparison with results at lower pion energies leads to the following conclusions:

a) The T = 0 absorption follows with good accuracy the energy dependence of the $\pi^+d \to pp$ reaction.

b) The T = 1 absorption shows also a decrease above the resonance . The isospin ratio increases below the resonance. The not well understood asymmetry is also present above the resonance.

c) Also the three-nucleon absorption shows up as a strong channel.

(1) S. Ljungfelt, Thesis University of Karlruhe 1984
KfK-report No 3792(1985)

[+] Physikinstitut der Universität Basel, Basel/Switzerland

[++] University of Zagreb, Zagreb, Yugoslavia

4.1.13 OBSERVATION OF A THREE-NUCLEON PION-ABSORPTION MECHANISM IN THE (π + ^{4}He)-INTERACTION

G. Backenstoss[+], S. Cierjacks, M. Furić[++], M. Izycki[+], S. Ljungfelt, T. Petković[++], P. Salvisberg[+], N. Šimičević[++], M. Steinacher[+], H. Ullrich, P. Weber[+], H.J. Weyer[+]

Pion absorption mechanisms involving more than two nucleons have been subject of speculations since many years. Only recently the discovery of a direct three-nucleon absorption process in ^{3}He[1)] has provided clear experimental evidence of such a mechanism. Other observations like the pion induced emission of composite particles (deuterons, tritons, alpha-particles etc.) also prove the participation of more nucleons, but possibly in a sequential process. This could be a two-nucleon absorption, followed by final state interaction of the nucleons.

In order to improve the understanding of this reaction type we have studied one of the most simple cases, namely the emission of deuteron-nucleon pairs following pion absorption in ^{4}He. Since in this case the residual nucleus is only a nucleon, the final state is determined in a kinematically complete way by the coincident measurement of the deuteron and the nucleon. The experiment has been made with positive and negative pions of 220 MeV/c on the reactions (π^+,dp) and (π^-,dn). The apparatus has been described elsewhere[2)]. For the present measurements several counter positions were used, covering a large part of the kinematically allowed region.

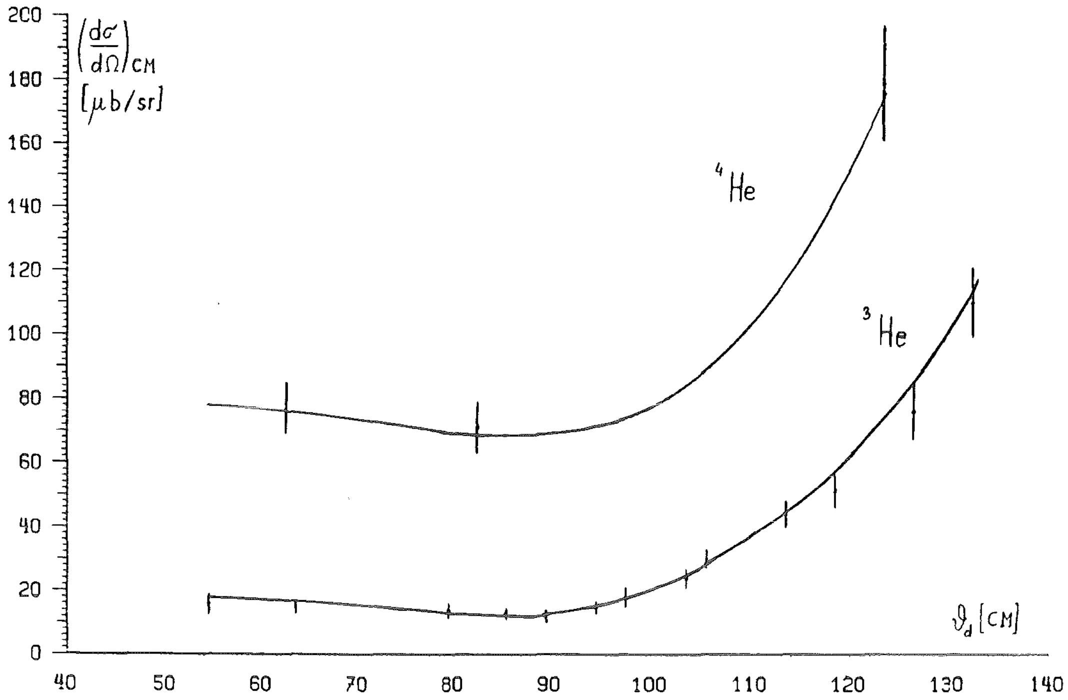

Fig. 1 Angular distribution of the quasifree absorption peak for the reaction $^4He(\pi^-,dn)n$ compared with the reaction $^3He(\pi^-,dn)$. Absolute differential cross sections are plotted vs the deuteron C.M.-angle relative to the beam axis

As expected the reactions show a pronounced correlation of the detected particles at 180° in the CM-system. First results for the angular distribution of these correlated pairs relative to the beam axis are given in Fig. 1. The deuterons are peaked in backward direction. Also shown in this figure are results from the respective reaction in ^3He. The similarity between the two distributions

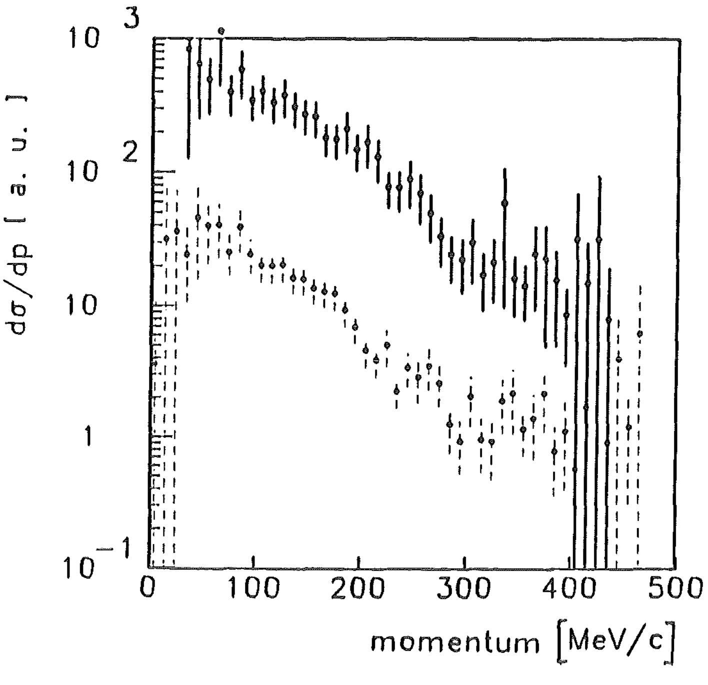

Fig. 2
Recoil momentum distribution for the reactions $^4He(\pi^+,pp)pn$ (upper points) and $^4He(\pi^+,dp)p$ (lower points) in the region of quasifree absorption.

is obvious and suggests, that the reaction in ^{4}He proceeds in a similar way as in ^{3}He i.e. on a three-nucleon sub system.

To pursue this idea we have determined the recoil momentum distribution of the (π^{+},dp)-reaction, which is the momentum distribution of the not detected nucleon. The result is shown in Fig. 2 (lower data points). This distribution is in good agreement with the Fermi distribution as determined from electron scattering experiments. The agreement proves, that the undetected nucleon was a pure spectator and hence the pion absorption process was quasifree on a three-nucleon subsystem.

(1) G. Backenstoss et al., Phys. Rev. Lett. 55(1985)2782
(2) S. Ljungfelt, Thesis University of Karlsruhe 1984
KfK report No. 3792 (1985)
S. Cierjacks et al., Nucl. Instr. and Methods A238(1985)354

+ Physikinstitut der Universität Basel, Basel, Switzerland
++ University of Zagreb, Zagreb, Yugoslavia

4.2 INTERACTION OF ANTIPROTONS AND ANTINEUTRONS

4.2.1 STRONG INTERACTION SHIFTS AND WIDTHS IN ANTIPROTONIC HELIUM ISOTOPES

R. Bacher, P. Blüm, J. Egger[+], K. Elsener[++], K. Heitlinger, W. Kunold,
D. Rohmann, M. Schneider, L.M. Simons[+]

The strong interaction effects in $\bar{p}\ ^3He$ and $\bar{p}\ ^4He$ atoms have been measured at LEAR using the cyclotron trap[1,2]. The antiprotonic X-rays were detected by semiconductor detectors (Tab. 1). The measurements have been performed at gas pressures between 36 and 600 mbar to investigate also the pressure dependence of the cascade.

In the last part of the experiment (june 1986) a novel technique was used to determine the in-beam efficiency of the detectors and the calibration energies. The $\bar{p}$ were stopped in gaseous nitrogen. From measurements of muonic and antiprotonic noble gases[3] it is known that at low pressures exotic atoms can be stripped off completely from electrons. The atomic cascade is almost circular and the relative intensities of the transitions are known to a high degree of accuracy. The absolute detection efficiency is achieved from a measurement with a ^{57}Co source at 6.4 and 14.4 keV. Fig. 1 shows the spectra from $\bar{p}\ ^4He$ and $\bar{p}N$.

Tab. 2 summarizes the results of the strong interaction shifts and widths together with a measurement at 30°K[4]. Theoretical predictions[5] deliver for $\bar{p}\ ^4He$ Γ_{3d} = 3.2 meV and Γ_{2p} = 42 eV, which are in good agreement with our values. Comparing the results of $\bar{p}\ ^3He$ and $\bar{p}\ ^4He$ the 2p-widths show the only clear signal for an isotope effect.

In Tab. 3 the absolute yields of the main transitions are given as a function of pressure, which are in good agreement with cascade calculations. Comparing the 72 mbar values there is no difference found between the two isotopes.

(1) P. Blüm, D. Gotta, H. Koch, W. Kunold, M. Schneider, L.M. Simons, Proposal PS 175, CERN/PSCC/S 27(1980)
(2) Annual report on Nuclear Activities 1984/85, KfK 3969(1985)100
(3) Annual report on Nuclear Activities 1984/85, KfK 3969(1985)110 and other contributions to this Annual Report in section 4.2
(4) J.D. Davies et al., Phys. Lett. 145B(1984)319
(5) W. Kaufmann, H. Pilkuhn, Phys. Lett. 166B(1986)279

+ SIN, Villigen, Schweiz
++ CERN, Genf, Schweiz

Detector	Type	Area inner/outer (mm²)	Thickness inner/outer (mm)	Be-window thickness (μm)	Resolution at 5.9 keV (eV)
Si I (1983)	planar	30	3.5	8	160
Si II (1985)	guard-ring	30/200	5/5	12	200
Si III (1986)	planar	300	2	50	460
Ge I (1985)	guard-ring	200/500	10/10	130	250
Ge II (1986)	guard-ring	200/900	3/10	500	365

Table 1

Properties of the semiconductor detectors

	Detector	ε_{2p} (eV)	Γ_{2p} (eV)	Γ_{3d}^{*} (meV)	p (mbar)
$\bar{p}\,{}^{3}He$	Si II (1985)	-11 ± 11	54 ± 26	2.32 ± .33	72
	Ge I (1985)	-18 ± 4	22 ± 9	2.12 ± .17	72
	weighted average	-17 ± 4	25 ± 8	2.16 ± .15	
$\bar{p}\,{}^{4}He$	Si I (1983)	-18 ± 6	44 ± 17	2.29 ± .15	375/600
	Si II (1985)	-19 ± 7	45 ± 16	2.24 ± .26	72
	Si III (1986)	-22 ± 4	49 ± 6	2.21 ± .22	36
	Ge I (1985)	-15 ± 3	43 ± 10	2.56 ± .18	72
	Ge II (1986)	-23 ± 7	33 ± 18	----	36
	weighted average	-18 ± 2	46 ± 5	2.34 ± .10	
$\bar{p}\,{}^{4}He$	ref. [5]	-7.4±5.3	35 ± 15	2.4 ± .5	

Table 2

Strong interaction shifts and widths in $\bar{p}\,{}^{3}He$ and $\bar{p}\,{}^{4}He$. Radiative 3d-widths including Fried-Martin correction: $\Gamma(\bar{p}\,{}^{3}He)$ = 1.46 MeV, $\Gamma(\bar{p}\,{}^{4}He)$ = 1.44 MeV

	$\bar{p}\,{}^{3}He$	$\bar{p}\,{}^{4}He$			
	72 mbar	600 mbar	375 mbar	72 mbar	36 mbar
3 - 2	26 ± 4	13 ± 3	10 ± 3	21 ± 3	23 ± 2
4 - 2	1.9 ± 0.5	1.5 ± 0.4	2.0 ± 1.5	2.2 ± 0.5	0.8 ± 0.2
Σ - 2	33 ± 8	-------	-------	33 ± 7	25 ± 2
4 - 3	45 ± 6	30 ± 7	24 ± 6	43 ± 4	48 ± 9
5 - 3	8.2 ± 1.5	4.5 ± 1.2	2.0 ± 1.2	5.5 ± 1.3	4.0 ± 0.4
6 - 3	2.3 ± 0.7	1.5 ± 0.9	1.1 ± 0.9	2.2 ± 0.4	1.4 ± 0.2
Σ - 3	64 ± 11	35 ± 9	26 ± 8	57 ± 6	57 ± 3
5 - 4	32 ± 9	-------	-------	37 ± 3	-------
6 - 4	5.7 ± 4.3	-------	-------	7.6 ± 2.9	-------
Σ - 4	42 ± 12	-------	-------	52 ± 16	-------

Table 3

Absolute yields of the X-ray transitions in $\bar{p}\,{}^{3}He$ and $\bar{p}\,{}^{4}He$

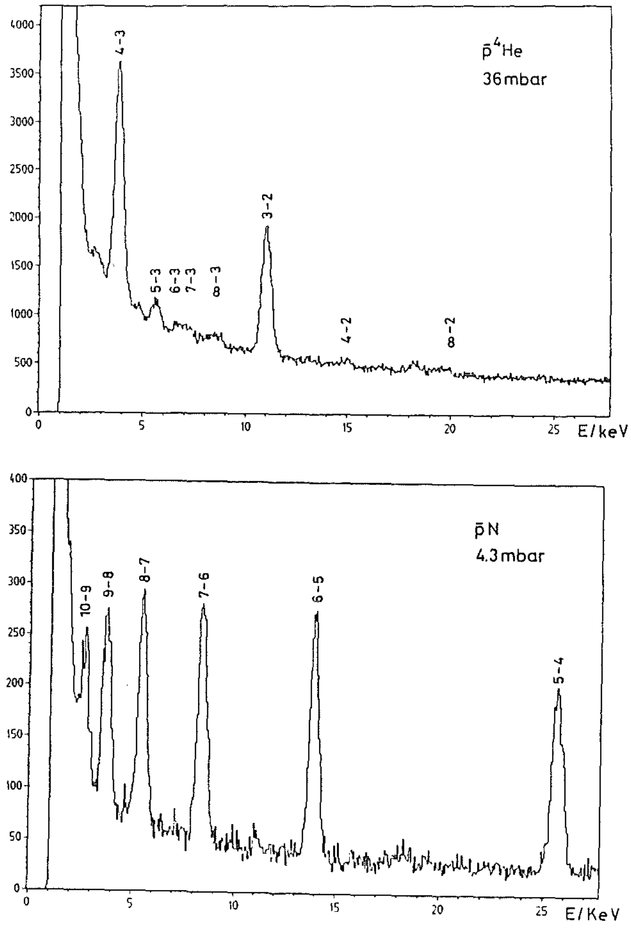

Fig. 1 X-ray spectra of $\bar{p}\,{}^{4}He$ and $\bar{p}N$ each 1 spill (about 1.3×10^{8} $\bar{p}$ stops) from detector Si III

4.2.2 PRESSURE DEPENDENCE OF THE ANTIPROTONIC CASCADE IN HYDROGEN

R. Bacher, P. Blüm, J. Egger[++], K. Elsener[+], D. Gotta, K. Heitlinger, W. Kunold, D. Rohmann, M. Schneider, L.M. Simons[++]

Due to the special principle of the cyclotron trap1) it is possible to form exotic atoms in gaseous targets down to lowest pressures. For the incoming antiproton beam at the LEAR facility at CERN with a beam momentum of 202 MeV/c it is possible to go down to 10 mbar in pressure. The cyclotron trap is therefore a mostly suited tool to study cascade effects in exotic atoms in a wide range of pressure. Only the detailed understanding of the atomic cascade provides the knowledge to make predictions about the processes which lead to the last observable transitions in exotic atoms. One point for example is the influence of the Stark mixing, which is expected to decrease in a pressure region below 1000 mbar. Here saturation of the line intensities should enable the measurement of very weak lines where good statistics is required.

At pressures below 1 atm the total intensity of the K-series is essentially shared by the K_α - and K_∞ ($\equiv K(\varkappa \geq 10)$)-transitions. The intensity ratio K_α to K_∞ is governed completely by the non hadronic parameters of the cascade. These are fixed by the measurement of the $\bar{p}$H L-series (d-level absorption is negligible), whereas the absolute intensities depend on the hadronic p-width.

Lowering the pressure means however to decrease the fraction of antiprotons which stop in the target gas because competing processes became dominant which stop the $\bar{p}$ elsewhere (deceleration foils, moderators, scintillators, etc).

So the aim of this measurement was to find out the optimum in pressure between these effects in order to prepare the measurement of the K-transitions in $\bar{p}$H.

The experiment was performed at the LEAR facility at CERN. The L-X-rays were measured with a 30 mm^2 high resolution Si(Li)-detector at 16, 30, 60 and 300 mbar hydrogen. Some characteristics of this detector are shown in Table 1. Inbeam efficiency and in beam resolution of the detector are monitored by measuring the observable transitions of nitrogen (Figure 1). This is a novel method to obtain these quantities and uses the fact that the electron shell in $\bar{p}$N is completely ionized and the cascade can develop itself without any disturbance. So a calibration can be performed down to 1 keV where calibrated sources are not available.

The results of the L-transition measurements are given in Figure 2 and Table 2. The yields obtained for $\bar{p}$H are in good agreement with cascade calculations of Borie and Leon2) using the cascade parameters k = 2 and $T_{\bar{p}p}$ = 1 eV (Fig. 3; k is a Stark effect mixing parameter which multiplies all Stark effect rates in the cascade, $T_{\bar{p}p}$ is the kinetic energy of the $\bar{p}$p-system). With this measurement it is possible to find cascade parameters which describe the cascade in the

Detector	Type	Area (mm²)	Thickness (mm)	Be-window thickness (µm)	Resolution at 5.9 keV (eV)
Si(Li)	planar	30	3.5	8	160

Tab. 1 Detector parameters

pressure (mbar)	$Y(L_\alpha)$ (%)	$Y(L_{tot})$ (%)
16	40 ± 8	57 ± 10
30	33 ± 6	48 ± 8
60	29 ± 6	41 ± 7
300	14 ± 8	26 ± 10

Tab. 2 Measured yields of L_α and L_{tot} in $\bar{p}H$

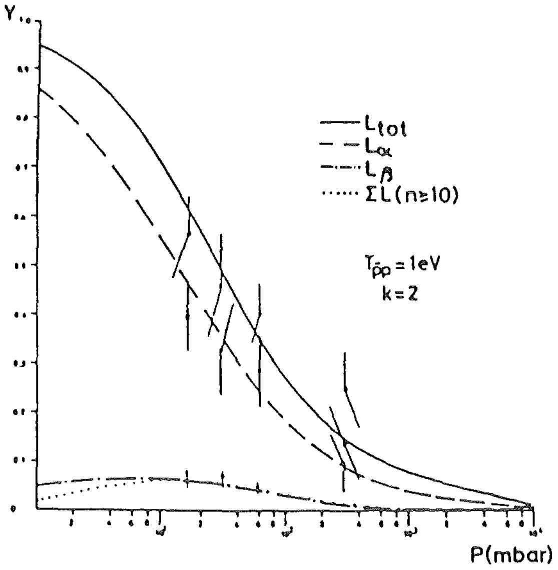

Fig. 3 Measured L-yields and cascade calculations based on the code of Borie and Leon [2)]

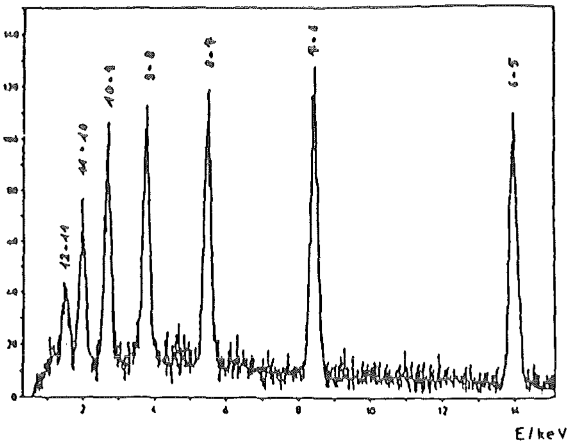

Fig. 1 Antiprotonic nitrogen measured at 21 mbar

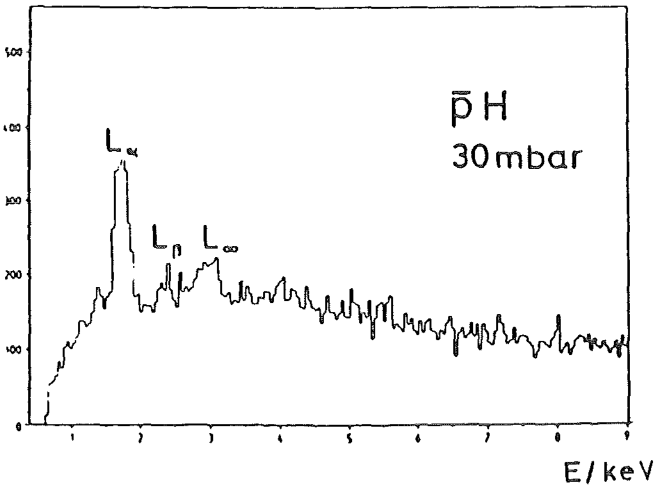

Fig. 2 Antiprotonic L-X-rays of $\bar{p}H$ at a pressure of 30 mbar

pressure region up to about 2 atm.

Fig. 2 would suggest a measurement below 10 mbar. Our decision however was to perform the measurement of the K-transitions at 30 mbar. This is a compromise considering concurrent processes described above. We expect 30% of all incoming antiprotons to be stopped at this pressure.

(1) P. Blüm, D. Gotta, R. Guigas, H. Koch, W. Kunold, M. Schneider, and L.M. Simons, CERN proposal PS 175 (1980)

(2) E. Borie, M. Leon, Phys. Rev. A21(1980)1460

+ CERN, Geneva, Switzerland

++ SIN, Villigen, Switzerland

4.2.3 STRONG INTERACTION SHIFTS AND WIDTHS IN ANTIPROTONIC HYDROGEN

R. Bacher, P. Blüm, J. Egger^{++}, K. Elsener^{+}, D. Gotta, K. Heitlinger, W. Kunold, D. Rohmann, M. Schneider, L.M. Simons^{++}

The X-rays of antiprotonic hydrogen have been measured using our cyclotron trap. The measurement was performed at the 202 MeV/c beam at the LEAR M1-area. The aim of this experiment is to determine the broadening and shift of the 1s level and the broadening of the 2p level from the measurement of the 2p → 1s transition in antiprotonic hydrogen.

The cyclotron trap gives the possibility to measure with very low pressure gas targets. At pressures below 1000 mbar the influence of the Stark mixing decreases rapidly thus yielding an increase of the intensities and a high sensitivity to cascade parameters.

The optimum pressure for this measurement was determined in a previous measurement of the L-X-rays in hydrogen to be 30 mbar$^{1)}$. The measurement of the K-transitions was performed with a 300 mm² Si(Li)-detector with characteristics as shown in Table 1. In the spectrum obtained from $2.8 * 10^9$ incoming antiprotons (11 spills, Figure 1) the two narrow peaks at 7.21 keV and 11.11 keV stem from the $\bar{p}O(8 \rightarrow 7)$ and $\bar{p}O(7 \rightarrow 6)$ transitions of the water contamination from the walls of the target chamber.

Detector	Type	Area (mm²)	Thickness (mm)	Be-window thickness (μm)	Resolution at 5.9 keV (eV)
Si(Li)	planar	300	2	50	460

Table 1 Detector parameters

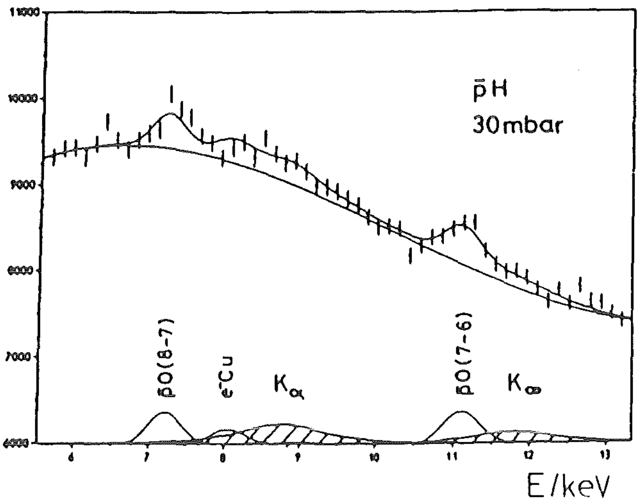

Fig. 1 Antiprotonic hydrogen measured at 30 mbar; together with a fit to the K-transitions and to the background lines

The intensities observed correspond to a partial pressure of 10^{-2} mbar H_2O within 30 mbar H_2, which could be confirmed by a mass spectroscopy measurement. Inside the detector the only electronic fluorescence X-rays produced stem from the copper cold finger which has been investigated in an irradiation measurement. The intensity ratio of the $\bar{p}$O-lines is known from a dedicated measurement. The intensity of the e^-Cu-line compared to the $\bar{p}$O-lines was determined from the spectra not correlated to $\bar{p}$-stops.

These quantities could therefore be kept fixed in the fitting procedure. The background is assumed to be flat, which is supported by the non correlated spectra. It originates from the low energy neutral component of the electromagnetic showers produced by the annihilation products in the materials of the target chamber and the detector itself.

For the fit of the K-X-rays the intensity ratio of K_α to K_∞ was fixed to 1.73 which is an input from the previous measurement of the L-X-rays in $\bar{p}$H. The distance of the two K-lines was fixed to the electromagnetic QED-energy difference. The Lorentz-widths are assumed to be equal. The background was fitted with a fourth order polynomial. From this we obtain:

Shift $\varepsilon = -(0.66 \pm 0.13)$ keV
Lorentz-width $\Gamma_L = (1.13 \pm 0.23)$ keV
Yield $Y(K_\alpha) = (4.9 \pm 1.6)\ 10^{-3}$
$Y(K_{tot}) = (7.8 \pm 1.9)\ 10^{-3}$

With the total L-yield of (48 ± 8)% at 30 mbar a hadronic 2p-width of (37 ± 13)meV is obtained which is a factor of 100 bigger than the radiative width.

An alternative way of evaluation proceeded without coupling the K_α-line to K_∞. Position, intensity and width were left free as independent fit parameters. This resulted in an energy shift of $\varepsilon = -(0.87 \pm 0{,}09)$keV, a Lorentz-width of $\Gamma_L = (0.74 \pm 0.27)$keV and a K_α-yield of $Y(K_\alpha) = (4.4 \pm 0.9)\ 10^{-3}$.

Fitting the K -transitions separately only a 1 to 2 standard deviation signal could be obtained.

To summarise we got (5224 ± 869) events in the K-lines which represents a 6 standard deviation signal. Our results for shifts and widths agree with a broad class of theoretical predictions from potential models[2,3,4].

However, a further measurement with a high resolution detector is needed with increased statistics in order to be able to determine the shift and width of the ground state more accurately and even to measure the two hyperfine ground state levels separately.

(1) R. Bacher et al., pressure dependence of the antiprotonic cascade in hydrogen, contribution 4.2.2 to this annual report
(2) J.M. Richard and M.E. Sainio, Phys. Letters 110B(1982)349
(3) W.B. Kaufmann and H. Pilkuhn, Phys. Letters 166B(1986)279
(4) W.B. Kaufmann and H. Pilkuhn, Phys. Review C17(1978)215

+ CERN, Geneva, Switzerland
++ SIN, Villigen, Switzerland

4.2.4 ON THE PRODUCTION OF HIGHLY IONIZED ANTIPROTONIC NOBLE GAS ATOMS

R. Bacher, P. Blüm, K. Elsener[+], D. Gotta, K. Heitlinger, M. Schneider, L.M. Simons[++]

Our experiments at SIN with muonic noble gases[1] demonstrated, that a muon is able to ionize completely a Neon atom via its deexcitation cascade. An antiproton should also deplete the electron shell of a Neon atom and it can be expected, that it will strip even atoms with more electrons, because it is captured at much higher levels than a muon. To proof this assumption we have measured low-energy-X-rays (up to 25 keV) of antiprotonic Neon, Argon Krypton and Xenon. The experiment was done at LEAR using our cyclotron trap. To suppress the selfabsorption in the gas and refilling processes low pressures (50 mbar) were used. The spectra were recorded by a thin-window silicon detector.

Fig. 1 shows a completely circular antiprotonic cascade (n=1) in Neon between the levels n=15 and n=16. Corrected by the detector efficiency all lines have the same yield of about 50%. The cascade process in Argon (Fig. 2) has the same behaviour as in Neon with the exception, that the X-ray transitions 17 → 16 and 16 → 15 are missing. These lines are converted by Auger effect, because their energies correspond to the binding energies of the two K-electrons in an Argon atom, which is stripped off all other electrons. Fig. 3 demonstrates the ionization of the L-shell in Krypton. The transitions 29 → 28 up to 25 → 24 are converted. Then all L-electrons are ejected and the radiative circular cascade rises up, because the energies of the lines are not sufficient to eject the K-electrons.

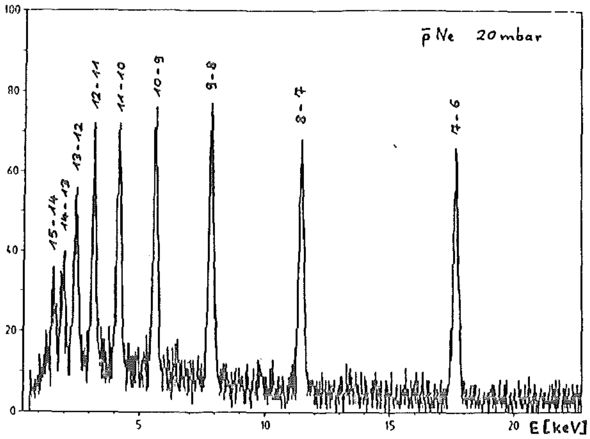

Fig. 1 X-ray spectrum of anti-
protonic Neon

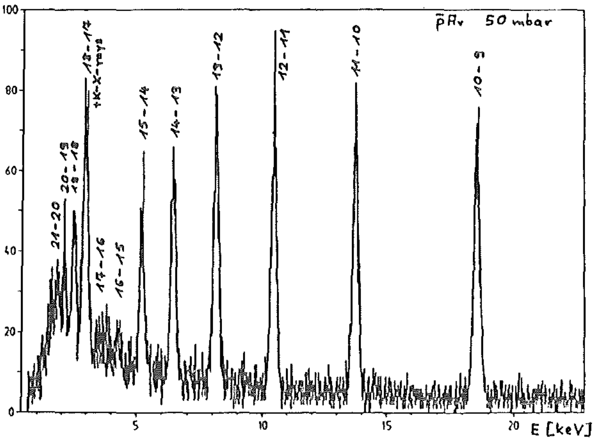

Fig. 2 X-ray spectrum of anti-
protonic Argon

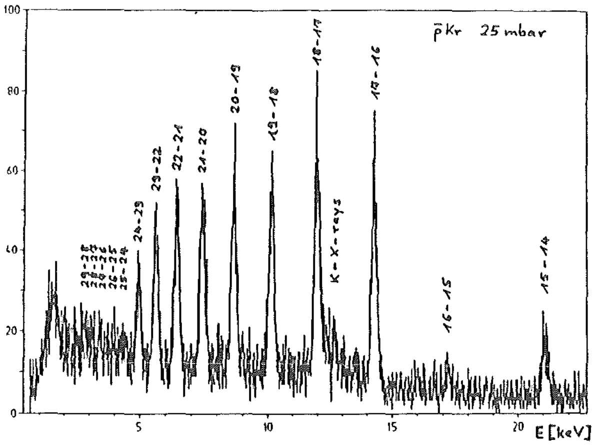

Fig. 3 X-ray spectrum of anti-
protonic Krypton

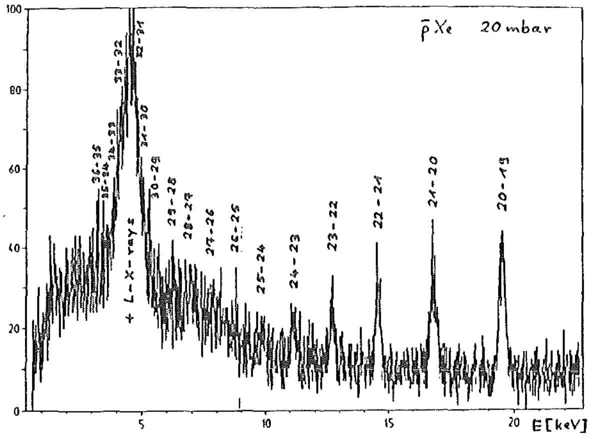

Fig. 4 X-ray spectrum of anti-
protonic Xenon

This can first be done via the Auger transitions 16 → 15 and 15 → 14. The corresponding lines are vanishing again. In an analogous way the Xenon spectrum (Fig. 4) shows - besides the depletion of the L-shell - the ionization of the M-shell.

The atomic capture process of the antiproton seems to be different to the previous approach, which predicts, that the antiproton is captured at n=43 by ejecting a K-elektron of the shell. The produced K-shell vacancy must be refilled via a radiative K-transition, which should show up in the spectrum. The measured K-line however has a yield of less than 20%. Therefore we conclude, that the antiproton is mostly captured at very high levels and peels off slowly the electron shell from the outer to the inner electrons.

(1) Annual report on nuclear physics activities
KfK 3969(1984)110

+ CERN, Genveva, Switzerland

++ SIN, Villigen, Switzerland

4.2.5 INVESTIGATIONS OF ANTIPROTONIC ATOMS AT LEAR

H. Barth, G. Büche, A.D. Hancock, H. Koch, Th. Köhler, A. Kreissl, H. Poth,
U. Raich, D. Rohmann, A. Wolf[+], L. Tauscher[++], A. Nilsson[+++],
M. Chardalas[IV], S. Dedoussis[IV], M. Suffert[V], W. Kanert[VI], T. von Egidy[VI],
F.J. Hartmann[VI], G. Schmidt[VI], J.J. Reidy[VII]

The measurements of antiprotonic atoms at LEAR were finished with the last run in August 1985. The data evaluation progresses well. A summary of the experimental outcome can be found in Refs. 1 and 2. The experiments can be classified as follows:

- global study of strong interaction effects in $\bar{p}$-atoms;
- study of details of the antiproton-nucleon interaction;
- measurement of the properties of the antiproton.

In the following we shall discuss the measurements in some detail.

We have chosen mainly light antiprotonic atoms to investigate strong interaction effects in the two last observable levels over a wide range of nuclei and isotopes to eliminate as far as possible nuclear medium corrections. For this purpose light atoms are well enough known so that their nucleon distribution can be calculated reliably. In our measurements we have scanned the range from A = 6 to A = 23$^{3)}$ to study strong interaction effects mainly in the 3d and 4f level.

Since the antiproton-nucleon interaction is very strong we expect that it takes place well localized at the surface of the nucleus. That means that shift and width should strongly depend on the overlap of the Coulomb wavefuntion with the nucleus which scales roughly as $(ZA^{1/3})^{2l+3}$. This scaling behaviour is demonstrated in Fig. 1 where we have plotted the strong interaction effects in the 3d level divided by $(ZA^{1/3})^{7}$. While the shifts obey this simple scaling law the widths increase less rapidly with A as one would expect from the overlap. A quantitative analysis on the basis of various antinucleon-nucleon potential models is presently done by a number of theorists.

In the last annual report we have reported the observation of large isotope effects in the stable oxygen isotopes. The data are evaluated and published$^{4)}$. This method was used to try to disentangle the antiproton-proton from the antiproton-neutron interaction. We have repeated this type of measurement in $^{6}Li/^{7}Li$ (Fig. 2) and in $^{58}Ni/^{60}Ni$. While in $^{6}Li/^{7}Li$ we do not observe an isotope effect whithin our statistical accuracy it is clearly seen again in Nickel.

The X-ray transitions in antiprotonic atoms are triplets where the splitting is proportional to the magnetic moment of the antiproton if the levels are not affected by strong interaction. In heavy nuclei these multiplets can be resolved. We measured the fine-structure splitting in the 11-10 and 10-9 transition of $\bar{P}$-Pb and determined from that the magnetic moment to be $-2.8007(91)\mu_N$. The

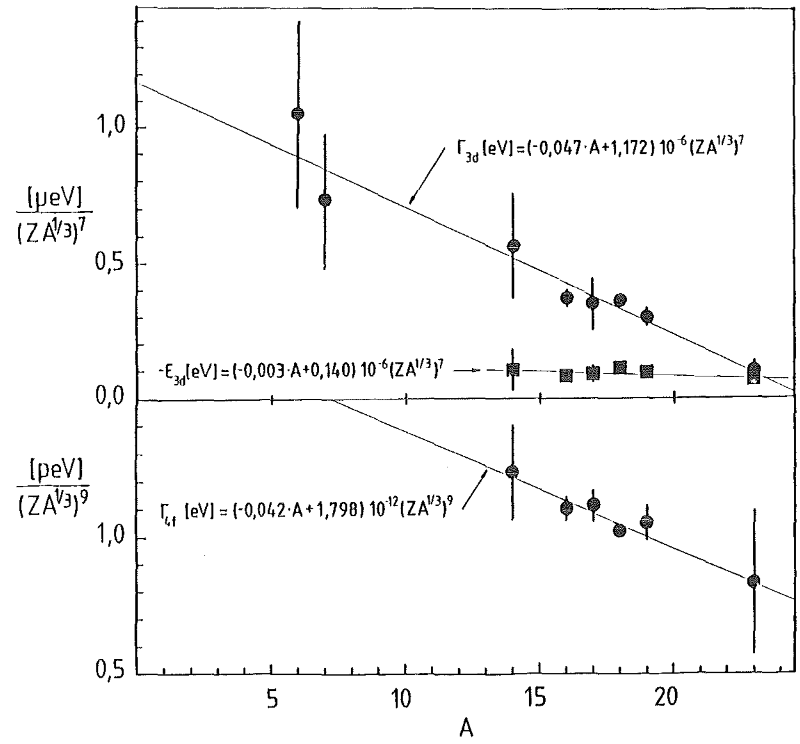

Fig. 1 Measured strong interaction shift and width devided by the overlap with the nucleus as a function of the nuclear mass A

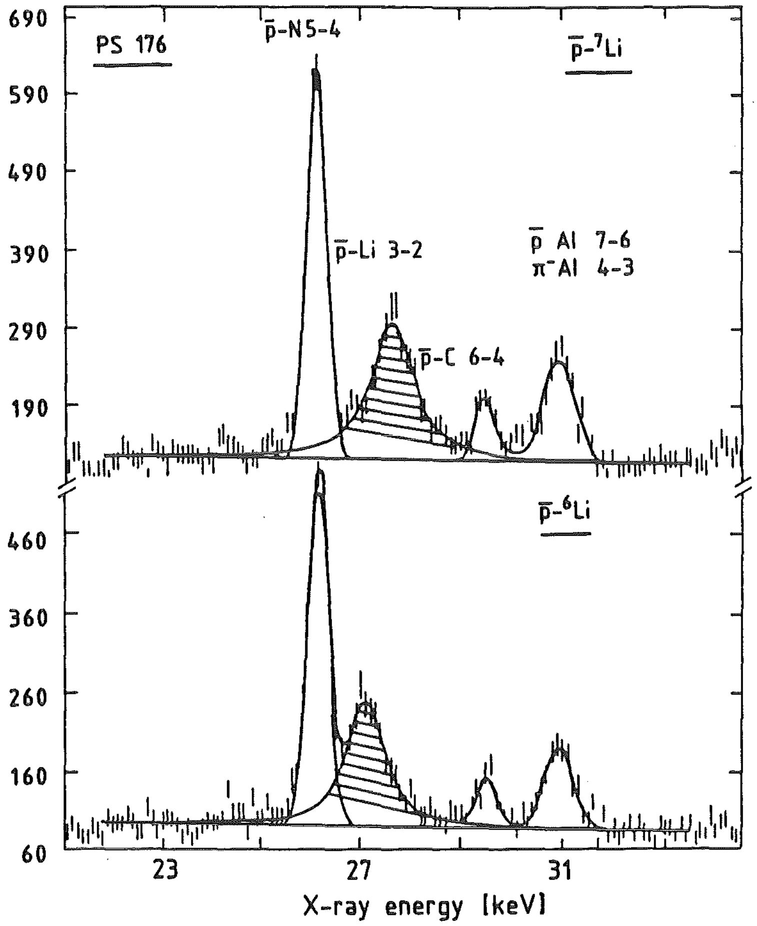

Fig. 2 X-ray spectrum of antiprotonic ^{6}Li/^{7}Li

precision of our measurement is about 2.5 times higher than the world average.

In levels which are closer to the nucleus strong interaction effects may contribute with different strength to the fine-structure components. This is due to a specific dependence of the strong force on angular momentum and spin. Hence the measurement of strong interaction effects in separated fine-structure compenents allows us to study these dependences. We have observed a significant difference in shift and width between the level where spin and angular momentum are parallel to the case where these vectors are antiparallel in ^{174}Yb. Our measured values are 5):

$$\varepsilon_{\uparrow\uparrow} - \varepsilon_{\uparrow\downarrow} = 59(30)\,\mathrm{eV} \qquad \Gamma_{\uparrow\uparrow} - \Gamma_{\uparrow\downarrow} = -195(60)\,\mathrm{eV}$$

This represents the first experimental evidence for a spin-orbit dependence in antinucleon-nucleon interaction.

(1) H. Poth, Antiprotonic, Hyperonic and Antihydrogen Atoms, Proc. Fermilab Antimatter Physics Conference, Batavia, April 10-12, 1986

(2) H. Koch, Antiprotonic atoms, 2nd Conf. on Intersection between Particle and Nuclear Physics, Lake Louise, Canada, May 24-31, 1986

(3) D. Rohmann et al., Mesurement of strong interaction width for the antiprotonic atomic 4f level, submitted to Zeitschrift für Physik

(4) Th. Köhler et al. , Precision Measurement of Strong Interaction Effects in Antiprotonic O16, O-17 and O-18 atoms, Phys. Lett. 176B(1986)327

(5) A. Kreissl, Thesis, University of Karlsruhe, KfK 4123, 1986

+ CERN, Geneva, Switzerland
++ Physikalisches Institut, University of Basel
+++ Institut for Nuclear Research, Stockholm
IV Physics Department, University of Thessaloniki
V CRNS, Strasbourg
VI Technische Universität München
VII University of Mississippi, University, USA

4.2.6 PARTICLE SPECTROSCOPY AFTER ANTIPROTON ANNIHILATION IN LIGHT ATOMS

R. Bacher, J. Egger[++], K. Elsener[+], D. Gotta, K. Heitlinger, D. Protic[+++], G. Riepe[+++], D. Rohmann, M. Schneider, L.M. Simons[++]

A Ge-seminconductor stack has been used to detect light charged particles originating from the annihilation of antiprotons stopped in gas targets of 4.2 to 36 mbar pressure.

The particles have been identified an E-E configuration of an E-counter (thickness 1 mm), 2 E-counters (11 mm + 12.5 mm) and a VETO-counter (14 mm). The active areas are about 3 cm^2. The counters were mounted on cooling fingers in a cryostat and flanged to the target chamber at the bore hole of the cyclotron trap outside the iron yoke yielding a solid angle of $(7 \pm 1)\ 10^{-5}$. The vacuum was separated from the target gases by a 7 µm HAVAR window.

The antiprotons were stopped in the cyclotron trap at the equivalent pressures of 30 mbar for H_2 and D_2, 36 mbar for ^{4}He and 4.2 mbar for N_2. The protons, deuterons and tritons are identified as isolated hyperbolas in the E-E-plane in the energy range of 18-80 MeV (Fig. 1). In a measurement with an extended energy range ^{3}He could be measured in the energy range of 30-60 MeV,

Fig. 1 Particle spectrum after $\bar{p}$ annihilation at rest in 36 mbar ^{4}He

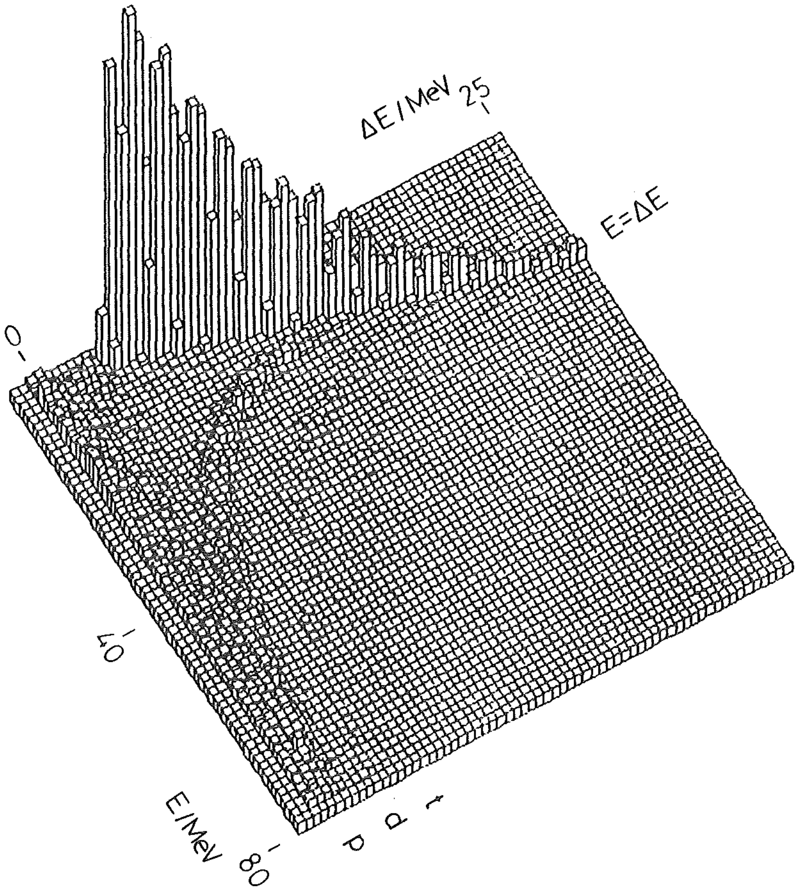

	p	d	t	^{3}He
T min/MeV	18	22	26	30
T max/MeV	80	80	80	60
$\bar{p}$ D	2.7 ± 1.8	-	-	-
$\bar{p}$ ^{4}He	7.2 ± 1.6	1.6 ± 0.4	0.14 ± 0.24	0.17 ± 13
$\bar{p}$ N	13.4 ± 2.1	3.3 ± 0.6	0.66 ± 0.33	
background ($\bar{p}$H and $\bar{p}$D)	4.7 ± 1.0	1.2 ± 0.2	0.51 ± 0.21	0.72 ± 0.06

Table 1 Relative yields of protons, deuterons, tritons and ^{3}He (background subtracted) Threshold ΔE = 2.5 MeV

when the particles stop in the E-counter.

Per annihilation about 2 negative pions are produced, which can stop in the materials of the target chamber and the cryostat walls. Assuming equal negative pion multiplicities for all targets$^{1)}$, the background of protons, deuterons, tritons and ^{3}He is known from the H_2-measurement. Except for protons this background is also determined by the D_2-measurement.

The relative rates (not corrected for the solid angle) normalized to 10^6 stop triggers are shown in Table 1. Errors include statistical errors, particle separation and normalization.

The measured rates given above are an average over the momentum dependent detection efficiency due to the imaging properties of the magnetic field, which leads to an increase of the solid angle. The correction factors for the solid angle has been estimated considering the number of turns in the magnetic field$^{2)}$. One obtains factors from 1.5 for protons of the minimum kinetic energy (T=18 MeV) to 1.14 for tritons of maximum energy (T=80 MeV). Absolute rates can be obtained applying a mean correction factor and dividing by the solid angle.

(1) A.S. Iljionov, V.I. Nazaruk and S.E. Chgrioniv, NP A382(1982)378
(2) I. Lindgren, G. Petterson and W. Schneider, NIM 22(1963)48

+ CERN, Geneva, Switzerland
++ SIN, Villigen, Switzerland
+++ KFA Jülich

4.2.7. CRITICAL ABSORPTION OF A 70-GE ANTIPROTONIC X-RAY TRANSITION

G. Zach, B. Jödicke, G. Büche, R. Frahm+, H. Koch, G. Materlik+

The precise knowledge of the energy of an antiprotonic X-ray transition is a matter of great interest. We applied the method of critical absorption to analyse a first case, where the transition energy coincides with the energy of the K-edge of an electronic atom$^{1)}$. The work was done within the scope of the experiment PS176 of LEAR at CERN in Geneva. In our experiment the X-ray transition 9 → 8 of antiprotonic ^{70}Ge was filtered by a natural mercury absorber$^{2)}$. To interprete the intensity measured behind the absorber in terms of the energy relative to the inflection point of the K-edge, the parameters of the edge and the thickness of the absorber are needed. The parameters of the edge and the extinction coefficient in its neighbourhood were measured using the double crystal monochromator RÖMO of the Synchrotronstrahlungslabor (HASYLAB) at DESY in Hamburg. The resulting transmission of the Hg absorber within the region of the K-edge is plotted in Fig. 1. The smooth curve is a fit of an arctangent to the logarithm of the data points. The thickness of the Hg absorber was calibrated from the transmission of a few lines of the antiprotonic ^{70}Ge below and above the energy of the K-edge. It was found to be 335 ± 10 mg/cm². A breakdown in the circuit of DESY prevented us from an absolute calibration of the energy as well as from a determination of the resolution of the monochromator at the unusually high energy of 83.1 keV.

Therefore we decided on the following compromise. In the literature we found the energy of the inflection point for the K-edge of elemental liquid Hg to

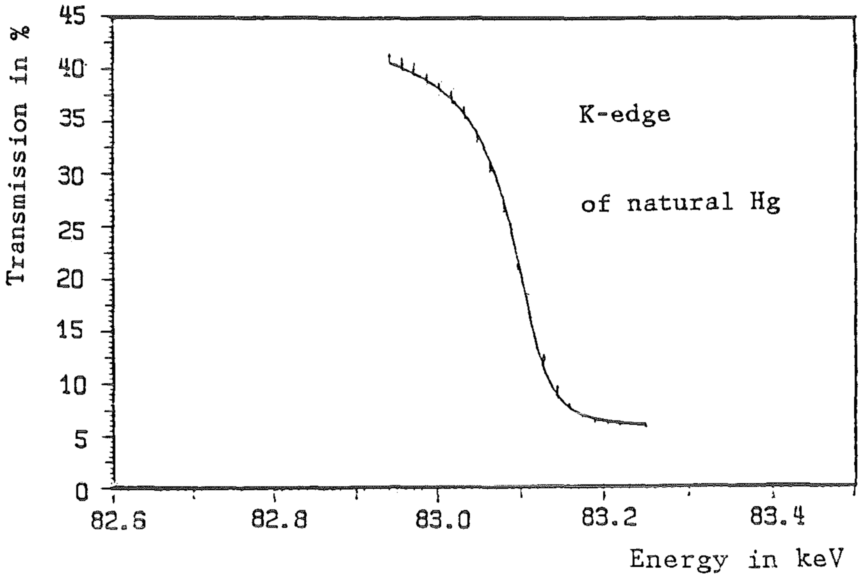

Fig. 1
The measured X-ray transmission of the Hg-absorber in the energy region of the K-edge

be within the region of about 83100 to 83110 eV. Consequently, we analysed our measurement relative to the median 83105 eV for the position of the K-edge, and to 54.6 eV for the width. The systematic errors due to this decision are ± 7 eV and ± 3 eV, respectively. The errors of our measurement are from the statistics of the intensity of the absorbed line (± 2 eV), from the unresolved line structure (± 2 eV), and from the thickness calibration (± 4 eV) leading to a final value of ± 5 eV. Based on the above choice for position and width of the Hg K-edge, we determine the energy of the transition $n_i, l_i, i_i = 9,8,{}^{17}/2 \rightarrow n_f,l_f,j_f = 8,7,{}^{15}/2$ of antiprotonic ^{70}Ge to 83074 ± 5 (± 10) eV, where the systematic error is added in parentheses. This value is in agreement with 83068 eV expected from a calculation using the program PBAR$^{1)}$.

From this feasibility study we feel sure that the errors of the X-ray energy induced from the width and the energy of the Hg K-edge can be reduced to about 2 eV and about 4 eV, respectively. Therefore with an absolute calibration it seems to be possible to lower the uncertainty of the transition energy from ± 5 eV (± 10 eV) to a total uncertainty of about ± 8 eV, which corresponds to an accuracy of 10^{-4}.

(1) B. Jödicke, "Über die Bestimmung von Röntgenenergien antiprotonischer Atome durch kritische Absorption an Kanten und die theoretische Deutung von Ergebnissen", KfK-Bericht 3933 (Juni 1985)

(2) B. Jödicke et al., "Critical absorption of antiprotonic X-rays", Annual Report on Nuclear Physics Activities, KfK 3969 (Oct. 85)

+ Hamburger Synchrotronstrahlungslabor (HASYLAB), DESY, Hamburg

4.2.8 SEARCH FOR NARROW LINES IN GAMMA SPECTRA FROM PROTON-ANTIPROTON ANNIHILATIONS AT REST

A. Angelopoulos[+], A. Apostolakis[+], T.A. Armstrong[++], B. Bassalleck[+++], J. Biard[++], G. Büche, L. Bürcker, P. Denes[+++], M. Fero[IV], M. Gee[IV], N. Graf[+++], R. Hill[+++], H. Koch, N. Komninos[+++], R.A. Lewis[++], M. Mandelkern[V], P. Papaelias[+], S.M. Playfer[a], R. Ray[IV], W. Rohrbach, H. Rozaki[+], L. Sakellion[+], D. Schultz[IV], J. Schultz[IV], J. Schwertel, G.A. Smith[++], M.J. Soulliere[++], M. Spyropoulou-Stassinaki[+], T. Usher[IV], D. Walther, K. Willuhn[++], D.M. Wolfe[+++]

A description of the magnetic pair spectrometer (PS183 at LEAR) and first results from the May 1985 run have been given in the last Annual Report$^{1)}$. The present contribution intends to give the methods of event analysis and of track reconstruction. The evaluation of the photon spectrum with respect to narrow photon lines from $\bar{p}p \rightarrow \gamma + X$ at energies of a few hundred MeV as well as to kinematical structures from neutral 2 body channels ($\pi^o\pi^o$, $\pi^o\omega, \ldots; \pi^o \rightarrow 2\gamma, \ldots$) is still in progress.

For calibration purposes a certain amount of charged particles has been recorded: delayed events of μ^+ and π^+ from decaying K^+ particles stopped in the liquid hydrogen target; prompt events from $\bar{p}p$ annihilations into $\pi^+\pi^-$ and K^+K^- channels. They all give rise to peaks in the momentum spectrum at well known energies and whose widths are studied using various track reconstruction methods. The photon spectrum which is reconstructed from the momenta of e^+e^--pairs has only one clear calibration signal. It is the line of 129 MeV photons emitted after radiative capture of negatively charged pions stopped in the liquid hydrogen target. This line was found after the application of a time cut at about 0.8 nsec excluding early events. Having set the magnetic field to a value of 3.5 kGauß this line appeared in the plots of RT- (i.e. returning and trapped tracks) and TT-events (see Fig. 1). The efficiency of additional cuts in the event spectrum was estimated from a visual inspection of a series of single events. An example of these events is plotted whithin a scheme of the spectrometer (Fig. 2). The magnetic field is oriented vertically to the plane. The event is initiated by a neutral particle which is found to have a vertex point whithin the target volume. The particle which is bent upwords (in the figure) returns from the magnet and triggers the A counter late. Its time is ordered to be in agreement with a particle of electron mass.

The momenta of the particles are reconstructed from an application of one of the following methods. The 3-point method uses a circle connecting the hits in the B, C2 and (D2 or E2 or Z or....) chambers. The momentum is calculated from the radius of the circle. The second method uses the hits in all chambers. In addition to that it takes into account the real distribution of the magnetic

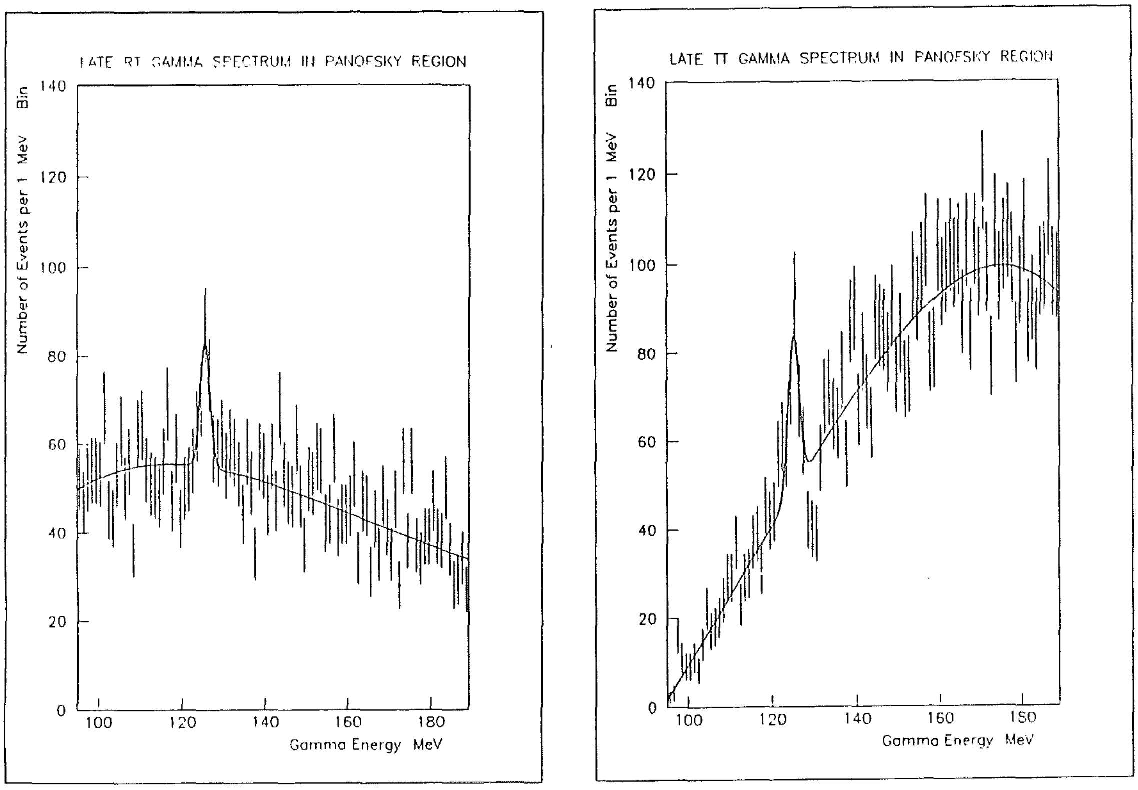

Fi. 1 Photon spectrum in the energy region of the Panofsky line reconstructed from the so-called RT-events (left) and TT-events (right)

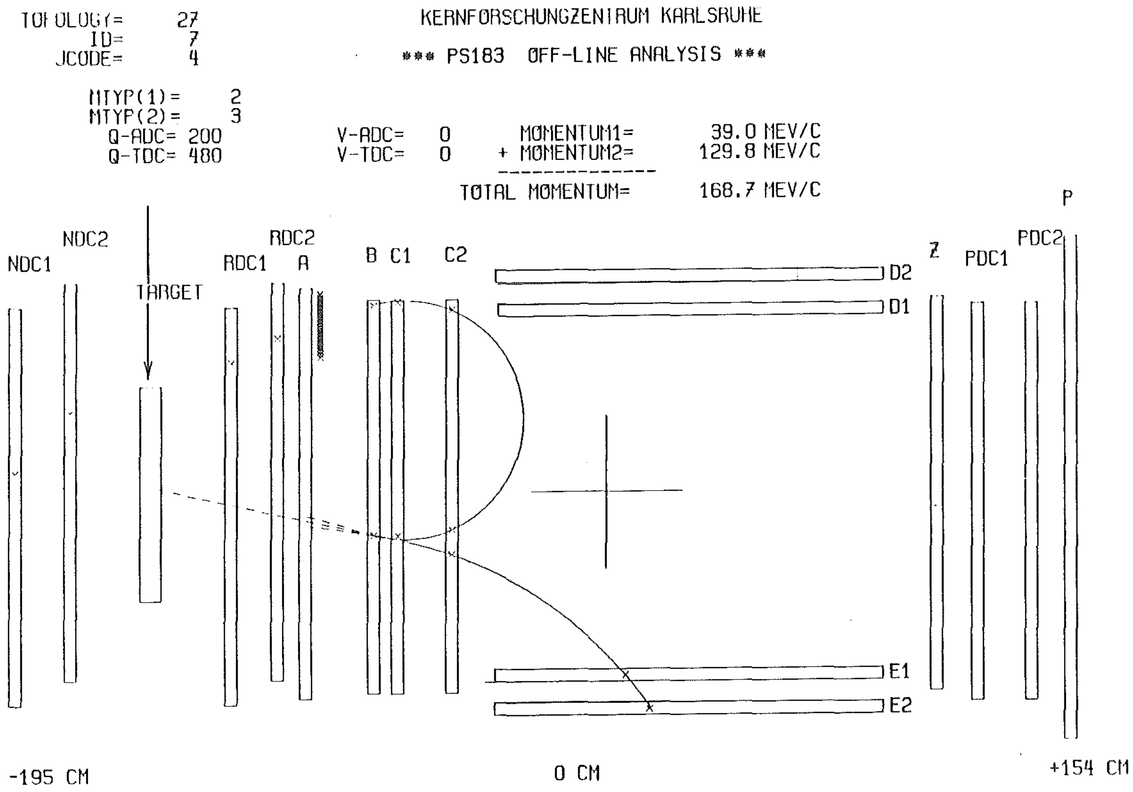
TOPOLOGY= 27
ID= 7
JCODE= 4
MTYP(1)= 2
MTYP(2)= 3
Q-ADC= 200
Q-TDC= 480
KERNFORSCHUNGZENTRUM KARLSRUHE
*** PS183 OFF-LINE ANALYSIS ***
V-ADC= 0
V-TDC= 0
MOMENTUM1= 39.0 MEV/C
+ MOMENTUM2= 129.8 MEV/C
TOTAL MOMENTUM= 168.7 MEV/C
NDC1
NDC2
TARGET
RDC1
RDC2
A
B
C1
C2
D2
D1
E1
E2
Z
PDC1
PDC2
P
-195 CM
0 CM
+154 CM

Fig. 2 From the topology of hits in this event a T-type and a R-type track is reconstructed

field (cf. Ref. 2). The last method integrates the equation of motion starting from the hits in B and C1 together with the initial momentum value from the 3-point method. The final momentum results from a minimisation procedure of the distances between the points of the track and the corresponding hits in the chambers. This way each type of track (R, T or P = penetrating the spectrometer) can be reconstructed economically with respect to the momentum value, resolution and computer time.

A further run in July 1986 using a LH_2 target was done to collect more statistics in the photon spectrum at a higher magnetic field and including a higher rate of charged events. In addition to that the measurements were extended to a liquid deuterium target to measure the $\bar{p}n$ annihilation process, too.

(1) Annual Report on Nuclear Physics Activities, KfK-Report 3969, October 1985, p. 107

(2) H. Wind, Nucl. Instr. Meth. 115(1974)431-34

+ Nuclear Physics Laboratory, University of Athens, Athens, Greece

++ Department of Physics, Pennsylvania State University, University Park, PA USA

+++ Department of Physics, University of New Mexico, Albuquerque, N.M. USA

IV Department of Physics, University of California, Irvine, CA, USA

4.2.9 MEASUREMENT OF THE ANTINEUTRON-PROTON CROSS SECTION AT VERY LOW ENERGY

T. Armstrong[+], B. Bassalleck[++], M. Furić[+++], A. Hicks[+], J. Kruk[IV], R. Lewis[+], W. Lochstedt[+], D. Löwenstein[V], B. Mays[VI], M. Moss[IV], G. Mutchler[IV], L. Pinsky[VI], H. Poth, G.A. Smith[+], L.S. Vinson[VI], W. von Witsch[VII], Y. Xue[VI]

In experiment E795 at the AGS in Brookhaven National Laboratory the $\bar{n}p$ annihilation cross section has been studied at very low energy ($T_{\bar{n}} < 1$ MeV). The antineutrons were produced by antiprotons through the charge exchange reaction. The experimental arrangement is shown in Fig. 1. The antineutrons annihilated in the same liquid hydrogen target in which they were produced.

The $\bar{n}p$ annihilation cross section is extracted from the measured time dependence of the $\bar{n}$ annihilation in the target[1)]. The lifetime of the antineutron in the target is derived from the arrival time of annihilation products in the M-counters. The annihilation vertex can be reconstructed from the tracks measured in the drift chambers (DC). Very slow antineutrons were tagged by recording the associated forward going neutron in a separate neutron detector.

It is expected that the annihilation cross section σ_a at this low energy scales as $1/\beta_{\bar{n}}$. Therefore the annihilation probability follows an exponential law with $1/\beta_{\bar{n}}\ \sigma_a)$ as the decay constant. The measured antineutron annihilation

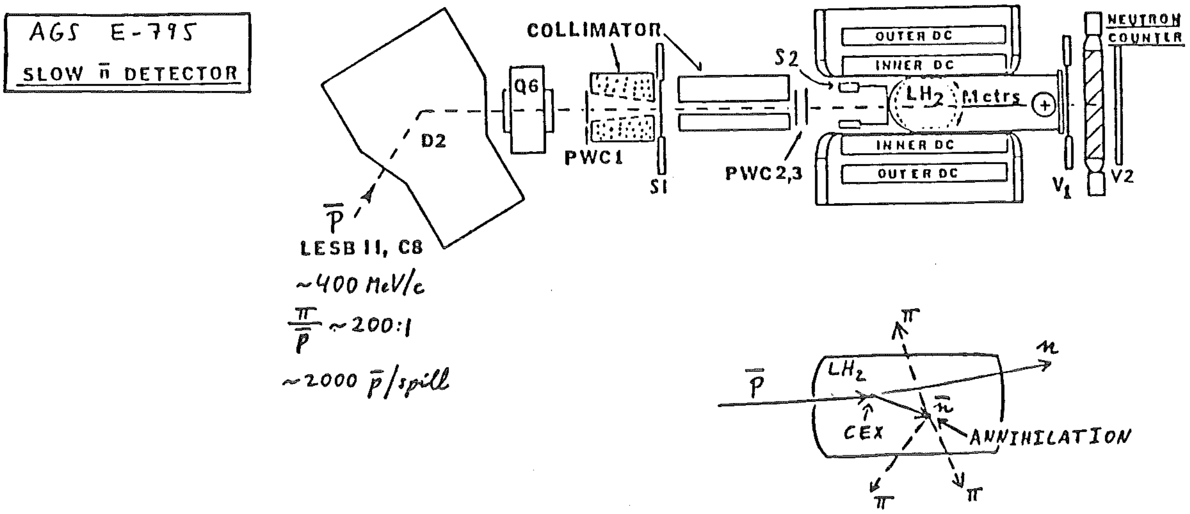
AGS E-795
SLOW $\bar{n}$ DETECTOR
D2
$\bar{p}$
LESB II, C8
~400 MeV/c
$\frac{\pi^-}{\bar{p}}$ ~200:1
~2000 $\bar{p}$/spill
Q6
COLLIMATOR
PWC1
S1
PWC2,3
S2
OUTER DC
INNER DC
LH2
1 Metrs
INNER DC
OUTER DC
V1
NEUTRON COUNTER
V2
π
n
$\bar{p}$
LH2
CEX
$\bar{n}$
ANNIHILATION
π
π

Fig. 1 Experimental set-up and schematic of a typical event of interest

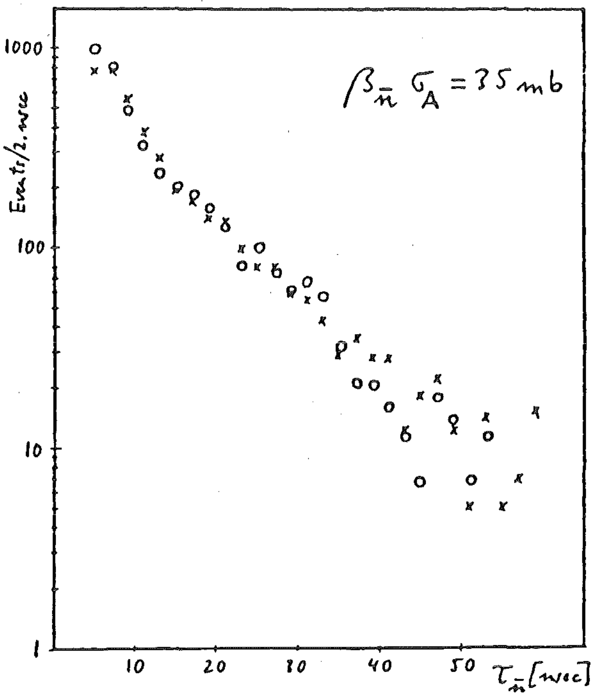

Fig. 2 $\bar{n}$ lifetime data (x's) and Monte Carlo with $\beta_{\bar{n}} \sigma_a$ mb (circles)

time distribution is shown in Fig. 2 and is compared with a Monte Carlo calculation. From these data we derive a tentative value for $\beta_{\bar{n}} \sigma_a$ of 35 mb 2).

(1) Annual Report 1984/85, KfK 3969, 1985, p. 108
(2) B. Bassalleck et al., Proc. 2nd Conf. on the Intersections between Particle and Nuclear Physics, Lake Louise, Canada, 1986

+	Pennsylvania State University
++	University of New mexico
+++	University of Zagreb
IV	Rice University, Houston
V	Brookhaven National Laboratory
VI	University of Houston
VII	University of Bonn

4.2.10 FEASIBILITY STUDY FOR ANTIHYDROGEN PRODUCTION

J. Berger[+], P. Blatt[+], C. Habfast, H. Haseroth[++], C.E. Hill[++],
R. Neumann[+], H. Poth, B. Seligmann, J.L. Vallet[++], A. Winnacker[+], A. Wolf[++]

In electron cooling of proton beams neutral hydrogen atoms are formed when cooling electrons are captured by circulating protons.

$$e + p \rightarrow H + h\nu$$

This process was observed in passed cooling experiments. Its dependence on the beam parameters is well understood. It was pointed out recently, that this reaction can be enhanced through induced capture¹⁾:

$$n\,h\nu + e + p \rightarrow H + h\nu + n\,h\nu$$

It was shown in Ref. 1 that the rate of hydrogen production can be increased by two orders of magnitude if a powerful laser is used and the capture into the second excited state of hydrogen is induced. The application of this technique to produce a beam of antihydrogen seems to be very promising.

We have performed a theoretical study concerning the feasibility of such an experiment at LEAR using the electron cooler, a powerful Eximer-pumped dye laser and a positron beam produced from a radioactive source²⁾. As a consequence of the encouraging outcome of this study a proposal was submitted to CERN³⁾ to do a pilot experiment at LEAR with the following aims:

- Experimental verification of the predicted gain of two orders of magnitude in the induced electron capture to be performed with protons stored in LEAR and electrons from the electron cooler as well as a 10 MW eximer laser pumping a dye laser.
- Producting of antihydrogen atoms through spontaneous capture of positrons in order to study the feasibility of merging a low intensity positron beam with an antiproton beam. This part of the experiment is supposed to be performed in straight section 2 (Fig. 1) of LEAR with circulating antiprotons and positrons produced from a 10Ci radioactive source. The production rate was estimated to be about 3 antihydrogen atoms per hour.

The intention was to use the information gained from this experiment to design an antihydrogen production facility based on stimulated capture and a time structured positron beam produced from a linac⁴⁾. Based on the present information and the validity of the predictions of Ref. 2 one could expect to produce then more than 10^4 antihydrogen atoms per second. This would be a very high intensity beam suitable for precision experiments⁴⁾ and opening the possibility to produce polarized antiproton beams⁵⁾.

(1) R. Neumann, H. Poth, A. Wolf, A. Winnacker, Z. Phys. A313(1983)253
(2) A. Wolf, H. Haseroth, C.E. Hill, J.L. Vallet, C. Habfast, H. Poth,
B. Seligmann, P. Blatt, R. Neumann, A. Winnacker, G. zu Putlitz,

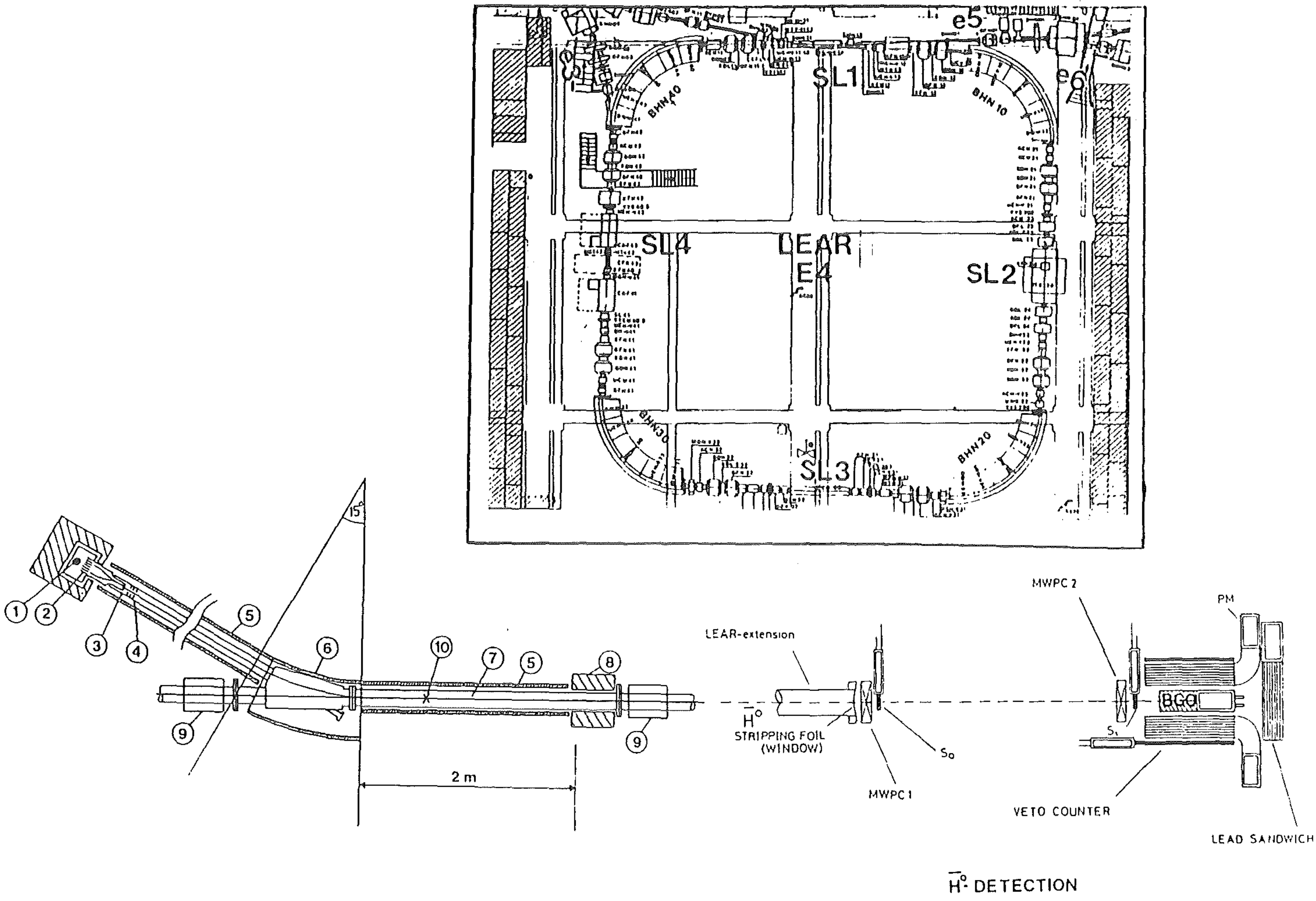
e5
e6
SL1
SL2
SL3
SL4
LEAR
E4
BHN 10
BHN 20
BHN 30
BHN 40
15°
①
②
③
④
⑤
⑥
⑦
⑧
⑨
⑩
2 m
LEAR-extension
H°
STRIPPING FOIL
(WINDOW)
S₀
MWPC 1
MWPC 2
PM
BGO
S₁
VETO COUNTER
LEAD SANDWICH
H̄° DETECTION

Fig. 1 Antihydrogen production and detection scheme

Electron cooling of low-energy antiprotons and production of fast antihydrogen atoms, Proc. Workshop on the design of a low-energy antimatter facility in the USA, Madison, Wisconsin, 1985.

(3) J. Berger et al., Feasibility Study for Antihydrogen Production at LEAR, Proposal to CERN, CERN-Heidelberg-Karlsruhe Collaboration, CERN/PSCC/85-45, PSCC/P86, CERN/PSCC/86-21, Add. 1 and CERN/PSCC/86-37 Add. 2 (extended collaboration includes Ann Arbor and Brookhaven National Laboratory) (spokesman H. Poth)

(4) H. Poth, Physics with Antihydrogen, Proc. 2nd Conf. on the Intersection between Particle and Nuclear Physics, Lake Louise, Canada, May 1986.

(5) H. Poth and A. Wolf, Antiproton polarization through antihydrogen, KfK 4098(1986)

+ Physikalisches Institut, Universität Heidelberg

++ CERN, Geneva, Switzerland

4.3 THE CRYSTAL BARREL PROJET AT LEAR

CB-Collaboration:

E. Aker, G. Büche, S. Cierjacks, D. Engelhardt, T. Henkes, H. Koch, A. Kreissl, F. Kröner, M. Kunze, H. Matthäy, J. Plotzitzka, D. Rohmann, W. Rohrbach, W. Schott, D. Walther, Ch. Weddigen; Kernforschungszentrum Karlsruhe GmbH und Universität Karlsruhe, Federal Republic of Germany

C. Amsler, B. Schmid, P. Truöl, Universität Zürich, Switzerland

C. Batty, Rutherford and Appleton Laboratory, Chilton, UK

P. Birien, CERN visitor, Geneva, Switzerland

J. Bisterlich, C.A. Meyer, K.M. Crowe, Lawrence Berkeley Laboratory, University of California, Berkeley, USA

D. Bugg , G. Hall, Queen Mary College, London, UK

A.S. Clough, R.L. Shypit, University of Surrey, Guildford, UK

E. Klempt, M. Guckes, H. Kalinowsky, R. Rieger, W. Weidenauer, Universität Mainz, Federal Republic of Germany

R. Haddock, University of California, Los Angeles (UCLA), USA

M. Suffert, Centre de Recherches Nucléaires, Strasbourg, France

H. Vonach, Institut für Radiumforschung und Universität, Wien, Austria

W. Wodrich, C. Zupancic, Universität München, Federal Republic of Germany

K. Braune, CERN-Fellow

An extended proposal for the project containing the maior physics ideas and all details of the technical realization was prepared in the fall of 1985 and presented to the CERN PSC-Committee in November$^{1)}$. As far as physics is concerned it stresses searches for exotic, nonmesonic states like Glue-Balls and Hybrids for which the detector is particularly suited (see Fig. 1). The proposal was unamimously approved by the PSCC and later by the Research Board of CERN and is considered as one of the essential Lear-experiments in the post-ACOL-period. After the completion of the work on the proposal more details of the components were worked out as basic for tenders to the industry. The replies to these tenders allowed a precise cost estimate which is 7.3 MDM. The most essential position there is the cost of the 1380 CsI-crystals which amount to 3.4 MDM. It is foreseen to finance these crystals exclusively by means of KfK and the University (BMFT) of Karlsuhe. The total amount of money provided by the member of the collaboration in the years '86-'88 sums up to 7.6 MDM, allowing a reserve for contingency. In order to reach a full financing in the years '86-'88 some cuts on specific items of the detector had to be performed which, however, don't affect the overall quality of the detector for the experiments foreseen at LEAR. At present, an agreement between CERN and the collaborators is in preparation. It foresees a Steering Committe which decides about the scientific programm and controls with the help of a secretary the flow of money and manpower during the set up phase of the experiment.

The distribution of task among the collaborators attributes to KfK/University Karlsruhe the following items:

- Set up and test of the CsI-detector, including read out-electronics and mechanics
- Preparation of the microprocessor-based trigger system (together with other collaborators)
- Help on the construction and test of the Jet-Drift-Chamber (JDC) and the proportional wire chamber (PWC).

(1) CERN/PSCC/85-56; PSCC/P 90

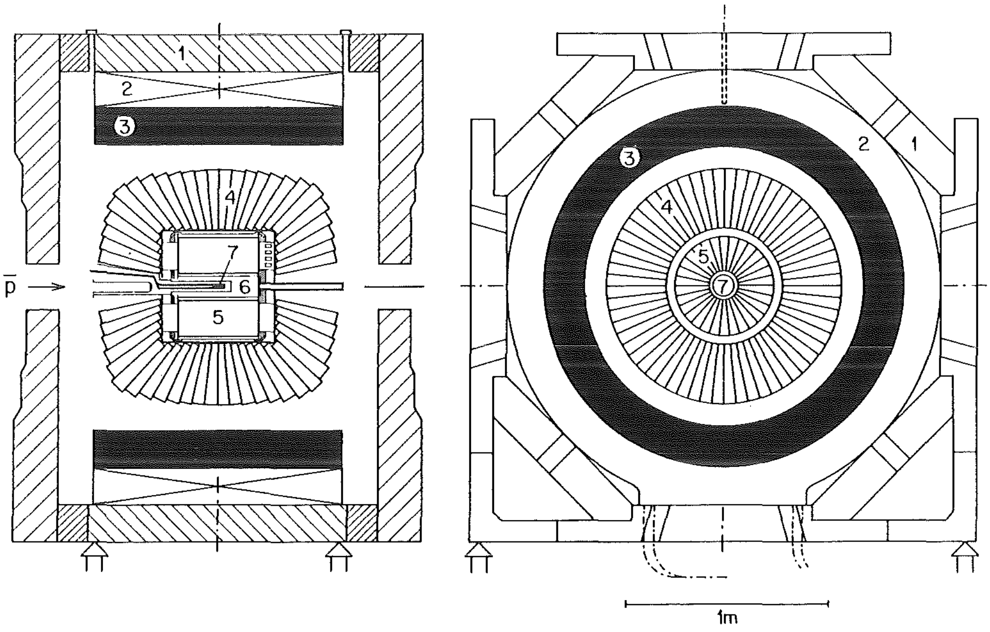

Fig. 1 CB-Detector
1: Magnet yoke; 2/3: Magnet coil, 4: CsI-crystals, 5: Jet-Drift-Chamber
6: X-Ray Drift chamber or Proportional-Wire-Chamber, 7: LH_2-Target

4.3.1 STATUS OF THE CB-Project

H. Koch, G. Büche, S. Cierjacks, D. Engelhardt, Th. Henkes, F. Kröner,
M. Kunze, H. Matthäy, J. Plotzitzka, W. Rohrbach, W. Schott, D. Walther,
Ch. Weddigen

In the following some comments are given on the present status of the work on the maior items of the project with special emphasis to the ones with participation from Karlsruhe.

CsI-Detector

CsI-crystals/Energy resolution/Calibration/Electronics

About 30 CsI-crystals of original shape and size were bought from three firms (BDH, Horiba, Bicron) and were tested with radioactive sources and on the

SC-Muon-channel with 200 MeV/c electrons. Very important for a good energy calibration is the homogenity of the crystals, and a method was worked out to test this feature with high precision. The in-beam test of a cluster of 20 CsI-modules at the SC was - because of beam schedule reasons - performed with a not optimized set up (only one photodiode/crystal; preliminary version of pre-amplifier chain) and with a beam of badly known $^{\Delta p}/_{p}$ (FWHM) $\approx$ 5-10%) momentum spread. The results of this test$^{1)}$ are discussed more in detail in 4.3.2 and show that the envisaged energy resolution $\frac{\Delta\sigma}{E} = 0.020/\{E[\mathrm{GeV}]\}^{1/4}$ is easily obtainable. A second test with a better beam and more refined electronic is foreseen for 1987 at SIN.

In the meanwhile quite successful tests have been performed (with the help of MPI München) replacing the four Si-diodes on the rear face of the crystals by only one diode attached side ways to an appropriate wave length shifter (see 4.3.3). If that solution turns out to be feasible, the cost and the complexity of the readout-system can be significantly reduced.

The energy calibration of the crystals will be done with radioactive sources (^{228}Th (2.6 MeV); Pu^{13}C (6.1 MeV)) and with the reaction $(\pi^{-})_{stop}p \rightarrow n\gamma$ (129 MeV). It is expected that an individual calibration of each crystal in an electron beam will not be necessary. The monitoring of the stability of the neutral detector will be done by a flash-light-system which is presently under construction.

In order to obtain a good energy resolution a low noise level on each individual crystal is mandatory. Two preamplifiers (KfK Karlsruhe, MPI München) built for similar applications in High Energy Physics were tested and yield r.m.s. noise equivalent levels of as low as 300 keV. The chain between preamplifier and the Fera-ADC's consisting of amplifier/shaper/discriminator needs special attention because of the large dynamical range and is presently under construction at KfK. A computer system allowing the test of the Fera-ADC's is also set up at KfK.

Mechanical support of the CsI-crystals

The mechanical support of the CsI-crystals presents a major problem because of the large solid angle (95% x 4 π) envisaged for the neutral detector which precludes massive walls between the crystals. Also the wall of the detector in the direction of the target must be as thin as possible, thus avoiding the conversion of Gamma-rays before they reach the sensitive volume of the detector. Extensive Monte-Carlo-studies (see 4.3.4) have been performed to get an idea on the effect of the material between and in front of the crystals concerning the energy resolution of the detector. It turns out that the wall in front of the crystals is not as critical as the material between the crystals which should be not thicker than .5 mm (carbon-fiber-material) or .2mm (Ti). These numbers put an upper limit to the thickness of the encapsulation of the crystals, which is necessary to attach the light-read-out-system to the crystals and allows for an easy removal of the crystals. Together with IT/M at KfK and the industry (Dornier, Stesalit) various solutions are worked out and tested at present: Carbon fiber/ glass fiber/Ti-material for the encapsulation of the modules or/and in front of the module. The feasibility of the design of the overall support structure will be tested with a 1:1 prototype for one half of the detector which should be ready early in 1987.

Design and realization of the trigger

Because of the low frequency of events of special interest per annihilation (e.g. search for exotic states with a complicated decay pattern) and the limitation of recordable events (300/s) the design and set up of a very effective trigger is one of the most important items of the experiment. Three stages are foreseen: (1) A hardware based trigger for a crude selection of the total multiplicity of an event. (2) A fast microprocessor (CAB) allowing the determination of the total energy and a more refined multiplicity definition. (3) A slower, but more powerfull microprocessor (Starburst), allowing the reconstruction of fast decaying particles, like π^0,$\eta(\rightarrow \gamma\gamma)$, $\rho(\rightarrow \pi\pi)$, $\omega(\rightarrow \pi\pi\pi)$, etc. The design of the hardware-trigger is finished, the CAB- and the Starburst-processors are bought and the programming has started. In order to check the reliability of the trigger a Monte-Carlo-programm is written which allows a simulation of the whole set-up on the basis of hit wires and fired CsI-modules, respectively.

Jet-Drift-Chamber (JDC)

At the beginning of 1986 two american groups (UC Irvine, Penn. State) have decided to leave the collaboration because of internal political problems in the U.S.. They were replaced by two other american groups (UC, Berkeley; UCLA) who took over the responsability for the construction and test of the JDC. The desired high spatial resolution (100µ) and the high magnetic field (1.5 T) requires the use of a slow gas-mixture (CO_2/Isobutan), which needs a very precise control of the gas pressure and the temperature. similar systems have been already successfully built at Berkeley, so that the project is expected to develop smoothly. The design of the chamber together with electrostatic calculations is completed, two test-modeules will be set up in the next months. Collaboration with chamber specialists from KfK is foreseen.

Magnet

The magnet has to produce a field of 1.5 T over the volume of the JDC (50 cm (Ø) x 50 cm (length)). Because of the relatively short running periods (low power costs), the price and the available manpower, it was decided a non-superconducting magnet. The modification of the already existing Asterix-magnet (former DM1-magnet from Orsay) will cost about 400 kDM, including a new coil and an enforced Fe-shielding. The Asterix experiment has finished running, so that the magnet is at our disposal. The modification of the magnet will be paid by the University of München and will start early in 1987.

(1) KfK-Primärbericht 14.02.01 P 18 A

4.3.2 TEST OF A MODULAR CsI(TL) PROTOTYPE CALORIMETER WITH PHOTODIODE READOUT AT 200 MeV/c

Th. Henkes, C. Amsler, H. Koch, F. Kröner, W. Rohrbach, B. Schmid, W. Schott, U. Straumann, M. Suffert, D. Walther

A test with a prototype calorimeter consisting of 20 CsI(Tl) crystals was performed in december 1985 at the CERN Synchro Cyclotron. The main goal of this experiment was to test the readout of CsI(Tl) crystals with photodiodes, as it is forseen in the design of the Crystal Barrel detector at LEAR, and to see whether we can achieve the energy resolution expected from electromagnetic shower calculations (EGS).

The 20 crystals were arranged in an aluminium container which could be rotated horizontally and vertically, so that the beam could penetrate each crystal along its axis. Each crystal was equipped with one photodiode. The signal of the photodiodes was amplified by a low noise charge sensitive preamplifier and shaping amplifier which were mounted on one printed circuit (KfK development by H. Keim). A 15 m shielded twisted pair cabel brought this pulse to a receiver, where the signal was attenuated in order to get a dynamical range of 300 MeV. Then it was feed into a charge sensitive 11 bit ADC (Le Croy FERA 4300). A DEC LSI computer was used to read out the ADC via CAMAC, to write the raw data to tape and to do the online monitoring of the experiment.

From the SC a beam of 200 and 108 MeV/c was available, The beam consisted of e^-, π^-, and μ^-. At a given momentum we could seperate the different particles by their time-of-flight between two scintillators which were positioned in the beam.

In order to get an initial calibration we shot negative pions of 200 MeV/c into each module. Their energy deposit peaks at 104 MeV (kinetic energy) which was used for the calibration. This calibration was improved in the offline analysis of the 200 MeV/c electron runs, using an iterative calibration method (1).

Once we got the final calibration constant of each channel, we summed up the energy of the module that was hit by an electron and its eight neighbouring moduls. From this distribution (Fig. 1) we find an energy resolution

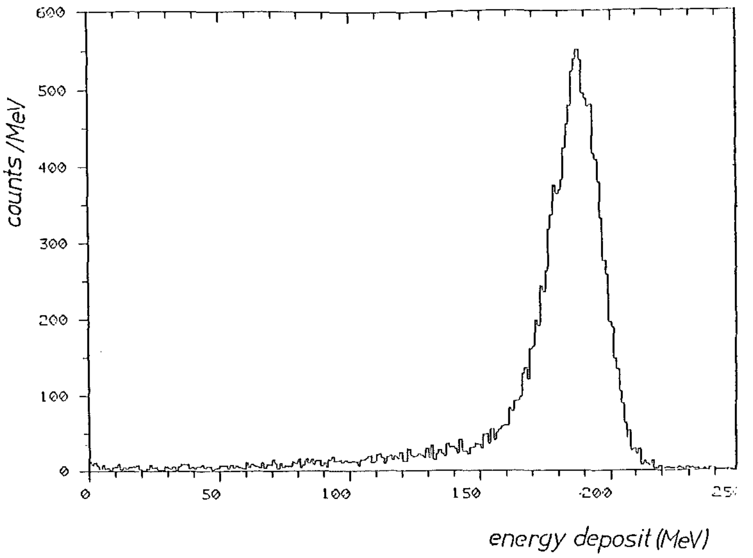

Fig. 1 Energy deposit of 200 MeV electrons in an array of 20 CsI-modules. The energy is summed over nine adjacent crystals.

of $\sigma/E = 4.7\%$ at 200 MeV/c. This is somewhat worse than the value we expect from electromagnetic shower calculations (EGS), where we get an energy resolution of $\sigma/E = 3.8\%$ for our experimental set up. The difference can be explained by the unknown but large momentum spread of the CERN - SC muon channel. A momentum spread in the order of 2.8% (σ) would explain the difference between data and EGS calculations. This value seems reasonable for a beam without momentum defining slits as the muon channel of the CERN - SC.

The intention of this experiment was mainly to learn about the problems with this new type of detector. To determine the precise energy resolution of a CsI(Tl) calorimeter the beam momentum spread has to be known. In the Crystal Barrel detector each crystal will be equipped with four photodiodes or a wave length shifter (see 4.3.3) which improves the signal to noise ratio and therefore the energy resolution. Due to delivery problems in industry only one photodiode per crystal could be used. An experiment which uses a fully equipped detector and the final version of the readout and trigger electronics is in preparation.

The results of this test were published as KfK Primärbericht (2).

(1) P. Blüm et al., Nuclear Instruments and Methods 213(1983)251
(2) C. Amsler et al., KfK Primärbericht 14.02.01 P 18 A

4.3.3 READ OUT OF CsI-CRYSTALS WITH WAVE LENGTH SHIFTERS (WLS)

W. Rohrbach, M. Suffert

The magnetic field of 1.5 Tesla demands for the read out of the CsI-crystals with photodiodes (PDs).

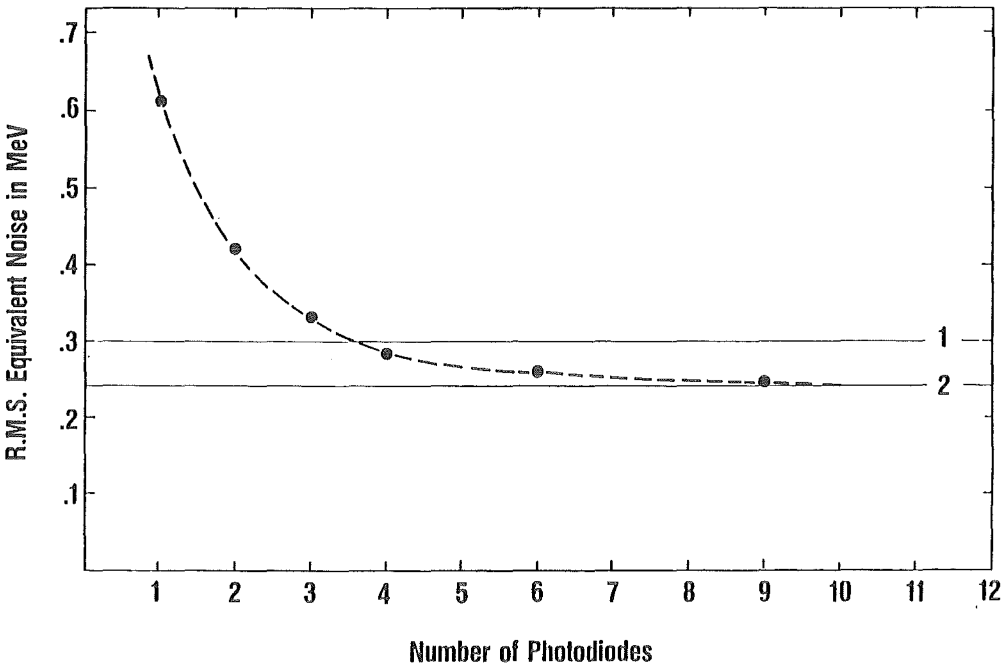

Fig. 1 R.M.S. equivalent noise as a function of the number of photodiodes attached to the rearface of a CsI-module (dotted curve). Lines 1 and 2 show results for the light read out by a wave length shifter with 1 or 2 photodiodes attached sideways to it.

The usual procedure is to use PDs directly coupled with optical grease on the crystal rearface. With four PD's of 1cm^2 area each, and a low noise charge-sensitive preamplifier, a r.m.s. noise equivalent < 300 keV could be obtained. By adding more PDs one samples more light but also adds more noise and a saturation in the signal to noise ratio (Grooms theorem) is observed (doted curve in Fig. 1).

To achieve a lower r.m.s. noise equivalent the idea is to sample as much as possible of the light leaving the crystal rearface and direct it to only one or two PDs with less capacities and therefore less noise than with a larger bunch of diodes. This can be realized with thin wave length shifters (WLS) which cover the whole crystal rearface. The light is converted with one or two PDs of about 30 x 30 mm^2 area placed along the sides of the WLS. At the same time this method has the advantage of reducing the nuclear counter effect.

For optimal results it is important to find a good match between the emission spectrum of the CsI-crystal, which has its maximum at 550 nm, and the absorption curve of the dye used in the WLS.

Furthermore it is very important to find an optimum mixture between dye and carrying material to minimize the losses by selfabsorption.

Measurements have been done with several WLS's which are commercially available or manufactured at the MPI Lab Munich after selection on the basis of their transmission characteristics.

Best results have been obtained with WLS's of 3 mm thickness, optically coupled via an air gap to the crystal rearface. They were covered with teflon tape on the small faces only allowing space for the PDs, and on the upper face with two layers of white filter paper.

With such a set up (2 PDs 30 x 3 mm^2) a r.m.s. noise equivalent of 240 keV was obtained which corresponds to the results of 9 PDs directly coupled on the crystal rearface (line 2 in Fig. 1). The result obtained with only one PD is also sketched in Fig. 1 (line 1).

Work along this line is going on and may eventually lead to a cleaner and less complex solution for the light read-out of the CsI-crystals.

4.3.4 MONTE CARLO STUDIES OF ELECTROMAGNETIC SHOWERS IN THE CRYSTAL BARREL DETECTOR

W. Schott, H. Koch, M. Suffert

The determination of the relevant parameters for the 4π neutral detector, like crystal dimensions and the effect of structure materials, was based on Monte-Carlo simulations of the development of electromagnetic showers using the SLAC-code EGS4[1]. For this a realistic geometrical description of a part of the detector was set up, including walls between and in front of the crystals.

Lengths of crystals/Energy resolution: In order to minimize the costs a realistic compromise for the crystal lengths has to be found. Fig. 1 shows the calculated energy resolutions (FWHM) for different energies as a function of the crystal length. The calculations include the effect of the unavoidable r.m.s. noise which was assumed to be 300 keV for 30 cm long crystals (16 radition lengths) and 250 keV for shorter crystals (e.g. 14 rad. lengths) because of their higher light output. The results show that a length of 16 radiation lengths would be desirable, but that also 14 radiation lengths (26 cm) crystals still yield satisfying results ($\Delta E/E$ (FWHM) = 7.5% at 100 MeV, which is near the maximum of the expected γ-energy distribution).

Nuclear counter effect: In case that the photodiodes are directly attached to the rear face of the crystals, particles from the electromagnetic shower may hit the diodes and cause a pulse of several MeV, thus deteriorating the energy resolution. This effect was calculated for various energies and crystal lengths. At 500 MeV e.g., the probability for this effect is 2% and 6% at 30 cm and 26 cm long crystals, respectively. It is much less probable at lower energies and thus can be neglected as far as the energy resolution is concerned.

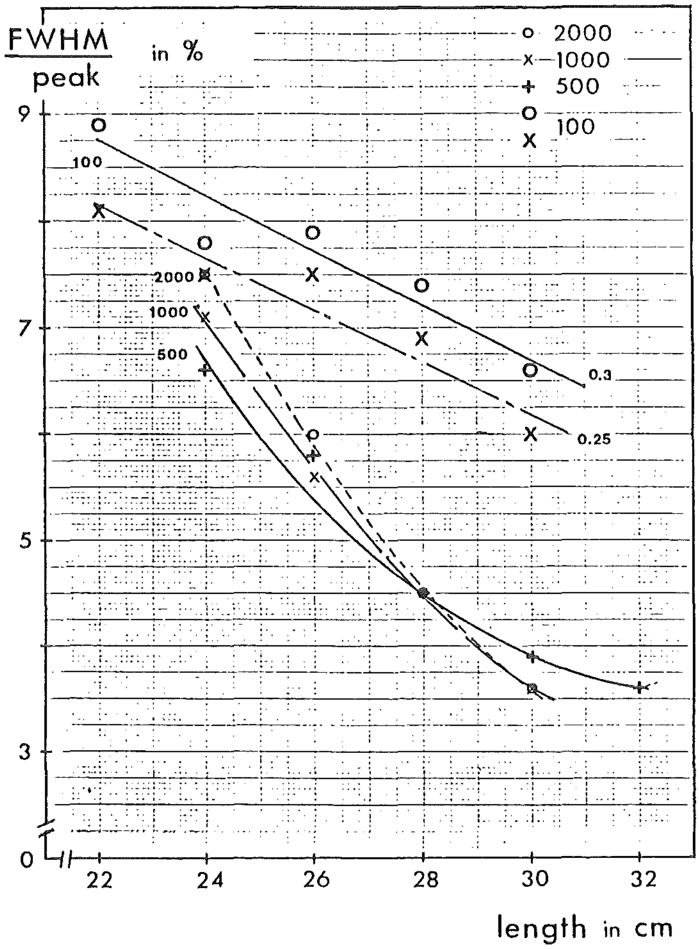

Fig. 1 Energy resolution depending on crystal lenght for incident photon energies of 100 MeV, 500 MeV, 1000 MeV. The simulation results are smeared with 0.3 MeV noise except for one calculation at 100 MeV where the noise was assumed to be 0.25 MeV. The energies of 25 crystals were summed.

Wall thicknesses of the mechanical support: Allowance was made in the simulations for encapsulations of the individual crystals and for support material in front of the modules. While the effect of the latter on the energy resolution is less important, walls between the crystals are critical for the energy resolution. It turned out e.g., that a wall of 0.4 mm of carbon fiber between the crystals deteriorates the energy resolution at 100 MeV by 0.7% and thus appears as an upper limit for the thickness of walls between adjacent modules.

(1) W.R. Nelson et al., SLAC-265 (Dec. 85)

4.4 THEORY

4.4.1 APPLICATIONS OF THE πNN BOUND-STATE PROBLEM: THE DEUTERON AND THE 4,4 RESONANCE

H. Garcilazo, L. Mathelitsch[+]

The relativistic three-body equations for the bound-state problem proposed by the authors[1)] are solved for the πNN system, in particular for the states with total isospin zero and two. In the case of isospin zero only one bound state is found which corresponds precisely to the deuteron and whose wave function is quite similar to those of phenomenological models. We show this "three-body" deuteron wave function in Fig. 1, where we compare it with the deuteron wave function of the Paris potential, and with the Moravcsik-Gartenhaus wave funtion. As we see, there is quite a good agreement between the three-body wave function and the two phenomenological ones, particularly with regard to the change of the sign of the S-state wave function at $k \sim 2 fm^{-1}$; this feature is well-known for all models having a strong repulsive core at short distances. In the traditional picture of the nucleon-nucleon interaction, this strong short-range repulsion is associated with the exchange of heavy mesons, such as ρ and ω. in Our picture, on the other hand, the deuteron is considered as a πNN bound state and the short-range repulsion is generated by the three-body dynamics alone. The D-state probability of the three-body wave function is 8.9%, which is somewhat higher than the values obtained from the Paris- (5.8%) and Moravcsik-wave function (6.7%).

In the case of isospin two the most favorable configuration to possess a bound state is with total angular momentum two and positive space parity. If the system is not bound, it will appear as a resonance of spin 2 and isospin 2 which we call the 4,4 resonance since it is the analog to the wellknown 3,3 resonance in the πN system which has spin 3/2 and isospin 3/2. The bound system would consist of a negative pion and two neutrons (or, its isobaric analog, of a positive pion and two protons). Such a possibility is a very attractive one, since, as the bound state can only decay by weak interactions, it means that it will be stable with a lifetime comparable to that of the charged pion. Even if it turns out that the system is unbound, as the result is in some of our solutions, this would mean that the state lies in the continuum; therefore, it should still be possible to observe it as a three-body resonance. Since this isospin-two resonance cannot couple directly to the nucleon-nucleon system, which can have only isospin zero or one, the observation is only possible via reactions like $\pi^- + d \rightarrow \pi^+ + \pi^- + n + n$ or $\pi^- + t \rightarrow p + \pi^- + n + n$, where in the first case the π^+

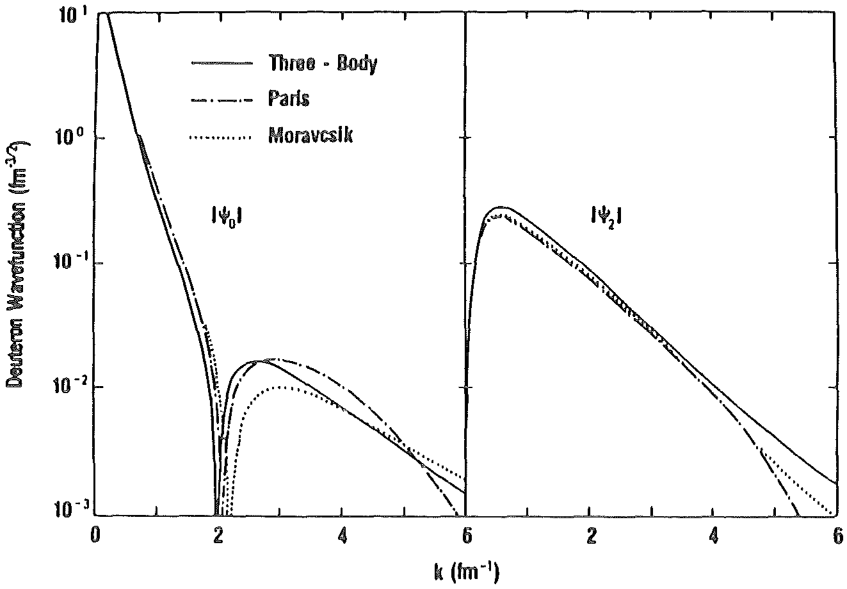

Fig. 1
The deuteron wave function of our three-body model as compared with the wave function of the Paris potential and the Moravcsik-Gartenhaus wave function

should be detected and in the second one the proton. Recent experiments on the first of these reactions[2,3] have found no evidence of a π^- nn bound state; the data, however, show a resonantlike behavior at 256 MeV incident pion energy, which can be interpreted as a resonance of mass equal to 2056 MeV, that is 38 MeV above the πNN threshold. Thus, if this result is confirmed by other experiments, it is very likely that one has observed the 4,4 resonance predicted by our three-body theory.

(1) H. Garcilazo and L. Mathelitsch, Phys. Rev. C28(1983)1272
(2) E. Piasetzky et al., Phys. Rev. Lett. 53(1984)540
(3) J. Lichtenstadt et al., Phys. Rev. C33(1986)655

+ Institut für Theoretische Physik, Universität Graz, A-8010 Graz, Austria.

4.4.2 STANDARD RELATIVISTIC FADDEEV THEORY OF THE πNN SYSTEM WITH APPLICATION TO πd SCATTERING

H. Garcilazo

The πNN system is probably one of the most basic problems in nuclear physics. It is certainly more basic than the NN system, since in order for two nucleons to interact there needs first to be a pion. Moreover, if the energy of the nucleon-nucleon system is sufficiently large, a real pion will be produced, so that in order to have a consistent theory of the NN system which is valid both above and below the pion-production threshold it must be a three-body theory. Also, since the pion can be absorbed, one has transitions of the form NN → πNN and NN → πd which are possible only if the pion or at least one of the nucleons are allowed to be off their mass shells. Thus, a theory of the πNN system must also be relativistic in order to be able to describe intermediate states in which some of the particles are off the mass shell.

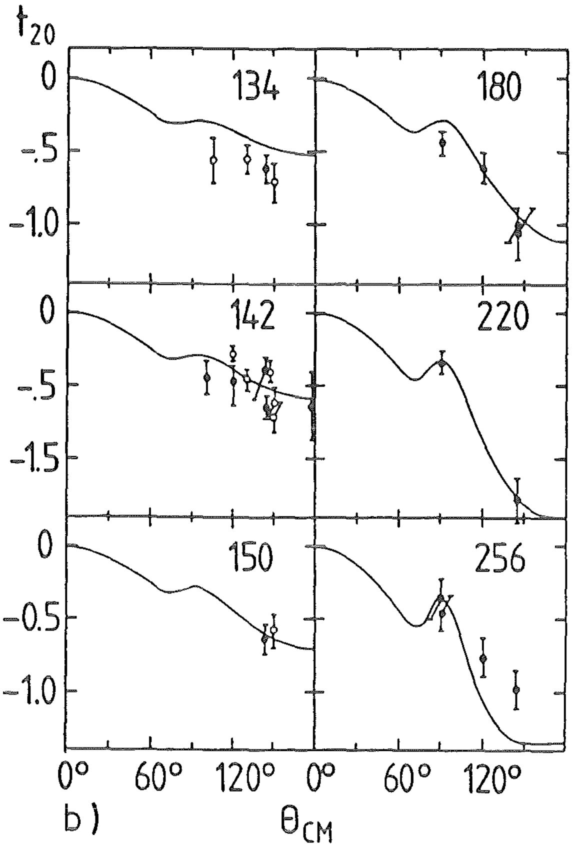

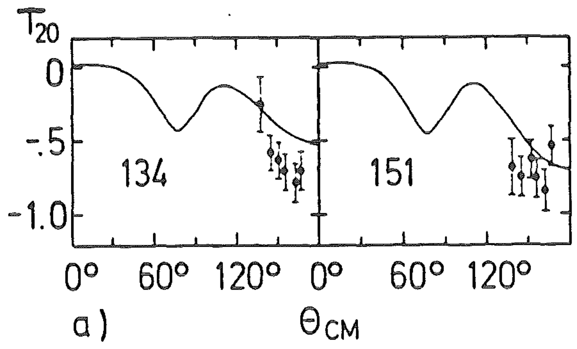

Fig. 1

a) The pion-deuteron tensor analyzing power T_{20} for two different kinetic energies of the pion (in MeV). The experimental data are from Ref. 4.

b) The pion-deuteron tensor polarization t_{20} for six different kinetic energies of the pion (in MeV). The experimental data are from Ref. 2 (solid circles) and from Ref. 3 (open circles)

We have formulated a standard relativistic Faddeev theory of the πNN system by using the isobar ansatz for the πN and NN amplitudes and the requirement that the spectator particles be allways on their mass shells. This theory takes into account the two possible time orderings in the propagator of the exchanged particle and describes correctly the coupling between the two-body and three-body channels. As a first application of this theory, we have studied pion-deuteron elastic scattering in the region of the 3,3 resonance by calculating all the observables for which data exists finding reasonably good agreement over the entire set. In Figs. 1a and 1b we present the results for the tensor analyzing power T_{20} and tensor polarization t_{20} respectively, where in the last case the results are calculated in the laboratory frame. As we see there is quite good agreement with most of the data and with the fact that t_{20} and T_{20} are large and negative. A set of controversial measurements by Grüebler et al.$^{1)}$ which gave values of t_{20} that were large and positive have now been contradicted by three different experimental groups $^{2,4)}$ while at the same time calculations of Afnan and McLeod$^{5)}$ that predicted large and positive values of t_{20} were the result of spurious effects introduced by the application of the Pauli principle in intermediate NN states. Some predictions for other polarization observables that will be measured in the near future have also been presented. Future applications of this theory will be the simultaneous description of all five reactions that can take place in the πNN system, that is πd → πd, πd → πNN, πd → NN, NN → NN and NN → πNN.

(1) W. Grüebler et al., Phys. Rev. Lett. 49(1982)444; Phys. Rev. Lett. 48(1982) 311
(2) E. Ungricht et al., Phys. Rev. Lett. 52(1984)333; Phys. Rev. C31(1985)934
(3) Y.M. Shin et al., Phys. Rev. Lett. 55(1985)2672
(4) G.R. Smith et al., submitted to Phys. Rev. Lett.
(5) I.R. Afnan and R.J. McLeod, Phys. Rev. C31(1985)1821

4.4.3 NONEXISTENCE OF Λnn OR Σ^-nn BOUND STATES

H. Garcilazo

Among the three-baryon systems with strangeness -1, there are three candidates which would be stable if they were bound; the Λnp, the Λnn and the Σ^-nn systems (plus the isobaric analogs of the last two, that is, the Λpp and Σ^+pp systems). Of these three candidates only the first one (the hypertriton) is known for sure to be bound. We are going to investigate if any of the other two possesses a bound state.

The application of the separable-model Faddeev method, has been very successful in the case of the hypertriton, where it predicts the binding energy within a fraction of an MeV. For simplicity we will neglect the tensor force in the spin-triplet hyperon-nucleon interaction which is known to have a negligible effect in the bound state of the Λnp system. Thus, with this approximation the Fadeev equations with separable potentials reduce to a set of three coupled integral equations which correspond to the hyperon-nucleon pair interacting in the $^3S_1$ and $^1S_0$ channels and the neutron-neutron pair interacting in the $^1S_0$ channel.

The two-body input of the Faddeev equations are the Yamaguchi separable potentials for each channel, which are completely determined by the low-energy parameters a and r, where a is the scattering length and r the effective range of that channel. We will use for the low-energy parameters of the $^1S_0$ neutron-neutron channel, the values $a = -17.612$ fm and $r = 2.881$ fm. For the Λn and Σ^-n subsystems, we will use the low-energy parameters obtained by Nagels et al.[1,2] from a combined analysis of nucleon-nucleon and nucleon-hyperon scattering with a one-boson-exchange model, where the coupling constants were calculated via SU(3) taking the coupling constants of the NN analysis as input.

The simplest way to visualize the amount of attraction or repulsion that a three-body channel has, when there is at most one bound state, is by looking at the Fredholm determinant $D_F(E)$ at zero energy. If there are no interactions then $D_F(0) = 1$. If the three-body channel is repulsive then $D_F(0) > 1$, while if it is attractive then $D_F(0) < 1$. A bound state exists if $D_F(0) < 0$. We have solved the three-channel Faddeev equations in the region $E \leq 0$, using a 40-point Gauss mesh for each channel so as to have a numerical error of less than 0.1%. We present in Table 1 the values of the Fredholm determinant at zero energy for the J = 1/2 and J = 3/2 channels of the Λnn system for the four models constructed by Nagels et

		$^1S_0$		$^3S_1$		FREDHOLM DETERMINANT	
	Model	a	r	a	r	J = 1/2	J = 3/2
Λnn	A	-2.67	2.04	-1.02	2.55	0.59	1.52
	B	-2.47	3.09	-1.66	3.33	0.49	1.60
	C	-2.03	3.66	-1.84	3.32	0.46	1.64
	D	-2.40	3.15	-1.84	3.37	0.46	1.63
Σ^-nn	A	-2.79	3.55	0.63	-0.76	1.95	0.64
	B	-3.29	3.29	0.41	-2.47	1.69	0.79
	C	-4.61	3.69	0.32	-6.01	1.59	0.87
	D	-3.84	4.03	0.62	-1.91	1.83	0.73

Table 1
Low-energy data (in fm) of the Yn $^1S_0$ and $^3S_1$ channels and the corresponding Fredholm determinant of the Ynn system at zero energy for the states with total angular momentum J = 1/2 and J = 3/2. The data for the four models A-D are those of Nagels et al.$^{1,2)}$.

al.$^{1,2)}$. The corresponding Λn $^1S_0$ and $^3S_1$ separable potentials are both attractive. As we see from this table the J = 1/2 channel is attractive but not attractive enough to produce a bound state, while the J = 3/2 channel is repulsive so that no bound state exists in either channel. In table I we present also the results for the Σ^-nn system for the four models of Nagels et al.$^{1,2)}$. The separable potentials of the Σ^-n subsystem are repulsive in the $^3S_1$ channel and attractive in the $^1S_0$ channel. As we see from this table the situation is the reverse from that of the previous case, since now the J = 1/2 channel is repulsive and J = 3/2 channel is attractive although again not sufficiently to be able to bind the system.

To conclude, we have searched for possible bound states of the Λnn and Σ^-nn systems without finding any evidence for them. This also rules out the possible existence of bound states in the Λpp and Σ^+pp systems which have in addition the repulsive Coulomb force.

(1) M.M. Nagels, T.A. Rijken, and J.J. DeSwart, Ann. Phys. (N.Y.)79(1973)338; Phys. Rev. D15(1977)2547; D20(1979)1633

(2) M.M. Nagels, T.A. Rijken, and J.J. deSwart, in Few Particle Problems in the Nuclear Interaction, edited by I. Slaus, S.A. Moszkowski, R.P. Haddock, and W.T.H. von Oers (North-Holland, Amsterdam, 1972)42

4.4.4 RELATIVISTIC ONE-PION-EXCHANGE POTENTIALS

H. Garcilazo, L. Mathelitsch⁺

We compare three different types of relativistic two-body equations, namely the Blankenbecler-Sugar equation, the Gross equation and an equation derived from relativistic three-body equations. Garcilazo showed how a two-body potential is changed, if one imbeds it into a three-body model satisfying both two- and three-body unitarity$^{1)}$. This three-body one-pion-exchange potential (three-body OPEP) has an energy-dependent range and it becomes complex above the pion-production threshold. In this paper we want to investigate, how this three-body potential with its related equation compares to other relativistic equations. As examples we choose the Blankenbecler-Sugar equation$^{2)}$ and the Gross equation$^{3)}$. The reason for this choice is that the OPEPs, which are derived in these approaches, differ from each other and also from the three-body OPEP. Other relativistic approximations yield one of the above potentials and differ just in the equations.

We have shown that the one-pion exchange potential, which was derived in Ref. 1 via a relativistic three-body model of the two nucleon interaction, deviates from other relativistic expressions for the same exchange mechanism. In particular, the three-body OPEP is energy dependent and shows a singular structure for full off-shell momenta. There can be two closed cuts in the momentum plane, but one cut just comes in at scattering energies above the one-pion-production threshold.

We have compared the resulting half-shell functions and phase shifts of the three-body potential (with its connected equation) to the corresponding results of the Lippmann-Schwinger, Blankenbecler-Sugar and Gross equations. Whereas features of the individual potentials are reproduced in the half-shell functions, the one-pion-exchange phase shifts are very similar for all three relativistic equations, but show some deviations from the nonrelativistic result. This finding, however, is dependent on the potential and also on the parameters of a given potential.

We have also included strong form factors for the πNN vertex. Their effect by far exceeds the differences caused by the various relativistic equations. Even the uncertainty due to the ill-determined value of the cuf-off parameter is larger than these relativistic deviations. The inclusion of full off-shell hadronic form factors yields smaller phase shifts than for the case where just the pion is treated off the mass shell in the form factor. The size of this effect can even be larger (depending on the considered partial wave) than the one caused by the inclusion of the (pion) form factor usually used.

(1) H. Garcilazo, Phys. Lett. 99B(1981)185
(2) R. Blankenbecler and R. Sugar, Phys. Rev. 142(1966)1051
(3) F. Gross, Phys. Rev. 186(1969)1448

+ Institut für Theoretische Physik, Universität Graz, A-8010 Graz, Austria

5. HIGH ENERGY PHYSICS

CELLO Collaboration

H.-J. Behrend, J. Bürger, L. Criegee, J.B. Dainton, H. Fenner, J.H. Field, G. Franke, J. Fuster, Y. Holler, J. Meyer, V. Schröder, H. Sindt, U. Timm, G.G. Winter, W. Zimmermann

Deutsches Elektronen-Synchrotron, DESY, Hamburg, Germany

P.J. Bussey, C. Buttar, A.J. Campbell, D. Hendry, G. McCurrach, J.M. Scarr, I.O. Skillicorn, K.M. Smith

University of Glasgow, United Kingdom

J. Ahme, V. Blobel, M. Feindt, J. Harjes, M. Poppe, H. Spitzer,

II. Institut für Experimentalphysik, Universität Hamburg, Germany

W.-D. Apel, A. Böhrer, J. Engler, G. Flügge, D.C. Fries, W. Fues, K. Gamerdinger, P. Grosse-Wiesmann, J. Hansmeyer, G. Hopp, J. Jung, J. Knapp, M. Krüger, H. Küster, P. Mayer, H. Müller, K.H. Ranitzsch, H. Schneider, J. Wolf

Kernforschungszentrum Karlsruhe and Universität Karlsruhe, Germany

W. de Boer, G. Buschhorn, G. Grindhammer, B. Gunderson, Ch. Kiesling, R. Kotthaus, H. Kroha, D. Lüers, H. Oberlack, B. Sack, P. Schacht, G. Shooshtari, W. Wiedenmann

Max-Planck-Institut für Physik und Astrophysik, München, Germany

A. Cordier, M. Davier, D. Fournier, M. Gaillard, J.F. Grivaz, J. Haissinski, P. Janot, V. Journé, F. Le Diberder, E. Ros, A. Spadafora, J.-J. Veillet

Laboratoire de l'Accélérateur Linéaire, Orsay, France

B. Fatah, R. George, M. Goldberg, O. Hamon, F. Kapusta, F. Kovacs, L. Poggioli, M. Rivoal

Laboratoire de Physique Nucléaire et Hautes Energies, Université de Paris, France

G. D'Agostini, F. Ferrarotto, M. Gaspero, B. Stella

University of Rome, Italy

R. Aleksan, G. Cozzika, Y. Ducros, Y. Lavagne, F. Ould Saada, J. Pamela, F. Pierre, J. Zacek

Centre d'Etudes Nucléaires, Saclay, France

G. Alexander, G. Bella, Y. Gnat, J. Grunhaus, A. Levy

Tel Aviv University, Israel

5.1 HARDWARE ACTIVITIES

5.1.1 CELLO OPERATION

PETRA operates actually at a constant beam energy of 17.5 GeV. At this energy CELLO collected a luminosity of about 60 pb^{-1} since the start-up in 1986. Due to the lower energy the quality of the new data is better since the background is appreciably reduced. Also the triggering has been continously improved. Fig. 1 shows as an example the threshold behaviour for single photons for the complete cylindrical LAr calorimeter. The mean threshold is now 1.6 GeV at a random trigger rate of about 1 Bq. This allows, e.g., a better search for supersymmetric particles and a stronger restriction in neutrino counting. Also the charged trigger could be improved by lowering the threshold for the minimum momentum required in a track. This is especially important for the two photon physics programme. Thresholds of as low as 250 MeV/c in the central and about 350 MeV/c in the forward region are realized.

The central tracking device is still the original version of intersperced proportional and drift chambers. The installation of the stereo-wire-chamber had to be abandoned due to high voltage problems in the wire feed-throughs. The feed-troughs of the mass production had a less good quality than the prototype series and the required high voltages on the wires could not be reached.

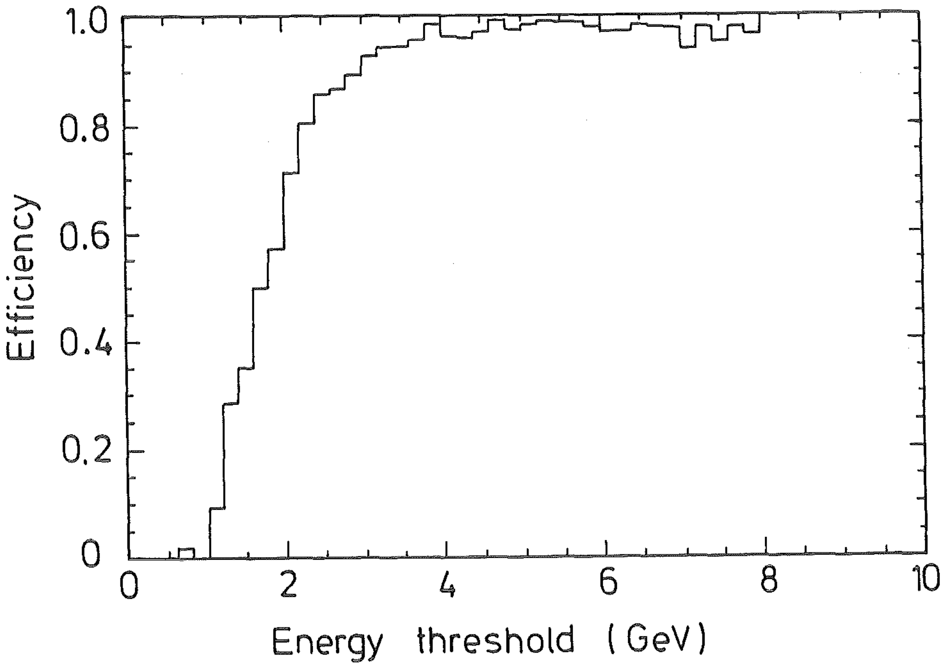

Fig. 1
Trigger threshold in the cylindrical LAr calorimeter for one single photon shower.

5.1.2 CALORIMETER DEVELOPMENT

Present and future high luminosity machines need particle detectors which are radiation resistant and exhibit long-term stability. Especially for calorimetry, liquid ionization sampling offers many obvious advantages, and room temperature liquids are the preferred active media.

The R&D work to introduce non-polar room temperature liquids for fast particle detection is being pursued. Most of the work is concentrated on TMS, tetramethylsilane, which is among the fastest liquids, i.e. 30 ns drifttime per mm at 30 kV/cm. It is relatively easy to purify and commercially available at reasonable prices. Chemically it resembles a pentane having at room temperature a vapour pressure of 800 mb. Work with Tetramethyltin, Neopentane and Tetramethylpentane is also under way.

A first prototype calorimeter has been tested in the institute and operated repeatedly at DESY (1). For the module, absorber slabs of carbon steel without any special surface treatment were chosen, in order to make it inexpensive and to demonstrate that possibly even a magnetic flux return yoke could be instrumented this way.

The charge yield in organic liquids at usual voltages is rather low and reaching saturation entails the use of high voltages. The yield in the calorimeter module was 60% of the charge collection expected in a very pure sample of the liquid. The preamplifier noise corresponds to 130 MeV electromagnetic shower energy. This is somewhat higher than in typical liquid argon calorimeters. For trigger purposes, this deficiency is well compensated by the fact that the preamplifiers are situated close to the detector capacitance, thus ensuring quiet operation, practically free of pick-up noise.

The electric signal decreased with time as shown in Fig. 1. Assuming an exponential decay, the lifetime of the signal is 1/2 year. The impurities responsible for the signal decreases are presumed to be outgassing compounds of the Kapton pick-up foils. In practice, we need lifetimes 10 times longer! The problem is therefore being followed up; two out of three modules presently under construction will have, at their bottoms, activated molecular sieves.

These three modules use 3 mm uranium plates encapsuled in 0.5 mm stainless steel sheets. The container will again be carbon steel, however chromium plated for protection and to ensure good electrical conductivity. The depleated uranium has been taken over from the SNEAK stock.

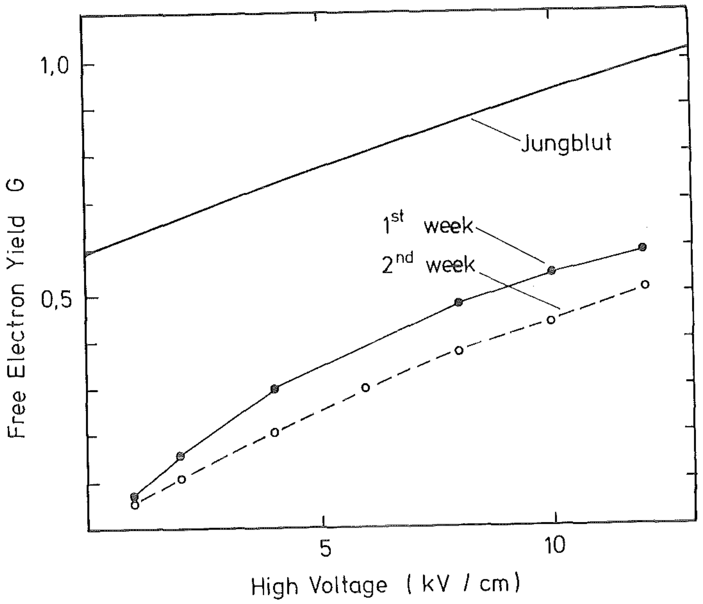

Fig. 1
The signal strength in the calorimeter module during two test periods separated by 5 1/2 weeks. The straight line indicates, as reference, the yield in a very pure sample of TMS. G is the number of electrons collected per 100 eV deposited ionization energy.

In addition to the calorimeter, a tracking chamber shown in the photograph of Fig. 2 has been tested (2). The chamber was operated in the ionization chamber mode. In a liquid layer of 2 × 4 mm, enough charge can be collected to operate such a chamber with a pulse-width shaped to shorter than 100 ns. The spatial resolution depends essentially on the strip pattern. A coarse pitch of 1.5 mm was used which gave the expected resolution of $\sigma = 470\ \mu$.

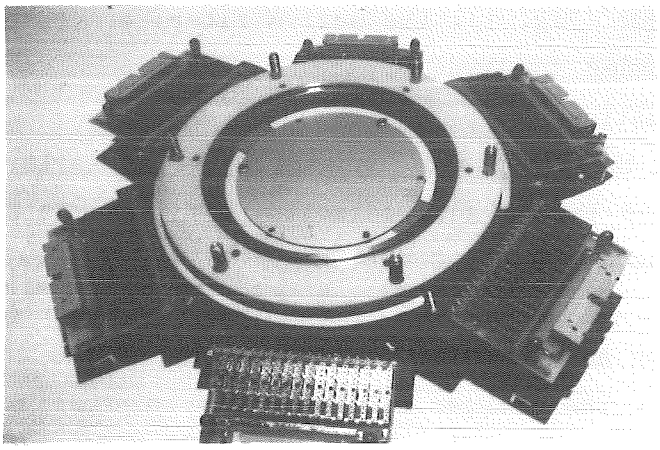

Fig. 2
Photograph of a liquid track chamber during assembly.

The idea of using liquid ionization chambers for tracking is that they offer new possibilities in cases of high background radiation. Presumably they will be very useful near the beam pipe in the forward direction for the new accelerators.

The purification system is a set-up which is able to purify 50 ℓ/week. It uses the rather straightforward method of (1) degassing, (2) vacuum distillation and (3) distillation over molecular sieves as described in (3). It is well suited and gives good results. We found it not to be necessary to pass the TMS vapour over special reducing compounds like NaK, hot metals, etc. But the sieves have to be well activated beforehand.

(1) J. Engler, H. Keim and B. Wild, Kernforschungszentrum Karlsruhe, Report 4086 (1986), to be published in Nucl.Instr.Meth.
B. Wild, Kernforschungszentrum Karlsruhe, Report 4119 (1986)
(2) J. Engler, H. Keim and C. Müller, Kernforschungszentrum Karlsruhe, Preprint 81-1 (1986), submitted to Nucl.Instr.Meth.
C. Müller, Kernforschungszentrum Kalrsruhe, Report 4166 (1986)
(3) J. Engler and H. Keim, Nucl.Instr.Meth. 223 (1984) 47

5.1.3 OPTICAL FIBER READ-OUT FOR SCINTILLATORS

In collaboration with the Institute for Nuclear Studies and the University Warsaw trigger counters have been developed for a High Density Projection Calorimeter (HPC).

The particular problem of the trigger counters is the necessity to carry the light output over a long distance (10-12 meters) before converting it into an electrical signal. The solution presently tested makes use of a readout system with optical fibers. The (blue) light signals of the scintillator are converted to wavelengths of about 520 nm by a layer of active (wavelength shifting) optical fibers. The fibers are attached to the small side of the scintillator (Fig. 1). The active fibers are coupled to optical neutral fibers in order to transmit the light signals over long distances with minimum attenuation.

Test measurements of the first two counters built at Karlsruhe in the e-testbeam at DESY showed that a good detection efficiency above 92% can be achieved for electrons above 1.5 GeV after about 4.5 X_0 (radiation length).

The trigger efficiency as a function of the energy of the incident electron is shown in Fig. 2. The trigger efficiency for minimal ionising particle for the two test counters was low (20-25%). Possibilities to increase of the light collection from the scintillator are examined at present.

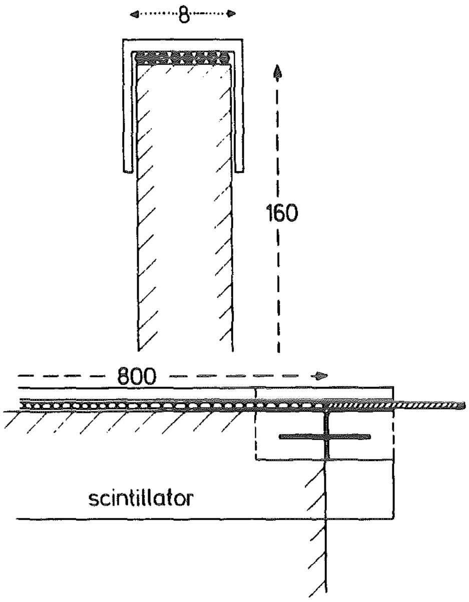

Fig. 1

Mounting of the wavelength shifting optical fibers to the scintillator.

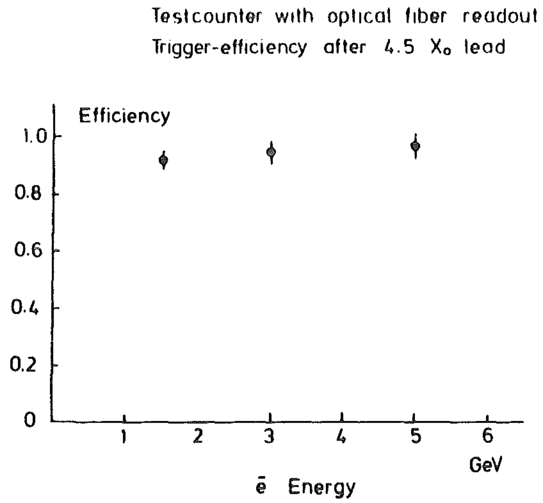

Fig. 2

Trigger efficiency of a scintillation counter with fiber readout as a function of the energy of the incident electrons of about shower maximum (after 4.5 radiation length).

5.2 ANALYSIS OF HADRONIC FINAL STATES AND TEST OF QCD

5.2.1 MEASUREMENT OF THE TOTAL HADRONIC CROSS SECTION IN e^+e^- ANNIHILATION BETWEEN CENTER OF MASS ENERGIES OF 14 AND 47 GeV

The total hadronic cross section in e^+e^- annihilation is determined by electroweak interactions (calculated in the Standard GWS Model) and strong interactions (calculated in Quantum Chromodynamics, QCD). The normalized cross section R is defined as the ratio

$$R = \frac{\sigma(e^+e^- \to \gamma, Z^0 \to \text{hadrons})}{\sigma(e^+e^- \to \gamma \to \mu^+\mu^-)}$$

R is dominated by the QED one photon annihilation. In the standard quark parton model it is given by

$$R = 3 \cdot \sum_{N_f} Q_f^2$$

where N_f is the number of quark flavors and Q_f is the electric quark charge. QCD corrections modify R by a factor

$$1 + \frac{\alpha_s(s)}{\pi} + C_2\left(\frac{\alpha_s(s)}{\pi}\right)^2 + \text{higher order corrections}$$

Here $\alpha_s(s)$ is the second order "running" strong coupling constant and C_2 is a constant, which depends on the renormalization scheme.

At the highest PETRA energies Z^0 exchange, and to a lesser extent the interference between γ and Z^0 exchange become important. For $\sin^2\theta_W$ = 0.22 and $\Lambda_{\overline{MS}}$ = 650 MeV at $\sqrt{s}$ = 14 GeV the QCD correction is 9%. At $\sqrt{s}$ = 46 GeV, QCD contributes 5.5%, Z^0 exchange 8.1%, and γZ^0 interference -2.8% to R (see Fig. 1).

So a precise measurement of the total hadronic cross section allows the determination of the weak mixing angle $\sin^2\theta_W$ and the strong coupling constant α_s. The α_s-value measured in this way does not depend on any fragmentation models for the hadronisation of quarks and gluons, because it is derived from an inclusive measurement, which does not refer to a certain event class.

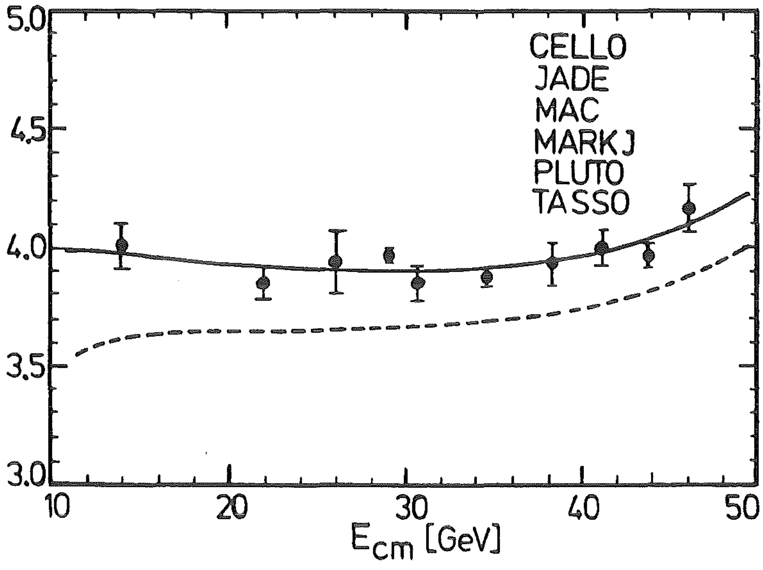

Fig. 1
Measured R value and best fit (solid line). The dotted line indicates the electroweak contribution alone (no QCD).

CELLO has taken data at center of mass energies $\sqrt{s}$ between 14.0 and 46.8 GeV with an integrated luminosity of 60.3 pb^{-1}.

For the multihadronic event selection we used only tracks and showers in the central detector inside $|\cos\theta| < 0.86$. We applied the cuts requiring more than 4 reconstructed "charged" tracks and some visible energy.

The R-value is determined from data by

$$R = \frac{(N_H - N_{BG})}{L\,\varepsilon_H(1 + \delta_H)\,\sigma_{\mu\mu}}$$

Here N_H and N_{BG} are the number of observed multihadron events and background events, respectively. L is the integrated luminosity, $\varepsilon_H(1+\delta_H)$ is the multihadron detection efficiency multiplied by a radiative correction factor and $\sigma_{\mu\mu}$ is the pointlike QED cross section.

For background events from beam-gas interactions and from off-momentum electrons an upper limit of 0.1% was obtained from scanning a large fraction of the data. Multihadronic events produced via two photon scattering show a low visible energy. Events with both initial state leptons leaving the detector outside the acceptance volume are suppressed to a level of 0.2% of the sample. Events from deep inelastic scattering with high Q^2 where one of the initial state leptons is scattered into the acceptance give a typical contribution of 0.7% at the highest energies. τ-pair background was estimated by Monte Carlo to be smaller than 0.1%.

The time integrated luminosity L was obtained from Bhabha scattering inside the acceptance of the cylindrical calorimeter. Bhabhas were defined by collinear shower clusters with an energy > 0.3 E_{beam} and at least 1 charged track that points at one of the clusters. The efficiency inside the acceptance is above 99%. Acceptance calculations and radiative corrections were performed with the Berends and Kleiss Bhabha generator.

The largest detection inefficiency comes from the fact, that we limited our acceptance to the central detector ($\cos\theta < .86$). But because the angular distribution of hadrons is well described by the Monte Carlo, the extrapolation to the full solid angle can be done reliably. Further inefficiencies arise from the multiplicity and energy cuts. We found the inefficiency to be independent of the specific fragmentation model, provided the tuning of them was done in similar ways. For example, if we change from string fragmentation to independent fragmentation, we find ε_H to change by less than 0.1%. These tunings of the different models of course had rather different values of α_s. For the further analysis the absolute systematic error on ϵ_H, δ_H, and L are combined quadratically. The absolute systematic error is in total 2.2% to 2.5%.

DETERMINATION OF α_s AND $\sin^2\theta_W$

The two parameters α_s and $\sin^2\theta_W$ can be determined by fitting the R-formula to the data. However, the data points at the different CM energies are not completely independent, since errors on radiative corrections and part of the Monte Carlo uncertainties are common to all points. We have used the following procedure to take these correlations in the errors into account:

One defines a n × n error correlation matrix V for n measurements. As diagonal elements it contains the square of the total error for each measurement and as off diagonal elements V_{ij} the common normalization error between the measurements i and j. The expression to be minimized is then:

$$\chi_R^2 = \Delta^T V_{ij}^{-1} \Delta .$$

Here Δ is a vector with the n residuals $R_i - R_{fit}$. In case the off-diagonal elements of V_{ij} are all zero, χ_R^2 reduces to the usual expression.

Previous determinations of α_s from R fitted the normalization as a free parameter to take the correlations into account. The separation of the systematic errors in point to point and overall normalization errors is not unique. For example, uncertainties in the luminosity, the tracking, and the Monte Carlo simulations are common to all energy points. However, small point to point variations still occur, because the agreement between Monte Carlo and data is not the same at all energies. Therefore we have performed the fit for different assumptions on the splitting of the systematic errors into point to point errors and normalization errors. The fit results and errors turn out to be rather insensitive to this splitting, although the correlation between the errors on α_s and $\sin^2\theta_W$ does depend on it. From a simultaneous fit to the CELLO data we find

$$\alpha_s(s = 44^2\ \mathrm{GeV}^2) = 0.18\ {}^{+0.05}_{-0.08}\ , \quad \text{and} \quad \sin^2\theta_W = 0.20\ {}^{+0.04}_{-0.03} \quad .$$

From a simultaneous fit to the combined data of CELLO, JADE, MAC, MARK J, PLUTO, and TASSO we find:

$$\alpha_s(s = 44^2\ \mathrm{GeV}^2) = 0.16\ {}^{+0.04}_{-0.05}\ , \quad \text{and} \quad \sin^2\theta_W = 0.23 \pm 0.03 \quad .$$

This value of $\sin^2\theta_W$ is in excellent agreement with the world average of 0.23 ± 0.003, which is determined by completely independent methods: neutrino scattering, masses of the weak gauge bosons, and asymmetries in lepton pair production. If we fix $\sin^2\theta_W$ to this value, we get for the strong coupling constant:

$$\alpha_s(s = 44^2 \text{ GeV}^2) \quad = \quad 0.16 \pm .03$$

The importance of the determination of α_s from R stems from the fact that it is an inclusive measurement, which does not depend on a certain event class and is therefore independent from the fragmentation model used to hadronise the quarks and gluons. As we have shown previously, α_s determinations sensitive to the fraction of 3-jet events strongly depend on the fragmentation model. The precision of the α_s determination from R approaches the precision obtainable with previous methods.

5.2.2 COMPARISON OF THE LOWEST ENERGY JET IN THREE-JET EVENTS AT 44 GeV WITH THE AVERAGE JET IN TWO-JET EVENTS AT 14 GeV

The multi-jet structures observed in e^+e^--annhilation at high E_{cm} are given by the processes:

$$e^+e^- \rightarrow \left.\begin{array}{l} qq \\ qqg \\ qqgg \\ qqqq \end{array}\right. \Rightarrow \quad \text{2-, 3-, 4-jet events}$$

Because of the higher colour charge and the self coupling of the gluons the gluon jet is expected to be broader than the quark jet.

We perform a phenomenological analysis of jet properties. From 2-jet events at 14 GeV we get reference jets at 7 GeV quark energy. We select 3-jet events from data around 44 GeV for which the energy of the third jet is about 7 GeV and compare the two samples. Models are used only to estimate systematic effects which might originate from the performance of the cluster routine and from efficiencies in our detector.

To find jets we use a cluster algorithm. Over a matrix of angles in space we search for maxima of a generalized energy flow S^{pw}, where at least 2 closely emitted particles are needed to create a local maximum of S^{pw}.

The directions of these maxima serve as initial jet axes. Particles are merged into the nearest jet if the angle to the proposed jet axis is below a present half cone angle, typically 45^0. After merging the jet axis is determined by the sum of the momenta of the particles in the jet and the procedure is repeated with this new axis until a stable situation is reached.

Two measures of the jet energy are used: The energy E_j^e is the sum of the measured energies of the particles within a jet. Due to particle losses it is smaller than the corresponding parton energy. The energy E_j^d is calculated from the angles between the jets. This value is not biased from random particle losses.

The jets are ordered according to $E_1^d > E_2^d > E_3^d$.

To have well reconstructed jets we request that the dip angles of the 3rd jets and the reference jets stay below 45^0 and that the angles between the three jets are above 60^0. 395 two-jet events at 14 GeV and 157 three-jet events at 44 GeV pass these cuts.

We present ratios of quantities from the lowest energy jet in three-jet events and the same quantities from the average jet in two-jet events.

$\langle p_\perp \rangle$	average transverse momentum of the particles with respect to the jet axis.
$\langle p_{\perp in} \rangle$	$p_\perp$ of each particle is split into two components. $p_{\perp in}$ of the 3rd jet is taken in the plane which is defined by jet #1 and #2.
$\langle p_{\perp out} \rangle$	is orthogonal both $p_{\perp in}$.

$\langle p_{\perp out} \rangle$ and $\langle p_{\perp in} \rangle$ for two-jet events at 14 GeV are given by $\langle p_\perp \rangle \cdot 2/\pi$.

The influence of the limited acceptance and efficiency of the detector has been studied by detector simulations. It largely cancels when ratios of quantities are taken.

3-jet events are used in the range 5 GeV $< E_3^d <$ 9 GeV. $\langle E_3^d \rangle$ at 44 GeV is near to 7 GeV, the energy of the reference jet. The measured energy $\langle E_3^e \rangle$ also agrees well with that of the reference jet.

The $p_\perp$-distributions of the particles in the 3rd jet and the reference jet are similar (Fig. 1). For the 3rd jet at 44 GeV we also compare $\langle p_{\perp in} \rangle$ with $\langle p_{\perp out} \rangle$ (Fig. 2).

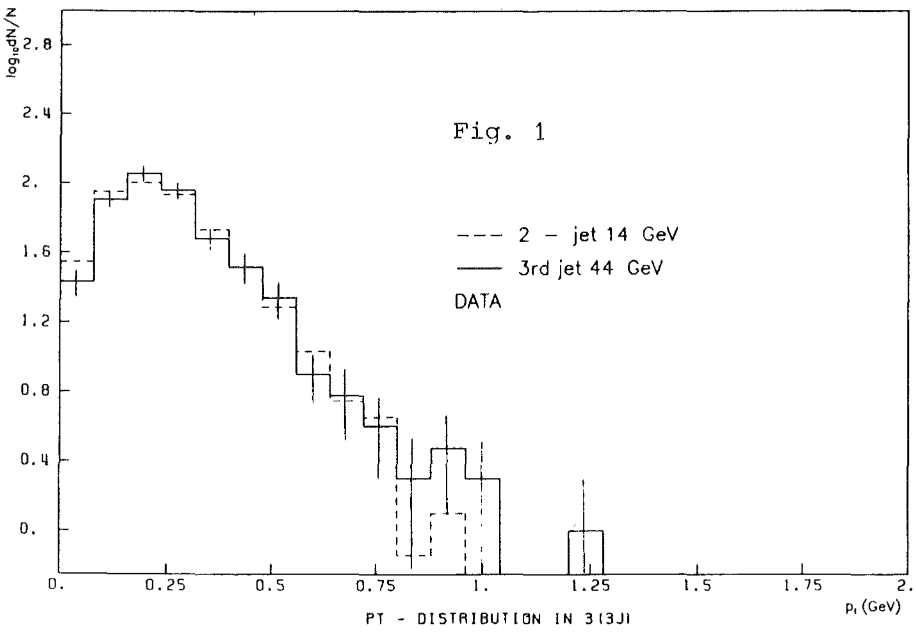

Fig. 1
The distributions of transverse momentum $p_\perp$ of charged particles within a jet relative to the jet-axis.
Solid line: third jet in 3-jet events at E_{cm} = 44 GeV;
dashed line: average jet in 2-jet events at 14 GeV.

The half cone angle for particle merging has been variied from 25^0 to 60^0. The changes of the results remain within the statistical errors. Thus the qualitative conclusions are independent from the opening of the cones used for the clusters.

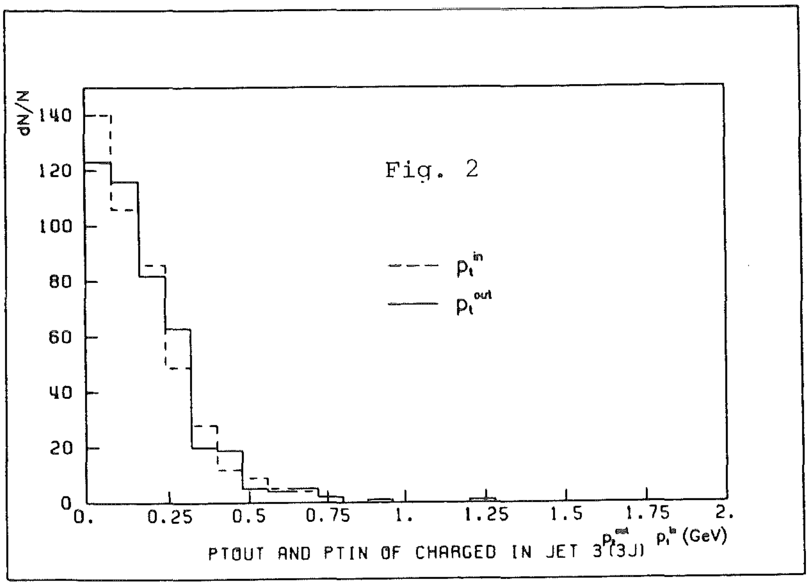

Fig. 2
Comparison of $p_{\perp in}$ and $p_{\perp out}$ for the 3rd jet at 44 GeV.
Solid line: $p_{\perp out}$
dashed line: $p_{\perp in}$

We get $\langle p_{\perp out} \rangle$ (3rd jet) / $\langle p_{\perp out} \rangle$ (ref. jet) = 1.08 ± 0.05 ± 0.06 which is consistent with the jet broadening observed at lower beam energies. The ratio $\langle p_{\perp in} \rangle / \langle p_{\perp out} \rangle$ = 0.96 ± 0.06 ± 0.06 shows that the 3rd jet is round within our experimental accuracy. While our Monte Carlo studies indicate that the latter ratio is sensitive to the type of fragmentation model (e.g. $\langle p_{\perp in} \rangle$ is about 10% larger than $\langle p_{\perp out} \rangle$ for string fragmentation) the current statistical accuracy of our data is insufficient to distinguish between them.

5.3 STUDY OF ELECTROWEAK INTERACTION

5.3.1 STUDY OF INCLUSIVE LEPTONS FROM b-QUARK PRODUCTION IN e^+e^- ANNIHILATIONS AT ENERGIES ABOVE 43 GeV

The data from 34 pb^{-1} luminosity at 43-46.4 GeV provided by PETRA in the last two years allow to test the standard model of Glashow, Salam and Weinberg at highest energies. The e^+e^- annihilation into fermion pairs proceeds via γ and Z^0 exchange. The presence of the weak amplitude and its interference with the electromagnetic one gives rise to a forward backward asymmetry in the production angle θ of the reaction $e^+e^- \to b\bar{b}$. The angular distribution has the form $(1 + b \cos\theta + \cos^2\theta)$. The integrated asymmetry is given by

$$A_{FB}(b) = \frac{F-B}{F+B} \simeq - \frac{3\ a_e a_b}{2\ Q_b} \cdot \frac{1}{16 \cos^2\theta_W \sin^2\theta_W} \cdot \frac{s}{s-M_Z^2} ,$$

where M_Z is the Z^0 mass, θ_W the weak mixing angle, a_e, a_b are the axial vector couplings and Q_b is the electric charge of the b quark. We expect $A_{FB}(b) = -0.41$ for the b quark asymmetry at the highest PETRA energies.

b events are identified by tagging leptons originating from the weak decay of the b quarks. The simplest picture for the semileptonic decay of heavy mesons is the spectator model where the b quark decays to a c quark emitting a virtual W boson, and the light quark in the heavy meson does not participate. W is predicted to decay in 10-15% of the cases into a lepton neutrino pair. Because of the heavy mass of the b quark the lepton has on average a high momentum transverse to the parent quark direction. Selecting high P_T of the lepton with respect to the jet axis therefore enriches leptons coming from b quark decays. We determine the jet axes by means of a cluster algorithm and cut at $p_T > 0.8$ GeV for the lepton which optimizes the b sample. Whether the lepton comes from a quark or an antiquark decay is derived from its charge. Leptons result from b or $\bar{c}$ decays, whereas antileptons come from $\bar{b}$ or c decays. Hence the observed asymmetry of the sample of lepton tagged events is decreased by a background of semileptonic c decays and b cascade decays ($b \rightarrow c \rightarrow l\nu X$). In addition initial state bremsstrahlung reduces the observed b asymmetry by a factor of around 0.86.

The electron identification in the CELLO detector exploits the measurements of charged tracks in the magnetic inner detector and of showers in the calorimeter. We use 3 measures to separate electrons from the much more abundant hadrons: we test the longitudinal shower development in the calorimeter, we check the alignment of the maxima in the lateral shower distribution and require good matching of shower energy and track momentum. At 75.5% identification efficiency for electrons with $p > 1.6$ GeV, $p_T > 0.8$ GeV we misidentify 0.8% of the hadrons.

Besides the background coming from misidentified hadrons, γ conversion and π/K decay from annihilation events there is a contamination of the electron sample due to events from two photon reactions $e^+e^- \rightarrow e^+e^- + X$, the deep inelastic electron photon scattering ($C = +1$) and the inelastic Compton scattering ($C = -1$), where X is a hadronic system with the charge conjugation C. Those events can have one electron and some hadrons in the central detector, whereas the other electron escapes undetected at small angles. Cuts on the event topology reduce this background to 3.8% of the e-candidate sample (Table 1).

	e - cand.	μ - cand.
$b \rightarrow l$	48.6 %	44.9 %
$b \rightarrow c \rightarrow l$	5.2 %	2.3 %
$c \rightarrow l$	9.7 %	15.8 %
DIS e	3.6 %	---
IC e	0.2 %	---
π/K decays	2.2 %	0.4 %
misid. hadrons	30.5 %	36.6 %
candidates	18	32

TABLE 1:
Contributions to the lepton yield for leptons with $p > 1.6$ GeV/c and $p_T > 0.8$ GeV/c using BR ($b \rightarrow l\nu X$) = 0.12 and BR ($c \rightarrow l\nu X$) = 0.08.

A muon passing the CELLO detector produces a track in the inner detector, deposits minimal ionizing energy in the calorimeter, penetrates the iron absorber and is detected in the muon chambers. To identify a muon the central detector track is extrapolated through the calorimeter and the iron to the muon chambers, and its quality of matching with the muon chamber hits is tested. Furtheron we require the energy deposition along the track through the calorimeter to be consistent with minimum ionisation. Random associations between tracks and background hits in the muon chambers, π/K decays and hadron punch through give rise to background to the muon signal. We achieve a muon identification efficiency of 73.7% for tracks with $p > 1.6$ GeV and $p_T > 0.8$ GeV while we misidentify 2.4% of the hadrons as muons.

From 6348 multihadrons we collect a sample of 18 electron and 32 muon candidates. The fraction of the lepton candidates as predicted by a Monte Carlo simulation are shown in Table 1. We derive semileptonic branching ratios for the b quarks

$$\mathrm{BR}\,(b \rightarrow e + \bar{\nu}_e + X) = 0.17 \pm 0.06$$
$$\mathrm{BR}\,(b \rightarrow \mu + \bar{\nu}_\mu + X) = 0.14 \pm 0.05 \quad .$$

Because of the low statistics we determine the b asymmetry from the forward and backward integrals of the angular distribution. We subtract all backgrounds with their Monte Carlo predicted asymmetries from the lepton signals and then calculate the asymmetry of the corrected forward and backward sums. The results are corrected for the limited detetor acceptance and initial state bremsstrahlung. The final value for the b asymmetry is

$$A^{e}_{FB}(b) = -0.15 \pm 0.61$$
$$A^{\mu}_{FB}(b) = -0.72 \pm 0.48$$ or combining the two measurements
$$A^{e+\mu}_{FB}(b) = 0.51 \pm 0.38$$

in good agreement with the standard model prediction of $A_{FB} = -0.41$.

The main sources of systematic errors are uncertainties in the fragmentation models and the semileptonic branching ratios of the heavy quarks, which change the expected number of leptons by 25%. The uncertainties of the branching ratios give a possible variation of the same size. Systematic errors of lepton identification are estimated to be 10%. We conclude a total systematic error for the b-quark asymmetry of 20% which is much smaller than our statistical error.

For energies $\sqrt{s} > 46.3$ GeV MARK J has observed an excess of multihadronic inclusive muon events with low thrust. They find 8 events with thrust $T < 0.8$ compared to an expectation from lower energy data of 1.9 events. In addition in these 8 events the muons are isolated, i.e. the angle δ between the muon and the thrust axis is large ($|\cos\,\delta| < 0.7$). Recently these findings have been confirmed by JADE who observe 5 events of this kind and expect 0.56 events from the extrapoltion from lower energies and 0.74 events from Monte Carlo simulation.

A search for such an anomly has been carried out using the CELLO data. For this search we included some additional data at 38 GeV. 8523 hadronic events corresponding to an integrated luminosity of 46.6 pb^{-1} are used.

No anomaly is found in the CELLO data. For $\sqrt{s} > 46.3$ GeV we observe 1 event in the region $T < 0.8$ and $\cos\delta < 0.7$ while we expect 0.6 from the extrapolation from lower energy data and 0.8 events from the Monte Carlo simulation.

We also have applied various harder and softer cuts for muon identification and found in each case good agreement between the two data samples. Thus the CELLO data do not support the findings of MARK J and JADE.

In conclusion we have measured the prompt electron and muon signals in hadronic events of e^+e^- annihilation at energies around 44 GeV with the CELLO detector. The semileptonic branching ratios of b quarks were found to be

$$BR\,(B \rightarrow e + \bar{\nu}_e + X) = 0.17 \pm 0.06 \pm 0.06 \quad \text{and}$$

$$BR\,(b \rightarrow \mu + \bar{\nu}_\mu + X) = 0.14 \pm 0.05 \pm 0.05 \quad .$$

The electroweak induced charge asymmetry of b quarks was measured to be

$$A_{FB}(b) = -0.51 \pm 0.38 \pm 0.20 \quad .$$

The results are compatible with the expectation of the standard model. The search for anomalous muon events at low thrust was negative. No excess of such events is observed at the highest PETRA energies.

5.4 SEARCH FOR NEW PARTICLES IN e^+e^- ANNIHILATION

The CELLO collaboration has devoted a considerable amount of work to the search for new phenomena at worldwide highest e^+e^- energies. Many of the predicted decay channels for new particles involve leptons. Thus, the CELLO detector with its large solid angle detection of electrons and muons is an excellent tool for this search.

In this chapter we will report on searches for compositeness (5.4.1 and 5.4.2), sequential leptons (5.4.3) and supersymmetry (5.3.4).

The analysis is mostly based on 48 pb^{-1} of data collected at center of mass energies between 38.3 GeV and 46.8 GeV with $\langle\sqrt{s}\rangle = 43.0$ GeV using the CELLO detector at the PETRA e^+e^- storage ring. The following detector components were relevant for this analysis: The central tracking chamber consists of interleaved drift and proportional chambers inside a solenoidal coil producing a magnetic field of 1.3 T. It covers the polar range $|\cos\theta| < .91$. Electromagnetic calorimetry is provided by a lead liquid argon calorimeter with fine lateral and longitudinal segmentation (sixfold sampling in depth). It consists of a central barrel of 16 modules in a single cryostat covering $|\cos\theta| < .86$ and two end caps covering $.92 < |\cos\theta| < .99$. Its energy resolution can be described by $\Delta E/E = 5\% + 10\%/\sqrt{E}$, where E is the shower energy in GeV. The acceptance gap between the central and end cap calorimeter is closed by a 2 layer lead scintillator sandwich (hole tagger), segmented eightfold in ϕ, with a sampling after 4 and 8 radiation lengths.

5.4.1 SEARCH FOR LIGHT LEPTOQUARK BOSONS

A perculiar two jet event with two isolated muons previously reported by our collaboration (1) was rather difficult to understand in terms of conventional electroweak processes. Some models accounting for this event and similar ones observed in $p\bar{p}$ collisions (2) suggested the production of a pair of leptoquark bosons (3,4) which decay subsequently into a muon and a jet.

Pair production of such leptoquarks χ leads to the following event signatures:

$$\mu^+\mu^- + \text{hadrons} \tag{a}$$
$$\mu^{+-} + \text{hadrons} + p_T^{miss} \tag{b}$$
$$p_T^{miss} + \text{hadrons} \tag{c}$$

We did not search for decays into electrons since a large background is expected from deep inelastic e^+e^- scattering, i.e. high Q^2 photon-photon interactions. The decays into τ leptons are difficult to detect.

Our results are interpreted within a specific model of B. Schrempp and F. Schrempp (4) where three leptoquarks, one per generation family, appear as coloured pseudo-Goldstone boson multiplets of charge 2/3. In our analysis we consider the leptoquarks of the second family decaying either into $s\mu^+$ or $c\nu$, i.e. $Br(\chi \to s\mu) + Br(\chi \to c\nu) = 1$.

To select events of the signature (a) we required that two muons be detected. Furthermore, the effective mass of all charged particles except the muons had to be larger than 5 GeV. This cut rejects events (1) from α^4 electromagnetic processes $e^+e^- \to q\bar{q}\mu^+\mu^-$.

One event which has been observed in the CELLO detector (1) passes our cuts. From the values of the effective masses of the combinations muon-jet we deduce that the lowest mass which can be attributed to the leptoquark is 14 GeV. A detailed study of background sources which could account for the event can be found in ref. (1). For our total luminosity of 47.8 pb^{-1} the numbers of predicted events from the reactions $e^+e^- \to q\bar{q}g$ and $e^+e^- \to \mu^+\mu^- q\bar{q}$ were found to be less than 9.5×10^{-3} and 2.3×10^{-2} respectively. This estimate corresponds to the range of effective masses, scaled to s, larger or equal to those observed in this particular event.

The acceptance for $\chi\bar{\chi}$ production varies from 35% to 4.3% for leptoquark masses between 20 GeV and 4 GeV. With one observed event we obtained a 95% C.L. limit on the branching ratios $\chi \to \mu s$ as a function of χ mass (see Fig. 1).

Events of topology (b) were selected by requiring only one muon to be identified. No event has been found and none is expected from background sources. The detection efficiency varies from 38% to 3.9% for leptoquark masses ranging from 20 GeV to 4 GeV. The 95% C.L. limit on the $Br(\chi \to \mu^+)$ for this topology is plotted in Fig. 1.

The main signature of events (c) is a high missing momentum carried away by neutrinos. The event selection can be performed by looking either for acoplanar jets or for isolated missing momentum. The latter possibility was included in our selection criteria. Two candidate events survived our cuts.

The detection efficiencies for the topology (c) decrease from 35% to 2% for the leptoquark masses in the range from 20 GeV to 8 GeV. The number of background events was estimated to be 3.2, which comes predominantly from the annihilation into qqg.

To conclude, we have searched for evidence of pair production of scalar leptoquarks of the Goldstone boson type in e^+e^- annihilations between the C.M. energies of 38.3 GeV and 46.8 GeV. Except for the CELLO event previously reported we have not found any other multihadronic event with isolated muons in spite of a tenfold increase of the integrated luminosity. No event with one isolated muon and missing energy was observed. Two candidates for the pair production of leptoquarks decaying both into

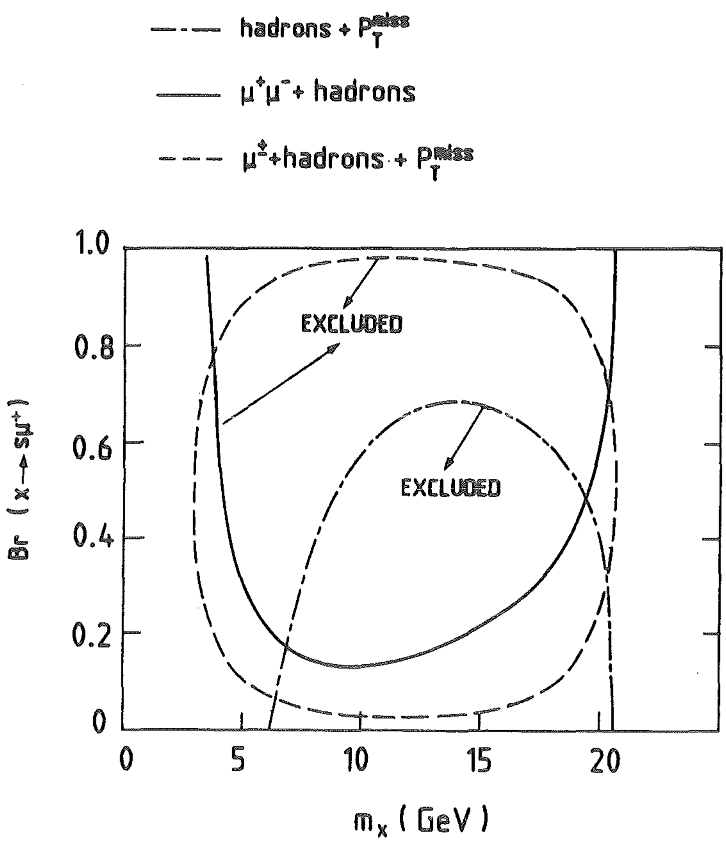

Fig. 1
95% C.L. limit contours for the leptoquark masses as a function of the branching ratio $\chi \to \mu$ s for the signatures $\mu\mu$ + hadrons (full line), μ + hadrons + p^{miss} (dotted line) and hadrons + p^{miss} (dashed-dotted line).

(c ν) pairs are compatible with the number of expected background events. The total of three candidates put an 95% C.L. limit on the $\chi\bar{\chi}$ production cross section of 0.44 pb. Combining the 95% C.L. limits on the cross sections for the three topologies we exclude the region from 7 to 20.5 GeV for any value of the branching ratio of $\chi \to s\mu$.

(1) CELLO coll., H.-J. Behrend et al., Phys.Lett. 141B (1984) 145
(3) UA1 coll., G. Arnison et al., Phys.Lett. 155B (1985) 442
UA2 coll., P. Bagnaia et al., Phys.Lett. 139B (1984) 105
(3) R.N. Mohapatra, G. Segre and L. Wolfenstein, Phys.Lett. 145B (1984) 433
(4) B. Schrempp and F. Schrempp, Phys.Lett. 153B (1985) 101

5.4.2 SEARCH FOR EXCITED QUARKS

One of the most direct predictions of composite models is the existence of excited states of quarks and leptons (1). Excited lepton (e*, μ*, τ*) searches have already been reported by us and by other collaborations (2). In the present analysis we have looked for multihadronic events coming from the production and subsequent decay of excited quarks.

In e^+e^- collisions such quarks can be produced either in pairs (due to the normal gauge coupling) or singly (with a magnetic coupling at the $qq^*\gamma$ vertex). Excited quarks can return to the ground state electromagnetically by emitting a photon $q^* \to q\gamma$ (c.f. $l^* \to l\gamma$, $l = e, \mu, \tau$), or strongly by the decay $q^* \to qg$; weak decays such as $q^* \to qZ$ and $q^* \to qW$ are also possible but they can be safely ignored at PETRA energies.

For single excited quark production we have considered an effective interaction lagrangian since the compositeness scale Λ_{comp} is expected to be in the TeV-range or above (3). The effective couplings are deduced from gauge and symmetry properties, under the simplifying hypothesis that excited quarks carry the same quantum numbers (1) as the normal ones (1,4).

Then the lagrangian leads to the decay widths (4):

$$\Gamma_{q^*\to q\gamma} = \frac{\alpha m_{q^*}}{2}\lambda_\gamma^2 \quad \text{and} \quad \Gamma_{q^*\to qg} = \frac{2\alpha_s m_{q^*}}{3}\lambda_g^2 \qquad (1)$$

where the only relevant parameters for the coupling constants are $\lambda_g^2 = |a^g| + |b^g|^2$, and, $\lambda_\gamma^2 = |a^\gamma|^2 + |b^\gamma|^2$. m_{q^*} is the mass of the excited quark, e_q and g_s are the electric and strong charge, and $a^{g,\gamma}$, $b^{g,\gamma}$ are free dimensionless parameters which determine the couplings.

The decay into gluon should dominate if $\lambda_g \approx \lambda_\gamma$. However, the possibility cannot be excluded that unknown dynamics might yield λ_γ larger than λ_g and inhibit the gluon decay. Because of that, our analysis has been performed for the two extreme cases $\Gamma_g \gg \Gamma_\gamma$ (only gluon decay), and $\Gamma_g \ll \Gamma_\gamma$ (only photon decay).

Therefore, we have looked for excited quarks in the following processes:

pair production

$e^+e^- \to q^*\bar{q}^* \to q\bar{q}gg$ (4-jets)

$e^+e^- \to q^*\bar{q}^* \to q\bar{q}\gamma\gamma$ (2-jets and 2-photons)

single production

$e^+e^- \to q\bar{q}^*, \bar{q}q^* \to q\bar{q}g$ (3-jets)

$e^+e^- \to q\bar{q}^*, \bar{q}q^* \to q\bar{q}\gamma$ (2-jets and 1-photon)

PAIR PRODUCTION

The process leading to $q^*\bar{q}^*$ production by one photon exchange is the same as for a pair of ordinary quarks. For this case only unknown quantity in the total cross section is m_{q^*}.

A - Gluon decay channel: For the reaction $e^+e^- \rightarrow q^*\bar{q}^* \rightarrow q\bar{q}gg$ we expect an excess in the number of four jet events.

B - Photon decay channel: For the production of q^*, via $e^+e^- \rightarrow q^*\bar{q}^* \rightarrow q\bar{q}\gamma\gamma$, we have searched for events with two jets and two hard photons.

SINGLE PRODUCTION

The process allows to produce excited quarks with $m_g^* \geqslant E_b$. The cross section has now two unknown parameters, m_{q^*}, and λ_γ.

A - Gluon decay channel: The cleanest signature for the q^* would be a peak in the two-jet invariant mass M_{jj} corresponding to the subprocess $q^* \rightarrow qg$ in the reaction $e^+e^- \rightarrow q\bar{q}^*, \bar{q}q^* \rightarrow q\bar{q}g$. So we have looked for such a peak in our three jet sample.

B - photon decay channel: The fourth q^* signal we looked for was a peak in the photon-jet invariant mass $M_{j\gamma}$ due to the decay $q^* \rightarrow q\gamma$- For that reason we searched for events with two jets and one energetic photon.

In conclusion, we have studied events with one of the following topologies: 4-jets, 2-jets and 2-photons, 3-jets, 2-jets and 1-photon. We observe good agreement of our data with the known QCD processes and thus conclude that no indication for an excited quark is found up to the highest PETRA energy of 46.8 GeV.

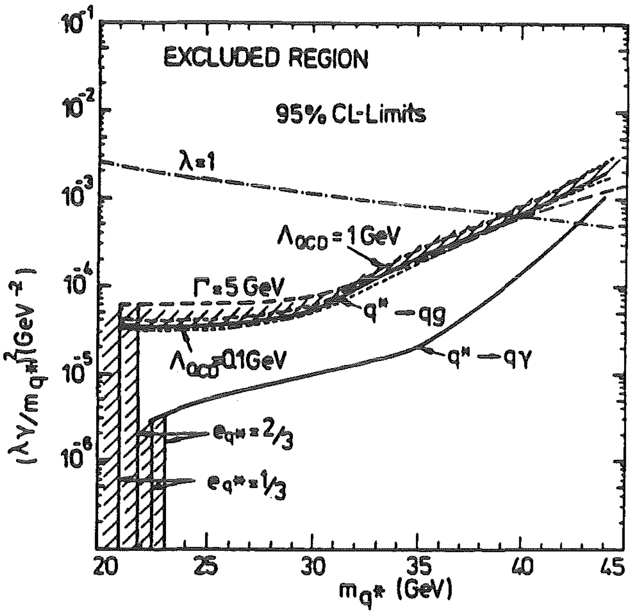

Fig. 1

Limits at 95% C.L. for all the cases considered in this analysis. In this plot the charged of excited quarks are taken into account only when they are pair produced and a limit independent from λ_γ is obtained (vertical lines).

If they are produced together with a normal quark the coupling of the $qq^*\gamma$ vertex is taken according to the gauge invariant effective lagrangian with e_q set to one.

In the case when the excited quark decays into an usual quark and a gluon we derive 95% C.L. lower limits on the excited quark mass of 20.8 GeV/c^2 and 22.3 GeV/c^2 for a quark charge 1/3 or 2/3, respectively. In the photon decay channel case we exclude them below 22.5 GeV/c^2 and 23.2 GeV/c^2.

Limits are also put for both channels on the $q^*q\gamma$ coupling strength, up to q* masses of about 40 GeV/c^2 (Fig. 1).

(1) A. de Rujula, L. Maiani, R. Petronzio, Phys.Lett. 140B (1984) 253
(2) CELLO coll., H.-J. Behrend et al., Phys.Lett. 168B (1986) 420
MARK-J coll., B. Adeva et al., Phys.Lett. 152B (1984) 439
S. Komamiya, Invited talk at the Lepton and Photon Symposium, Kyoto, 1985 (it includes JADE latest results).
(3) W. Buchmüller, D. Wyler, Nucl.Phys. 268B (1986) 621
(4) F.M. Renard, Nuovo Cimento 77A (1983) 1
J.H. Kühn, CERN-TH, 4131/85 (1985)

5.4.3 SEARCH FOR CHARGED AND NEUTRAL HEAVY LEPTONS

The repetitive nature of the three known fermion generations suggests a search for new leptons of a possible fourth generation. Charged heavy leptons can be pair produced by photon annihilation. Neutral particles can be pair produced by annihilation into a (at present energies virtual) Z^0. At the present PETRA energy ($\sqrt{s}$ = 44 GeV) the neutrino pair production cross section is:

$$\sigma(e^+e^- \to Z^0 \to \nu_\mu\bar{\nu}_\mu) = 1.1 \text{ pb} \quad .$$

Correspondingly: the total cross section for Z^0 production at PETRA is

$$\sigma(e^+e^- \to Z^0 \to \text{anything}) = \frac{\sigma(e^+e^- \to Z^0 \to \nu_\mu\bar{\nu}_\mu)}{BR(Z^0 \to \nu\bar{\nu})} = 19 \text{ pb} \quad .$$

This means that ~ 900 Z^0's have been produced at each of the four PETRA interaction regions. Seen this way, at present PETRA (and PEP) are the largest Z^0 factories available! In this chapter we describe first the detector and the search for charged and neutral heavy leptons, respectively.

CHARGED HEAVY LEPTON

A new charged lepton would be pair produced via one photon annihilation with a cross sectin (neglecting Z^0 effects)

$$\sigma(e^+e^- \rightarrow L^+L^-) = \frac{\beta(3-\beta^2)}{2}\,\sigma_{\mu\mu} \quad ,$$

where $\sigma_{\mu\mu}$ is the μ pair cross section. It is expected to decay via W exchange into a lighter lepton and neutrinos or into hadrons and neutrino with a leptonic branching fraction of $\sim 3 \cdot 11\%$. The signatures for a new charged heavy lepton are jets and lepton pairs or a jet plus and isolated lepton together with missing energy and momentum carried away by neutrinos.

The selection of acoplanar jets and electrons is identical to be one described in the search for winos and zinos (5.4.4), while the search for jets plus an isolated muon has been described in our search for leptoquarks.

NEUTRAL HEAVY LEPTON

The two possible mechanisms are the $N\bar{N}$ pair production through the Z^0 annihilation or the production of a single heavy neutrino together with a light neutrino through a W exchange. The cross section for the production of a single heavy neutral lepton can be calculated using a V-A or a V+A current at the vertex eWN.

It is obvious that with this mechanism, one is sensitive to heavier neutral leptons. One should however note that in the cross section, the e-N mixing $|U_{eN}|^2$ has been set to 1. If $|U_{eN}|^2 \ll 1.$, the cross section is scaled down and becomes too small to be measured.

It is commonly assumed that a heavy neutral lepton decays in the same way as a charged lepton through a W boson (Fig. 1) and has the following width:

$$\Gamma(N^0 \rightarrow \ell X) = \frac{G^2 M_{N^0}^5}{3(4\pi)^3}\;\frac{\Sigma_\ell |U_{N^0\ell}|^2}{B(N^0 \rightarrow \ell \nu_e e)}$$

leading to a lifetime of:

$$\tau_N = \frac{M_\mu^5}{M_N^5}\,\tau_\mu\,\frac{B(N^0 \rightarrow \ell \nu_e e)}{\Sigma |U_{N^0\ell}|^2}$$

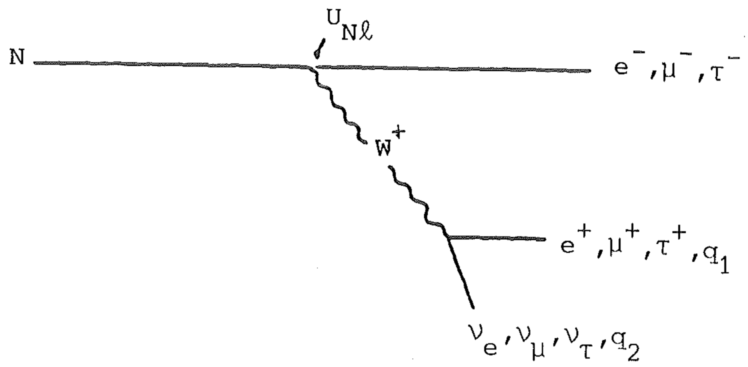

Fig. 1 Decay mechanism of a heavy neutral lepton

It is clear from this expression that in order to observe the neutrino decay in our detector, the value $M_N^5\Sigma|U_{N\ell}|^2$ has to be large enough.

Depending upon the mass of the heavy neutrino, the decay channels are different. A naive estimation of the branching ratios gives for masses bigger than 2 GeV:

$$B(\ell\nu_e e) : B(\ell\nu_\mu\mu) : B(\ell\nu_\tau\tau) : B(\ell\,ud) : B(\ell\,cs) = 1 : 1 : 1 : 3 : 3$$

which is slightly modified by QCD radiative corrections. ℓ stands for the charged lepton which is preferentially coupled to the heavy neutral lepton.

Taking advantage of the good ability of our detector to identify electrons and muons, we have searched for a heavy neutral lepton coupled to one of these leptons.

We are finally left with 2 events. One 4 prong events having 3 identified electrons and a high multiplicity events with 2 identified muons.

We have summarized in Table 1 the different types of candidates found and the expected background.

In conclusion we have searched for a heavy neutral lepton pair-produced through the Z^0 boson or produced together with a usual neutrino in the t channel. No evidence has been found in both cases. We have set 95% C.L. limits in a range going from 3.1 to 18.0 GeV/c^2 in the first mode (Fig. 2) while in the second mode we exclude the region between .6 to 34.6 GeV/c^2 with a V-A current at the eWN vertex and between .4 to 37.4 GeV/c^2 with V+A. These results improve earlier limits from JADE (1).

(1) JADE coll., W. Bartel et al., Phys.Lett. 123B (1983) 353

Table 1

Signatures	Number of events	Expected background
4 charged particles with 2 leptons	1	0.74 ± 0.07
> 5 charged particles with 2 electrons	0	1.4 ± 0.3
> 5 charged particles with 2 muons	1	0.13 ± 0.03

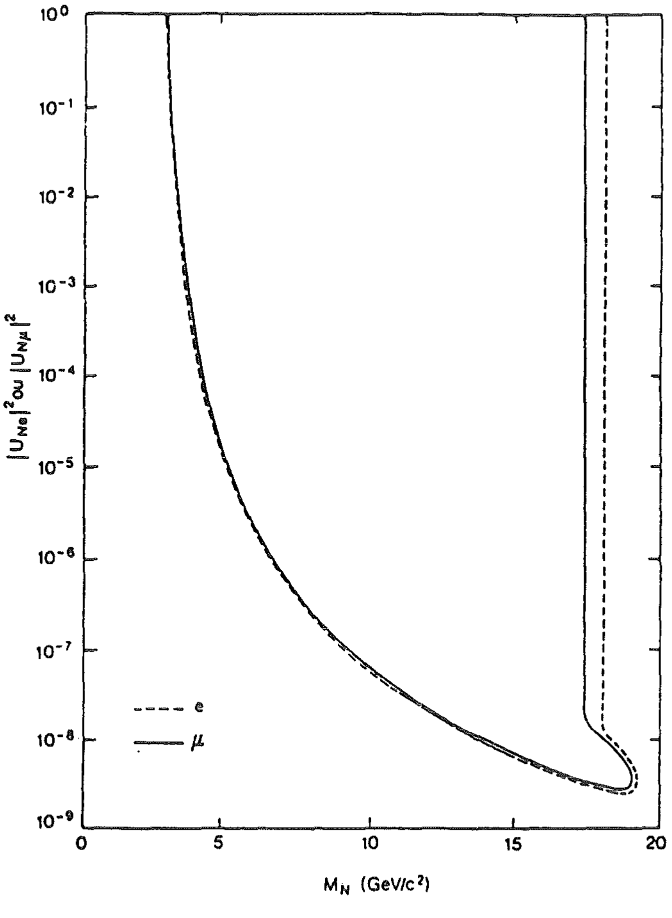

Fig. 2
95% C.L. exclusion contour of heavy neutral leptons versus the $|U_{N\ell}|^2$. The solid line is for $|U_{N\mu}|^2$ and the dashed line for $|U_{Ne}|^2$.

5.4.4 SEARCH FOR SUPERSYMMETRIC PARTICLES

Supersymmetry relates the fermion (matter) fields and the gauge fields which are the origin of particle interactions. The main features of supersymmetric models is the prediction of a supersymmetric partner for each known particle with the same couplings and quantum numbers except spin which differs by $|\Delta j| = 1/2$. In this case many divergencies in Feynman graphs are cancelled, since the fermions and bosons contribute equally with opposite signs, provided the supersymmetric particles are not too heavy. The absence of mass degenerate supersymmetric partners of the known particles shows that supersymmetry must be broken. The details of this symmetry breaking are unknown. Therefore there are essentially no firm predictions for the masses of the supersymmetric particles.

SERACH FOR PHOTINOS

In supersymmetric theories, there is no general prediction for the mass spectrum of the partners of the ordinary particles. Because of the expected R-parity conservation, it is commonly believed that the lightest supersymmetric particle (LSP) must be stable, and cosmological arguments lead to the conjecture that it is neutral and colorless. Candidate LSP's are therefore the photino $\tilde{\gamma}$, the zino $\tilde{z}$ or the higgsino $\tilde{h}$, and in some models a scalar neutrino $\tilde{\nu}$; the gravitino $\tilde{g}$ can also be considered as the LSP. The couplings of these particles are completely fixed, except for possible mixings in the gaugino sector. Here, we will assume that the $\tilde{\gamma}$ is unmixed. The LSP is in all cases expected to interact only weakly with ordinary matter. As a consequence, pair production of LSP's in e^+e^- collisions can be detected only in association with an initial state radiation photon (1).

It is evident that an experiment aiming at the study of such a reaction needs good photon detection at low angle. In addition, to ensure that only weakly interacting particles are produced in association with the tagged photon, the veto capability of the detector must be extended to the largest possible solid angle. However, e^+e^- storage rings, it is unavoidable that a hole be left for the beam pipe. This causes the reaction $e^+e^- \rightarrow e^+e^-\gamma$ to be the major experimental background, when both electrons are scattered at small polar angles. For the results reported here, the minimum veto angle is 50 mrad.

The acceptance gap between the barrel and end cap calorimeters was filled in 1984 by a crude lead-scintillator sandwich array read by wavelength shifters, the so-called hole tagger. This upgrade of the detector was instrumental in this analysis, since it allowed the elimination of the large potential background coming from the reaction $e^+e^- \rightarrow \gamma\gamma\gamma$, with one photon remaining inside the beam pipe, another one going into the hole tagger region, and only one detected. Finally, a lead glass array closes the acceptance from 130 mrad (lower limit of the angular coverage of the end

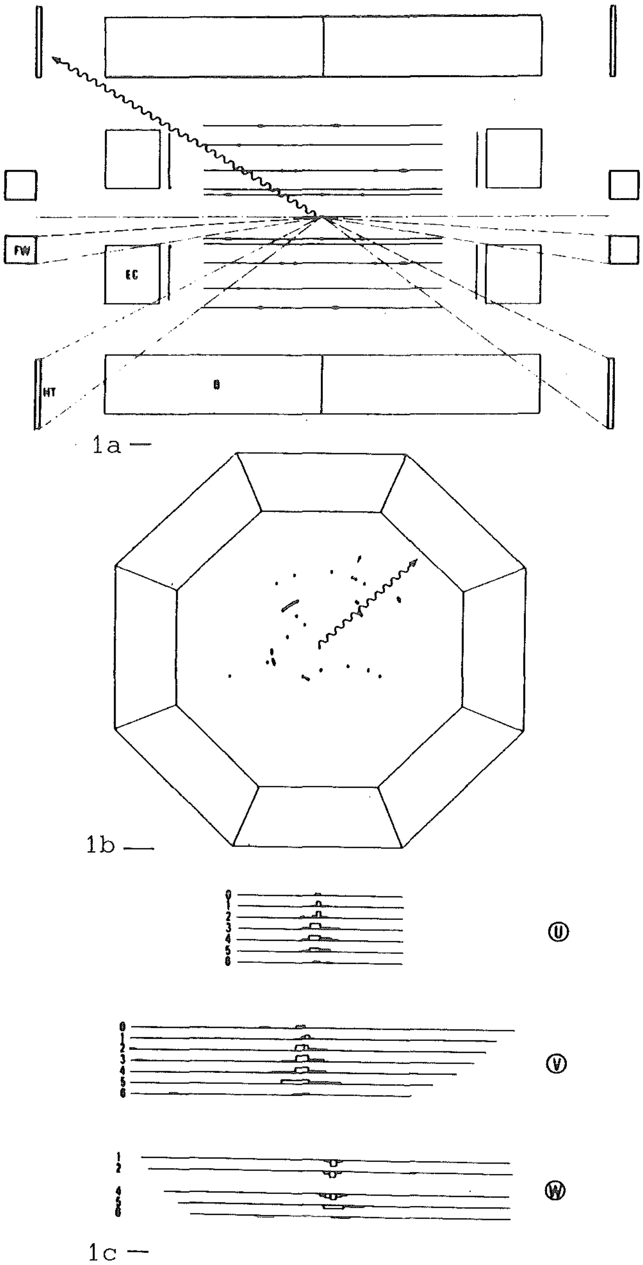

Fig. 1

Example of an event with a single photon in the barrel calorimeter, vetoed in the hole tagger.

1a and 1b are projections into planes containing the beam axis and transverse to it respectively. The various components of the calorimetric coverage are indicated: barrel (B) and end cap (EC) lead-liquid argon calorimeter, hole tagger (HT) and forward lead glass array (FW). The wiggled lne indicates the direction of the additional photon detected in the hole tagger. The hits in the central detector are due to synchrotron radiation. The data of the liquid argon calorimeter module containing the showers are displayed in 1c. The lead strips of the 7 layers in the U direction run parallel to the beam, those of the 7 layers in the V direction transverse to it, and those of the 5 layers in the W direction at 45^0 with respect to U and V. The magnification variies with the depth so that a shower pointing to the interaction vertex always appears perpendicular to the layers.

cap calorimeter) down to 50 mrad. High energy muons can be identified over 92% of the solid angle in the large drift chambers which surround the detector beyond an 80 cm thick iron absorber (Fig. 1).

Single photon events were triggered by a total energy deposit in excess of an adjustable threshold in any of the 16 modules of the barrel calorimeters. This threshold (50% of the maximum efficiency) was set at ~ 3 GeV for the first half of the data (set A), and decreased to ~ 2 GeV afterwards (set B). This improvement was made possible by a better rejection of the out of time signals (cosmics and electronic noise) at the trigger level. This rejection is achieved by sampling the 1.5 μs-long liquid argon signal at a set of times fixed with respect to the beam crossing (twice in A, four times in B). After all cuts, no events survived.

The visible cross section expected from the three known neutrino species is 18 fb. With our integrated luminosity the corresponding number of events is 0.68, which gives a 51% probability of not observing any event. The 90% and 95& C.L. upper limit on the total number of light neutrino species set by this experiment are 14.9 and 20.1 respectively. Similar results have been obtained recently using the same method (2) and from studies of the production and decay of the intermediate vector bosons at the CERN $p\bar{p}$ collider (3). Combining our result with the most recent ones from the ASP and MAC collaborations (2), ones obtains a 90% (95%) C.L. limit of 8 (10) on the total number of light species.

We now turn to the interpretation of this result in terms of bounds on masses of supersymmetric particles.

The most commonly considered LSP is the photino, which could be produced by the reaction $e^+e^- \to \gamma\bar{\gamma}\bar{\gamma}$. Since $e^+e^- \to \bar{\gamma}\bar{\gamma}$ goes by t-channel $\tilde{e}$ exchange ($\tilde{e}$ is either one of $\tilde{e}_L$ or $\tilde{e}_R$, the scalar partners of the left and right handed electrons), the number of single photon events expected in this case will depend on both the photino and scalar electron masses. The domain we exclude is presented in Fig. 2 for the two cases where i) $\tilde{e}_L$ and $\tilde{e}_R$ are degenerate in mass, ii) one is much heavier than the other. In Fig. 2 we also combine the results obtained here and in Ref. (4), where single and pair productions of scalar electrons are investigated, to obtain the largest domain excluded by this experiment. For massless photinos, a 90% C.L. lower limit of 37.7 GeV/c^2 is set on the mass of degenerate scalar electrons.

The case where the LSP is the zino can be readily deduced from the former one, by replacement of the $e\tilde{e}\tilde{\gamma}$ coupling by the $e\tilde{e}\tilde{z}$ coupling. However, even in the most favorable case (equal mass scalar electrons,

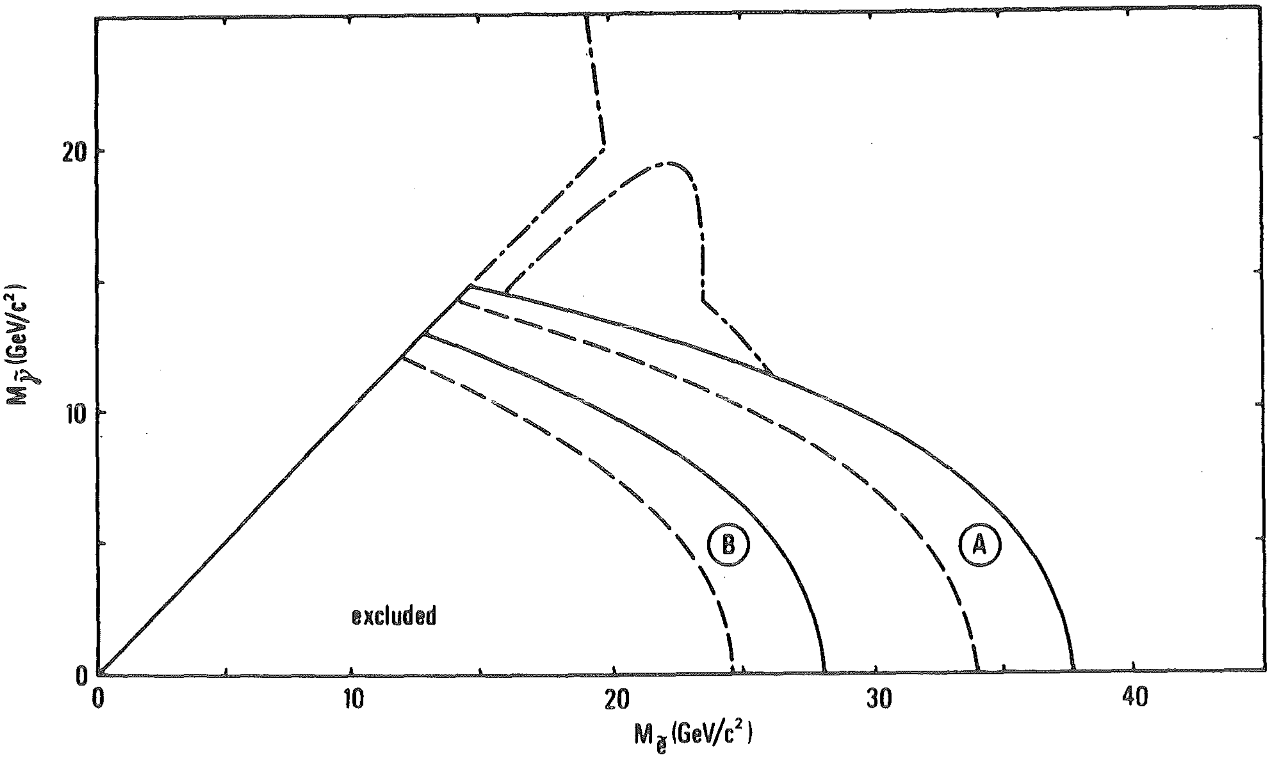

Fig. 2 Boundaries of 90% C.L. (full lines) and 95% C.L. (dotted lines) domains excluded by this analysis for mass degenerate scalar electrons (A), and if one of the scalar electrons is very heavy (B). The dash-dotted contour indicates the additional domain excluded at 90% C.L. by another CELLO analysis (4), for mass degenerate scalar electrons.

massless zinos, and no $\tilde{z}$-$\tilde{h}$ mixing), the 90% C.L. lower limit which can be set on the mass of the scalar electron is far less stringent than that provided by pair production.

In the case where the LSP is an electron-type scalar neutrino $\tilde{\nu}$, the t-channel exchanged particle is now a wino $\tilde{w}$. We have used $\sigma(e^+e^- \rightarrow \tilde{\nu}\nu)$ as given in Ref. (5) to obtain the excluded domain shown in Fig. 3. For the sake of simplicity, we have assumed no wino-charged higgsino mxing, and we did not take into account other scalar neutrino species (which in any case contribute only by s-channel Z^0 exchange). Also shown in Fig. 3 is the additional domain excluded by CELLO in a search for single and pair production of winos (4). For massless $\tilde{\mu}$, a 90% C.L. lower limit of 40.2 GeV/c^2 is set on the mass of the wino.

Finally, we consider the case of radiative photino-gravitino production. Here the LSP is the gravitino. The photino should be sufficiently light not to conflict with the standard model of cosmology (6), in which case its lifetime is such that it can be considered as stable in this expe-

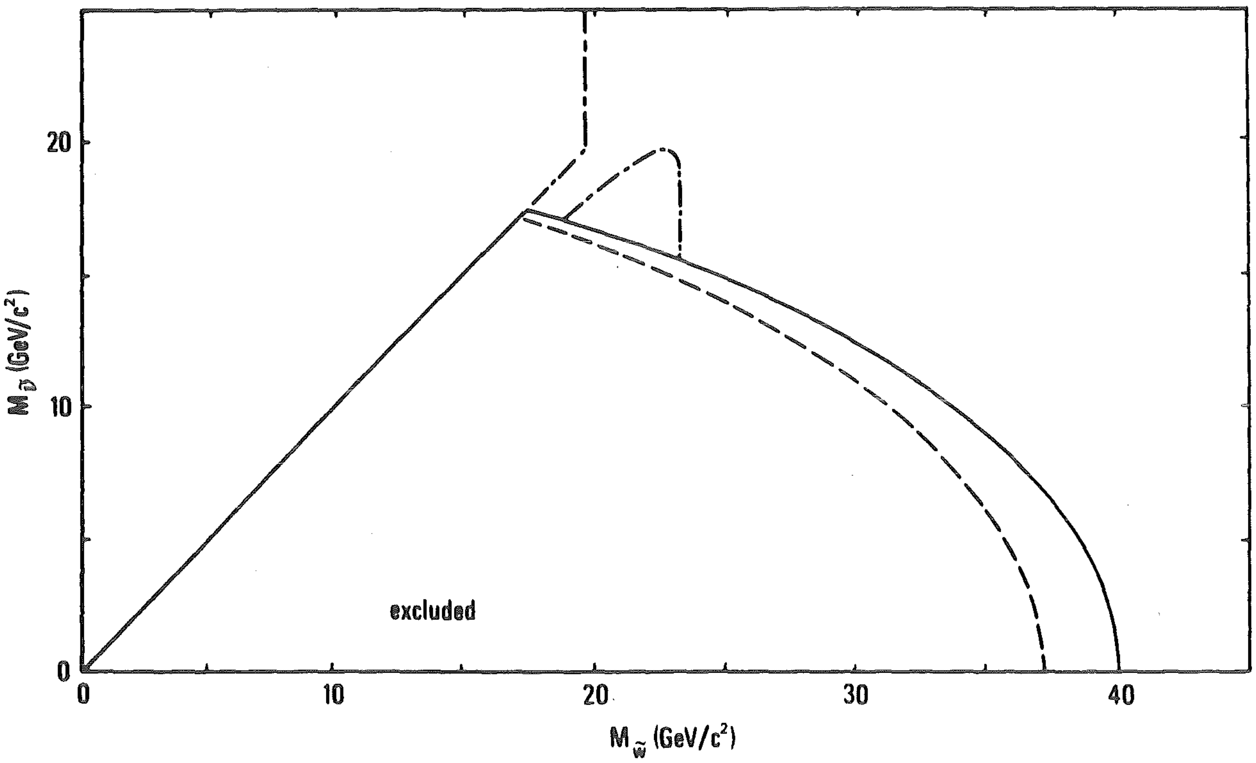

Fig. 3 Boundaries of 90% C.L. (full lines) and 95% C.L. (dotted lines) domains excluded by this analysis. The dash-dotted contour indicates the additional domain excluded at 90% C.L. by another CELLO analysis (4).

riment. The cross-section for this process is given in Ref. (1), and leads to a 90% C.L. lower limit of 1.1×10^{-6} eV for the mass of the gravitino.

Our results improve all comparable previous PETRA limits (7,8) and the most recent PEP limits (2,9) for high photino or scalar neutrino masses. Our limit on the gravitino mass is two orders of magnitude better than that obtained from J/Ψ decays.

To summarize, we have searched for single photons produced in e^+e^- collisions at $\sqrt{\langle s \rangle}$ = 42.6 GeV. No event was observed, which is compatible with the expectation from $e^+e^- \rightarrow \gamma\mu\bar{\mu}$ for the three know neutrino species. This result sets a limit of 15 (90% C.L.) on the total number of light neutrino species, and restricts the allowed mass range for various supersymmetric particles.

(1) P. Fayet, Phys.Lett. 117B (1982) 460
(2) ASP coll., G. Bartha et al., Phys.Rev.Lett. 56 (1986) 685
MAC coll., E. Fernandez et al., Phys.Rev.Lett. 54 (1985) 1118
(3) UA1 coll., G. Arnison et al., Phys.Lett. 166B (1986) 484
UA2 coll., J.A. Appel et al., Z.Phys. C30 (1986) 1

(4) CELLO coll., H.-J. Behrend et al., Search for Scalar Electrons and Photinos in e^+e^- Interactions, to be published

(5) J.S. Hagelin, G.L. Kane, and S. Raby, Nucl.Phys. B241 (1984) 638

(6) N. Cabibbo, G.R. Farrar, and L. Maiani, Phys.Lett. 105B (1981) 155

(7) CELLO coll., H.-J. Behrend et al., Phys.Lett. 114B (1982) 287,
JADE coll., W. Bartel et al., Phys.Lett. 152B (1985) 385,
MARK J coll., B. Adeva et al., Phys.Lett. 152B (1985) 439,
TASSO coll., R. Brandelik et al., Phys.Lett. 117B (1982) 365

(8) JADE coll., W. Bartel et al., Z. Phys. C29 (1985) 505,
MARK J coll., B. Adeva et al., Phys.Rev.Lett. 53 (1984) 1806

(9) MAC coll., E. Fernandez et al., Phys.Rev.Lett. 52 (1984) 22,
MARK II coll., L. Gladney et al., Phys.Rev.Lett. 51 (1983) 2253

SEARCH FOR ZINOS

The final particles in electron positron collisions are quarks, leptons, and gauge bosons so that one can produce also squarks, sleptons, and gauginos, provided they are not too heavy. This is an update of the report on a search for the supersymmetric partner of the neutral intermediate vector bosons Z^0, called the zino $\tilde{z}$ already given in 1985.

In electron positron collisions zinos can be produced in association with the supersymmetric partner of the photon, the photino $\tilde{\gamma}$:

$$e^+e^- \rightarrow \tilde{\gamma}\tilde{z}$$

via t-channel exchange of a scalar electron which is the spin 0 partner of the electron. This channel will open up at lower energies than the pair production of two zinos, if the photino is lighter than the zino. Therefore, we do not consider the pair production of two zinos.

The experimental signature for this reaction of course depends on the decay modes of the zino. Depending on the unknown SUSY mass spectrum, various scenarios are possible:

Heavy gluino ($M(\tilde{g}) > m(\tilde{z})$), heavy sneutrino ($M(\tilde{\nu}) > M(\tilde{z})$): The zino decays via scalar exchange into a fermion anti-fermion pair and a photino.

Light gluino ($m(\tilde{g}) < m(\tilde{z})$): In this case the dominant zino decay would be hadronically into $q\bar{q}\tilde{g}$ followed by $\tilde{g} \rightarrow q\bar{q}\tilde{\gamma}$ due to the stronger hadronic $\tilde{q}q\tilde{g}$ coupling.

Light sneutrino ($m(\tilde{\nu}) < m(\tilde{z})$): The scalar neutrino may be light, possibly even the lightest SUSY particle. Then the zino would decay exclusively into an invisible $\tilde{\nu}\nu$ final state. In this case, which will not be considered here, the zino production can only be observed by searching for single photons from the reaction $e^+e^- \rightarrow \gamma\tilde{\gamma}\tilde{z}$ (see above).

The process $e^+e^- \rightarrow \tilde{\gamma}\tilde{z}$ followed by the decay $\tilde{z} \rightarrow e^+e^-\tilde{\gamma}$ leads to the signature of an acoplanar electron pair with momentum and energy carried

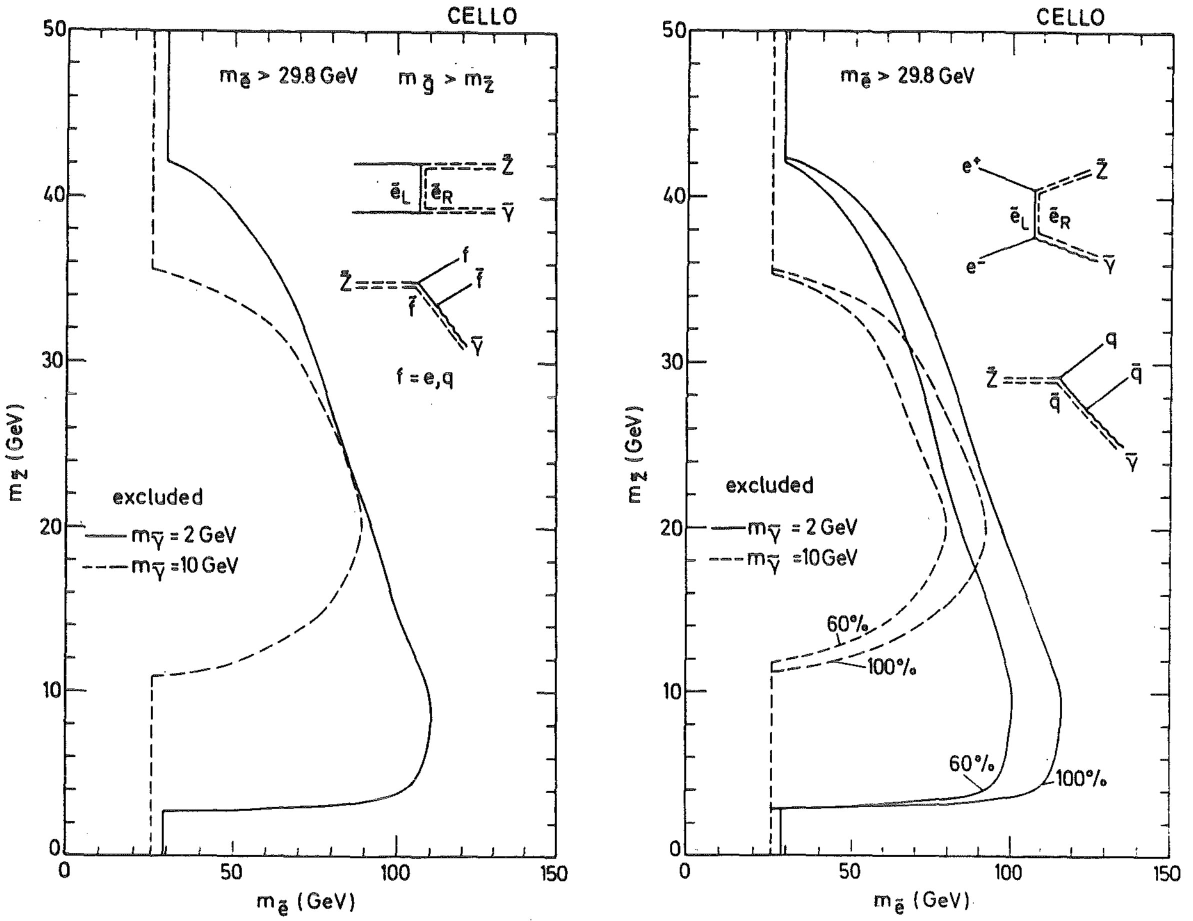

Fig. 4 Excluded zino masses (95% C.L.) as a function of the scalar electron mass. Scalar electron masses below 29.8 GeV (26.1 GeV) are excluded for $m(\tilde{\gamma})$ = 2 GeV (10 GeV) by a previous search for scalar electrons.

a) for $\tilde{z} \rightarrow q\bar{q}\tilde{\gamma}$ with $m(\tilde{\gamma})$ = 2 GeV (full lines) and $m(\tilde{\gamma})$ = 10 GeV (dashed lines) for two different branching ratios: $BR(\tilde{z} \rightarrow ee\tilde{\gamma})$ = 100% and 60%, respectively.

b) Combined limit search for $\tilde{z} \rightarrow ee\tilde{\gamma}$ and $\tilde{z} \rightarrow q\bar{q}\tilde{\gamma}$ assuming an hadronic branching fractions of 60% with a 2 GeV (full line) and 10 GeV (dahsed line) photino.

away by the two unobserved photinos. In analogy, the decay $\tilde{z} \rightarrow q\bar{q}\tilde{\gamma}$ gives rise to a pair of acoplanar jets which for smaller zino masses are boosted into a single hemisphere giving rise to one handed 'zen'like event topologies. If the zino decays predominantly into $q\bar{q}\tilde{g}$ the average momentum of the decay photino is reduced but the general feature of missing energy and momentum, although less distinctive for high zino masses, is maintained.

Thus signatures of zino production and decay in e^+e^- collisions will be jets or lepton pairs with missing energy and momentum (Fig. 4).

In conclusion we have searched for such unusual lepton and quark pairs with missing energy and momentum. No signal has been found. This excludes copious production of SUSY type neutralinos within the PETRA energy range. The upper limits on the visible cross sections for acoplanar jets and acoplanar lepton pairs have been compared with specific models of zino production. Typcal limits on the mass of the zino are found to be 30 - 40 GeV assuming the scalar electron to be lighter than 80 GeV. Since we searched for both leptonic and hadronic final states from zino decay these limits are quite insensitive to the leptonic branching fraction of the zino. Similar limits have been obtained by other PETRA experiments (1).

(1) JADE coll., W. Bartel et al., Phys.Lett. 146B (1984) 126
MARK J coll., B. Adeva et al., Phys.Rev.Lett. 53 (1984) 1806

SEARCH FOR WINOS AND HIGGSINOS

We have also searched for the supersymmetric partners of the weak intermediate vector bosons Z^0 and W, called th zino $\tilde{z}$ and the wino $\tilde{w}$. Here we report on search for the wino $\tilde{w}$ and the higgsino $\tilde{h}^{\pm}$, the supersymmetric partner of the charged Higgs particle. In general the higgsino and wino are expected to mix forming mass eigenstates usually called charginos $\tilde{\chi}^{\pm}$ (1).

Charginos can be pair produced in electron positron annihilation

$$e^+e^- \rightarrow \tilde{\chi}^+\tilde{\chi}^-$$

via one photon annihilation and via t channel exchange of a scalar electron neutrino (Figs. 5a,b). The latter amplitude is proportional to the wino content in the chargino due to the small $\tilde{h}^{\pm}e\tilde{\nu}$ coupling.

The experimental signature for this reaction depends on the chargino decay mode. For definiteness, we first assume the case of a pure wino and postpone the discussion of gaugino higgsino mixing. Depending on the unknown SUSY mass spectrum, various scenarios are possible.

Heavy gluino ($m(\tilde{g}) > m(\tilde{w})$), heavy sneutrino ($m(\tilde{\nu}) > m(\tilde{w})$): The wino decays into $l\nu\tilde{\gamma}$ or $q\bar{q}'\tilde{\gamma}$ via W (Figs 5e,f) or via scalar exchange (Figs. 5c,d) with the decay width being proportional to $1/m^4(W)$ and $1/m^4_{scalar}$ respectively (1). One expects acoplanar lepton pairs (not neccessarily of the same flavour) and hadronic final states with missing transverse momentum carried away by unobserved photinos and neutrinos. Unless otherwise noted,

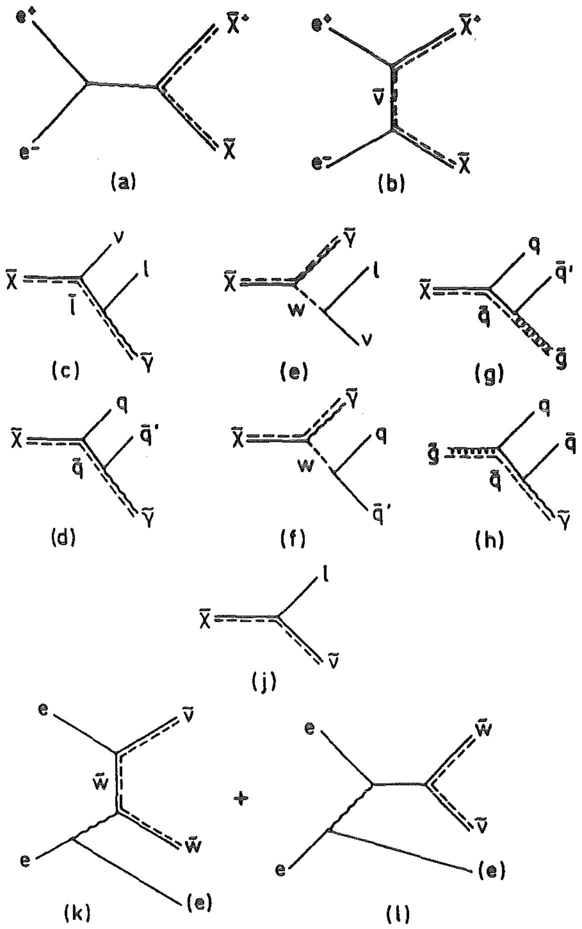

Fig. 5
Feynman diagrams for chargino production and decay
a,b: chargino pair production
c-f: chargino decay, both $\tilde{g}$ and $\tilde{\nu}$ heavy ($> m(\tilde{\chi}^{\pm})$)
g,h: chargino decay, light $\tilde{g}$
j: chargino decay, light $\tilde{\nu}$
k,l: single wino production in eγ scattering.

in this chapter we make the usual assumption that the photino is the lightest supersymmetric particle and is thus stable and non-interacting in the detector. Unstable photinos decaying inside the detector are excluded for scalar electron masses up to 100 GeV by our previous search for photon pairs with missing energy (2,3).

Light gluino ($m(\tilde{g}) < m(\tilde{w})$): In this case the dominant wino decay would be hadronically into $q\bar{q}'\tilde{g}$, followed by $\tilde{g} \rightarrow q\bar{q}\tilde{\gamma}$ (Figs. 5g,h), due to the stronger hadronic $q\bar{q}'\tilde{g}$ coupling. Winos are pair produced, so that there are 8 quarks in the final state resulting in spherical events with relatively small missing energy and momentum

Light sneutrino ($m(\tilde{\nu}) < m(\tilde{w})$): The scalar neutrino might be light, possibly even the lightest SUSY particle (4). Then the wino would decay exclusively into $l\tilde{\nu}$ final states (Fig. 5j) with a branching ratio of 1/3 for each lepton generation. The sneutrino escapes unseen, resulting in a final state of two acoplanar leptons.

Winos can also be produced singly in association with a scalar neutrino (5):

$$e^+e^- \rightarrow (e)\tilde{w}\tilde{\nu} \quad .$$

This process, in contrast to pair-production, is sensitive to $\tilde{w}$ masses above the beam energy, provided the $\tilde{\nu}$ is light. Figs. 5k,l show the dominant diagrams contributing to this reaction if the final electron is scattered at small angle. Here one of the beam electrons radiates a quasi real photon which interacts with an electron of the other beam producing a wino and a scalar neutrino, either by t-channel $\tilde{w}$ exchange or via a virtual electron in the s-channel. The electron is scattered at very small angles and escapes unobserved down the beam pipe. The decay of the $\tilde{w}$ into an electron an a sneutrino (branching ratio 1/3) gives rise to an energetic electron distributed almost isotropically for high $\tilde{w}$ masses plus unobserved photino. So the signature of this process is one energetic electron in the detector and nothing else.

As follows from the above discussion, signatures of chargino production and decay in e^+e^- collisions will be jets or lepton pairs with missing energy and momentum and single electrons.

In conclusion, we have searched for such unusual lepton and jet pairs with missing energy and momentum and for single energetic electrons. No signal was observed. Lower limits on the mass of the wino are between 22.0 GeV and 26.4 GeV depending on the wino decay mechanism. The first limit also holds for a charged higgsino and we can conclude that charginos are excluded for $m < 22$ GeV independent of assumptions on mixing or decay properties. Similar limits have been obtained by other PETRA experiments (6). If the scalar neutrinos are very light $(m(\tilde{\nu}_e) + m(\tilde{\nu}_\tau) \lesssim m(\tau))$ wino masses up to $\sim m(W)$ can be excluded from data on τ lifetime and decay lepton momentum spectra (7).

(1) J.M. Frere and G.L. Kane, Nucl.Phys. B223 (1983) 331
(2) CELLO coll., H.-J. Behrend et al., Phys.Lett. 123B (1983) 127
(3) CELLO coll., H.-J. Behrend et al., Search for Scalar Electrons and Photinos in e^+e^- Interactions, to be published
(4) L.E. Ibanez and C. Lopez, Nucl.Phys. B233 (1984) 511
J.S. Hagelin, G.L. Kane, and S. Raby, Nucl.Phys. B241 (1984) 638
(5) J.A. Grifols and R. Pascual, Phys.Lett. 135B (1984) 319
G. Eilam and E. Reya, Phys.Lett. 145B (1984) 425 and erratum, Phys.Lett. 148B (1984) 502
(6) JADE coll., W. Bartel et al., Z. Phys. C (1985) 505
MARK J coll., B. Adeva et al., Phys.Rev.Lett. 53 (1984) 1806
(7) G.L. Kane and W.B. Rolnick, Nucl.Phys. B232 (1984) 21

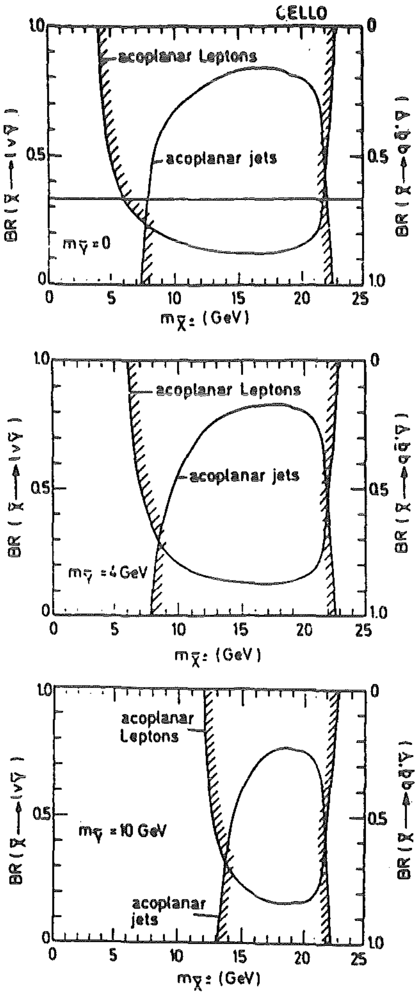

Fig. 6

Excluded chargino masses as function of the leptonic branching fraction for the decay modes $\tilde{\chi}^{\pm} \rightarrow l\nu\tilde{\gamma}$. $q\bar{q}'\tilde{\gamma}$ i.e. for the case of both heavy $\tilde{g}$ and heavy $\tilde{\nu}$.

a) $m(\tilde{\mu}) = 0$ GeV

b) $m(\tilde{\mu}) = 4$ GeV

c) $m(\tilde{\mu}) = 40$ GeV

The horizontal line in a) indicates a leptonic branching fraction of 3 × 11% as expected for a chargino decaying via W exchange. For this branching ratio the limit on the mass of $\tilde{\chi}^{\pm}$ is 22.1 GeV.

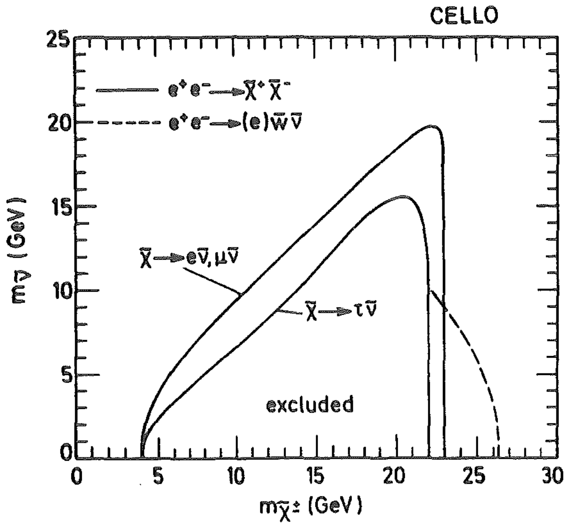

Fig. 7

Excluded chargino mass as function of the scalar neutrino mass for the case of a light scalar neutrino $m(\tilde{\nu}) < m(\tilde{\chi}^{\pm})$). The full lines are for equal decay widths into $e\tilde{\nu}$, $\mu\tilde{\nu}$, and $\tau\tilde{\nu}$ and for $BR(\tilde{\chi}^{\pm} \rightarrow \tau\tilde{\nu}) = 1$ (as expected for a pure higgsino) respectively. The limit indicated by the dashed contour comes from single wino production.

6. DEVELOPMENTS AND INSTRUMENTATION

6.1 DETECTORS

6.1.1 PROTOTYPE CRYSTALS FOR THE KARLSRUHE 4π BARIUM FLUORIDE DETECTOR

K. Wisshak, F. Käppeler, H. Müller, (1)

The energy and time resolution of big BaF_2 crystals has been improved significantly by the use of a PTFE reflector and a modified voltage divider chain. We found that an energy resolution of 8.7 % (662 keV) and a time resolution of 325 ps (^{60}Co, 300 keV threshold) can be obtained simultaneously from a cylindrical test crystal of 1 l volume. The respective results as obtained from prototype crystals for the Karlsruhe 4π detector are only slightly worse (9.6 % and 400 ps). These crystals are truncated hexagonal and pentagonal pyramids shaped from cylindrical single crystals of 14 cm diameter and 15 cm thickness.

(1) Nucl. Instr. and Meth. A 251 (1986) 101

6.1.2 COMPLETION OF THE MECHANICAL SUPPORT FOR THE 4π BaF_2 DETECTOR

K. Wisshak, F. Käppeler, J. Krisch$^+$

The mechanical support for the 4π BaF_2 detector has been completed and installed at a beam line of the 3.75 MV Van de Graaff accelerator (Fig. 1). The central part is a sphere composed of 30 hexagonal and 12 pentagonal honeycomb frames mounted

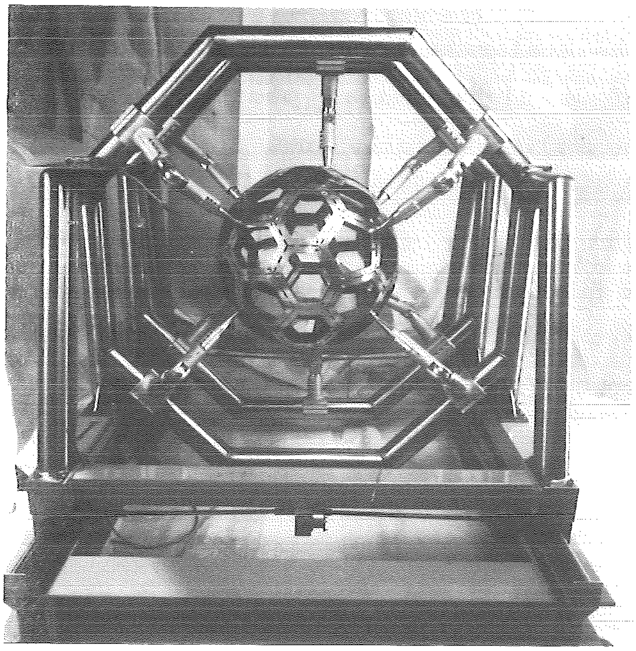

Fig. 1 The mechanical support of the 4π BaF_2 detector at the 3.75 MV Van de Graaff accelerator.

together by means of fitting screws. Extreme care had to be taken during the machining of the honeycomb frames as - due to their complicated shape - the exact dimensions could be verified only by mounting the final sphere. It proved that the diameter of the sphere of 840 mm was reproduced with an accuracy of better than 0.1 mm.

The sphere is subdivided into two parts of 17 and 25 modules. This is necessary for access to the sample position in the centre. Each part is fixed by 4 - 6 arms in an oktogonal frame. In principle, these arms can be connected to the sphere in each corner where 3 hexagons or pentagons fit together. This versatile construction allows to remove any desired part of the 4π detector if this is required for special experiments.

The two oktogonal frames are mounted on sledges and can be moved independently in the direction of the beamline. In this way, the position of the detector relative to the neutron target can be changed by 1.3 m. The detector can also be opened for mounting of the samples. The adjustment of the overall support is such that the horizontal axis of the honeycomb sphere deviates by less than 0.2 mm from the beam axis in any possible detector position.

+ Hauptabteilung Ingenieurtechnik, Kernforschungszentrum Karlsruhe

6.1.3 TEST MEASUREMENTS WITH THE FIRST SIX DETECTOR MODULES OF THE 4π BaF_2 DETECTOR

K. Wisshak, K. Guber

The Karlsruhe 4π BaF_2 detector for precise neutron capture cross section measurements consists of 42 detector modules which form a spherical shell of 15 cm thickness around a central sample (see also contribution 6.1.2 of this report). A subassembly of the detector has been mounted and tested. It consists of a central pentagon, surrounded by five hexagons. The energy and time resolution of the individual modules are given in Table 1. This sample of six detectors, yielding an average energy resolution of 10.6 %, is representative for the quality of the crystals delivered up to now. The spectrum of a ^{137}Cs source as obtained from the best module is shown in Fig. 1. The time resolution was measured in a coincidence experiment, using a ^{60}Co source and a Pilot U plastic scintillator as a reference detector. Events due to detector-detector scattering of gamma-rays were minimized by means of a lead collimator. On the average a time resolution of 460 ps was observed using CAMAC controlled constant fraction discriminators.

The time resolution of the whole assembly was determined by combining the CFD signals of the six modules by a fast OR circuit. The delay in the individual branches was adjusted via CAMAC delays to an accuracy of 250 ps. As shown in Fig.2, an overall time resolution of 500 ps was obtained. This result is only slightly worse compared to that obtained with a single detector. The tails of the time peaks on the right hand side (see Fig. 2) are caused by detector-detector scattering.

Finally, the setup was used as an anti-Compton spectrometer. Signals of the central pentagon were registered only if they were not coincident with an event in one of the surrounding modules. The result for the 4.4 MeV gamma-ray line of an ^{241}Am-Be source is shown in Fig. 3. It demonstrates that the Compton background and the single escape peak can be reduced significantly. (A threshold of ∿ 600 keV was placed on the fast component in order to suppress pulses from the α-decay of Ra in the BaF_2 crystals).

Table 1 Energy and time resolution of the first six modules of the 4π BaF_2 detector

detector	energy resolution (662 keV) (%)	time resolution (^{60}Co, 100 keV threshold) (ps)
1	10.6	460
2	9.8	500
3	10.0	480
4	10.7	400
5	12.6	440
6	10.0	480

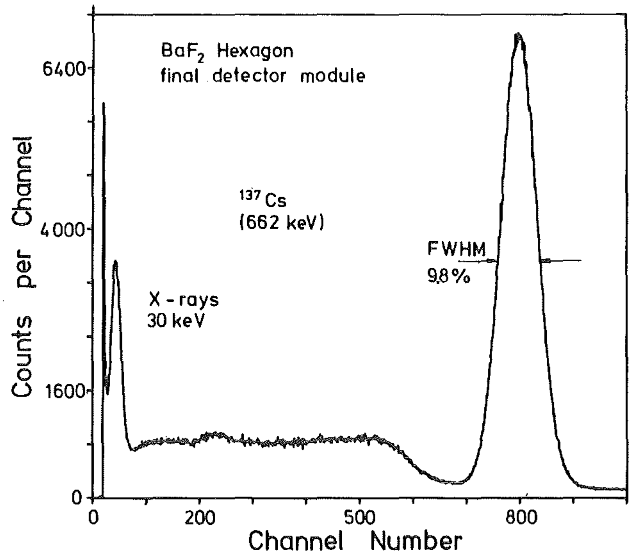

Fig. 1

Optimum energy resolution as measured with one module of the 4π detector

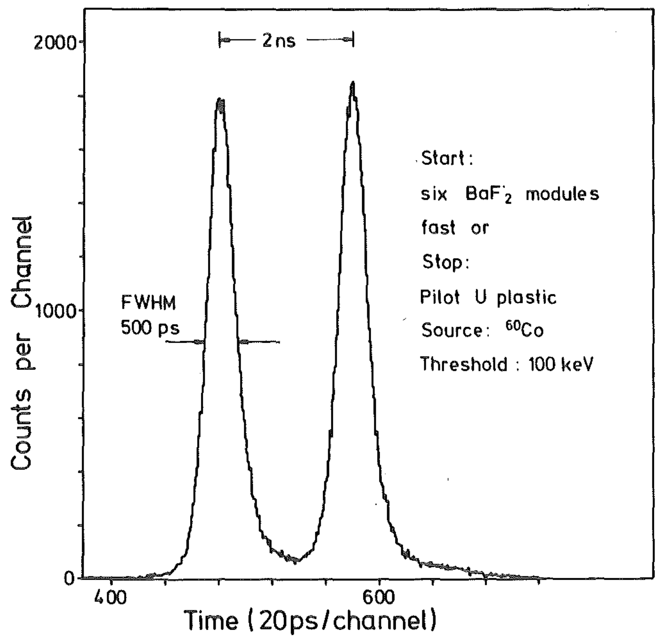

Fig. 2
Time resolution as measured by combining six detector modules with a fast OR circuit

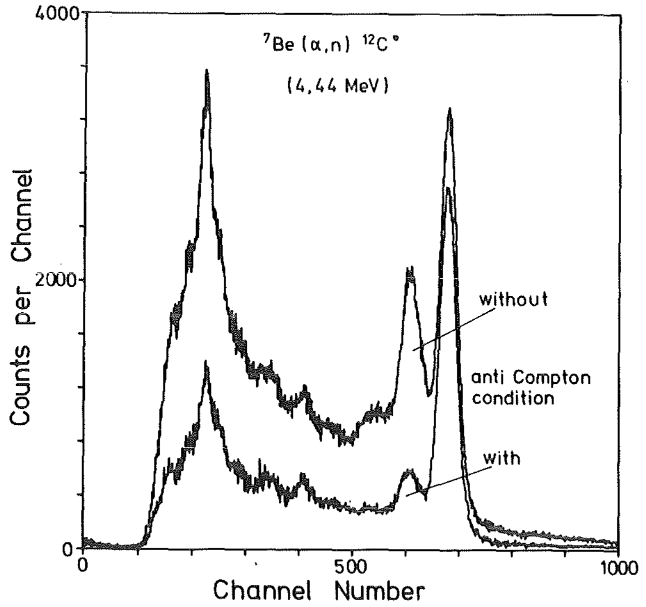

Fig. 3
Spectrum of the 4.4 MeV gamma-ray line from a ^{241}Am-Be source as obtained from the central pentagon with and without anti-Compton condition.

6.1.4 A GAS IONIZATION CHAMBER FOR ON-LINE HEAVY ION IDENTIFICATION

Z. Sosin[+], T. Kozik[+], S. Micek[+], and K. Grotowski

A gas ionization chamber is described for an on-line identification of products from nuclear reactions. The chamber can work with two different anodes: the resistor type or the split one. Response of the device, proved experimentally, enables fast identification of Z values subtending some defined region. Possible modifications of the detector are discussed. The concept of extending the Z value flexibility of the system is proposed.

(1) Nucl. Instr. and Meth. A249 (1986) 344

[+] Institute of Physics, Jagellonian University, Cracow, Poland

6.1.5 A TEN-FOLD COINCIDENCE PULSE GENERATOR FOR THE ELECTRONIC SET-UP OF THE FOCAL PLANE DETECTOR OF THE MAGNETIC SPECTROGRAPH

S. Zagromski, H. Neudold, C. Samanta[+]

The magnetic spectrograph at the Karlsruhe cyclotron is in use for inclusive type measurements of charged particle spectra and in combination with solid state detector telescopes for coincidence measurements. For several reasons it is very useful to install a coincidence pulser in the electronic set up of the system, for

a) deadtime correction of the measurements
b) linearity-tests of the electronic paths
c) off-line adjustment possibilities of the coincidence branches.

A device in NIM-Standard was built up and tested for this purpose.

A particle, passing the magnetic spectrograph is stopped in the focal-plane detector. This detector consists of two position-sensitive-, one energy-loss- and one plastic-scintillator stopping-detector. The position-sensitive-detectors have a charge division readout with one preamplifier on each end of a resistive wire. The energy-loss-detector is an ionisation-chamber with one preamplifier and the scintillator has one photomultiplier with preamplifier on each side. For the readout of one event in the focal-plane detector therefore seven preamplifiers send their signals to the electronic system. In addition to this, the signals of the coincidence-detectors, which are two for one $\Delta E,E$ silicon-detector telescope, arrive on the electronic system and built a complete set of 9 preamplifier-signals. These signals have to be reproduced by the pulser, matching the pulse-form, pulse-height -polarity and -decay of each signal. Fig. 1 shows the block diagram of the pulse generator.

For offline-adjustments of the electronics, specially of the coincidence branches, the preamplifiers receive their signals from the pulse generator instead of the respective detector and all electronic elements may be adjusted before actually starting the measurements with the beam.

A linearity test in each amplifier path for calibration purposes has to be done. Therefore a pulse-height scanner is included. It generates 8 different calibrated pulse heights being adjusted over the full range of each branch.

Due to a high number of pulses of inclusive events in each detector branch and a low number of coincidence events, a deadtime in the electronic system appears. This may be corrected by dividing the integral of a pulser peak in a coincidence-spectrum by the number of "Counter out" signals of the pulser. The frequency-divides fits for this purpose the number of pulser signals with the number of coincidence events.

[+] Permanent address: Saha Institute of Nuclear Physics, Calcutta (India)

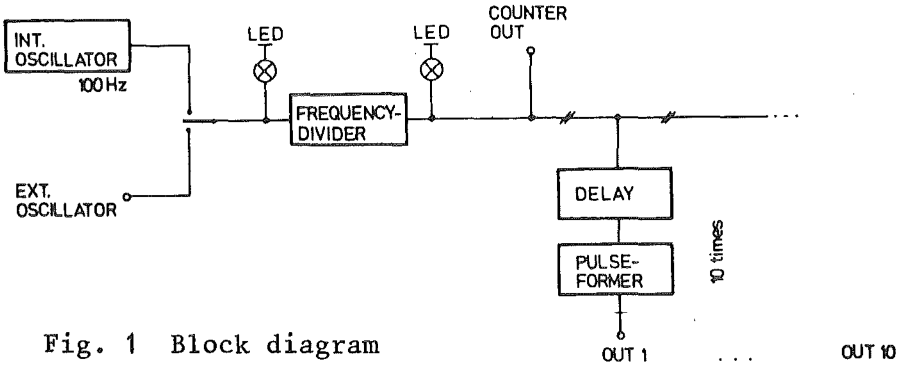

Fig. 1 Block diagram

6.1.6 A LIQUID ARGON TIME PROJECTION CHAMBER

G.Giorginis, D.Mann, H.Gemmeke, R.Maschuw, B.Zeitnitz

A precise measurement of the differential cross section of neutrino electron scattering at low energies can provide information about the nature of the weak interaction and the elctromagnetic form factors of the neutrino. Such an experiment requires a large calorimeter with excellent energy as well as good spatial resolution. As a suitable detector a 50 t liquid time projection chamber (LTPC) is currently discussed in the KARMEN* collaboration.

Long distance drift of electrons has been studied in a 20 l LAr ionization chamber described in the annual reports 1982 - 1985. Drift distances up to 10 cm and attenuation lengths up to 100 cm have been achieved. The above test detector has been rebuilt to operate as LTPC. It is an ionization chamber with subdivided anode surface providing X-Y spatial information; the Z coordinate results from drift time and drift velocity. Particle track reconstruction is straightforward; the particle energy is deduced from the sum of signal amplitudes of anode subdivisions.

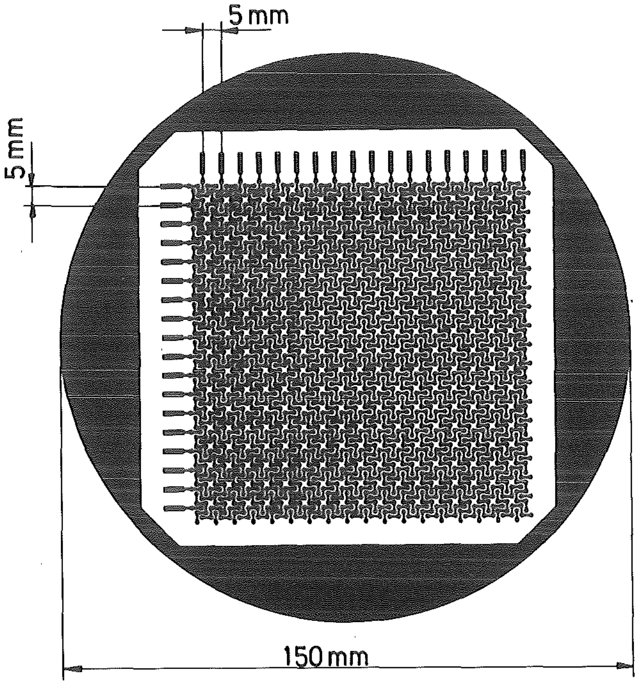

Fig.1: Segmented anode of the LAr-TPC.

The segmented anode shown in fig.1 as adopted from ref.1, consists of orthogonal X-Y copper strips on a fiber glass plate. At the crossing points the strips are connected on the back side of the anode. The zig-zag shape of the strips ensures an almost uniform sampling of the collected charge in X and Y direction. Each X and Y strip as well as the cathode has an analog read out via a charge sensitive amplifier. The analog signals are digitized as function of time, thus providing amplitude and time information simultaneously. Apart from the drift time the knowledge of the drift velocity in the actual LAr filling is very important for track reconstruction. Therefore ionization electrons starting from a ^{207}Bi source on the cathode are drifted over a well known distance.

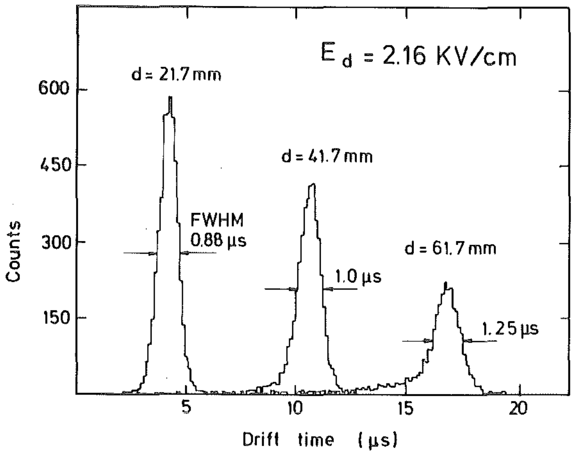

Fig.2: Drift time distributions of ionization electrons from a ^{207}Bi source for three drift distances at constant drift field in LAr.

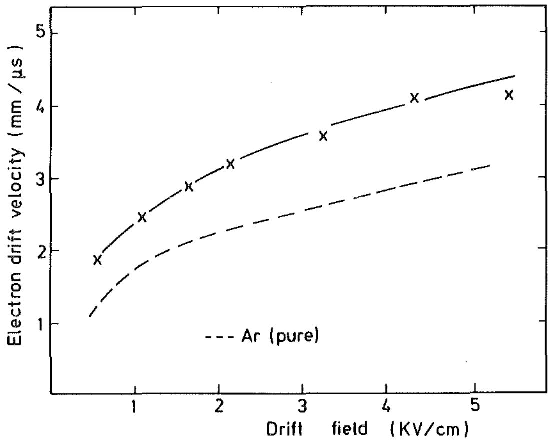

Fig.3: Electron drift velocity in LAr as function of drift field.

The drift time is derived from the time difference between cathode and anode signal. Time spectra for three drift distances in a constant drift field are demonstrated in fig.2. A spatial resolution σ = 1.6 mm for a drift distance d = 62 mm and a drift field ε_d = 2.16 kV/cm has been deduced. The drift velocity calculated from drift distance and drift time is shown in fig.3 as a function of the drift field. Our higher values compared to those for pure argon from ref.2 may be due to hydrocarbon impurities from the vacuum pump.

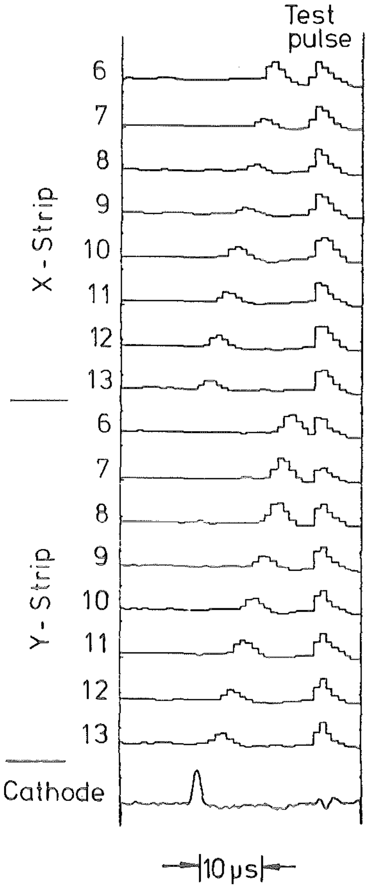

Cosmic rays penetrating the LAr-TPC were used to test its track recognition capability. The TPC was operated in a self triggered mode. Straight tracks were clearly identified by their measured X-Z and Y-Z projections as shown in fig.4. The next step would be to improve the electronics to achieve high energy resolution.

Fig.4: Digitized signals as function of time induced on the anode strips and on the cathode by a cosmic particle.

(1) H.J.Mahler, P.J.Doe, H.H.Chen, IEEE Trans. Nucl.Sci., NS-30 (1983) 87

(2) E.Shibamura, A.Hitachi, T.Doke, T.Takahashi, S.Kubota and M.Miyajima, Nucl.Instr.Meth., 131 (1975) 249

6.1.7 STUDY OF n-γ PULSE-SHAPE-DISCRIMINATION (PSD) WITH A LARGE NaI(Tl)-CRYSTAL

P.Doll, G.Fink, R.W.Finlay*, M.Haupenthal, B.Kasten**, F.Smend**, G.Wicke**

Neutron capture reactions bear great problems because the cross section of capture reactions are much smaller than neutron scattering (1.3.4). To separate neutrons and gammas we used a pulse-shape-discrimination (PSD) method, which is discussed in detail elsewhere (1,2,3). In an experimental setup at POLKA we used a 16 x 16 x 24 cm^3 NaI(Tl) crystal with active and passive shielding. The passive shield consisted of 10 cm Pb and 20 cm boron loaded polyethylene. A carbon sample was set in the continuous energy ($E_n \leq$ 50 MeV) neutron beam. With this type of shielding, about 50% of the count rate comes from the sample and $\simeq$ 50% is background. Therefore, in further experiments, the shielding has to be improved.

Fig.1 shows a pulse-shape versus pulse-height-spectrum. Clearly a separation is seen between γ-ray events and neutron-induced reactions in the NaI detector. The peak at ~ 15 MeV, which is very dominant, results mainly from the reaction $^{12}C(n,n'\gamma)^{12}C$. Even in this first test the neutrons and γ's can be separated better than discussed in literature (4)

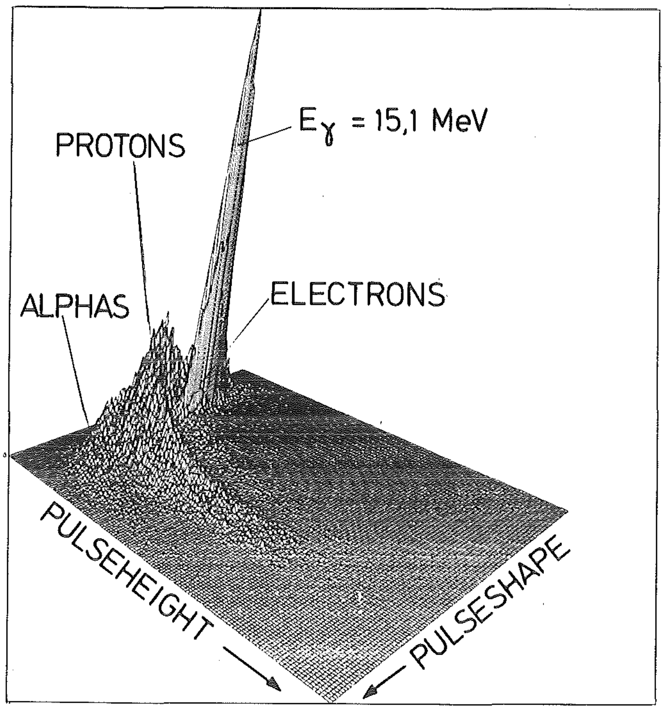

Fig.1: Two dimensional representation of pulse-shape versus pulse-height in a large NaI crystal. The pulse-shape exhibits electrons from photon interactions in the crystal and protons, deuterons and alphas from neutron interactions in the crystal.

(1) R.Bass et al., Nucl.Instr. and Meth. 30 (1964) 237

(2) C.M.Bartle, Nucl.Instr. and Meth. 124 (1975) 547

(3) D.M.Whittal, C.M.Bartle, Nucl.Instr. and Meth. in Phys. Research A247 (1986) 390

(4) G.H.Shave et al., Nucl.Instr. and Meth. 148 (1978) 531

* Ohio State University, Athens, USA

** University of Göttingen, W.-Germany

6.1.8 DETECTOR DEVELOPMENTS FOR NEUTRON FLUX MEASUREMENTS

V.Eberhard, R.W.Finlay*. W.Heeringa, H.O.Klages, Chr.Wölfl

The measurement of the spin-spin cross section of nuclei for neutrons requires the determination of the flux ratio for neutrons with spin up and spin down with very high precision. Scintillators placed directly in the beam have an increasing effeciency towards low-energy neutrons. At the neutron facility POLKA this is a disadvantage, because the useful energy spectrum between 16 and 50 MeV is contaminated with lower energy neutrons. Moreover, the steep increase in count rate towards small energy signals makes the detectors very sensitive to drifts in electronic thresholds or gains.

A stable flux monitor which we routinely employ consists of a PE (polyethylene) foil placed in the beam combined with pairs of ΔE-E detectors positioned at small angles, which detect recoil protons from the PE converter. The ΔE-E coincidence suppresses the smallest signals, thus removing the sensitivity for electronic drifts. The drawback of this system is its rather small count rate, which is insufficient for spin-spin cross section measurements.

We now have constructed two other detector types which are a compromise between the concepts mentioned above. Their properties are being investigated at present.

1. Converter-absorber-ΔE array. It consists of a 15-20 mm PE converter followed by a 0.5 mm Al absorber and a 0.5-1.0 mm NE102A scintillator (fig.1a). Low energy protons generated in the PE are stopped within the PE itself or in the Al absorber giving rise to a largely decreased efficiency for lower energy neutrons.

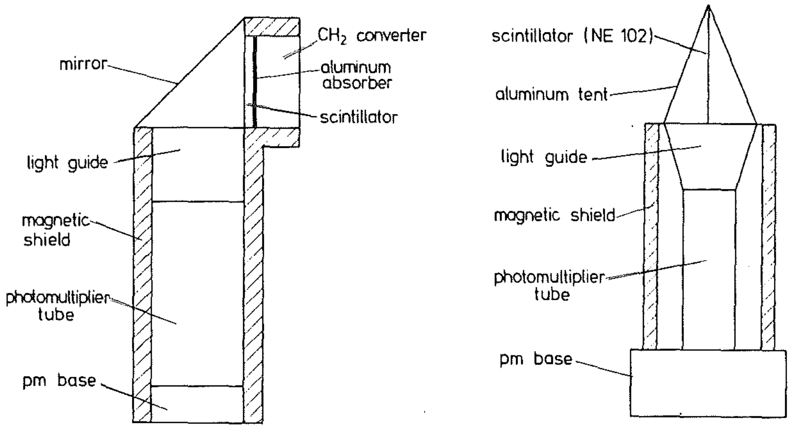
CH_2 converter
aluminum absorber
scintillator
mirror
light guide
magnetic shield
photomultiplier tube
pm base
scintillator (NE 102)
aluminum tent
light guide
magnetic shield
photomultiplier tube
pm base

Fig.1: Converter-absorber-ΔE detector (left), ΔE detector from the converter-ΔE-ΔE array (right).

2. Converter-ΔE-ΔE array. It consists of a 15-20 mm thick PE converter followed by two ΔE detectors separated by a diaphragm to reduce edge effects. The construction of the ΔE-detectors (0.5-1.0 mm NE102A) is shown in fig.1b. The coincidence requirement between the ΔE's yields a very good reduction of background and of small energy signals. The thick PE converter again increases the efficiency for high energy neutrons.

* Ohio State University, Athens, USA

6.1.9 PRECISE THRESHOLD DETERMINATIONS FOR ABSOLUTE NEUTRON COUNTING

S. Cierjacks, B. Rzehorz, H. Ullrich, H.-J. Weyer+

In recent pion absorption studies at SIN a large NE 102A plastic scintillation counter$^{1)}$ has been used for charged particle and neutron detection in the energy range from 10 to 300 MeV. Its use for absolute neutron counting depends strongly on the accurate knowledge of the neutron detection efficiency as a function of the incident energy. This quantity can be calculated with good accuracy with modern Monte-Carlo codes (e.g. Ref. 2), provided the effective threshold applied in the measurements is well known. The strong dependence of the detection efficiency on the threshold is illustrated in Fig. 1 which shows the calculated results for our counter at three different thresholds of 3,5 and 10 MeV electron-equivalent energies (MeV$_{ee}$).

A determination of low thresholds (below 1 MeV) can easily be accomplished with standard γ-sources by observation of Compton edges for a few γ-lines. Similar measurements at higher thresholds are, however, more complicated, since suitable pure γ-sources providing γ-rays in the several MeV range are lacking. In this range Am-Be and Pu-^{13}C sources providing γ-rays of 4.43 and 6.13 MeV, respectively, can in principle, be used. But without n-γ pulse-shape discrimination (which is not possible with NE 102A scintillators) the observation of the corresponding Compton edges is obscured by superposition of an intense high-energy neutron background spectrum. This difficulty was circumvented by measuring pulse-height spectra with and without 5 cm lead around the sources. The difference spectra from both measurements allowed largely to subtract the contributions from high-energy neutrons, and thus to separate pulse-height distributions for high-energy γ-rays. A typical difference spectrum is shown in Fig. 2a which displays the results for the Am-Be source. The Compton edge at 4.16 MeV is clearly visible.

The determination of effective thresholds for our counter was performed by using γ-rays from ^{88}V (1.85 MeV), Am-Be (4.43 MeV) and Pu-^{13}C (6.13 MeV) sources together with cosmic-ray muons (providing a peak at 21.4 MeV$_{ee}$). A typical calibration of pulse-heights in electron-equivalent energies is shown in Fig. 2b. From the linear dependence of pulse-height versus energy effective experimental thresholds around 5 MeV$_{ee}$ were determined with an accuracy of $\leq$ 3%. This proved that the counter can be used for absolute neutron counting at an accuracy level of ~ 10%.

(1) S. Cierjacks et al., Nucl. Instrum. Meth. A238(1985)354
(2) S. Cierjacks et al., Nucl. Instrum. Meth. 192(1982)407

+ Institute for Physics, University of Basel, Basel, Switzerland

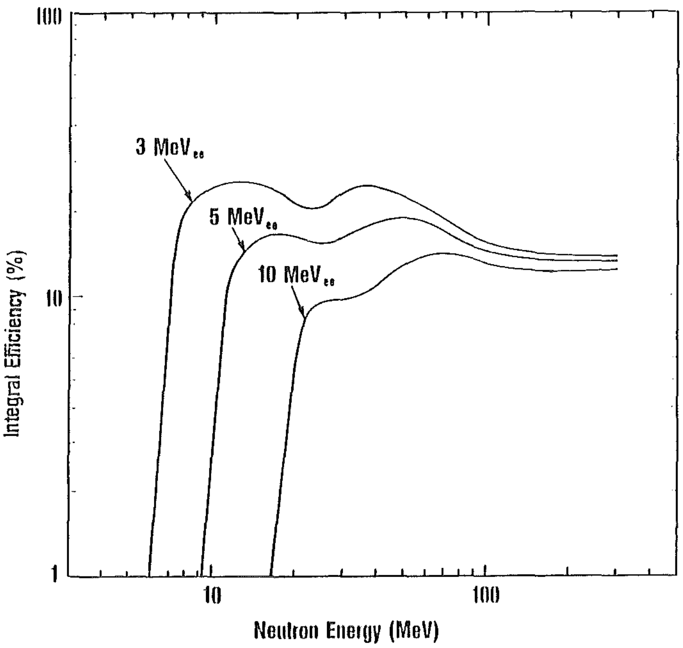

Fig. 1 Neutron detection efficiencies calculated with the KfK Monte-Carlo code$^{2)}$ for three different counter thresholds. It can be seen that neutron detection efficiencies, especially below ~ 50 MeV, change drastically with threshold.

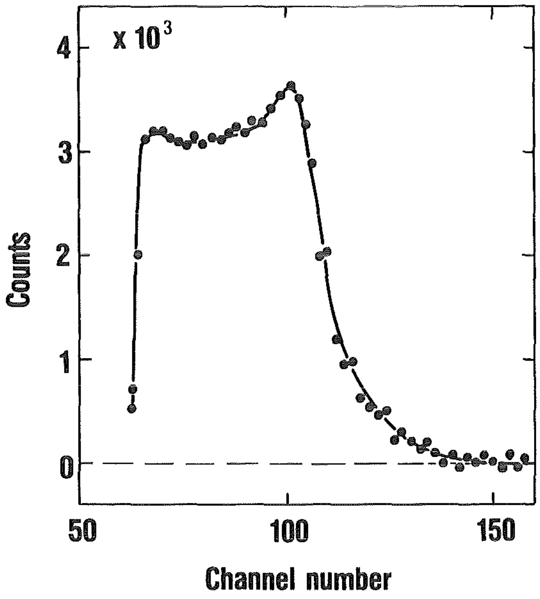

Fig. 2 a) Typical difference spectrum for a Am-Be source with and without 5 cm of lead shielding. By elimination of neutron background the Compton edge of the 4.43 MeV γ-rays is clearly visible.

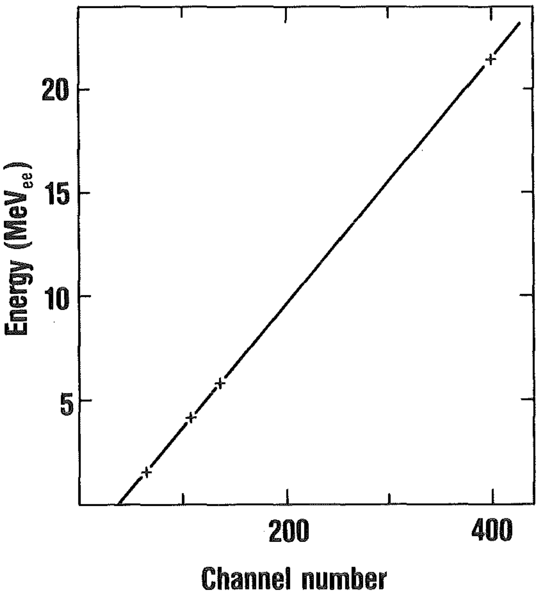

Fig. 2 b) Energy calibration of a typical counter for employing ^{88}Y , Am-Be and Pu-^{13}C γ-sources and Cosmic-ray muons. From these calibration effective thresholds in the MeV range have been determined with a total uncertainty of $\leq$ 3%.

6.2 INSTRUMENTATION

6.2.1 A DEVICE PRODUCING AN ULTRAPURE STOPPED MUON BEAM OF HIGH INTENSITY

L.M. Simons[+]

Modern experiments aiming to measure or to put at least upper limits for rare muon decay or reaction experiments require beams with a high flux, high stopping density and a low pion contamination. A low momentum muon beam with an intensity higher than 10^8 μ^-/s and a pion contamination of less than 10^{-9} pions/muon is necessary for the next generation of experiments.

A new approach to achieve this is shown in Fig. 1. The apparatus consists of a split-coil magnet (injection magnet) (I), a decay solenoid (II), two purification solenoids (IIA, IIB), a free space for an experiment (III) and two mirror magnets (IVA, IVB). The whole system is in a vacuum. Pions of momentum (85 ± 4.5) MeV/c are injected perpendicular to the rotational axis of the system in region I at a distance of 120 mm from the axis. Two moderators provide an efficient injection. Radial and axial betatron oscillations are excited in order to avoid hitting the moderators again.

The length of the decay region II is sufficient to let more than 90% of the pions decay. The basic idea for the device is that by decay the phase space of the muons is separated from the one of the pions. Whereas muons produced from pion decay inside a certain radial region can move freely forth and back between the two mirrors, the pions have to come back to the radial and azimuthal coordinates where they originated. Thus a cylindrical collimator with decreasing radius inside the purification solenoids IIA, IIB is sufficient to eliminate the pions. More than three scatter processes are needed for them to reach the experimental zone which results in the required suppression factor.

With a target diameter of 140 mm and a diameter of the collimator of 200 mm about one muon per four pions can be stopped in the target in the center of region III.

The momentum spectrum of the muons ranges from 10 to 60 MeV/c. With the possibility of multiple traversals through the target the thickness of the target can well be less than 200 mg/cm^2.

For the planned high proton current at SIN of 1mA a muon flux of more than 10^8 particles can be stopped then.

[+] Now at Schweizerisches Institut für Nuklearforschung, CH 5234 Villigen

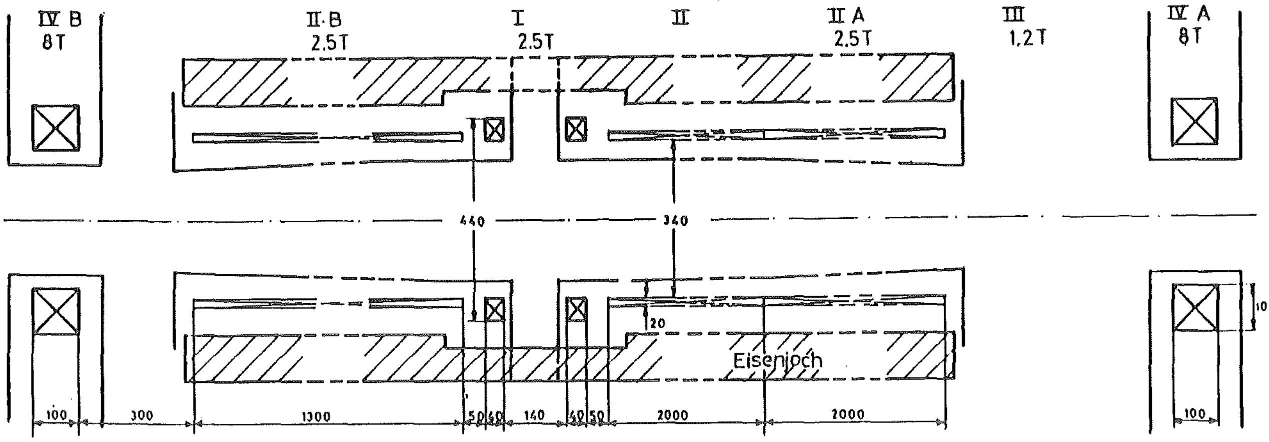

Fig. 1 Approach to a new low momentum muon beam

6.2.2 COMMISSIONING OF THE LOW ENERGY PION SPECTROMETER (LEPS) AT SIN

B. Barnett[+], H. Clement[+], K. Göring, W. Gyles, A. Höhne, J. Jaki,
K. Kärcher, W. Kluge, S. Krell[+], H. Matthäy, M. Metzler, D. Renker[+++],
R. Tacik, G. Wagner[+], Ch. Wiedner[++], U. Wiedner

During the last year the Low Energy Pion Spectrometer has been commissioned at the πE3 channel of SIN, which now can be operated in a dispersed mode appropriate for LEPS. The detector system, i.e. the multiwire proportional chamber at the intermediate focus, the vertical drift chamber and the scintillation trigger counters in the focal plane of the split pole have been finally assembled[1,2,3]. A photograph of LEPS is shown in Fig. 1. In the foreground at the left side the scattering chamber can be seen, followed by the quadrupole triplet, the intermediate focus detector (not visible), the split pole magnet and the vertical drift chamber up in the focal plane.

The results, although some components of the entire set-up are not yet optimised (in particular the final beam tuning is still ahead), are already very satisfying. All essential optical parameters of the beam, determined so far, agree well with the design specifications: Beam spot size 10×6 cm^2, dispersion $D = 5$ cm/%, angular divergences $|\theta| \leq 40$ mr, $|\varphi| \leq 25$ mr. Further tests covered a broad range of measurements in order to determine the imaging characteristics of the quadrupole triplet, the phase space acceptance of LEPS and the momentum resolution of the whole system.

As an example Fig. 2 demonstrates the imaging performance of the quadrupole triplet. It shows reconstructed images of a scintillation counter, which has been designed as a ladder with 5 mm steps, 15 mm apart and mounted at the scattering target position. They have been obtained by tracing back the tra-

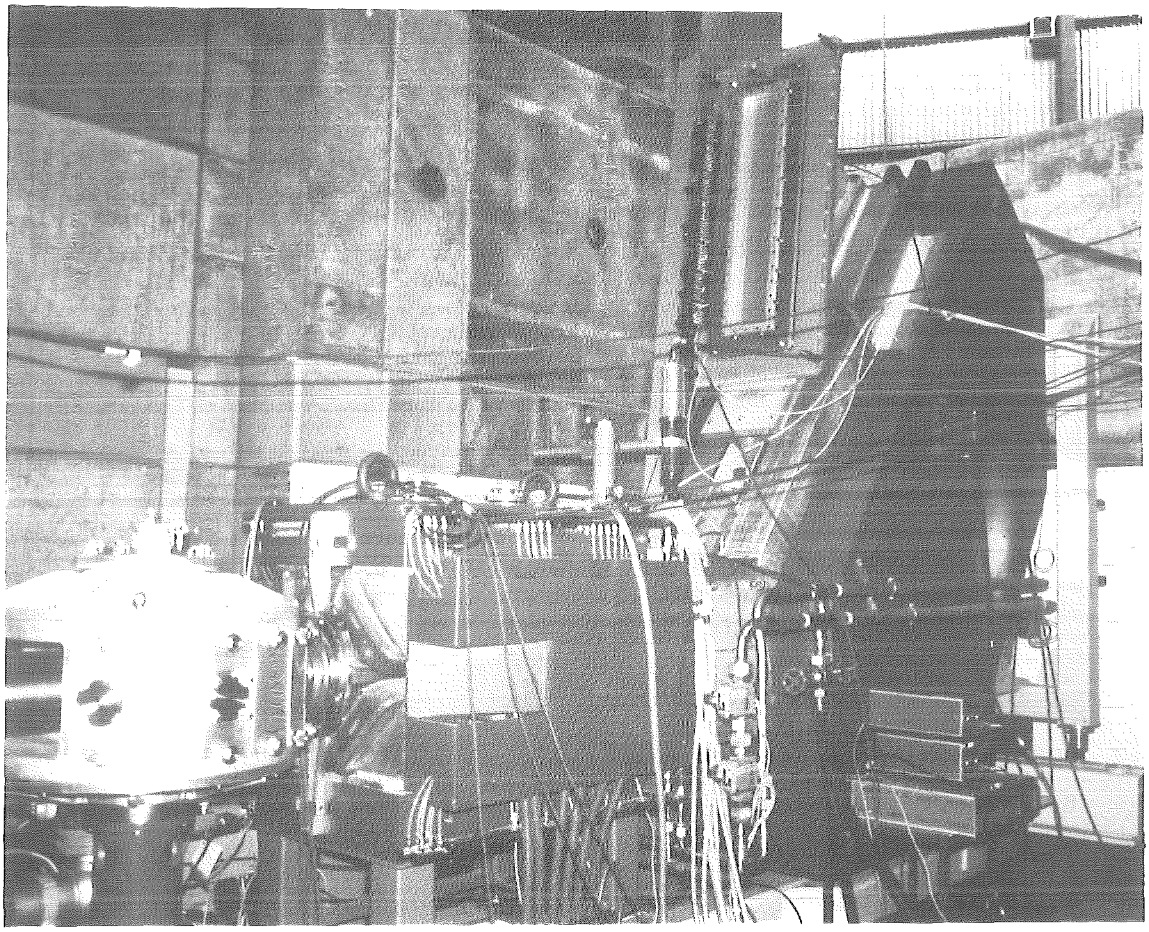

Fig. 1 LEPS: In the foreground at the left side the scattering chamber can be seen, followed by the quadrupole triplet, the intermediate focus detector (not visible), the split pole magnet and the vertical drift chamber up in the focal plane.

jectories from the intermediate focus detector to the target position. According to the symmetric lay-out of the quadrupole triplet the ratio of image to object size is: 1:1. Fig. 2a shows the image for the direct pion beam of 150 MeV/c. Due to the limited angular divergences of the beam no corrections for optical aberrations had to be applied. The result is a practically perfect image caused by the good spatial and angular resolution of the intermediate focus detector. Fig. 2b shows the same image for pions of 156.3 MeV/c, scattered on the scintillator target at 50°, again without any soft ware corrections. The accepted phase space is huge in that case: $|\theta| \leq 200$ mr, $|y| \leq 3.5$ cm, $|\varphi| \leq 70$ mr and causes the reduced spatial resolution of the image as a result of aberrations. After their correction up to the 3rd order the good spatial resolution is fully restored (Fig. 2c). Fig. 3 depicts our first momentum spectrum taken with LEPS. It has been obtained by the scattering of 156.3 MeV/c (70 MeV) π^- on the scintillator target at 50°. The large peak represents the elastic scattering on ^{12}C and the smaller peak (better visible in the insert of Fig. 3) the inelastic scattering to the first excited state of ^{12}C at 4.43 MeV. The momentum resolution

Imaging with the quadrupole triplet:

a) restricted phase space (unscattered pion beam) uncorrected for aberrations

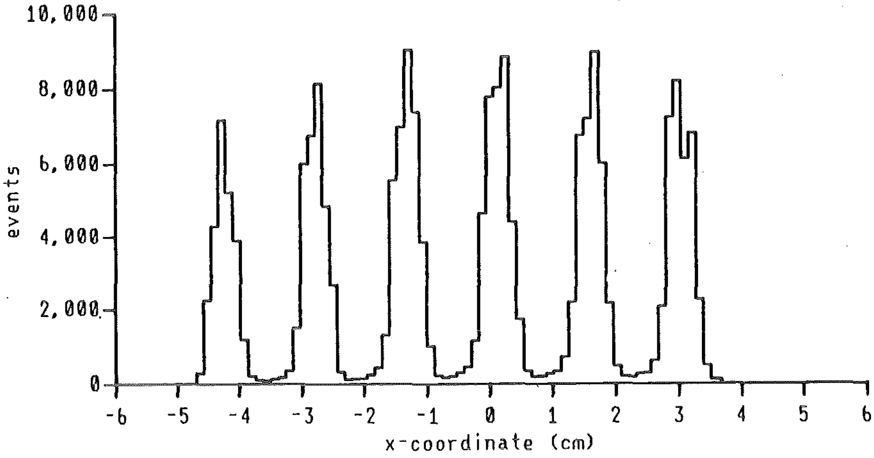

b) unrestricted phase space (scattered pion beam) uncorrected for aberrations

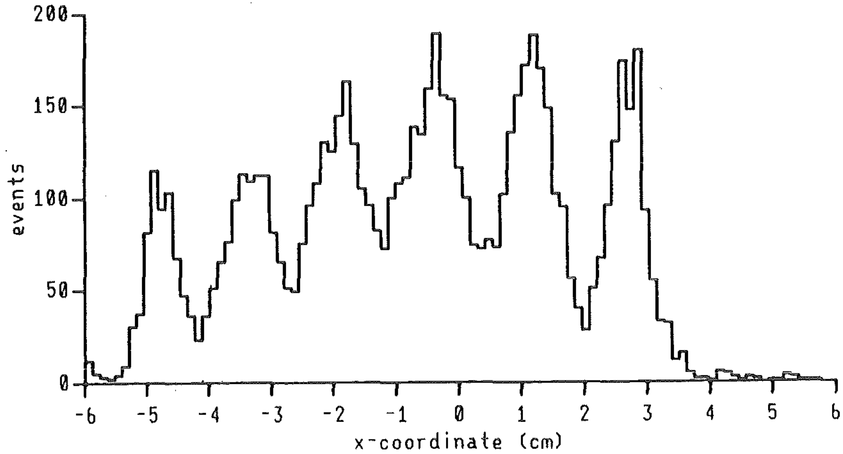

c) unrestricted phase space (scattered pion beam) corrected to third order aberrations

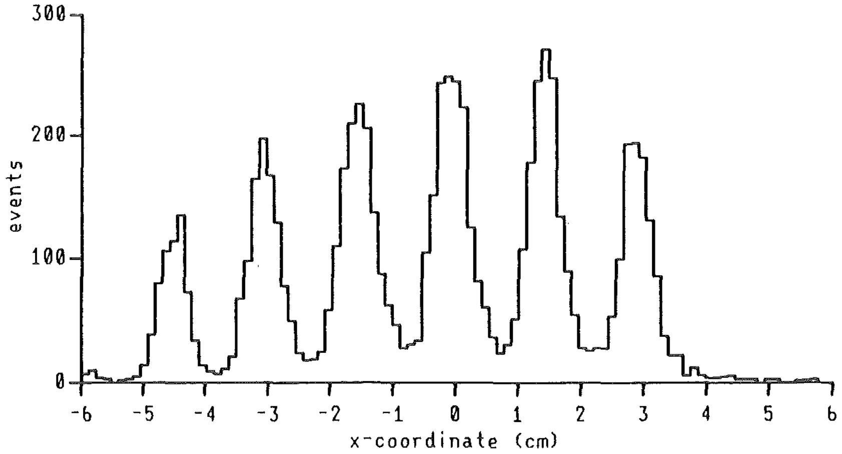

Fig. 2 Imaging of the quadrupole triplet: The image of a scintillation counter, which has been built as a ladder with 5 mm steps, 15 mm apart and mounted in the centre of the scattering chamber has been detected at the intermediate focus and traced back to the scattering target position by calculation.

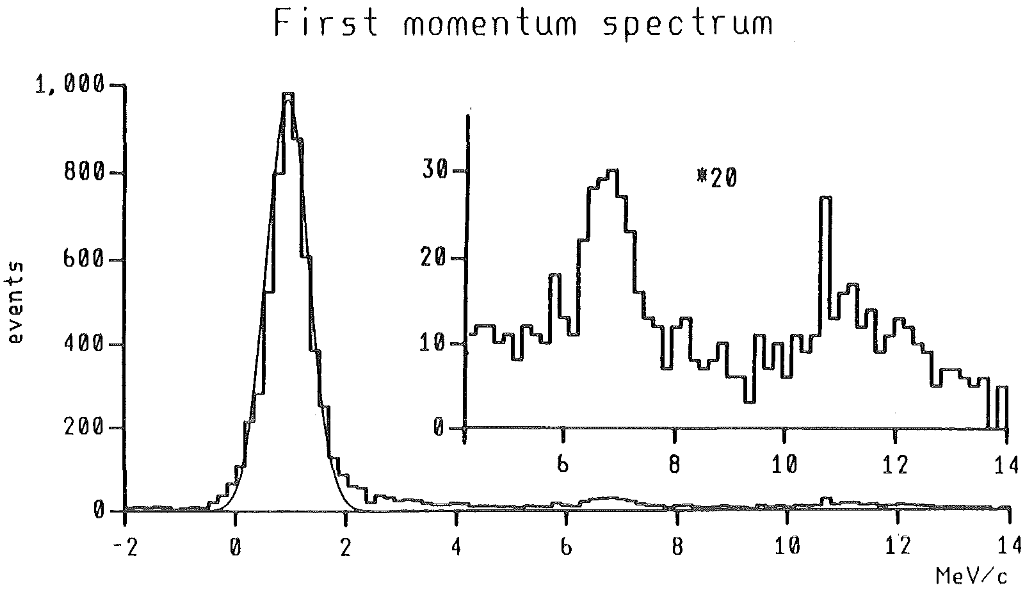

Fig. 3 Momentum resolution of LEPS: momentum spectrum obtained by the scattering of 70 MeV π^- on a scintillator target at 50°. The momentum resolution of both beam and LEPS is 0.4% after correcting aberrations up to the 3rd order. The result has been obtained without any optimisation of the beam resolution and without minimisation of scattering material. The left peak represents the elastic scattering on ^{12}C while the smaller peaks (better visible in the insert) arise from inelastic scattering to the first excited state at 4.43 MeV of ^{12}C and from elastic scattering on hydrogen.

0.4% competes favourably with the low energy pion spectrometers at LAMPF and TRIUMF. The resolution has been achieved after correcting for aberrations up to the 3rd order, but must still be regarded as preliminary, because no final optimisation of the beam resolution has been carried out, and further reduction of scattering material within LEPS is possible. The hope to achieve a final momentum resolution of 0.2% seems realistic after this "first shot" if further optimisation measures will have been taken.

(1) Annual Report on Nuclear Physics Activities 1982/83, p. 208, P. 210, 1983/84, p. 164, 1984/85, p. 181
(2) SIN Jahresbericht 1984, p. JB 25
(3) J. Jaki, Diploma Thesis, Karlsruhe 1983
M. Metzler, KfK-Report 4010B(1986), Diploma Thesis, Karlsruhe 1986
K. Göring, Diploma Thesis, Karlsruhe 1986

+ Physikalisches Institut, Universität Tübingen, Auf der Morgenstelle 12, 7400 Tübingen
++ Max Planck-Institut für Kernphysik, Saupfercheckweg, 6900 Heidelberg
+++ SIN, CH-5234 Villigen

6.2.3 AN INEXPENSIVE TEMPERATURE-COMPENSATED HALL-PROBE DEVICE FOR MONITORING THE MAGNETIC FIELD OF THE SPECTROGRAPH "LITTLE JOHN"

M. Neudold, H.J. Gils

The magnetic field of the dipole magnet of the spectrograph "Little John" should be measured and monitored with an accuracy of about 2×10^{-4} for calibration purposes and stability control. A nuclear magnetic resonance (NMR) probe was not taken into consideration because of its costs and of the problems in operating such a system in HF stray-fields existing in the cyclotron laboratory.

Based on the experiencies made with a less precise prototype assembly a Hall-probe magnetic field monitor device was developed which is characterized by the following features.

- Hall-probe with small temperature effects (Siemens, FC 34)
- temperature stabilization of the Hall-probe by a Peltier-element
- selected, temperature insensitive electronical components
- NIM - modul

The non-linearity of the Hall-voltage and of the ADC with respect to the magnetic field is measured with an NMR-field measuring device (accuracy 2×10^{-7}). The measured curve is programmed into an EPROM memory, which linearizes it by software. The linearized ("true") value of the measured magnetic field strength is displayed digitally in the control room of the spectrograph and also transmitted to the data-acquisition system, where it may be written on magnetic tape according to the requirements of the experimenter.

6.2.4 A LOW TEMPERATURE ^{3}He GAS TARGET SYSTEM

A.Vollmer, P.Doll, W.Heeringa, P.Jany, H.O.Klages, H.Skacel

For the study of neutron-induced reactions on ^{3}He a gas target system has been developed for use in an evacuated scattering chamber. The design was made to combine high target thickness, small dimensions and thin foils to avoid excessive energy loss for the charged reaction products. Therefore, a cryogenic target system was chosen. The systems consists of three parts: the target, the cooling system, and the gas supply system.

The features of the target chamber are shown in fig.1. The neutron beam ($\varnothing_n \simeq 20$ mm) enters through a 40 mm Ø stainless steel foil (25 µm thick). The exit window for the neutrons and for the charged reaction products is made out of 12 µm thick HAVAR foil. It is glued by epoxy to the stainless steel target body whereas the entrance window is welded to a flange which is sealed to the body by an indium sealing. On top of the chamber there is the connection to the cooling device, a temperature sensor, and the ^{3}He gas tube.

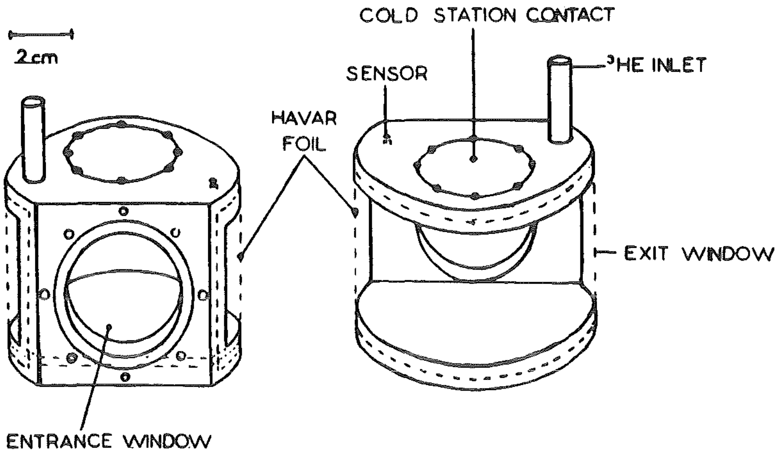
2cm
COLD STATION CONTACT
SENSOR
³HE INLET
HAVAR FOIL
EXIT WINDOW
ENTRANCE WINDOW

Fig.1: ^{3}He gas target chamber

Fig.2 shows a schematic view of the complete system. The ^{3}He gas is contained in a storage tank at low pressure: 0.5 - 1.0 bar. The connection to the filling system is made through a cold trap filled with Zeolith to absorbe air and water at liquid nitrogene temperature. A small "cold buffer" of about 1 l volume is used as an intermediate stage. It is surrounded by liquid ^{4}He to make the ^{3}He gas flow from the storage tank to the buffer. After closing the valve 1 the buffer is warmed up and the target can be filled to higher pressure, if necessary.

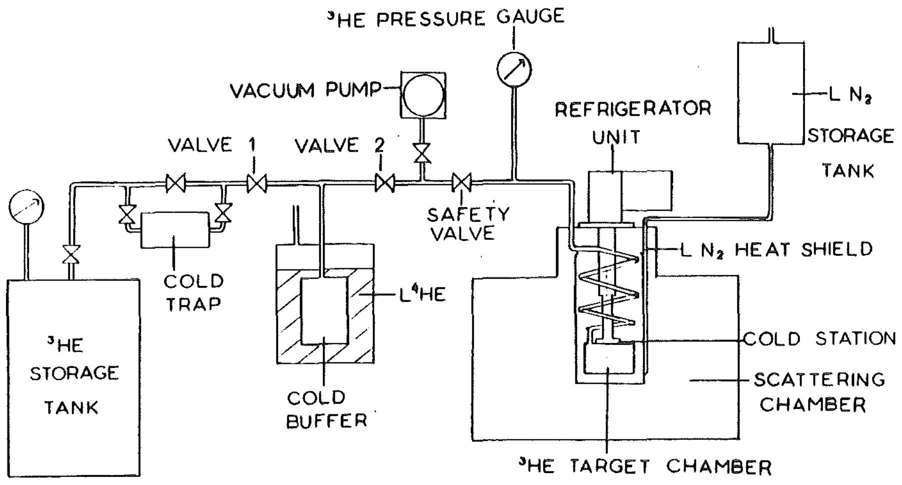
³HE PRESSURE GAUGE
VACUUM PUMP
VALVE 1
VALVE 2
REFRIGERATOR UNIT
L N₂
STORAGE TANK
SAFETY VALVE
L N₂ HEAT SHIELD
COLD TRAP
L⁴HE
³HE STORAGE TANK
COLD STATION
SCATTERING CHAMBER
COLD BUFFER
³HE TARGET CHAMBER

Fig.2: Schematic view of the ^{3}He gas target system

The refrigerator unit used is a ^{4}He expansion cooler CTI 21 (Cryophysics) with a nominal cooling power of 2 Watts at 20 Kelvin. It is connected to the target chamber by a 25 cm long copper tube. The temperature of the gas target is measured by a silicon sensor. To avoid excessive heat load from the walls of the scattering chamber, the gas target is surrounded by a heat shield on liquid nitrogen temperature.

In a first experiment, the target system was used succesfully for three weeks at 18 K and 3 bar.

6.2.5 A NEW CAMAC SYSTEM FOR HIGH RATE,LOW DEAD TIME MULTI-PARAMETER DATA ACQUISITION

T.D.Ford, H.O.Klages, P.Plischke

Data collection rates for multi parameter experiments through CAMAC interfaced with an LSI 11-73 have been limited to a few hundred Hertz. This has prompted the seeking of faster ADCs, CAMAC based memory modules and the necessary software. A complete system for multi parameter (list mode) experiments capable of very high data throughput rates has been purchased from LeCroy. Software is currently being developed for this system to allow one to eight model 3512 ADCs to be connected to two model MM8201A CAMAC list mode memories through one model 3587 data router. The units are all contained in a single standard CAMAC crate.

The ADCs were selected for the relatively fast conversion time, which is fixed at 5 μsec for all conversion lengths up to 8192 channels. The system as a whole was chosen for its versatility. Many other possibilities besides pure list mode experiments are available. Further technical details are easily obtainable from LeCroy and so will not be presented here.

Software is being developed for a LSI 11-73 operating under a RT-11 single user system. The software is intended to be "user friendly" in that changes in the acquisition parameters are easily accomplished through an input data file. No changes to the program code are necessary. Also, all user interactive routines are written in FORTRAN, providing for easier changes of the code and better transportability between computers. If necessary one could create a much more streamlined code for specific very high rate applications. It is hoped to attain completely dead time free count rates of 1 to 3 KHz. For even higher rates, 10 to 30 KHz, the sampling of only a fraction of the incoming data for display and on-line analysis purposes is possible.

The CAMAC system operates, once enabled, independently of the CAMAC dataway. ADC signals are transferred, in order, by the router into the list mode memories. Only when a memory becomes full, a LAM is generated and the dataway taken for data transfer to LSI memory. The second list mode memory is enabled as soon as the first is full, so no dead time results due to memory read-out. Since the list mode memory changing is handled within the LeCroy system, with each address simply overwritten, the limitation is imposed that the LSI finish the read-out and re-enable the memory before the router tries to access it again.

In a first application, four-dimensional list mode aquisition has been performed with data transfer to magnetic tape and full on-line evaluation of the data to 9 spectra. For count rates of ~ 1 KHz no additional dead time from the data aquisition system was observed.

6.3 ACCELERATORS

6.3.1 OPERATION OF THE ISOCHRONOUS CYCLOTRON (KIZ)

F.Schulz, H. Schweickert

During the period of the report the machine was in full operation (see Tables I, II). The use of the axial injection system has now reached about 60 % of the total beam time. Two thirds of this time is used with polarized deuterons and one third with ^{6}Li^{3+} ions at 156 MeV.

In a shut-down period of 3 weeks in January after the Christmas vacations, a large number of maintenance and measurement activities were carried out:

- installation of a new control-console for the improved computer control of KIZ,

- installation of a new extraction element whereby the thin graphite septum foil can now be easily exchanged and where also the cooling has been improved, allowing the extraction of higher currents, especially for the dual beam facility,

- replacement of the 15 year old vacuum system of the cyclotron. The new system (Fig. 1) consisting of two large 12,000 l/s diffusion pumps with an additional diffusion pump in the foreline, is especially designed for low oil backstreaming. The system is completely automatic and reaches a final pressure of 2 x 10^{-6} mbar in the cyclotron. The reduced oil backstreaming compared to the old system has resulted immediately in a smoother operation of the rf-system,

- installation of an improved Penning ion source (Fig. 2), which delivers much higher currents especially for α-particles (> 80 μA accelerated). The success of this source arises from a very small inner diameter of the chimney and a reflector at the same potential as the heated cathode. The lifetime for high current α-particle operation is now more than 2-3 weeks, whereas the lifetime for high-current p,d-particles is now more than 3-4 months.

Statistics of the cylotron from July 85 to June 86

Table I

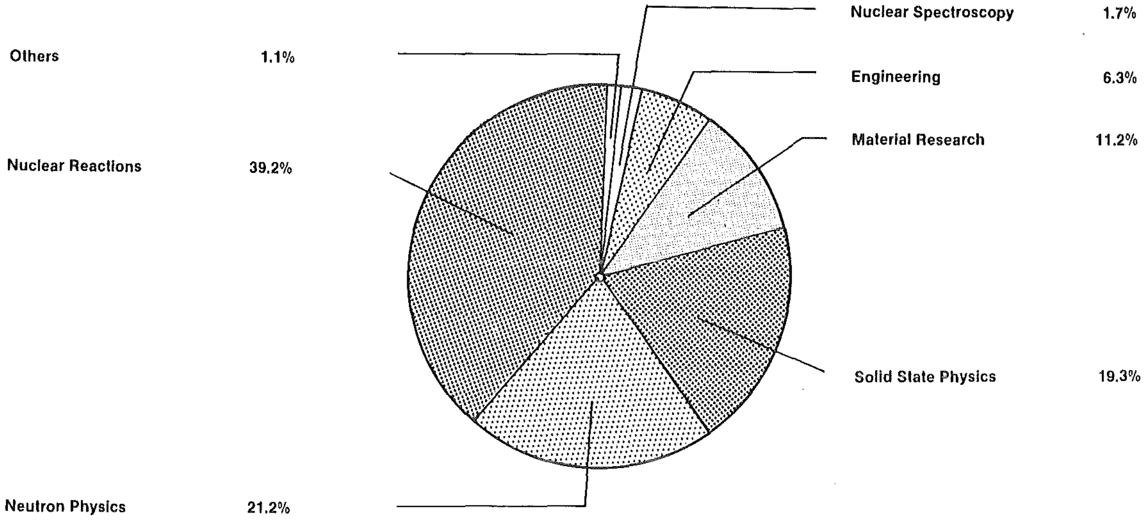

Table II

Internal Users		
Institut für Kernphysik I	1305.3 h	22.2%
Institut für Kernphysik III	1073.5 h	18.2%
Institut für Material u. Festk.-Forsch.	627.2 h	10.7%
Institut für Radiochemie	52.4 h	0.9%
Hauptabteilung Sicherheit/Dosimetrie	4.2 h	0.1%
	3062.6 h	52.0%
External Users		
Universität Tübingen	626.2 h	10.6%
Universität Erlangen	625.9 h	10.6%
Technische Universität München	571.5 h	9.7%
Freie Universität Berlin	552.3 h	9.3%
Max-Planck-Institut Heidelberg	165.1 h	2.8%
Universität Ulm	59.5 h	1.0%
Universität Konstanz	42.1 h	0.7%
Universität Münster	20.6 h	0.3%
Technische Hochschule Darmstadt	19.3 h	0.3%
Universität Bonn	8.0 h	0.1%
Universität Heidelberg	6.6 h	0.1%
Universität Mainz	6.5 h	0.1%
Universität Hamburg	5.6 h	0.1%
Universität Frankfurt	2.0 h	0.1%
	2711.2 h	45.8%
Irradiation of Machine Parts	150.4 h	1.9%
Total	5924.2 h	100.0%

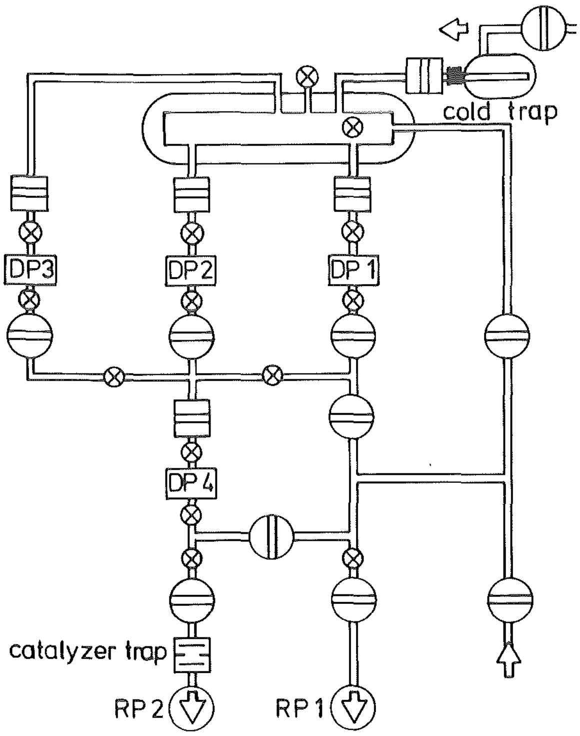
cold trap
DP3
DP2
DP1
DP4
catalyzer trap
RP2
RP1

Fig. 1: New vacuum system for KIZ. An additional diffusion pump (DP4) in the fore line and a special catalyzer trap were used to reduce oil backstreaming.

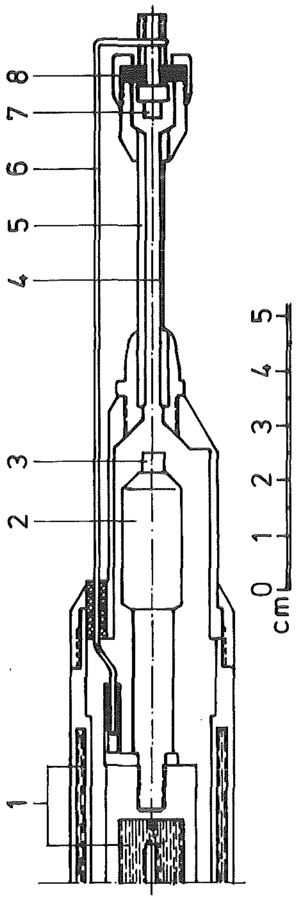
8
7
6
5
4
3
2
1
0
1
2
3
4
5
cm

Fig. 2: Modified internal Penning ion source for higher currents and longer life times.
1 = water cooling
2 = graphite cathode holder
3 = hafnium carbide cathode
4 = extraction slit
4.5×1.2 mm^2.
5 = tantalum chimney
6 = molybdenum connection
7 = tungston reflector
8 = boron nitride insulator.

6.3.2 OPERATION OF THE KARLSRUHE COMPACT H^--CYCLOTRON (KAZ)

J. Möllenbeck, H. Schweickert

During the period of the report the cyclotron was operated for isotope production, activation of machine parts and occasionally for the production of radioisotopes for nuclear physics experiments. The cyclotron is normally operated from late Sunday afternoon until Thursday. However, since June it is being operated additionally from Friday until Sunday for materials research within the Fusion Project using the dual-beam technique.

The availability of the machine was good and no major breakdowns occurred during operation. Repairs of the power supplies of the exciter coils and the high frequency system were necessary. During the hot period of the year the very high outside-air temperatures led to problems with the central back-cooling system for KIZ and KAZ.

In order to prevent radiation damage and high activation of the machine and the beam guiding system, measuring probes were installed at the exposed positions of the machine and the beam guiding system. These probes automatically switch off the ion source when the preset maximum values are exceeded.In this way a false optimization of the machine is prevented and at the same time the activation of the machine is reduced to a minimum.

Stable beam currents > 100 μA at 40 MeV can be extracted.

6.3.3 STATUS OF THE EXTERNAL ION SOURCES OF THE KARLSRUHE ISOCHRONOUS CYCLOTRON

H.P. Ehret, R. Ernst, L. Friedrich, A. Hurst$^+$, E. Huttel,
J. Kaltenbaek, F. Schulz, L. Wiss, P. Ziegler

The polarized atomic beam source has operated for 2800 h for nuclear physics experiments over the past year. Typically 150 nA of 52 MeV polarized deuterons could be extracted from the cyclotron. The measured vector-polarization was 0.55. The remaining time was used for extensive studies of the source in order to improve the brightness of the extracted ion beam and the reliability of the source. As a result the polarized beam current delivered from the source increased by a factor of two (mainly due to an improved ionizer tune), but the current extracted from the cyclotron could not be increased. The main parameters of the source are given in table 1.

D_2 flow:	0.5 mbar l/s
Dissociation degree:	0.35
Nozzle-temp.:	100° K
Sextupoles:	1. l:100 mm, r = 4-8 mm, B_{max} = 0.8 T 2.. l:100 mm, r = 8 mm, B_{max} = 0.8 T distance 1.-2. sextupole: 200 mm distance 2. sextupole-ionizer 300 mm
Atomic-Beam-Intensity:	1 x 10^{16} atoms/sec
Vacuum:	1 x 10^{-4} mbar dissociator chamber 2 x 10^{-6} mbar sextupole chamber 5 x 10^{-7} mbar ionizer chamber
Current below the ionizer:	80 µA* 0.05 x 10^{16} D^+/sec
Emittance:	100 mm mrad MeV $^{1/2}$
Current behind the 90° deflection:	30 µA*
Energy spread:	± 75 eV (estimated from emittance degradation by 90° deflection)

* The quoted currents are the differences of measurements taken with the sextupoles on and off.

Table 1: Main parameters of the atomic beam source PASKA

Several attempts will be made to reduce the 60 % loss of the 90° deflection; an electrostatic mirror has been built, and spherical deflection plates are under construction. Cooling down the dissociator nozzle to 20°K and changing the geometry of the remaining two hexapoles should result in an increase by a factor 2 of the source output.

The ECR-source LISKA has operated for 1700 h for nuclear physics experiments over the past year. In Nov. 1986 it became necessary to rebuild the source because it was no longer possible to repair the cooling system of the hexapole magnet and as a consequence the plasma chamber heater was destroyed. This shutdown was used for major modifications of the source.

Motivated by the good experiences of the Berkeley Group (1), a smaller gradient of the hexapolar magnetic field is now used, allowing an increase in the diameter of the main plasma chamber from 80 to 125 mm. The microwave power is split and transmitted separately to the first and second stages. Figure 1 shows the new design of LISKA. The source was in operation again in March 86 but some debugging is still necessary. The heating of the plasma chamber has to be completed and optimized, which will be carried out in the following months.

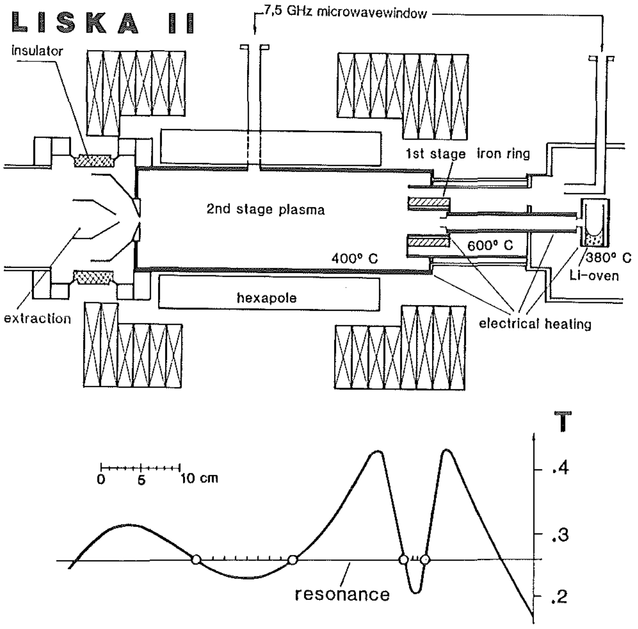
LISKA II
7,5 GHz microwavewindow
insulator
1st stage
iron ring
2nd stage plasma
400° C
600° C
380° C
Li-oven
hexapole
extraction
electrical heating
T
.4
.3
.2
0
5
10 cm
resonance

Fig. 1:
The new design of the ECR-source for Li^{+++} ions

$^{+}$on leave from TRIUMF, Vancouver, Canada, April-Sept. 86

(1) C.W. Lyneis, Proc. of the 6th Int. Workshop on ECR-ION-SOURCES Berkeley 1985, p. 51

6.3.4 AN ECR ION SOURCE WITH A HIGH IONIZATION EFFICIENCY

V. Bechtold and S.A. Sheikh

The most important requirement of an ion source used for the purification of accelerator-produced radioisotopes is the ionization efficiency. As the amounts of radioisotopes produced are extremely small (nano- to microgramme range) the ionization efficiency governs the economical feasability of the purification process. A high ionization efficiency also prevents the accumulation of long-lived isotopes in the system, which is important as far as the radiation protection aspects are concerned.

An efficient, medium-temperature ($\leq 1000^{o}C$) ECR ion source has been developed in Karlsruhe for the production of radioactive beams of volatile elements. Although still in a prototype state it has demonstrated the application of an ECR ion source in an isotope separator, with an emphasis on high ionization efficiency.

The first possible application of the ECR ion source is in the nuclear medical field and involves the purification of I-123 (13.2 h) from its possible contaminants I-124 (4.2 d) and I-125 (60.14 d). For the latter case the radioxenon precursors are separated. The second possibility is the production of Be-7 ions for implantation into modern materials such as ceramics for wear analysis. The third possible application involves the on-line production of radioactive beams of volatile elements for nuclear astrophysics. With these applications in mind the ionization efficiencies of Xe, C, N, O and Ne have been measured using the prototype ECR ion source.

The Karlsruhe prototype ECR ion source for radioactive beams is a single-stage, multiple-mirror machine operating in the continuous mode at a microwave frequency of 6.4 GHz, corresponding to resonance at a magnetic field of 0.229 T. The minimum-B field configuration is created by the superposition of an axial mirror field and a radial hexapole feld. Two sets of four double-helix water-cooled copper solenoid coils induce the axial mirror field, while the radial hexapole field is established by means of a compact assembly of samarium cobalt permanent magnets. Plasma generation in the inner quartz tube is achieved by radially injecting the microwaves into the multimode cavity through an open-ended waveguide positioned between the hexapole bars.

For the measurements of ionization efficiencies it is very important to know the flow rate of the test gas into the ion source with a high enough accuracy. This was achieved by the use of commercially-available calibrated gas leaks, which provide reliable sources of low leak rates of specific gases with an accuracy better than ± 10 %. With the flow rate of the test gas known, the determination of the ionization efficiencies was carried out by measuring the extracted and separated current of the test gas ions using a Faraday cup biased for secondary electron emission. The ionization efficiencies were measured as functions of microwave powetr and support gas flow rate. The support gas used was hydrogen because of the high ionization efficiency measured for natural xenon (1). The hydrogen was introduced via a palladium valve in order to filter out air for the nitrogen and oxygen measurements. Additionally a correction factor due to the rest gas and desorption from the quartz surface was determined for both nitrogen and oxygen. This was carried out by isolating the calibrated leak from the ion source and measuring the remaining current. The ion source was tuned by optimizing all the adjustable parameters to obtain the maximum ionization efficiency of the test gas.

Table 1 summarizes the maximum ionization efficiencies of q = 1+, 2+ and 3+ ions and compares them with those of ,other on-line sources.

		Ionization efficiency	
Element		Karlsruhe ECR ion source	On-line ion source
Carbon (CO)	1+	10.0 %	0.23 % (2)
	2+	0.7 %	-
	3+	0.01 %	-
Nitrogen	1+	26.0 %	0.01 % (2)
	2+	1.7 %	-
	3+	0.03 %	-
Oxygen	1+	53.0 %	-
	2+	3.5 %	-
	3+	0.1 %	-
Neon	1+	30.0 %	1.0 % (2)
	2+	1.5 %	-
	3+	0.05 %	-
Xenon	1+	80.0 %	48.0 %
	2+	11.0 %	-
	3+	1.0 %	-

Table 1: Summary of measured ionization efficience

It has been shown that an ECR ion source has much higher ionization efficiencies than conventional ion sources for both light ions as well as for heavy ions such as natural xenon. The Karlsruhe ECR ion source is in addition well-suited for use in isotope separators due to the absence of electrodes, which results in no wear and corrosion, and therefore no maintenance, and a long lifetime.

(1) V. Bechtold and S.A. Sheikh, p. 110, Proceedings of the Radioactive Beams Workshop, Vancouver, Canada 1985
(2) H.L. Ravn et al., p. 94, Proceedings of the Radioactive Beams Workshop, Vancouver, Canada 1985
(3) R. Kirchner et al., Nuclear Meth. and Instr. 186 (1981) 295-305

6.3.5 STATUS OF THE ELECTRON COOLING DEVICE UNDER CONSTRUCTION AT CERN

P.F. Dittner+, C. Habfast, H. Haseroth++, C.E. Hill++, H. Poth,
B. Seligmann, J.-V. Vallet++, A. Wolf++

The LEAR electron cooler entered into the final phase of the development before it is installed in LEAR in spring 1987. The earlier stages of the development were described in previous reports(1). In the past year (Juli 85 - June 86) the following work was done:

- generation of the first electron beam in the conditioned vacuum system within the full energy range up to 40 keV,
- determination of operation parameters and establishment of scaling laws; optimization of performance,
- measurement of the vacuum pressure in the presence of the electron beam under various conditions,
- improvement of the pumping speed by installation of specific vacuum pumps,
- set-up of microwave detection system and measurement of microwave spectrum emitted from the electrons.

In Fig. 1 the actual status of the electron cooler is shown. In particular the microwave antenna in the cooling section and the new pumps at the collector can be seen. A major part of the vacuum mesurements are summarized in(2). The major achievements are:

- lowest vacuum with cold cathode: $3.5 \cdot 10^{-12}$ Torr
- lowest vacuum with 3 keV beam: $1.0 \cdot 10^{-11}$ Torr
- lowest vacuum with 26 keV beam: $9.0 \cdot 10^{-11}$ Torr

The electron cooler had been under operation for many hours and was trimmed to an easy and realiable handling. In particular beam studies were made in order to decrease the electron losses, which yielded the lowest electron loss of $6 \cdot 10^{-4}$ of primary electron beam.

The synchrotron radiation emitted by the electrons spiraling in the longitudinal magnetic field allows to determine the transverse electron temperature non-destructively. It is therefore an important means of diagnostics for the electron beam. The low transverse temperature of the electron beam makes the measurement of the microwave radiation difficult. Owing to the overall noise temperature of 900°K for the entire one octave receiver, we obtained for the first time a detailed spectrum. It is shown in the upper part of Fig. 2 can be reproduced quantitatively with a model based on the coupling of the electron oscillator to a microwave cavity which is the vacuum tube. This calculated spectrum is shown in the lower part of Fig. 2. The evaluation leads to a transverse temperature of the electron beam of 1.6 ± 0.8 eV which is probably so high, because at the time of the measurement the electron beam guiding system was not fully optimized yet.

In view of the upgrading of the LEAR electron cooler to 100 keV as required for a LEAR experiment we have designed a set-up which serves to test different components (e.g. collectors) of future coolers. In particular we will test a new high voltage concept for cooling devices4). This set-up is constructed within a collaboration between groups of the KfK, the KfA, GSI Darmstadt and MPI Heidelberg and will also be used to study aspects relevant for cooler projects in these institutions.

(1) H. Budig, M. Girardini, C. Habfast, H. Haseroth, C.E. Hill, L. Hütten, H. Poth, B. Seligmann, J.-L. Vallet, A. Wolf, Electron Cooling at LEAR, Annual Report, KfK 3969(1985)193
A. Wolf, Dissertation, Universität Karlsruhe, 1986, KfK 4023

(2) C. Habfast, M. Girardini, L. Hütten, H. Poth, A. Poncet, B. Seligmann, A. Wolf, Das Ultrahochvakuumsystem des Elektronenkühlers für LEAR, Vakuum-Technik 7(1985)195

(3) C. Habfast, H. Poth, B. Seligmann, A. Wolf, Mikrowellendiagnose eines relativistischen Elektronenstrahls, DPG-Tagung für Plasmaphysik, 11.-14.3.1986, Stuttgart

(4) C. Habfast, H. Poth, B. Seligmann, A. Wolf, An alternative concept for high-voltage systems used in electron cooling, Nucl. Instr. Methods in Phys. Research A248(1986)562

+ Visitor from Oak Ridge National Laboratory
++ CERN, Geneva, Switzerland

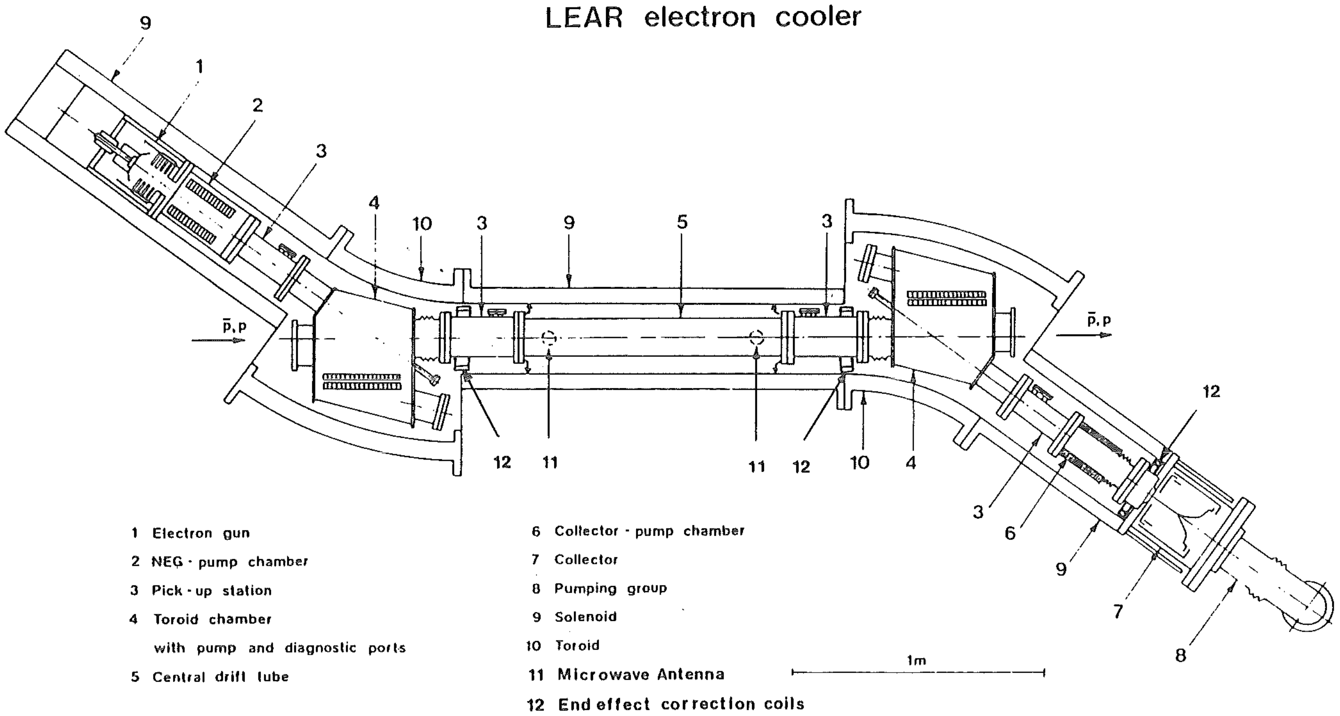
LEAR electron cooler
9
1
2
3
4
10
3
9
5
3
p̄,p
p̄,p
12
11
11
12
10
4
12
3
6
9
7
8
1 Electron gun
2 NEG - pump chamber
3 Pick - up station
4 Toroid chamber with pump and diagnostic ports
5 Central drift tube
6 Collector - pump chamber
7 Collector
8 Pumping group
9 Solenoid
10 Toroid
11 Microwave Antenna
12 End effect correction coils
1m

Fig. 1 Assembly drawing of the LEAR electron cooler

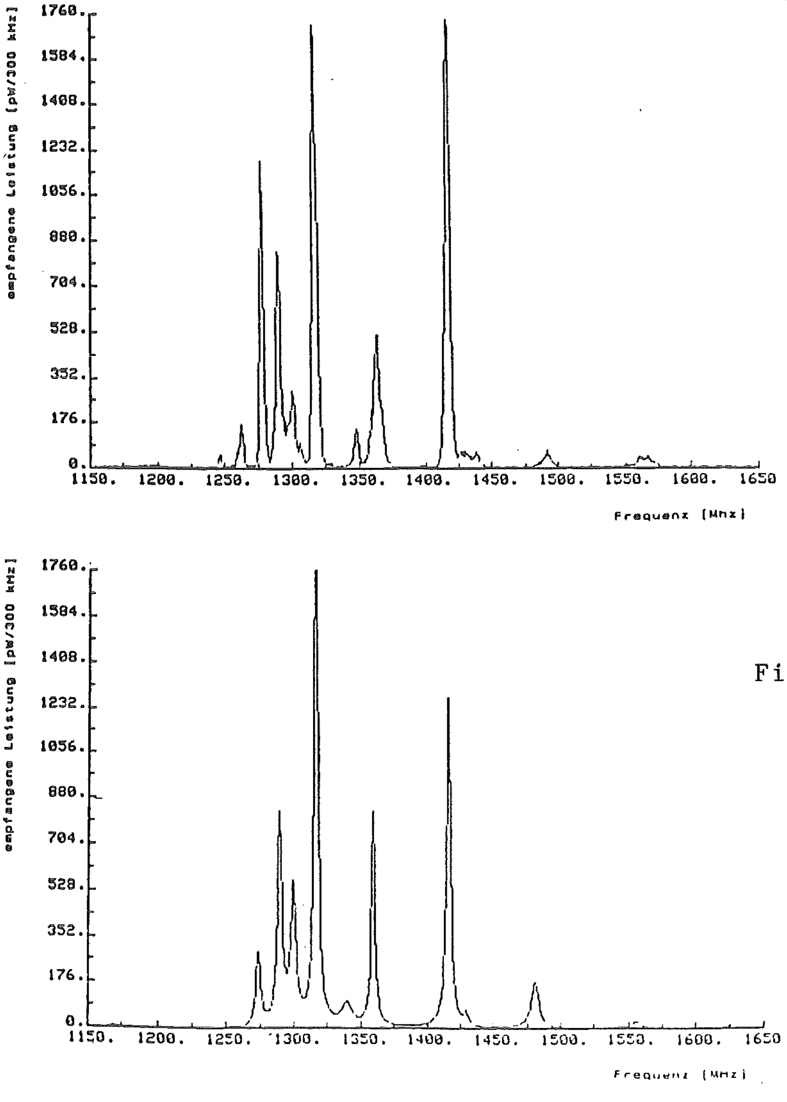

Fig. 2 Measured (above) and calculated (below) spectra of the electrons measured with an antenna in the drift region

6.3.6 GENERAL ISSUES FOR THE DESIGN OF LATTICES FOR EHF

P. Blüm

The conceptual design of the European Hadron Facility (EHF) has been developed and described$^{1)}$. The design objectives (30 GeV maximum energy, 100μA average current, 100% duty cycle or fast extraction, and acceleration of polarized protons) are given by the need of a wide faceted research program in Medium Energy and Modern Nuclear Physics.

The projected beam intensity of 100μA average current ($6.24 \cdot 10^{14}$ protons per sec) is almost two orders of magnitude higher than that of the AGS or CERN-PS, and requires special attention on beam stability and minimal beam losses. These considerations leads to several, fundamental design criteria for the lattices:

Crossing of transition should be avoided. Though the crossing of transition energy is considered to be a standard procedure in existing synchrotrons we believe that in presence of space charge transition crossing may be a source of considerable particle losses. Several methods can be used to avoid transition crossing:

Transition can be below injection or above extraction.

The lattice can have imaginary transition energy.

Choose the principle of variable optics$^{2)}$.

Transverse space charge effects should be accomodated. Magnet apertures have to be large enough to account for tails and nonlinear effects in the particle distributions.

Coupling between horizontal and vertical betatron motion should be avoided.

Coupling between radial and longitudinal motion should likewise be avoided. Due to the high repetition rates high accelerating voltages are needed which may lead to large synchrotron oscillations. Thus-coupling resonances may be excited, if the rf-cavities are not located at places with zero or small dispersion.

A further constraint for the lattice design is given by the requirement, that this new facility should be able to preserve polarization during acceleration up to the maximum energy. Therefore one has to consider depolarizing resonances, which occur whenever the precession frequency of the spin $f_p = G \cdot \gamma$ coincides with a disturbing magnetic field. $G = 1.7928$ is the anomalous gyromagnetic ratio of the proton. The expected depolarization during the passage through an intrinsic resonance driven by special harmonics in the betatron motion ($f_p = kS \pm Q_y$) or an imperfection resonance driven by special harmonics in the closed orbit distortion ($f_p = k$), is given by the Froissart-Stora formula$^{3)}$:

$$P_f/P_i = 2\exp(-\pi|\varepsilon|_p^2/2\alpha) - 1 ,$$

which however is only valid for isolated resonances. The quantity ε_p represents the strength of a resonance and has been evaluated with help of the computer program DEPOL$^{4)}$. α gives the crossing speed of the resonance and is:

$$\alpha = (G \cdot \Delta\gamma \pm \Delta Q)2\pi \quad .$$

$\Delta\gamma$ is the energy gain per turn. In the case of instrinsic resonances ΔQ describes the tune shift per turn due to pulsed quadrupoles. For imperfection resonances ΔQ is omitted. We have the choice of different methods to preserve polarization up to 30 GeV:

Choose the periodicity of the lattice such high, that the first intrinsic resonance occurs above maximum energy. Imperfection resonances can be corrected with careful alignment of the elements.

A high lattice periodicity leads to few resonances only, which may be crossed with fast Q-jumps or adiabatically spin flips. Both methods were already used at Saturne$^{5)}$ and AGS$^{6)}$.

For lattices with few resonances one may spin match the lattice by careful spacing of the magnets in order to reduce the strength of the resonance. One may even achieve this spin transparency with help of a set of slowly varying quadrupoles correcting the harmonic of the betatron motion during the passage of the resonance.

In lattices of low periodicity with long, dispersionfree straights one or more Siberian snakes$^{7)}$ may be installed.

Starting with these considerations lattices of the Booster and the Main Ring have been designed and are summarized in the study report$^{1)}$.

(1) Feasibility Study for a European Hadron Facility EHF-86-33
(2) B. Franczak, LA-10260-MS
(3) M. Froissart, R. Stora, Nucl. Instr.& Meth. NIM 7(1960)297
(4) E. Courant, Amer. Inst. of Phys. Conf. Proc. 42(1977)94
(5) E. Grorud et al., Amer. Inst. of Phys. Conf. Proc. 95(1982)407
(6) L. Ratner et al., IEEE Trans. on Nucl. Sci. NS-32(1985)1656
(7) E. Courant, Amer. Inst. of Phys. Conf. Proc. 95(1982)388

6.4 APPLICATIONS

6.4.1 APPLICATION OF PROTON-INDUCED X-RAY EMISSION (PIXE) TO THE DETERMINATION OF TRACE ELEMENTS IN BIOLOGICAL SAMPLES

C. Spieker⁺, D. Heck, W. Zidek⁺, T. Stratmann⁺, D.P. v. Bassewitz⁺⁺, H. Vetter⁺ and H. Zumkley⁺, (1)

Charged particle reactions are used in the Karlsruhe nuclear microprobe for the analysis of light elements in organic tissue. In this method (PIXE) a well-focussed ion beam is directed at the sample under investigation. The secondary radiation induced by the ion impact gives the information on the elemental composition of the target mass. In this study, samples from lumbar aorta, renal artery, rat heart muscle and human heart muscle were examined. The results demonstrate that PIXE yields a good insight into the spatial distribution of trace elements in tissue. The spatial resolution of this technique is limited to about 4 µm. Further developments will be necessary to achieve a resolution sufficient for analysing subcellular components.

(1) ditto, Trace Elements in Medicine 3 (1986) 87-89

+ Medizinische Universitäts-Poliklinik, Münster
++ Pathologisches Institut der Universität Münster

6.4.2 PROTON MICROBEAM STUDY OF CALCIUM-PHOSPHATE COMPLEXES IN HUMAN ARTERIES

T. Cichocki⁺, D. Heck, L. Jarczyk⁺⁺, E. Rokita⁺⁺, A. Strzalkowski⁺⁺, M. Sych⁺, (1)

The proton microprobe was used for the determination of the elemental composition of Ca-P deposits in 3 types of human arteries (abdominal aorta, coronary artery, circle of Willis). The PIXE and RBS techniques were used for elemental analyses and the distribution of concentrations of the element C, N, O, P, S, Cl, K, Ca, Fe, Cu, Zn, Br, Se and Pb was measured. The chemical structure of the Ca-P deposits as well as the role of certain elements in the calcification process were considered. The comparison between different investigated arteries was also made.

(1) ditto, Nucl. Instr. Meth. in Phys. Res. B (1986) (in print)

+ Adademy of Medicine, Kopernika 7, Pl-31034 Kraków, Poland
++ Institute of Physics, Jagellonian University, Reymonta 4, Pl-30059 Kraków, Poland

6.4.3 ELEMENTAL COMPOSITION IN OCULAR TISSUE OF RAT

T. Cichocki[+], D. Heck, L. Jarczyk[++], E. Rokita[++], A. Strzalkowski[++], M. Sych[+], (1)

Proton microprobe and proton induced X-ray emission (PIXE) methods were used for examination of the elemental composition of rat eyes. The concentrations of the elements Cl, K, Ca, Cr, Fe, Zn, Br and Rb were determined in the different ocular tissue structures. The observed differences in the elemental composition of different layers were correlated with known physiological facts. The applicability of the micro-PIXE for the investigation of the ocular tissue is also considered.

(1) ditto, Experimental Eye Research (in print)

+ Academy of Medicine, Kopernica 7, Pl-31034 Kraków, Poland

++ Institute of Physics, Jagellonian University, Reymonta 4, Pl-30059 Kraków, Poland

6.4.4 Ca^{2+} ANALYSIS IN ARTERIES OF SPONTENEOUSLY HYPERTENSIVE RATS BY PROTON-INDUCED X-RAY EMISSION

C. Spieker[+], D. Heck, W. Zidek[+], and H. Vetter[+], (1)

Numerous investigations have shown that Ca^{2+} plays an important role in the pathogenesis of hypertension. Intracellular Ca^{2+} measurements have been carried out with Ca^{2+}-selective electrodes and the Quin 2 method. The present study used particle induced X-ray emission to investigate the Ca^{2+} distribution in arterial smooth muscle. This method correlates Ca^{2+} distribution with the morphological structure of the tissue. The Ca^{2+} content of the aortas and renal arteries was measured in 22 spontaneously hypertensive and 11 normotensive rats.

The findings demonstrate significant Ca^{2+} elevation in the aortas of spontaneously hypentensive rats compared with the aortas of normotensive rats (3124.9 ± 790.0 versus 2031 ± 478 µg Ca^{2+}/g; $P < 0.05$), whereas there was only a tendency to Ca^{2+} elevation in the renal arteries of spontaneously hypertensive rats compared with normotensive rats (3336.0 ± 1798.0 versus 1533.2 ± 1082.0 µg Ca^{2+}/g; NS). The Ca^{2+} was mainly detected in the muscle containing tunica media.

(1) ditto, Journal of Hypertension 1985, 3 (suppl 3):S53-S55

+ Medizinische Universitäts-Poliklinik, D-4400 Münster

6.4.5 TRACE ELEMENT DISTRIBUTIONS IN HUMAN LIVERS DETERMINED WITH MICRO-PIXE

D. Heck, A. Ochs[+], A. Klempnow[++], C. Kratt[++], K.P. Maier[++], (1)

Most trace element (TE) determination methods show no pronounced spatial resolutions of the sample. Therefore the TE concentrations of liver tissue determined with such methods can only be correlated with gross structures, while the detailed architecture of the liver lobules (typical size 1 mm) is averaged out. Microscopic determination with the electron microprobe suffers from a low elemental sensitivity. We use the method of proton induced X-ray emission (PIXE) with microfocussing. A beam of 3 MeV protons is tiny focussed (diameter 3 μm) onto the liver samples, which are prepared as cryo-microtome cuts. In the point of impact (∿ 25 pg mass) this beam produces characteristic X-rays. By sweeping the proton beam across the sample the distributions of all TE with $Z \geq 13$ and concentrations above some μg/g are determined simultaneously. Out of 40 investigated human biopsy samples the healthy ones reflect rather homogeneous distributions of Fe, Cu and Zn. The average Br-content of hepatocytes amounts to ∿ 5 μg/g DW (dry weight) in contrast with the local enhancements up to 50 μg/g DW at the fibrotic boundary between the lobules. We observe a similarly enlarged Br-concentration in the fields of histological inactive and scarred areas of fibrosis in 3 samples of liver cirrhosis (alcohol-toxic and primary biliary cirrhosis). In these cirrhotic livers within the areas of blooming fibrotic degeneracy we find a strictly localized enhancement of the Cu-concentration up to 1500 μg/g DW which must be compared with the normal Cu-concentration of 30 μg/g DW.

These results demonstrate that with the micro-PIXE method the TE distributions in the micro range can be determined to give hints onto the enzymatic reactions; by macroscopic TE determinations these detailed structures are averaged out.

(1) ditto, Trace Element Analytical Chemistry in Medicine and Biology, Vol. 4 (P.Brätter, P. Schramel ed; Walter de Gruyter, Berlin, 1986) (in print)

[+] Medizinische Universitätsklinik, 7800 Freiburg

[++] Städtische Krankenanstalten, 7300 Esslingen

6.4.6 LOCALIZED CHANGES OF TRACE ELEMENT CONCENTRATION WITHIN DISEASED HUMAN LIVER LOBULES

D. Heck, A. Ochs[+], A. Klempnow[++], K.P. Maier[++], C. Kratt[+++], (1)

The Karlsruhe ion microprobe was used in the investigation of healthy and cirrhoticly diseased human liver samples. Target preparation and irradiation is described. The PIXE spectra above 4 keV are dominated by the trace elements Fe, Cu, Zn, and Br. These elements are distributed rather homogeneously in healthy livers. Their concentration levels fluctuate from patient to patient by factors up to 10.

For cirrhotic livers we tried to elaborate typical trace element patterns. A locally increased Cu content indicates onto inflammatory activity, while fibroticly scarred tissues show a markedly higher Br concentration. Fe concentrations up to some per cent are found in granular deposits within the parenchyma of hemochromatotic livers.

(1) ditto, Nucl. Instr. Meth. in Phys. Res. B (1986) (in print)

+ Medizinische Universitätsklinik, 7800 Freiburg
++ Medizinische Klinik, Fachbereich Gastroenterologie, Städtische Krankenanstalten, 7300 Esslingen
+++ Institut für Pathologie, Städtische Krankenanstalten, 7300 Esslingen.

6.4.7 MEASUREMENT OF REGIONAL PERFUSION OF THE MYOCARD BY RECORDING THE DISTRIBUTION OF ^{81}Rb-^{81m}Kr WITH A SPECT-SYSTEM

E. Oberhausen[+], A. Hanser, A. Steinsträßer[+], M. Müller[++], E.L. Schmidt[+], and R. Berberich[+], (1)

The activity ratio of ^{81}Rb and its short living daughter product ^{81m}Kr meets the requirements for the direct measurement of the perfusion of organs. Because of the short half life of ^{81m}Kr the deviation from radioactive equilibrium is only 25 % at a perfusion rate of 100 ml/min x 100 g. The pure ^{81}Rb needed for such measurements is produced by means of electromagnetic isotope separation.

We use a SPECT-system with simultaneous recording in the two energy windows of ^{81}Rb and ^{81m}Kr. As the tomograms are without superposition of other tissues the possibilities of the ^{81}Rb - ^{81m}Kr can be fully utilized. In the examination of 106 patients we have found that with the Rb-Kr-tomograms, recorded at rest, we are able to differentiate between sites of infarction and regions of ischemia. All examinations have been compaired with coronary angiography and a part of them also with ^{201}Tl scintigraphy. The method can also be used for objectivation of coronar dilatation and bypass-surgery.

(1) ditto, Radioaktive Isotope in Klinik und Forschung, 17. Band, R. Höfer und H. Bergmann (Herausg.), Egermann-Verlag, Wien (1986) s. 233

+ Radiologische Universitätsklinik Homburg/Saar, Abt. Nuklearmedizin
++ Medizinische Universitätsklinik Homburg/Saar, Innere Medizin III

6.4.8 EVALUATION OF SEVERE CORONARY ARTERY STENOSES USING TOMOGRAPHIC ^{81}Rb^{81m}Kr MYOCARDIAL IMAGES

M. Müller[+], E. Oberhausen[++], H.P. Stoll[++], E.L. Schmidt[++], A. Hanser und W. Vogel[+], (1)

^{81}Rb scintigrams at rest, ^{201}Tl scintigrams after exercise, and coronary angiography were performed in 28 patients with 1 - 3 vessel diseases. All myocardial infarctions were recognized with both scintigraphic methods (7 x posterolateral wall, 8 x inferior wall and 7 x anterior wall). In the inferior wall and posterolateral wall 6 ^{201}Tl- and 5 ^{81}Rb defects were detected without any support of infarction. In 13 regions distal to > 75 % diameter stenoses 5 irreversible and 8 reversible ^{201}Tl defects corresponding to the absence or presence of redistribution in a 3-hour delayed image were detected. In 12 of these 13 regions the ratio of ^{81m}Kr / ^{81}Rb was increased. 8 completely occluded vessels showed 2 reversible and 3 irreversible ^{201}Tl defects and 5 increased ratios of ^{81m}Kr / ^{81}Rb. 10 vessels with 50 - 75 % stenoses showed 4 reversible and 1 irreversible ^{201}Tl defect and 3 increased ratios of ^{81m}Kr / ^{81}Rb. In 7 vessels without detection on stenoses 4 reversible ^{201}Tl defects and 4 increased ratios of ^{81m}Kr / ^{81}Rb were proved. The results indicate the possibility to detect high grade coronary stenoses using ^{81}Rb-scintigrams recorded at rest, and they indicate the superiority of ^{81}Rb imaging in separating resting hypoperfusion from myocardial scar.

(1) ditto, Herz/Kreislauf 18 (1986) 128

+ Medizinische Universitätsklinik Homburg/Saar, Innere Medizin III

++ Radiologische Universitätsklinik Homburg/Saar, Abt. Nuklearmedizin

6.4.9 PERFORMANCE OF PLUTONIUM ISOTOPIC ANALYSIS BY GAMMA SPECTROMETRY IN REPROCESSING PRODUCT SOLUTIONS

H. Eberle, H. Ottmar

The KfK K-Edge Densitometer provides as an additional option the possibility to determine the isotopic composition of plutonium from the spectrometry of the isotope-specific gamma self-radiation (1). The measurement data produced so far have been examined for an assessment of the actual measurement performance from routine instrument operation.

A handicap of the gamma-spectrometric analysis is the lack of a gamma-ray signature from the isotope ^{242}Pu, which for this reason has to be estimated from an isotopic correlation with the measurable isotopes. A generally valid and accurate isotopic correlation for ^{242}Pu, however, does not exist, because the plutonium isotopic composition is known to be reactor dependent. For plutonium generated in standard power reactors the ^{242}Pu abundance estimated from the presently used correlation may have a systematic error of up to 10 %, which in turn then also leads to small systematic measurement errors for the remaining isotopes.

We have therefore modified the software, allowing the input of the correct ^{242}Pu abundance in those cases, where this information is available from other sources. Table 1 compares 14 isotopic analysis results from gamma spectrometry and mass spectrometry for the two situations, where in the gamma analysis ^{242}Pu once is estimated from the correlation, and once taken as known input. In the latter case the average deviations for the major isotopes 239, 240 and 241 are $\lesssim$ 0.2 %, and the observed standard deviations are close to the precision values expected from a 2000 s gamma counting. The poorer agreement for ^{238}Pu most probably arises from uncertainties in the reference values, which have been determined by the less accurate alpha-spectrometry method. This is supported by the observed standard deviation of 4.1 % between two independent alpha-spectrometric ^{238}Pu determinations for the set of 14 samples.

Table 1 Measured plutonium isotope abundances, given as ratio of results from gamma spectrometry and mass spectrometry.

Sample No.	^{238}Pu	^{239}Pu	^{240}Pu	^{241}Pu	^{242}Pu
		^{242}Pu from isotope correlation			
1	1.0247	0.9991	1.0002	1.0068	0.9857
2	1.0173	1.0013	1.0026	0.9922	0.9748
3	1.0464	0.9968	1.0039	1.0042	0.9962
4	1.0252	1.0023	0.9919	1.0043	0.9991
5	1.0487	0.9955	1.0014	1.0002	1.0280
6	1.0459	1.0036	1.0035	1.0019	0.9241
7	1.0949	0.9977	1.0062	1.0036	0.9615
8	1.0312	1.0053	0.9989	1.0112	0.9074
9	1.0244	1.0020	1.0048	0.9928	0.9502
10	1.0290	1.0005	1.0038	1.0027	0.9656
11	1.0290	1.0020	0.9970	1.0061	0.9659
12	1.0444	0.9986	1.0001	1.0057	0.9755
13	1.0272	1.0001	1.0045	1.0129	0.9326
14	1.0447	1.0030	1.0023	1.0189	0.8974
Mean	1.0381	1.0006	1.0015	1.0045	0.9617
RSD (%)	1.86	0.28	0.37	0.71	3.81
		Operator value for ^{242}Pu as input			
1	1.0220	0.9984	0.9995	1.0060	1.0000
2	1.0165	1.0002	1.0030	0.9911	1.0000
3	1.0464	0.9966	1.0037	1.0040	1.0000
4	1.0252	1.0022	0.9918	1.0043	1.0000
5	1.0500	0.9971	1.0029	1.0017	1.0000
6	1.0412	0.9996	0.9995	0.9978	1.0000
7	1.0929	0.9955	1.0039	1.0014	1.0000
8	1.0262	1.0007	0.9944	1.0065	1.0000
9	1.0214	0.9988	1.0016	0.9897	1.0000
10	1.0267	0.9983	1.0015	1.0004	1.0000
11	1.0268	0.9998	0.9949	1.0039	1.0000
12	1.0420	0.9960	0.9975	1.0030	1.0000
13	1.0214	0.9945	0.9989	1.0073	1.0000
14	1.0388	0.9975	0.9968	1.0134	1.0000
Mean	1.0355	0.9982	0.9993	1.0022	-
RSD (%)	1.89	0.22	0.38	0.62	-

---

(1) H. Eberle, H. Ottmar, P. Matussek, Report JOPAG/04.85-PRG-113, Kernforschungszentrum Karlsruhe (1985).

(2) Annual Report on Nuclear Physics Activities 1984/85, KfK 3969 (1985), 201.

6.4.10 HOW TO SIMPLIFY THE ANALYTICS FOR INPUT-OUTPUT ACCOUNTABILITY MEASUREMENTS IN A REPROCESSING PLANT

H. Ottmar, H. Eberle, P. Matussek, I. Michel-Piper, (1)

An analytical approach to high-performance uranium and plutonium accountancy measurements in reprocessing input and output solutions is presented, which provides larger operational simplicity than the conventionally applied chemical methods. The proposed alternative is based on energy-dispersive absorption edge and fluorescence X-ray spectrometry, using the proven and reliable K-edge densitometry technique as reference method. Two X-ray densitometers developed for accurate and reliable uranium and plutonium analysis in both the feed and product solutions are described. Practical experiences and results from their performance evaluation on actual process solutions from a reprocessing plant are presented and discussed.

(1) ditto, KfK-Report 4012 (1986)

6.4.11 CALIBRATION OF X-RAY DENSITOMETERS FOR THE DETERMINATION OF URANIUM AND PLUTONIUM CONCENTRATIONS IN REPROCESSING INPUT AND PRODUCT SOLUTIONS

H. Ottmar, H. Eberle, I. Michel-Piper, E. Kuhn+, S. Johnson+

Two different instruments for uranium and plutonium analysis in reprocessing solutions, both developed in the KfK Institute for Nuclear Physics, are presently installed and operated at the European Institute for Transuranium Elements (TUI), Karlsruhe:

1. A K-Edge densitometer for the precise determination of uranium and plutonium elemental concentrations in reprocessing product solutions from a measurement of the energy-differential X-ray transmittance at the K-absorption edge ('K-edge densitometry').
2. A Hybrid K-edge / K-XRF X-ray densitometer for uranium and plutonium elemental analysis in highly radioactive reprocessing input solutions, which incorporates the techniques of K-edge densitometry and X-ray fluorescence analysis (1).

For accurate measurements both instruments need to be calibrated with suitable reference solutions. A calibration of the K-edge densitometer for quantitative plutonium analysis has been carried out in 1983. Due to the observed high long-term stability of the instrument of better than 0.2 %, this calibration is still valid in 1986. A second calibration exercise, which included the calibration of the K-edge densitometer for uranium analysis and the initial calibration of the Hybrid Instrument for uranium and plutonium analysis in the reprocessing input solutions, has been undertaken in 1985 (2). Different sets of reference solutions have been characterized independently at 3 analytical laboratories (3).

The calibration for uranium measurements from K-edge densitometry in both instruments involves, according to the known densitometry equation

$$U(g/\ell) = \frac{\ln T(E_\ell)/T(E_u)}{\{\mu(E_u)-\mu(E_\ell)\} \cdot D} \cdot 1000 ,$$

the determination of the quantity $\Delta\mu = \mu(E_u)-\mu(E_\ell)$. It represents the difference of the effective total mass attenuation coefficients (in units of $cm^2 \cdot g^{-1}$) of uranium at the energies E_ℓ and E_u below and above the absorption edge, where the ratio of X-ray transmittance $R = T(E_\ell)/T(E_u)$ across the K-edge is experimentally measured. D is the length (in cm) of the densitometry cell, which is known with a relative accuracy of $\pm$ 0.01 %.

With the same method of spectrum analysis the derived calibration constants $\Delta\mu$ for the two different instruments agreed within 0.07 %. We can therefore conclude that the K-edge densitometry calibration appears to be instrument-invariant for highly collimated systems.

The calibration of the XRF measurement in the Hybrid Instrument is simplified by the fact that in the present case this method is only used for a U/Pu ratio measurement. The calibration thus involves the determination of a calibration factor R(U,Pu), which converts the measured peak ratio of the uranium and plutonium $K\alpha_1$ X-rays into the corresponding element ratio. The calibration factor R(U,Pu) is physically described by the ratio of excitation probabilities for the emission of $K\alpha_1$ X-rays from uranium and plutonium in the interrogation X-ray beam. It is not a single calibration constant, but depends slightly on the total element concentration in the sample. This is because the interrogating X-ray beam, while passing through the sample, suffers a change of its spectral distribution in the sense that the beam will be slightly hardened. As a result the excitation probability for emission of plutonium K X-rays will slightly increase relative to that for uranium with increasing total heavy element concentration. For the variations of the U/Pu ratio reasonably to be expected in dissolver solutions from LWR fuels it is sufficient to represent the XRF calibration factor R(U,Pu) just as a function of the concentration of the major heavy element uranium as shown in Fig. 1. The dependence on the uranium concentration is relatively weak, changing R(U,Pu) by only about 2 % over the concentration range from 100 to 300 g U/ℓ. Variations of the matrix density and composition have a negligible influence on R(U,Pu) as verified from calculations.

The calibration factor derived from the calibration measurements agreed within 1.3 % with that calculated from published data on photon cross-sections and spectral distributions of industrial X-ray units. The calculated calibration factor is also shown in Fig. 1.

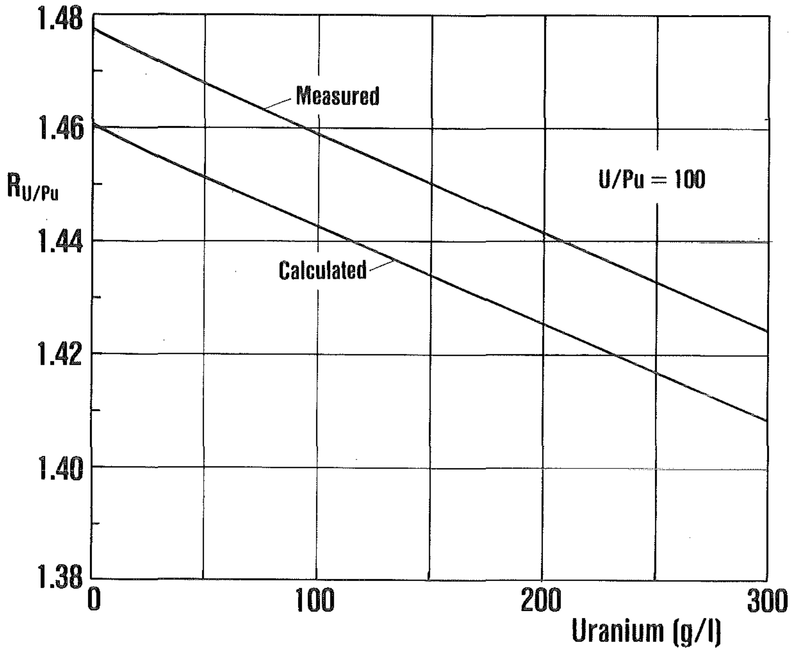

Fig. 1
Calibration factor R(U,Pu) for the U/Pu ratio determination from the XRF measurements.

(1) H. Ottmar, H. Eberle, Annual Report 1984/85, KfK 3969 (1985) 203.
(2) H. Ottmar, H. Eberle, I. Michel-Piper, E. Kuhn, S. Johnson, Report JOPAG/11.85-PRG-123, Kernforschungszentrum Karlsruhe (1985).
(3) E. Kuhn, S. Johnson, L. Koch, H. Ottmar, B. Stojanik, Report JOPAG/10.85-PRG-118, Kernforschungszentrum Karlsruhe (1985).

+ International Atomic Energy Agency, Vienna, Austria.

6.4.12 PERFORMANCE EVALUATION OF AN X-RAY SPECTROMETER FOR URANIUM AND PLUTONIUM ELEMENTAL ANALYSIS IN DISSOLVED SPENT NUCLEAR FUELS

H. Ottmar, H. Eberle, L. Koch[+]

The performance of the previously described X-ray spectrometer for elemental analysis of uranium and plutonium in dissolver solutions from spent nuclear fuels (1) has been evaluated from measurements on real process solutions. The dissolver solutions received for analysis from the Karlsruhe Reprocessing Plant (WAK) arise from recent reprocessing campaigns of this plant on spent fuels from two different pressurized water reactors. The burnup values of the respective fuels were typically within the range of 30 to 35 GWd/tU, giving U/Pu ratios of about 100 to 150. The cooling time was about 3 years, resulting in total ß, γ- activities of between $4 \cdot 10^{12}$ and $7 \cdot 10^{12}$ Bq/l in the dissolver solutions.

The X-ray spectrometer determines the major element uranium from the differential X-ray transmittance at the K-absorption edge of uranium, while the minor element plutonium is obtained from a simultaneous analysis of fluoresced K X-rays. The results have been compared with those obtained from the conventional technique of isotope dilution mass-spectrometry (IDMS). The IDMS analyses were performed by the European Institute for Transuranium Elements.

Table 1 lists for a set of 15 samples the percentage differences between results from the X-ray measurements ('nondestructive assay' = NDA) and from the IDMS analyses ('destructive assay' = DA). The uranium and plutonium concentrations, and the corresponding U/Pu ratios, were determined from truly parallel analyses of the same sample. The IDMS analyses were done twice on two aliquots, and the X-ray measurements include 3 repeat runs of 1000 s counting time each. The reproducibility of the U and Pu determination from the NDA and DA measurements are given in Table 2 for the given set of 15 samples. The errors of the X-ray measurements are dominated by counting statistics. For the total counting time of about 1 h the standard errors ($\sigma\sqrt{n}$, n=3) reduce to 0.12 % for U and to 0.48 % for Pu.

The mean differences of -0.3 % between the compared NDA and DA results (Table 1) for both uranium and plutonium are statistically not significant at the obtained standard deviations of 0.7 %. For plutonium a scatter of 0.7 % in the compared data is within the expected combined uncertainties of the NDA and DA measurements. However, one would have expected a somewhat better precision for the uranium results, because both in the X-ray measurements and in the IDMS analyses the measurement precision is significantly better for uranium than for plutonium (see Table 2).

Table 1: Percentage differences between NDA and DA results for the U and Pu concentration and for the U/Pu ratio.

Sample No.	U	Pu	U/Pu
1	-1.75	-1.51	-0.24
2	-0.44	-0.07	-0.36
3	0.12	-0.13	0.26
4	0.18	-0.54	0.87
5	-0.47	-0.55	0.09
6	-0.58	-0.87	0.29
7	0.11	-0.19	0.30
8	0.73	0.67	0.06
9	0.32	-0.19	0.51
10	0.00	0.59	-0.59
11	-0.22	0.41	-0.63
12	-0.88	0.00	-0.85
13	0.53	-0.06	0.59
14	-1.26	-0.52	-0.77
15	-1.06	1.77	0.72
Mean Diff. (%)	-0.31	-0.32	0.02
S.D. (%)	0.70	0.69	0.56

Table 2: Reproducibility (%) of U and Pu determination from 2 repeat IDMS analyses and 3 repeat K-Edge/K-XRF measurements (counting time 1000 s).

Input Sample	IDMS		K-Edge/K-XRF	
	U	Pu	U	Pu
1	*	0.45	0.13	0.48
2	0.1	0.2	0.19	0.28
3	0.4	0.2	0.32	1.69
4	0.06	0.5	0.02	0.88
5	0.3	1.2	0.44	0.95
6	0.1	0.3	0.23	0.87
7	0.1	*	0.28	1.15
8	0.0	0.6	0.31	0.50
9	0.1	0.2	0.34	0.40
10	0.2	0.1	0.07	0.96
11	0.2	0.05	0.26	0.26
12	0.5	0.4	0.14	1.26
13	0.02	0.7	0.12	1.23
14	0.04	*	0.17	0.46
15	0.3	0.5	0.02	1.29
Mean	0.17	0.42	0.20	0.84

* Only 1 aliquot analysed

Very good agreement between NDA and DA has been so far obtained from all available results for the U/Pu ratio. For the present data set the mean difference is 0.02 % with a standard deviation of 0.56 %. When averaging over all available experimental data, a standard deviation of about 0.8 % is observed as a representative value for the compared U/Pu ratios from NDA and DA. This is well within the range of expectation.

(1) H. Ottmar, H. Eberle, Annual Report 1984/85, KfK 3969 (1985) 203.

+ European Institute for Transuranium Elements, Karlsruhe

6.4.13 KFKPU - A COMPUTER PROGRAM FOR THE EVALUATION OF THE PLUTONIUM ISOTOPIC COMPOSITION FROM GAMMA SPECTRA

P. Matussek

The non-destructive determination of the plutonium isotopic composition by means of high-resolution gamma-ray spectrometry is being widely used for the characterization of plutonium bearing materials in the nuclear fuel cycle. However, due to the complexity of the measured gamma spectra sophisticated data evaluation techniques are required in order to arrive at accurate results. Especially the determination of the ^{240}Pu content may present problems because of strong interferences of the characteristic ^{240}Pu gamma radiation with gamma lines emitted from other isotopes, thus requiring complex unfolding procedures of the gamma-line multiplets. Moreover, the sample characteristics of plutonium materials in the nuclear fuel cycle may differ significantly with respect to parameters such as size, geometry, matrix, canning, age, burn-up etc. This may necessitate different approaches for the counting equipment used (detectors) and for the selection of the spectral range to be analyzed if the highest possible accuracy for a particular measurement problem is required.

Therefore the computer program 'KFKPU' has been developed (1) that provides a high degree of flexibility, and that can easily be tailored to varying measurement problems. The data evaluation methodology includes the following principle steps:

- Energy calibration,
- Determination of the peak-shape parameters using two reference gamma lines,
- Subtraction of the background continuum,
- Evaluation of net-peak counting rates using least-squares-fit techniques,
- Determination of the total counting efficiency as a function of the gamma-ray energy,
- Determination of Pu isotope ratios from selected pairs of efficiency-corrected gamma peaks.

All relevant evaluation parameters can be selected by the user according to his needs: the reference peaks used, the gamma lines and the energy regions of interest, the windows for the subtraction of the background continuum, the peaks to be included in the efficiency evaluation, the values of the gamma branchings used for the determination of the isotope ratios from the peak-area ratios, etc. In addition to this several options are provided with the program 'KFKPU', as, e.g., alternate peak-shape parametrizations, peak stripping, split background subtraction. The flow of the evaluation program and the selection of various options is controlled by the evaluation parameters and the control parameters, respectively. All parameters are combined in a parameter list and are stored separately from the code portion of the program. This concept allows easy modifications of the evaluation program simply by changing the parameter list, thus avoiding the time-consuming and error-prone recompilation of the program when changes are required.

At present the program 'KFKPU' is implemented in a small microprocessor-controlled, NIM based multichannel analyzer system. The parameter list is contained in a separate EPROM. Program modifications require the exchange of the parameter EPROM. In future assay systems equipped with fast mass storage devices (e.g.,floppy disks) various sets of parameter lists can be stored and can be loaded according to the particular measurement problem. The program 'KFKPU' is considered as a first step towards an expert system for gamma-spectrometric plutonium isotope assay.

(1) P. Matussek, Report JOPAG/04.86-PRG-129, Kernforschungszentrum Karlsruhe (1986)

6.4.14 INVESTIGATIONS OF X-RAY FLUORESCENCE FOR URANIUM MONITORING IN A REPROCESSING PLANT

I. Michel-Piper, H. Ottmar

For automated control of the uranium concentration in aqueous and organic waste streams of a reprocessing plant the use of in-line instrumentation is highly desirable. The expected uranium concentration in the waste streams of the first three extraction cycles considered here typically range from about 10 mg/l (1 CW stream) to about 100 mg/l (2 DW stream). The plutonium content in the waste streams is much lower than the uranium content (by a factor of 10^2 to 10^6), so that interferences are not expected. However, one should remark that the neptunium concentration may be in the same order of magnitude as that of uranium in some cases. The expected total activity of fission products is in the range of $2x10^4$ to $2x10^8$ Bq/l.

Given these boundary conditions the X-ray fluorescence analysis (XRFA) seems to be a candidate for solving the measurement problems. Therefore we have investigated the potential of the XRFA as an in-line instrument for monitoring the uranium concentration in particular waste streams of a reprocessing plant. The work is restricted to energy-dispersive XRFA.

Many parameters will influence the performance of an energy-dispersive XRFA instrument:

1. The energy of the observed X-rays
   K-X-Rays at about 100 keV
   L-X-Rays between about 13 to 17 keV

2. Selection of the excitation radiation
   Radioactive gamma- or X-ray sources
   Radiation from suitably filtered X-ray tubes
   - thin-anode line emitting tube
   - thick-anode emitting bremsstrahlung continuum

   use of secondary X-ray emitters stimulated by gamma- or X-rays

3. Selection of the X-ray detector
   High-resolution semiconductor detector operated at liquid-nitrogen temperature (Si(Li))
   Semiconductor detector operated with peltier cooling (here stabilized at room temperature)
   Scintillation detector or proportional counter.

Certain selection criteria have to be applied in order to arrive at a suitable in-line instrument for monitoring the uranium concentration in waste streams:

- a lower detection limit of below 10 mg U/l is required
- the counting time should not exceed about 1000 s per assay

- the instrument should be simple and ruggedized with low maintenance requirements and low operating costs
- high operating stability is required
- a single type of instrument should be used for measurements at various waste streams.

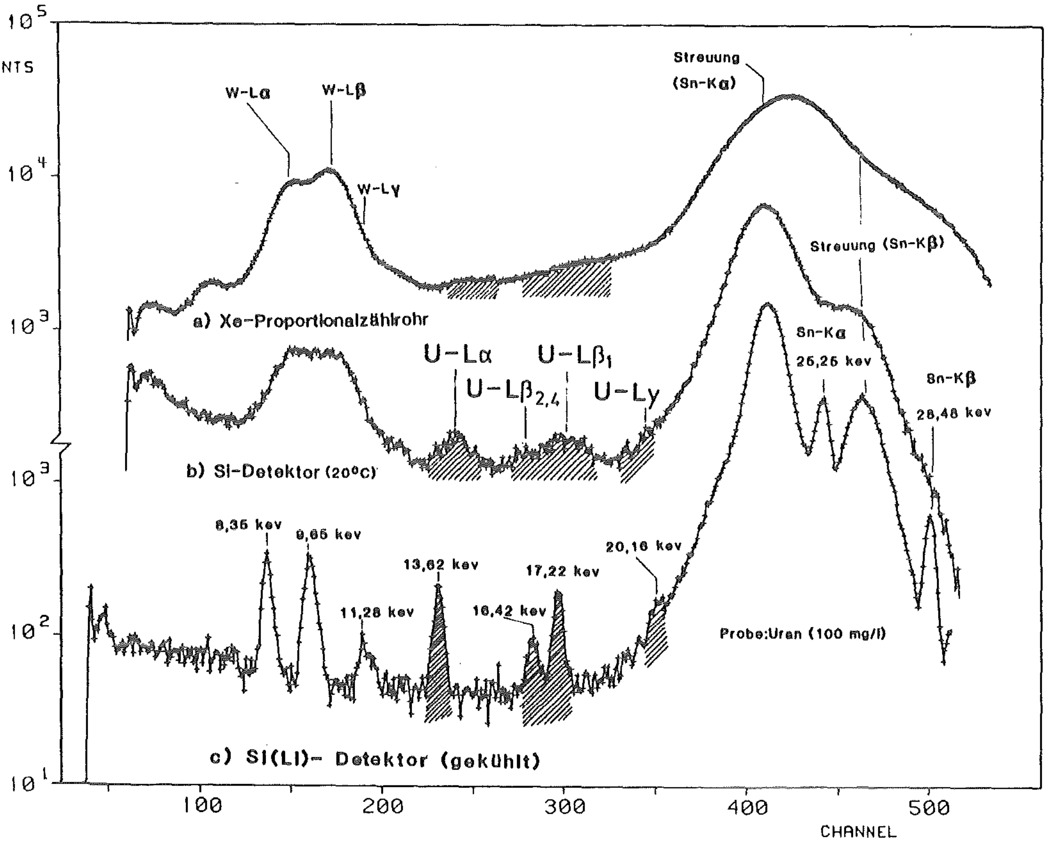

Fig. 1 Uranium XRFA spectra taken with three different detectors
a) Xe proportional counter
b) Si detector operated at room temperature
c) high-resolution Si(Li) detector operated at liquid nitrogen temperature

Target: uranium solution 100 mg U/l
Radiation source: Sn K-X-rays stimulated by a ^{241}Am source

Several experiments have been carried out to identify suitable excitation sources and detectors. The investigations were concentrated on the uranium L-X-rays because of their higher sensitivity. Measurements have been performed with a ^{241}Am source and a thick-anode tungsten X-ray tube as radiation sources, using both the direct and secondary excitation mode. The performance study is not yet completed, but preliminary results can be given. As an example, Fig. 1 shows the uranium XRFA spectra taken with three different detectors. In all three cases the sample was an inactive uranium solution with an uranium concentration of 100 mg U/ℓ, and the excitation radiation was Sn K-X-rays stimulated by a ^{241}Am source. The uranium X-ray peaks are indicated by hatched areas in the figure. The energy resolution

Table 1 Lower detection limits (LDL) of uranium concentrations using different detectors

	High-resolution Si(Li)	Si detector at room temperature	Xe proportional counter
Lower detection limit	3 mg U/ℓ	5 mg U/ℓ	25 mg U/ℓ

and, accordingly, the sensitivity of the detectors show an improvement from top to bottom in Fig. 1. The corresponding lower detection limits for the detectors are shown in Table 1. The lower detection limit (LDL) is defined here at the 3σ level, i.e., the LDL is reached if the net counts in the X-ray peak are equal to three times the expected statistical error in the background below the peak. Further it was assumed that the analyzing system is capable to handle 10.000 events per second, and that the counting time is 10 min, resulting in a number of 6×10^6 events analyzed. Therefore all measurements were normalized to 6×10^6 total counts. In practical applications strong ^{241}Am sources (Ci) will be necessary to arrive at a total counting rate of 10.000 cps. in the secondary excitation mode. Table 1 shows that with this premise a Si detector operated at room temperature will meet the requirements of in-line uranium concentration assays.

6.4.15 PRODUCTION OF ISOTOPES FOR MEDICAL APPLICATIONS

K.H. Assmus, S. Augstein, V. Bechtold, H.D. Dennerlein,
H. Dohrmann, D. Erbe, E. Foßhag, A.Hanser, R. Hüfner, N.Kernert,
W. Maier, J.W. Peters, H. Ripp, U. Sahm, M. Seidler,
H. Schweickert, S. Sheikh, S. Uhlemann

Radioisotopes for applications in nuclear medicine are produced routinely at the compact cyclotron (CP42H$^-$). The customers are several pharmaceutical companies and research hospitals in Germany. The status of the various isotopes is discussed in the following:

Ultra-pure I-123

Compared to last year the demand for I-123 has again increased by 20 %. This could be fulfilled by taking the new target system into operation, which has a production capacity 3 times higher than the old one.

This new target system (fig. 1) is characterized by:

- a high production yield
- continuous operation
- microprocessor control
- remote target-window changer
- low dose rate to personnel

A duplicate of the production target system could be sold as a 'push button ready system' to a radiopharmaceutical company in Japan. This system will be ready for first production runs in Japan in September 86.

Rb-81/Kr-81m-Generator

The routine production of generators could be increased by 50 % compared to last year. The main production was used for generators for ventilation studies in hospital. A third of the generators are delivered for subsequent mass-separation in order to produce ultra-pure Rb-81 for IV-injection. Improvements have been made in the application system 'Kryptovent' such as simplified handling and reduction of radiation exposure.

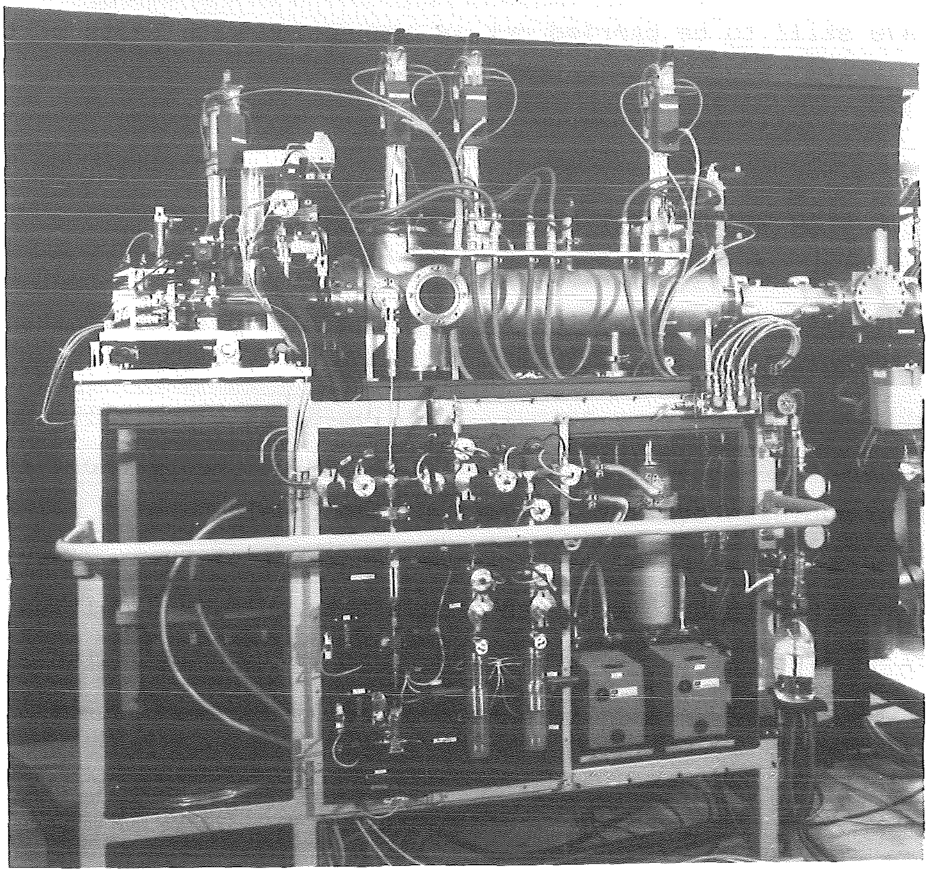

Fig. 1: New I-123 production target with diagnostic system

Rb-81/Kr-81m liquid generator

In FRG there is a certain demand for the application of Kr-81m not only for lung ventilation but also for perfusion- and myocardial studies. From the pharmaceutical viewpoint the infusion of dissolved Kr into the human blood system is more difficult than breathing Kr-contaminated air. Therefore at the end of 1984 the development of a modified Rb/Kr generator system and a new corresponding application system was initiated.

The application system allows the alternative usage of Kr-81m either dissolved in water or added to breathing air. A prototype of the application system, controlled by two independently working microprocessors is now under construction. Most of the components consist of commercially available modules.

The resin of the generator column was selected by considering the distribution, capacity and breakthrough of Rb-activity, as well as the elution efficiency when eluting the generator with poor 'aqua injectabilia'.

The elution efficiency is in the range of 80 to 90 % at flow rates of 10 to 15 ml per minute. The Rb breakthrough is less than 20 ppm per liter eluent up to a volume of 6 l corresponding to more than 6 h continuous operation. Pharmaceutical tests concerning sterility and pyrogenity of the generator have still to be carried out in connection with tests of the loading equipment.

6.4.16 BLOOD FLOW MEASUREMENT USING ULTRA-PURE RB-81

U. Baßler, J. Bialy, J.W.Peters, M. Schmitt,

Up till now, no method is known for routine medical application to measure the blood flow quickly, noninvasively, and exactly. In many situations this possibility would be very helpul. Rubidium-81 is especially qualified for this purpose because of its physical and chemical properties. Injected intravenously, Rubidium behaves similarily to potassium, being principally incorporated within the intracellular pool. Radioactive Rb-81 decays with a half live of 4.6 h to Kr-81m, which decays to stable Kr-81 with a half live of only 13 s. While the amount of Rb-81 in the intracellular space changes only relatively slowly, Kr-81m, being a freely diffusible inert-

gas, is washed out instantly by the regional blood flow. So the ratio of Kr-81m to Rb-81 is a good measure of the blood flow.
For a fast and accurate determination of this ratio, there are two main difficulties to overcome. First, the energy resolution of the detection system must be good enough to clearly resolve the different gamma-lines of Rb-81 and Kr-81m for fast automatic activity determination. Second, the use of pure Rb-81 is necessary, because radioactive contaminants (esp. Rb-82m) severely increase the number of decay lines and the amount of Compton background.

Worldwide ultra-pure Rb-81 is only produced routinely at the Karlsruhe cyclotron laboratory.But normal medical gamma camera systems are not applicable for the Rb-Kr method because of their bad energy resolution. So a data acquisition and analysing system has been designed, which meets the necessary requirements. It consists of a high-purity Ge-detector, analog and digital electronics, which are all able to handle extremely high data rates.

For this system data acquisition and processing software was written. Main attention was given to a flexible and modular design to enable later modifications and additions without the need of changes in the basic routines. Also easy handling was taken into account.

The complete system was set up in a first version during the last year. First tests and phantom measurements have already been carried out successfully (Fig. 1).

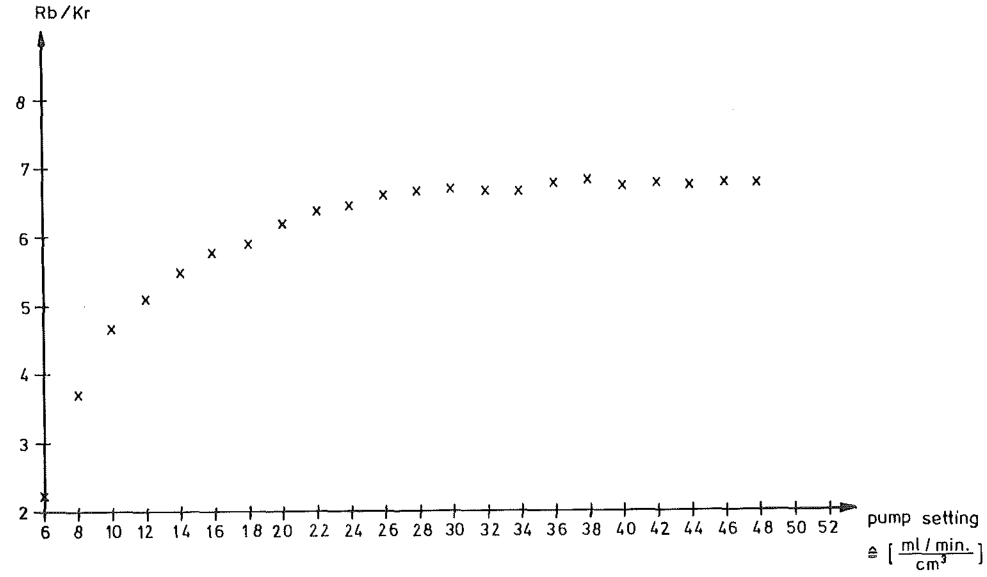

Fig. 1: Results of a phantom measurement

6.4.17 ACTIVATION OF MACHINE PARTS FOR MECHANICAL ENGINEERING

E. Bollmann, P. Fehsenfeld, B. Gegenheimer, H. Roth, A.Kleinrahm

The activation service, supplying radioactively labeled machine components to industry and research institutes, increased by about 20 % compared to the preceding year. A positive aspect is the start of two more important companies in applying the radionuclide technique for corrosion and wear measurements: One great firm of the chemical engineering industry, the other new customer is an important manufacturer of marine diesel engines.

The second stage of the new facility for serial activation has been installed and put into operation at the end of the year 85 (see Fig. 1)

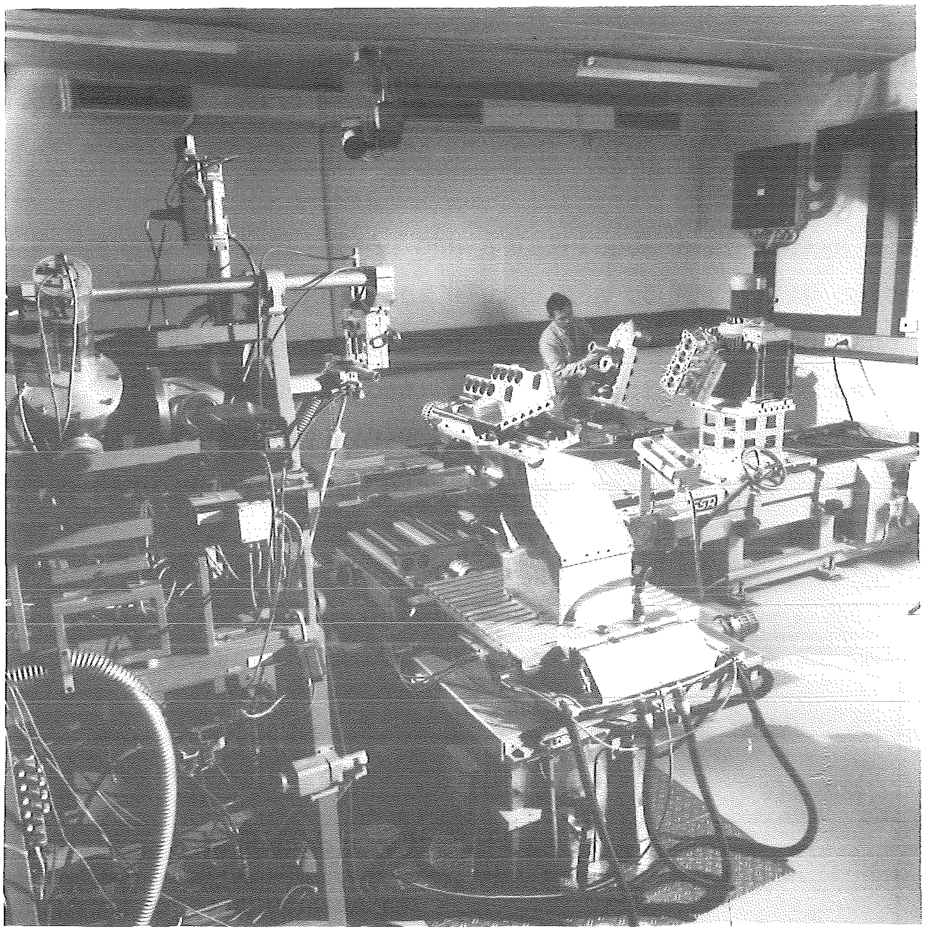

Fig. 1: The fully automatic, computer controlled system for serial irradiation of machine components at the Karlsruhe Compact Cyclotron (KAZ). From the left: The head of the beam tube with the aiming and adjusting device, in front of that the positioning unit with the machine parts to be activated on it, adjacent the friction wheel supply system, bearing six standard plates. Up to 50 small parts or six larger parts of different form and weight (max. 6000 N) can be mounted on the plates and irradiated in one batch.

In developing the thin layer activation technique to new industrial materials and new forms of machine components and in testing new measuring methods for maximum accuracy, the engine test bench and the tribometer apparatus have been used intensively. Primary parameters for thin layer activation of ceramic materials have been established and have to be optimized in subsequent work.

The wear behavior of ion implanted nitrogen steel compared to unimplanted material and simple salt bath hardened steel has been measured with the radionuclide technique at the tribometer apparatus in the region of mixed friction. The ion implanted material did not show any improvement against the unimplanted steel, but a higher wear rate was measured compared to the salt bath hardened material.

7. LIST OF PUBLICATIONS

7.1 PUBLICATIONS AND REPORTS

ABELA, R.; BACHER, R.; BLUEM, P.; GOTTA, D.;
KUNOLD, W.; MISSIMER, J.; SCHNEIDER, M.;
SIMONS, L.M.
Cascade studies in light muonic atoms at high
stop densities.
SIN-Newsletter, 17(1985) S.NL38

AKER, E.; BRISSOT, R.; ENGELHARDT, D.;
GELTENBORT, P.; GINDLER, J.; GOENNENWEIN, F.;
OED, A.; WILKINS, B.
Mass and energy distribution of fission
fragments in ^{249}Cf(nth, f).
Proc.of the Internat.Conf.on Nuclear Data for
Basic and Applied Science, Santa Fe, N.M.,
May 13-17, 1986

ALBINSKI, J.; BUDZANOWSKI, A.; DABROWSKI, H.;
ROGALSKA, Z.; WIKTOR, S.; REBEL, H.;
SRIVASTAVA, D.K.; ALDERLIESTEN, C.; BOJOWALD,
J.; OELERT, W.; MAYER-BOERICKE, C.;
TUREK, P.
α-particle scattering from Ni-isotopes at
$E(\alpha)=172.5$ MeV.
Nuclear Physics A, 445(1985) S.477

ANSELMENT, M.; BEKK, K.; HANSER, A.;
HOEFFGEN, H.; MEISEL, G.; GOERING, S.; REBEL,
H.; SCHATZ, G.
Charge radii and moments of tin nuclei by
laser spectroscopy.
KfK-4071

ANSELMENT, M.; FAUBEL, W.; GOERING, S.;
HANSER, A.; MEISEL, G.; REBEL, H.; SCHATZ, G.
The odd-even staggering of the nuclear charge
radii of Pb isotopes.
Nuclear Physics A, 451(1986) S.471

BACKENSTOSS, G.; IZYCKI, M.; KOWALD, W.;
WEBER, P.; WEYER, H.J.; LJUNGFELT, S.;
MANKIN, U.; SCHMIDT, G.; ULLRICH, H.
Measurement of the ratio
$(\pi^- {}^3He \to \pi^0 t)/(\pi^- {}^3He \to dn)$ and of the respective
partial K X-ray yields.
Nuclear Physics A, 448(1986) S.567

BACKENSTOSS, G.; IZYCKI, M.; SALVISBERG, P.;
STEINACHER, M.; WEBER, P.; WEYER, H.J.;
CIERJACKS, S.; LJUNGFELT, S.; ULLRICH, H.;
FURIC, M.; PETKOVIC, T.
Evidence for a direct three-nucleon
pion-absorption process.
Physical Review Letters, 55(1985) S.2782

BECK, R.; DICKMANN, F.; LOVAS, R.G.
Quasielastic cluster knock-out reactions and
the microscopic cluster model.
Nuclear Physics A, 446(1985) S.703

BEER, H.
s-process nucleosynthesis below A=90.
Audouze, J. [Hrsg.]
Proc. of the NATO Advanced Research Workshop,
5th Moriond Astrophysics Meeting,
Les Arcs, F, March 17-23, 1985
Dordrecht [u.a.] : Reidel, 1986. - S.263

BEER, H.
A measurement of the ^{139}La capture cross
section and a study of the s-process at magic
neutron number 82.
Astronomy and Astrophysics, 162(1986) S.330

BEER, H.; WALTER, G.
Analysis of Zr and Tc abundances from S-stars
using the s-process with an exponential
distribution of neutron exposures.
Jaschek, M. [Hrsg.]
Cool Stars with Excesses of Heavy Elements :
Proc.of the Strasbourg Observatory
Colloquium, Strasbourg, F, July 3-6, 1984
Dordrecht [u.a.] : Reidel, 1985. - S.373

BEER, H.; WALTER, G.; MACKLIN, R.L.
The ^{163}Dy-^{163}Ho branching: an s-process
barometer.
Raman, S. [Hrsg.]
Capture Gamma-Ray Spectroscopy and Related
Topics : 5th Internat.Symp., Knoxville,
Tenn., September 10-14, 1984
New York, NY : American Inst.of Physics,
1985. - S.778

BEER, H.; WALTER, G.; MACKLIN, R.L.;
PATCHETT, P.J.
Neutron capture cross sections and solar
abundances of (160,161)Dy, (170,171)Yb,
(175,176)Lu, and (176,177)Hf for the
s-process analysis of the radionuclide ^{176}Lu.
In: Quaim, S.M. [Hrsg.]
Progress Report on Nuclear Data Research in
the Federal Republic of Germany for the
Period April 1, 1984 to March 31, 1985
NEANDC(E)-262 U Vol. 5(June 1985) S.11

BEER, H.; MACKLIN, R.L.
supra(198,199,200,201,202,204)Hg(n,γ) cross
sections and the termination of s-process
nucleosynthesis.
Physical Review C, 32(1985) S.738

BEKK, K.; DOLL, P.; WEDDIGEN, CH.; [HRSG.]
Annual report on nuclear physics activities.
KfK-3969

BERTHOLD, G.H.; ZANKEL, H.; MATHELITSCH, L.;
GARCILAZO, H.
Momentum space calculation of ^{3}He bound-state
energies.
Nuovo Cimento A, 93(1986) S.89

BLUEM, P.; BRADAMANTE, F.; CRAWFORD, F.;
[HRSG.]
Feasibility study for a European hadron
facility.
EHF-86-33 (1986) (University of Trieste, I)

BODENKAMP, J.; FRIES, D.C.; MARKOU, A.;
SEITZ, E.; BEHREND, H.J.; HESSE, W.P.;
MIYACHI, T.; MCNEELY JR, W.A.; SCHROEDER, V.
Measurement of the reaction $\gamma p \to ppp$ at photon
energies $4.7 <= E(\gamma) <= 6.6$ GeV.
Nuclear Physics B, 255(1985) S.717

BOSCHITZ, E.T.
The interaction of pions with deuterons.
Symp.'Mesons and Light Nuclei', Bechyne, Cs,
May 27 - June 1, 1985
Czechoslovak Journal of Physics B, 36(1986)
S.215

BROUET, M.; GIRARDINI, M.; PONCET, A.; WOLF,
A.; HUETTEN, L.; POTH, H.; HABFAST, C.
An ultra-high vacuum system for coolers.
Poth, H. [Hrsg.]

ECOOL 1984. Proceedings of the Workshop on
Electron Cooling and Related Applications,
Karlsruhe, September 24-26, 1984
KfK-3846 S.267

CELLO-COLLABORATION
An investigation of the processes $e^+e^-\rightarrow\mu^+\mu^-\gamma$
and $e^+e^-\rightarrow e^+e^-\gamma$.
Physics Letters B, 158(1985) S.536

CELLO-COLLABORATION
A search for single photons at PETRA.
DESY-86-050 (Mai 86) LAL-86-11 (Mai 86)

CELLO-COLLABORATION
Experimental limit on monojet production in
e^+e^--annihilation.
Physics Letters B, 161(1985) S.182

CICHOCKI, T.; HECK, D.; JARCZYK, L.; ROKITA,
E.; STRZALKOWSKI, A.; SYCH, M.
Elemental Composition of the human
atherosclerotic artery wall.
Histochemistry, 83(1985) S.87

CIERJACKS, S.; PETKOVIC, T.; ULLRICH, H.;
GOTTA, D.; LJUNGFELT, S.; SIMICEVIC, N.;
IZYCKI, M.; WEBER, P.; WEYER, H.J.
A large-area position-sensitive
time-of-flight counter for energetic neutrons
and charged particles.
Nuclear Instruments and Methods A, 238(1985)
S.354

CIERJACKS, S.; HINO, Y.; RAUPP, F.; HOWE,
S.D.; BUTH, L.
Systematics of angular-dependent neutron
production by 585 MeV protons on targets with
12<=A<=238.
Quaim, S.M. [Hrsg.]
Progress Report on Nuclear Data Research in
the Federal Republic of Germany for the
Period April 1, 1984 to March 31, 1985
NEANDC(E)-262 U Vol. 5(June 1985) S.1

CIERJACKS, S.; HINO, Y.; FILGES, D.;
ARMSTRONG, T.W.; CLOTH, P.
Validation of intranuclear-cascade-
evaporation-model calculations for
proton-induced neutron production.
Quaim, S.M. [Hrsg.]
Progress Report on Nuclear Data Research in
the Federal Republic of Germany for the
Period April 1, 1984 to March 31, 1985
NEANDC(E)-262 U Vol. 5(June 1985) S.1

CLERC, H.G.; LANG, W.; MUTTERER, M.; SCHMITT,
C.; THEOBALD, J.P.; QUADE, V.; RUDOLPH, K.;
ARMBRUSTER, P.; GOENNENWEIN, F.; SCHRADER,
H.; ENGELHARDT, D.
Cold fragmentation in thermal-neutron-induced
fission of ^{233}U and ^{235}U.
Nuclear Physics A, 452(1986) S.277

CORVI, F.; BASTIAN, C.; WISSHAK, K.
Neutron capture in the 1.15-keV resonance of
^{56}Fe using Moxon-Rae detectors.
Nuclear Science and Engineering, 93(1986)
S.348

DIERCKX, R.; KLEY, W.; VERGA, A.; BENTON,
E.V.; BUSCHMANN, J.
The stopping of deuterons in lithium.
Nuclear Engineering and Design/Fusion,
2(1985) S.337

DOERR, M.; FETSCHER, W.; GOTTA, D.; REICH,
J.; ULLRICH, H.; BACKENSTOSS, G.; KOWALD, W.;
WEYER, H.J.
Composite particle emission following
π^--absorption in ^6Li.
Nuclear Physics A, 445(1985) S.557

DOLL, P.; FINK, G.; BRADY, F.P.; GARRETT, R.;
KLAGES, H.O.; KRUPP, H.
ΔE-E telescope systems for detecting charged
particles produced with a 'white' neutron
beam.
Nuclear Instruments and Methods A, 250(1986)
S.526

EGIDY, T.VON; KANERT, W.; HARTMANN, F.J.;
DANIEL, H.; MOSER, E.; SCHMIDT, G.; REIDY,
J.J.; NICHOLAS, M.; LEON, M.; POTH, H.;
BUECHE, G.; HANCOCK, A.D.; KOCH, H.; KOEHLER,
TH.; KREISSL, A.; RAICH, U.; ROHMANN, D.;
CHARDALAS, M.; DEDOUSSIS, S.; SUFFERT, M.;
NILSSON, A.
Antiprotonic molybdenum: resonant coupling of
atomic and nuclear states and the impact of
annihilation on the nucleus (PS 186).
Pennington, M.R. [Hrsg.]
Antiproton: Proc.of the 7th European Symp.on
Antiproton Interactions, Durham, GB, July
9-13, 1984
Bristol[u.a.]: Hilger, 1985. - S.181

ENGLER, J.; KEIM, H.; WILD, B.
Performance test of a TMS calorimeter.
KfK-4085

FLUEGGE, G.
Search for new particles in e^+e^-
annihilation.
KfK-4035

FLUEGGE, G.
Jet fragmentation.
KfK-4034

FLUEGGE, G.
Experimentelle Aspekte der
Elementarteilchenphysik.
Umschau, 86(1986) S.222-27
Fridericiana - Zeitschrift der Universitaet
Karlsruhe, (1986) Nr. 36, S.24-33

FUCHS, K.; EYRICH, W.; HOFMANN, A.;
MUEHLDORFER, B.; SCHEIB, U.; SCHLOESSER, H.;
REBEL, H.
Neutron decay of the isoscalar giant
resonance region in ^{90}Zr.
Physical Review C, 32(1985) S.418

GARCILAZO, H.; MATHELITSCH, L.; ZANKEL, H.
Relativistic effects in the neutron-deuteron
scattering lengths.
Physical Review C, 32(1985) S.264

GYLES, W.; BOSCHITZ, E.T.; GARCILAZO, H.;
LIST, W.; MATHIE, E.L.; OTTERMANN, C.R.;
SMITH, G.R.; TACIK, R.; JOHNSON, R.R.
$\pi^+d\rightarrow\pi^+pn$ reaction as a test of relativistic
Faddeev theories: Differential cross section.
Physical Review C, 33(1986) S.583

GYLES, W.; BOSCHITZ, E.T.; GARCILAZO, H.;
MATHIE, E.L.; OTTERMANN, C.R.; SMITH, G.R.;
MANGO, S.; KONTER, J.A.; JOHNSON, R.R.
$\pi^+d\rightarrow\pi^+pn$ reaction as a test of relativistic
Faddeev theories: Vector analyzing power.
Physical Review C, 33(1986) S.595

HABFAST, C.; POTH, H.; SELIGMANN, B.;
HASEROTH, H.; HILL, C.E.; VALLET, J.L.; WOLF,
A.
Status and perspectives of the electron
cooling device under construction at CERN.
Gastaldi, U. [Hrsg.]
Physics with Antiprotons at LEAR in the Acol
: Proc.of the 3rd LEAR Workshop, Tignes, F,
January 12-26, 1985
Gif-sur-Yvette : Ed. Frontieres, 1985. -
S.129

HABFAST, C.; POTH, H.; SELIGMANN, B.; WOLF, A.
An alternative concept for high-voltage systems used in electron cooling.
Nuclear Instruments and Methods A, 248(1986) S.562

HARTMANN, F.J.; DANIEL, H.; KANERT, W.; MOSER, E.; SCHMIDT, G.; EGIDY, T.VON; REIDY, J.J.; NICHOLAS, M.; LEON, M.; POTH, H.; BUECHE, G.; HANCOCK, A.D.; KOCH, H.; KOEHLER, TH.; KREISSL, A.; RAICH, U.; ROHMANN, D.; CHARDALAS, M.; DEDOUSSIS, S.; SUFFERT, M.; NILSSON, A.
The antiprotonic X-ray cascade in Mo isotopes.
Pennington, M.R. [Hrsg.]
Proc.of the 7th European Symp.on Antiproton Interactions, Durham, GB, July 9-13, 1984
Bristol[u.a.]: Hilger, 1985. - S.507

HASEROTH, H.; HILL, C.E.; VALLET, J.L.; HABFAST, C.; HUETTEN, L.; POTH, H.; WOLF, A.
The LEAR electron cooler.
Poth, H. [Hrsg.]
ECOOL 1984. Proceedings of the Workshop on Electron Cooling and Related Applications, Karlsruhe, September 24-26, 1984
KfK-3846 S.93

HASSE, R.W.
Semiclassical description of multiparticle-multihole excitations in nuclei.
Di Toro, M. [Hrsg.]
Topical Meeting on Phase Space Approach to Nuclear Dynamics, Trieste, I, September 30 - October 4, 1985.
Singapore : World Scientific 1986. - S.685

HEERINGA, W.
Static nuclear polarisation and polarised targets.
Hyperfine Interactions, 22(1985) S.263

HEERINGA, W.; AURES, R.; MASCHUW, R.; SCHMIDT, F.K.
Brute-force polarization and demagnetization of protons in TiH$_2$.
Cryogenics, 25(1985) S.369

HOFMANN, K.
Untersuchungen zum Neutron-Deuteron-System im Energiebereich von 20 bis 50 MeV.
KfK-4008

HOPP, G.
Energieabhaengigkeit von Jet-Strukturen und Bestimmung der starken Kopplungskonstanten αsub(s) in der e^+e^- annihilation mit dem Detektor CELLO.
KfK-3952

KAEPPELER, F.
s-process nucleosynthesis - stellar aspects and the classical model.
Audouze, J. [Hrsg.]
Nucleosynthesis and its Implications on Nuclear and Particle Physics : Proc.of the NATO Advanced Research Workshop, 5th Moriond Astrophysics Meeting,
Les Arcs, F, March 17-23, 1985
Dordrecht [u.a.] : Reidel, 1986. - S.253

KAEPPELER, K.; WALTER, G.; MATHEWS, G.J.
Stellar neutron capture rates for ^{46}Ca and ^{48}Ca.
Qaim, S.M. [Hrsg.]
Progress Report on Nuclear Data Research in the Federal Republic of Germany for the Period April 1, 1984 to March 31, 1985
NEANDC(E)-262 U Vol. 5(June 1985) S.7

KANERT, W.; HARTMANN, F.J.; DANIEL, H.; MOSER, E.; SCHMIDT, G.; EGIDY, T.VON; REIDY, J.J.; NICHOLAS, M.; LEON, M.; POTH, H.; BUECHE, G.; HANCOCK, A.D.; KOCH, H.; KOEHLER, TH.; KREISSL, A.; RAICH, U.; ROHMANN, D.; CHARDALAS, M.; DEDOUSSIS, S.; SUFFERT, M.; NILSSON, A.
First observation of the E2 nuclear-resonance effect in antiprotonic atoms.
Physical Review Letters, 56(1986) S.2368

KLAGES, H.O.; HEERINGA, W.; DOBIASCH, H.; FISCHER, R.; HAESNER, B.; SCHWARZ, P.; WILCZYNSKI, J.; ZEITNITZ, B.
Analyzing power of the n-^{3}He elastic scattering from 3.7 to 22.0 MeV.
Nuclear Physics A, 443(1985) S.237

KOCH, H.
Antiprotonische Atome bei LEAR.
KfK-Nachrichten, 17(1985) S.49

KOCH, H.; BUECHE, G.; HANCOCK, A.D.; HAUTH, J.; KOEHLER, TH.; KREISSL, A.; POTH, H.; RAICH, U.; ROHMANN, D.; FINDEISEN, CH.; REPOND, J.; TAUSCHER, L.; NILSSON, A.; CARIUS, S.; SUFFERT, M.; CHARALAMBUS, S.; CHARDALAS, M.; DEDOUSSIS, S.; EGIDY, T.VON; HARTMANN, F.J.; KANERT, W.; REIDY, J.J.; NICHOLAS, M.
Antiprotonic atom sepctroscopy at LEAR.
Pennington, M.R. [Hrsg.]
Antiproton: Proc.of the 7th European Symp.on Antiproton Interactions, Durham, GB, July 9-13, 1984
Bristol[u.a.]: Hilger, 1985. - S.175

KOCH, H.
CsI-crystal-barrel at LEAR.
Gastaldi, U. [Hrsg.]
Physics with Antiprotons at LEAR in the Acol : Proc.of the 3rd LEAR Workshop, Tignes, F, January 12-26, 1985
Gif-sur-Yvette : Ed. Frontieres, 1985. - S.389

KOEHLER, TH.; BLUEM, P.; BUECHE, G.; HANCOCK, A.D.; KOCH, H.; KREISSL, A.; POTH, H.; RAICH, U.; ROHMANN, D.; BACKENSTOSS, G.; FINDEISEN, CH.; REPOND, J.; TAUSCHER, L.; NILSSON, A.; CARIUS, S.; SUFFERT, M.; CHARALAMBUS, S.; CHARDALAS, M.; DEDOUSSIS, S.; DANIEL, H.; EGIDY, T.VON; HARTMANN, F.J.; KANERT, W.; SCHMIDT, G.; REIDY, J.J.; NICHOLAS, M.; WOLF, A.
Precision measurement of strong interaction isotope effects in antiprotonic ^{16}O, ^{17}O, and ^{18}O atoms.
Physics Letters B, 176(1986) S.322

KOZIK, T.; BUSCHMANN, J.; NEUDOLD, M.
A gas-silicon telescope for medium-heavy ion detection.
KfK-3988B

KREISSL, A.
Messung des magnetischen Momentes des Antiprotons und eine Bestimmung des LS-Terms der Antiproton-Kern-Wechselwirkung.
KfK-4128

KUESTER, H.
Search for supersymmetric particles at PETRA.
KfK-4011

KUHN, E.; JOHNSON, S.; KOCH, L.; OTTMAR, H.;
STOJANIK, B.
Characterization of calibration solutions for
the KfK K-edge densitometer and the hybrid
K-edge/K-XRF solution assay system.
JOPAG/10.85-PRG-118

LOVAS, R.G.
On Fliessbach's approaches to direct
reactions.
Zeitschrift fuer Physik A, 322(1985) S.589

MARTOFF, C.J.; POCANIC, D.; WHITLOW, L.W.;
HANNA, S.S.; ULLRICH, H.; CIERJACKS, S.;
FURIC, M.; PETKOVIC, T.; WEYER, H.J.
Search for the emission of nucleons and
nucleon pairs following muon capture in
selected light nuclei.
Czechoslovak Journal of Physics B, 36(1986)
S.378

MATHELITSCH, L.; GARCILAZO, H.
Separable potentials for relativistic
three-body calculations of the NNN, $NN\pi$, $N\pi\pi$,
and $\pi\pi\pi$ systems.
Physical Review C, 32(1985) S.1635

MATHEWS, G.J.; KAEPPELER, F.
Neutron capture nucleosynthesis of neodymium
isotopes and the s-process from A = 130 to
150.
The Astrophysical Journal, 286(1984) S.810

METZLER, M.
Untersuchung der magnetoptischen
Eigenschaften des Magnetspektrometers LEPS.
KfK-4010B

MICEK, S.; REBEL, H.; GILS, H.J.;
KLEWE-NEBENIUS, H.; ZAGROMSKI, S.;
SRIVASTAVA, D.K.
Single nucleon transfer reactions in ^{6}Li+^{6}Li
collisions at 156 MeV.
Nuclear Physics A, 435(1985) S.621

MONTOYA, M.; HASSE, R.W.; KOCZON, P.
Coulomb effects in cold fission.
Informe Nuclear, 3(1986) S.54

MUELLER, M.; OBERHAUSEN, E.; STOLL, H.P.;
SCHMIDT, E.L.; HANSER, A.; VOGEL, W.
^{81}Rubidium (81m)Krypton-SPECT-
Untersuchungen zur Beurteilung hochgradiger
Koronarstenosen.
Herz-Kreislauf, 18(1986) S.128

NAQVI, A.A.; KAEPPELER, F.; DICKMANN, F.;
MUELLER, R.
Fission fragment properties from fast neutron
induced fission of ^{237}Np.
Physical Review C, 34(1986) S.218

OBERHAUSEN, E.; HANSER, A.; STEINSTRAESSER,
A.; MUELLER, M.; SCHMIDT, E.L.; BERBERICH, R.
Measurements of regional perfusion of the
myocard by recording the distribution of
^{81}Rb-(81m)Kr with a SPECT-system.
Hoefer, R.; Bergmann, H. [Hrsg.]
Radioaktive Isotope in Klinik und Forschung.
Bd. 17 1986 S.233
Wien: Egermann

OTTERMANN, C.R.; BOSCHITZ, E.; GYLES, W.;
LIST, W.; TACIK, R.; MANGO, S.; KONTER, J.A.;
VAN DEN BRANDT, B.; SMITH, G.R.
Measurement of the $\pi d \rightarrow pp$ reaction at T
= 65 MeV.
Physical Review C, 33(1986) S.1802

OTTERMANN, C.R.; BOSCHITZ, E.T.; GYLES, W.;
LIST, W.; TACIK, R.; JOHNSON, R.R.; SMITH,
G.R.; MATHIE, E.L.
Large angel πd scattering in the region of
the (3,3) resonance.
Physical Review C, 32(1985) S.928

OTTMAR, H.; EBERLE, H.; MATUSSEK, P.;
MICHEL-PIPER, I.
How to simplify the analytics for
input-output accountability measurements in a
reprocessing plant.
KfK-4012

OTTMAR, H.; EBERLE, H.; MICHEL-PIPER, I.;
KUHN, E.; JOHNSON, S.
Calibration of X-ray densitometers for the
determination of uranium and plutonium
concentrations in reprocessing input and
product solutions.
JOPAG/11.85-PRG-123

PILKUHN, H.; POTH, H.
An ion beam lamp for monochromatic X-rays.
Poth, H. [Hrsg.]
ECOOL 1984. Proceedings of the Workshop on
Electron Cooling and Related Applications,
Karlsruhe, September 24-26, 1984
KfK-3846 S.413

POTH, H.; [HRSG.]
ECOOL 1984. Proceedings of the workshop on
electron cooling and related applications,
Karlsruhe, September 24-26, 1984.
KfK-3846

POTH, H.
Review of electron cooling experiments.
Poth, H. [Hrsg.]
ECOOL 1984. Proceedings of the Workshop on
Electron Cooling and Related Applications,
Karlsruhe, September 24-26, 1984
KfK-3846 S.45

ROTH, H.; BOLLMANN, E.; SCHUESSLER, B.
Verfahren und Einrichtung zur Messung der
Energie geladener Teilchen.
DE-OS 34 12 978

SAKURAGI, Y.; KAMIMURA, M.; MICEK, S.; REBEL,
H.; GILS, H.J.
^{6}Li break-up effect on elastic and inelastic
scattering of ^{6}Li+^{6}Li at 156 MeV.
Zeitschrift fuer Physik A, 322(1985) S.627

SCHAEFER, H.; WISSHAK, K.
CAD-Studien fuer einen 4π Detektor im
Kernforschungszentrum Karlsruhe.
CAD-CAM, 4(1985) S.69

SELIGMANN, B.; ERNST, J.; KLEINFELLER, J.;
KELLER, K.; LASSEN, L.; LUECKING, W.;
SCHRECK, R.; GEMMEKE, H.
Limits of the post-form DWBA from
neutron-proton correlations observed in the
breakup of 15 MeV deuterons on gold.
Physics Letters B, 157(1985) S.345

SPIEKER, C.; HECK, D.; ZIDEK, W.; VETTER, H.
Ca^{2+} analysis in arteries of spontaneously
hypertensive rats by proton-induced X-ray
emission.
Journal of Hypertension, 3(1985) Suppl. 3,
S.S53

SRIVASTAVA, D.K.
Break up of light ions in the nuclear and
Coulomb field of nuclei.
KfK-4007

SRIVASTAVA, D.K.; REBEL, H.
Resonant and nonresonant Coulomb break up of ^{6}Li.
Journal of Physics G, 12(1986) S.717

SRIVASTAVA, D.K.; REBEL, H.
Alternative formulation of post-form distorted-wave Born approximation theory of nuclear breakup.
Physical Review C, 33(1986) S.1221

TACIK, R.; BOSCHITZ, E.T.; GYLES, W.; LIST, W.; OTTERMANN, C.R.
Measurement of three protons in coincidence following absorption of 228 MeV π^{+} in carbon.
Physical Review C, 32(1985) S.1335

THIELEMANN, F.K.; NOMOTO, K.; YOKOI, K.
Explosive nucleosynthesis in carbon deflagration models of Type I supernovae.
Astronomy and Astrophysics, 158(1986) S.17

TRAUTVETTER, H.P.; BECKER, H.W.; HEINEMANN, U.; BUCHMANN, L.; ROLFS, C.; KAEPPELER, F.; BAUMANN, M.; FREIESLEBEN, H.; LUETKE-STETZKAMP, H.J.; GELTENBORT, P.; GOENNENWEIN, F.
Destruction of ^{26}Al in explosive nucleosynthesis.
Zeitschrift fuer Physik A, 323(1986) S.1

WALTER, G.; BEER, H.; KAEPPELER, F.; PENZHORN, R.D.
The s-process branching at ^{85}Kr.
Astronomy and Astrophysics, 155(1986) S.247

WALTER, G.; LEUGERS, B.; KAEPPELER, F.; REFFO, G.; FABBRI, F.
KeV-neutron capture cross sections of the krypton isotopes.
In: Quaim, S.M. [Hrsg.]
Progress Report on Nuclear Data Research in the Federal Republic of Germany for the Period April 1, 1984 to March 31, 1985
NEANDC(E)-262 U Vol. 5(June 1985) S.9
INDC(Ger)-28/LN + Special
Nuclear Science and Engineering, 93(1986) S.357

WEDDIGEN, CH.; JUENGST, W.
Elektronik. Einfuehrung fuer Naturwissenschaftler und Ingenieure.
Berlin [u.a.] : Springer 1986

WEYER, H.J.; BACKENSTOSS, G.; IZYCKI, M.; SALVISBERG, P.; STEINACHER, M.; WEBER, P.; CIERJACKS, S.; LJUNGFELT, S.; ULLRICH, H.; FURIC, M.; PETKOVIC, T.
π-absorption on ^{3}He.
Czechoslovak Journal of Physics B, 36(1986) S.243

WINTERS, R.R.; KAEPPELER, F.; WISSHAK, K.; MENGONI, A.; REFFO, G.
(148,150)Sm: a test for s-process nucleosynthesis.
The Astrophysical Journal, 300(1986) S.41

WISSHAK, K.; KAEPPELER, F.
A 4π barium fluoride detector for precision measurements of neutron capture cross sections in the keV range.
Radiation Effects, 95(1986) S.313

WOLF, A.
Elektronenkuehlung fuer niederenergetische Antiprotonen.
KfK-4023

WOLF, A.; HASEROTH, H.; HILL, C.E.; VALLET, J.L.; HABFAST, C.; POTH, H.; SELIGMANN, B.; BLATT, P.; NEUMANN, R.; WINNACKER, A.; ZU PUTLITZ, G.
Electron cooling of low-energy antiprotons and production of fast hydrogen atoms.
Proc.of a Workshop on the Design of a Low-Energy Antimatter Facility in the USA, Madison, Wis., 1985

YOKOI, K.; TAKAHASHI, K.; ARNOULD, M.
The production and survival of ^{205}Pb in stars, and the ^{205}Pb-^{205}Tl s-process chronometry.
Astronomy and Astrophysics, 145(1985) S.339

7.2 CONFERENCE CONTRIBUTIONS

10th European Symp., Balatonfuered, H, June 3-7, 1985

BECK, R.; DICKMANN, F.; KRUPPA, A.T.; LOVAS, R.G.
Decomposition of ^{6}Li into α+d.

BECK, R.; DICKMANN, F.; LOVAS, R.G.
Appraisal of macroscopic cluster models.

BRADY, F.P.; DOLL, P.; FINK, G.; GARRETT, R.; HEERINGA, W.; HOFMANN, K.; KLAGES, H.O.; KRUPP, H.; WILCZYNSKI, J.
Status of n-p measurements and phase-shift analyses up to 50 MeV neutron energy.

DOLL, P.; GARRETT, R.; HEERINGA, W.; HOFMANN, K.; KLAGES, H.O.; KOIKE, Y.; KRUPP, H.; NITZ, W.
Neutron-deuteron experiments in the energy range up to 50 MeV.

6th Internat.Symp.on Polarization Phenomena in Nuclear Physics, Osaka, J, August 26-30, 1985

DOLL, P.; GARRETT, R.; HALE, G.M.; HEERINGA, W.; JANG, P.; KLAGES, H.O.; MAIER, CHR.
Analyzing powers of elastic n-^{3}He scattering from 1-2 MeV and from 16-50 MeV.

BRADY, F.B.; DOLL, P.; FINK, G.; HEERINGA, W.; HOFMANN, K.; KLAGES, H.O.; NITZ, W.; WILCZYNSKI, J.
Analyzing powers of elastic and inelastic n-d scattering between 16 and 50 MeV.

HEERINGA, W.; KLAGES, H.O.; MAIER, CHR.
Performance and Improvement of the Karlsruhe Polarized Target Facility KRYPTA.

CERN Accelerator School, Oxford, GB, September 25, 1985

POTH, H.
Electron cooling.

Internat.Europhysics Conf.on High Energy Physics, Bari, I, July 18-24, 1985

CELLO-COLLABORATION
Measurement of the muon pair and tau pair asymmetry in e^+e^- annihilations at $39.8<=\sqrt{s}<=46.6$ GeV.

CELLO-COLLABORATION
Search for gauginos in e^+e^- interactions.

CELLO-COLLABORATION
Excited lepton search.

Internat.Symp.on Lepton and Photon Interactions at High Energies, Kyoto, J, August 19-24, 1985

CELLO-COLLABORATION
Search for scalar electrons and photinos in e^+e^- interactions.

CELLO-COLLABORATION
Excited lepton search.

Workshop on Radioactive Ion Beams, Vancouver, CDN, September 4-7, 1985

BECHTOLD, V.; SHEIKH, S.A.
Karlsruhe ECR ion source for radioactive beams.

10th Hawaii Topical Conf. on Particle Physics, Honolulu, Hawaii, August 27, 1985

FLUEGGE, G.
Search for new particles in e^+e^- annihilation.

ARTTA '85 Workshop, Amman, JOR, September 7-14, 1985

KAEPPELER, F.
Neutron physics at Van de Graaff accelerators.

KAEPPELER, F.
Neutron cross section measurements on radioactive isotopes.

40. Tagung der Deutschen Gesellschaft fuer Verdauungs- und Stoffwechselkrankheiten gemeinsam mit der 17. Tagung der Deutschen Gesellschaft fuer Gastroenerologische Endoskopie, Freiburg, 19.-21.September 1985

OCHS, A.; HECK, D.; KELMPNOW, A.; KRATT, C.; MAIER, K.P.; GEROK, W.
Bestimmung der Spurenelementverteilung bei Leberzirrhose mittels protoneninduzierter Roentgenemission (PIXE).

Herbstsitzung der Studiengruppe fuer Nukleare Elektronik, Erlangen, 23.-25.September 1985

GEMMEKE, H.
Neutrinoexperiment KARMEN.

Meeting on the Quark Structure of Matter, Strasbourg, F, September 26 - October 1, 1985

FLUEGGE, G.
Jet fragmentation.

Topical Meeting on Phase Space Approach to Nuclear Dynamics, Trieste, I, September 30 - October 4, 1985

HASSE, R.W.
Semiclassical description of multiparticle-multihole excitations in nuclei.

KTG/ENS Internat.State of the Art Seminar on Nuclear Data Cross Section Libraries and their Application in Nuclear Technology, Bonn, October 1-2, 1985

CIERJACKS, S.
Nuclear data needed in research of advanced intense neutron sources.

1985 IUCF Workshop on Nuclear Structure at High Spin, Excitation and Momentum Transfer, Bloomington, Ind., October 21-23, 1985

SAMANTA, C.; CHANT, N.S.; ROOS, P.G.
Experimental study of ^{16}O(α,αp) and ^{40}Ca(α,αp) reactions.

Nuclear Structure Weekend, Daresbury Laboratory, Daresbury, GB, October 26-27, 1985

KAEPPELER, F.
Maesurements on nuclei far from stability of astrophysical interest.

7.Nuklear Symp. - PET, Medizinische Hochschule Hannover, 8.-9.November 1985

SCHWEICKERT, H.
Erfahrungen im Routinebetrieb eines 'Negativ-Ion'-Zyklotrons in Karlsruhe.

Internat.Workshop on Polarized Sources and Targets, Montana, CH, January 13-17, 1986

HEERINGA, W.; MAIER, CHR.; SKACEL, H.
Exchange of polarized targets in a high magnetic field and at mK temperatures.

Tagung 'Radioaktive Isotope in Klinik und Forschung, Badgastein, 13.-16.Januar 1986

OBERHAUSEN, E.; HANSER, A.; STEINSTRAESSER, A.; MUELLER, M.; SCHMIDT, E.L.; BERBERICH, R.
Measurement of regional perfusion of the myocard by recording the distribution of Rb-81 Kr-81 with a SPECT-system.

24th Internat.Winter Meeting on Nuclear Physics, Bormio, I, January 20-25, 1986

HASSE, R.W.
The nuclear self energy - semiclassically.

REBEL, H.; BAUER, G.; SRIVASTAVA, D.K.
Coulomb break up as a source of information of astrophysical interest.

Wire Chamber Conf., Vienna, A, February 25-28, 1986

ENGLER, J.; KEIM, H.; MUELLER, C.
A strip chamber using tetramethylsilane.

Workshop on the Conceptual Design for the European Hadron Facility (EHF), Karlsruhe, March 1-4, 1986

BLUEM, P.
9 and 30 GeV lattice design.

BLUEM, P.
Acceleration of polarized protons in EHF.

Fermilab Antimatter Physics Workshop, Batavia, Ill., March 12-13, 1986

POTH, H.
Antiprotonic, hyperonic and antihydrogen atoms.

Fruehjahrstagung DPG, Kurzzeitphysik, Plasmaphysik, Stuttgart, 11.-14.Maerz 1986. Verhandlungen der Deutschen Physikalischen Gesellschaft, R.6, Bd.21(1986)

CITRON, A.; KUEHN, W.; ROGNER, A.; SCHIMASSEK, W.; STOLTZ, O.
Untersuchungen an einer selbstmagnetisch Bsub(Theta)-isolierten Diode.
Investigation of a self-magnetically insulated Bsub(Theta) diode.

BAUER, W.; BRANDELIK, A.; CITRON, A.; EHLERS, H.; MELCHIOR, G.; MITTAG, K.; SCHULTHEISS, C.
Pseudofunken-Ionendiode.
Pseudospark - ion diodes.

HABFAST, C.; POTH, H.; SELIGMANN, B.; WOLF, A.
Mikrowellendiagnose eines relativistischen Elektronenstrahls.

50.Physikertagung gemeinsam mit der Fruehjahrstagung DPG, Atomphysik, Kern- und Hochenergiephysik, Molekuelphysik, Quantenoptik, der Arbeitsgemeinschaft Massenspektrometrie, Wechselwirkung von Strahlung mit Werkstoffen, Energietechnik - Physikalische Grundlagen, Heidelberg, 17.-21.Maerz 1986

Verhandlungen der Deutschen Physikalischen Gesellschaft, R.6, Bd.21(1986)

AKER, E.; ENGELHARDT, D.; BRISSOT, R.; GELTENBORT, P.; GOENNENWEIN, F.; OED, A.; GINDLER, J.; WILKINS, B.;
Massenausbeute der Spaltfragmente der Reaktion ^{249}Cf(nth,f) als Funktion der kinetischen Energie.

ANSELMENT, M.; FAUBEL, W.; GOERING, S.; HANSER, A.; MEISEL, G.; REBEL, H.; SCHATZ, G.
Das 'Odd-Even Staggering' der nuklearen Ladungsgradien der Blei-Isotope.

ANSELMENT, M.; HANSER, A.; HOEFFGEN, H.; GOERING, S.; MEISEL, G.; REBEL, H.; SCHATZ, G.
Nukleare Ladungsgradien und elektromagnetische Momente von Sn-Isotopen aus laserspektroskopischen Untersuchungen.

BACHER, R.; BLUEM, P.; GOTTA, D.; KUNOLD, W.; ROHMANN, D.; SCHNEIDER, M.; SIMONS, L.M.
Antoprotonische X-rays von Wasserstoff- und Heliumisotopen.

BAUR, G.; BERTULANI, C.A.; REBEL, H.
Vorschlag zur Untersuchung von astrophysikalisch interessanten Strahlungseinfangsreaktionen mit Hilfe der Coulombdissoziation.

BEER, H.; WALTER, G.; KAEPPELER, F.; RUPP, G.; VOSS, F.; PENZHORN, R.D.
Die Messung der ^{22}Ne(n,γ)^{23}Ne Reaktion mit der Aktivierungsmethode.

BERG, G.P.A.; GAUL, G.; HACKER, U.; HAGEDORN, H.; HARDT, A.; HENN, K.; HINTERBERGER, F.; JAHN, R.; ERNST, J.; KILIAN, K.; KREJCIK, P.; KOEHLER, M.; LANG, H.; MARQUARDT, N.; MARTIN, S.A.; MAYER-KUCKUK, T.; MEISSBURGER, J.; OSTERFELD, F.; PAETZ GEN.SCHIECK, H.; POTH, H.; PRASUHN, D.; PROBST, H.J.; RIEPE, G.; ROGGE, M.; ROSSEN, P.VON; SCHUG, G.; TUREK, P.; WUESTEFELD, G.
Planungsstand des Kuehler-Speicherrings COSY.

BUECHE, G.; BUERCKER, L.; KOCH, H.; ROHRBACH, W.; SCHWERTEL, J.; WALTHER, D.
Messung des inklusiven Spektrums der Photonen aus dem Vernichtungsprozess von pp in Ruhe.

CHONGKUM, S.; BEKK, K.; GOERING, S.; HANSER, A.; MEISEL, G.; REBEL, H.; ANSELMENT, M.
Kernmomente und die Variation der Ladungsradien von Sr-Isotopen aus Messungen mittels der Atomstrahl-Laserspektroskopie.

CLEMENT, H.; ECKLE, G.; ECKLE, F.J.; ERMER, M.; FRIEDRICH, L.; GRABMAYR, P.; GRAW, G.; KADER, H.; KIHM, TH.; KNOEPFLE, K.T.; MAIRLE, G.; MERZ, F.; NURZYNSKI, J.; REUTER, W.; SCHIEMENZ, P.; WAGNER, G.J.
Die effektive Deuteron-Kern-Wechselwirkung aus der Streuung polarisierter Deuteronen.

CRYSTAL-BARREL-COLLABORATION; KOCH, H.
Das Crystal-Barrel-Projekt bei LEAR.

CRYSTAL-BARREL-COLLABORATION; KUNZE, M.
Monte-Carlo-Simulation von p-p-Annihilationen fuer des Crystal-Barrel-Projekt.

CRYSTAL-BARREL-COLLABORATION; SCHOTT, W.
MC-Simulation von elektromagnetischen Schauern in CsI.

DANIEL, H.; EGIDY, T.VON; HAGN, H.; HARTMANN, F.J.; KANERT, W.; MOSER, E.; PLENDL, H.; SCHMIDT, G.; SCHUG, C.A.; RIEPE, G.; REIDY, J.J.; NICHOLAS, M.; POTH, H.; BUECHE, G.; HANCOCK, A.D.; KOCH, H.; KOEHLER, TH.; KREISSL, A.; RAICH, U.; ROHMANN, D.; CHARDALAS, M.; DEDOUSSIS, S.
Starke Wechselwirkung und Annihilation von Antiprotonen mit Atomkernen.

DOLL, P.; GARRETT, R.; HEERINGA, W.; HOFMANN, K.; JANY, P.; KLAGES, H.O.; KRUPP, H.; VOELKER, G.
Messung der Analysierstaerke der elastischen n-d Streuung bei niedrigen Energien.

DOLL, P.; FINLAY, R.W.; HEERINGA, W.; KLAGES, H.O.; KRUPP, H.; MAIER, CHR.; REPPENHAGEN, D.
Bestimmung von sigmasub(ss) von ^{27}Al fuer Neutronen zwischen 18 und 50 MeV.

DOLL, P.; FINLAY, R.; FORD, T.; HEERINGA, W.; KLAGES, H.O.; KRUPP, H.; MAIER, CHR.; REPPENHAGEN, D.; VOLLMER, A.
Ein $\Delta E/\Delta E$-Teleskopsystem zur schwellenfreien Messung von Neutronenfluessen.

DOLL, P.; KRUPP, H.
Operational features of MWPC's in the neutron beam.

DOLL, P.; EBERHARD, V.; FINK, G.; GARRETT, R.; HEERINGA, W.; HOFMANN, K.; JANY, P.; KLAGES, H.O.; KRUPP, H.; MAIER, CHR.; REPPENHAGEN, D.; VOELKER, G.
Neutron-Proton-Streuexperimente und Phasenanalysen fuer das n-p System.

EBERHARD, V.; KLAGES, H.O.; SCHMALZ, G.
Neutronen-Detektoren mit LED-Verstaerkungsmonitor.

ENGLER, J.; KEIM, H.; WILD, B.
Test eines elektromagnetischen Kalorimeters mit TMS.

ENGLER, J.; KEIM, H.; MUELLER, C.
Test einer TMS-Streifen-Ionisationskammer.

EYRICH, W.; HOFMANN, A.; LEHMANN, A.; MUEHLDORFER, B.; SCHLOESSER, H.; TRESP, M.; WIRTH, H.; GILS, H.J.; REBEL, H.; ZAGROMSKI, S.
Untersuchung von isoskalaren Riesenresonanzen mit ^{6}Li-Teilchen.

FETSCHER, W.; GERBER, H.J.; GOERING, K.; KLEIN, U.; KLUGE, W.; MATTHAEY, H.; METZLER, M.; PEDRONI, E.; WIEDNER, U.
Messung des Realteils der isospin-geraden Vorwaertsstreuamplitude der Pion-Nukleon-Streuung bei 55 MeV als Test der Quantenchromodynamik.

FINLAY, R.W.; MELLEMA, S.; PETLER, J.S.; DIETRICH, F.S.
Microscopic DWBA analysis of nucleon scattering from $^{89}\gamma$.

FORD, T.D.; ROMERO, J.L.; BRADY, F.P.; CASTANEDA, C.M.; DRUMMOND, J.R.; MCEACHERN, B.C.; WEBB, M.L.; KING, N.S.P.
The (n,px) reaction at 65 MeV on ^{12}C and ^{90}Zr.

GAMERDINGER, K.; JUNG, H.; CELLO-COLLABORATION
Der neue Kalorimetertrigger des Detektors CELLO auf einzelne Photonen.

GARCILAZO, H.
Relativistic three-body calculations of the πNN system.

GEMMEKE, H.; GRANDEGGER, W.; MASCHUW, R.; PLISCHKE, P.; RAUPP, F.
Nachweis der Neutronen aus der Reaktion νsub(e)$+p\rightarrow e^{+}+n$.

GEMMEKE, H.; GRANDEGGER, W.; GRIMM, A.; MASCHUW, R.; RAUPP, F.; REUSCHER, M.
Simulation von Neutrinoereignissen im Detektor KARMEN 1.

GEMMEKE, H.; GIORGINIS, G.; MANN, D.; MASCHUW, R.; OTTMANN, K.H.; ZEITNITZ, B.
KARMEN fluessig Argon Test-TPC.

GYLES, W.; BOSCHITZ, E.; GARCILAZO, H.; MATHIE, E.L.; OTTERMANN, C.R.; LIST, W.; SMITH, G.R.; VAN DEN BRANDT, B.; MANGO, S.; KONTER, J.A.; JOHNSON, R.R.
Comprehensive measurements of the $\pi^{+}d\rightarrow\pi^{+}pn$ reaction as test of relativistic Faddeev theories.

HEERINGA, W.; KLAGES, H.O.; MAIER, CHR.; SKACEL, H.
Temperaturverhalten des Karlsruher polarisierten Protonentargets bei 'schnellem' Targetwechsel und unter hohem Neutronenfluss.

JELITTO, H.; BUSCHMANN, J.; GILS, H.J.; KIENER, J.; REBEL, H.; ZAGROMSKI, S.
Experimentelle Untersuchungen des Aufbruchs von 156 MeV ^{6}Li-Ionen unter extremen Vorwaertswinkeln.

JUNG, H.; GRIVAZ, J.F.; SPADAFORA, A.; CELLO-COLLABORATION
Ergebnisse des 'Single Photon Experiments' am CELLO Detektor bei PETRA.

KAEPPELER, F.; NAQVI, A.A.; AL-OHALI, M.
Das Isomerenverhaeltnis von ^{85}Kr bei kT = 54 keV.

KNAPP, J.; CELLO-COLLABORATION
Untersuchung semileptonischer Zerfaelle schwerer Quarks mit dem CELLO Detektor bei hoechsten Energien.

KOZIK, T.; BUSCHMANN, J.; GROTOWSKI, K.; GILS, H.J.; KLEWE-NEBENIUS, H.; PLANETA, R.; REBEL, H.
Highly dissipative pick up reactions of 26 MeV/amu ^{6}Li ions with Al, Ti, and Ni nuclei.

KREISSL, A.; BUECHE, G.; HANCOCK, A.D.; KOCH, H.; KOEHLER, TH.; POTH, H.; ROHMANN, D.; NILSSON, A.; SUFFERT, M.; CHARDALAS, M.; DEDOUSSIS, S.; DANIEL, H.; EGIDY, T.VON; HARTMANN, F.J; KANERT, W.; SCHMIDT, G.; REIDY, J.J.; RAICH, H.; WOLF, A.; PLENDL, H.
Praezisionsmessung des magnetischen Momentes des Antiprotons und eine Bestimmung des LS-Terms der starken Wechselwirkung

KRUEGER, M.; CELLO-COLLABORATION
Eine praezise Messung des hadronischen Wirkungsquerschnittes R in e^+e^- Annihilationen im Schwerpunktsenergiebereich von 14.0 bis 46.8 GeV.

LIEWEHR, W.; BEKK, K.; KAELBER, W.; MEISEL, G.; REBEL, H.
Optogalvanische Untersuchung der Hyperfeinstruktur und Isotopieverschiebung von Am I - Spektrallinien.

LUECKING, W.; KELLER, K.; LASSEN, L.; GEMMEKE, H.; SCHROEDER, W.U.; HOLUB, E.; HILSCHER, D.; INGOLD, G.; JAHNKE, U.; ORF, H.; ROSSNER, H.; ZANK, W.P.
Neutronenemission in peripheren Stoessen im System ^{12}C + ^{165}Ho bei 25 MeV/amu.

MATHELITSCH, L.; GARCILAZO, H.
Untersuchungen zu Dreiteilchenresonanzen.

OLSZEWSKI, R.; BARAN, R.; HOFMANN, A.; KRELL, S.; ORTNER, H.W.; ORZECHOWSKI, J.; VOGLER, F.; DEHNHARD, D.; LIST, W.; SMITH, G.R.
π-γ Winkelkorrelationen an ^{12}C(2^+, 4.44 MeV).

OTTERMANN, C.R.; BOSCHITZ, E.; GYLES, W.; LIST, W.; TACIK, R.; VAN DEN BRANDT, B.; MANGO, S.; KONTER, J.A.; SMITH, G.R.
Messung der $\pi d \rightarrow pp$ reaction bei Tsub(π) = 65 MeV.

ROESCH, W.; BRENDEL, C.; RICHTER, A.; SCHRIEDER, G.; GENTNER, R.; KELLER, K.; LASSEN, L.; LUECKING, W.; SCHRECK, R.; GEMMEKE, H.; SCHUELL, D.
Praeaequilibriumsemission von Nukleonen fuer das System ^{40}Ar + ^{40}Ca bei 20 MeV/amu.

ROHMANN, D.; BUECHE, G.; HANCOCK, A.D.; KOCH, H.; KOEHLER, TH.; KREISSL, A.; POTH, H.; WOLF, A.; BACKENSTOSS, G.; TAUSCHER, L.; NILSSON, A.; DEDOUSSIS, S.; CHARDALAS, M.; DANIEL, H.; EGIDY, T.VON; HARTMANN, F.J.; KANERT, W.; SCHMIDT, G.; REIDY, J.J.
Effekte der Starken Wechselwirkung im 3d- und 4f-Niveau von leichten antiprotonischen Atomen.

SCHATZ, G.
Nukleare Uhren und Thermometer der Astrophysik.

SRIVASTAVA, D.K.; REBEL, H.
Der resonante und nichtresonante Coulomb-Aufbruch von ^{6}Li.

STAUBER, K.; VOETISCH, D.; BOETTCHER, J.; FINCKH, E.; HUELSMANN, B.; KRETSCHMER, W.; STEGEN, R.; ZELL, E.; MASCHUW, R.
Der Antizaehler fuer das KARMEN-Projekt.

TACIK, R.; BOSCHITZ, E.; GYLES, W.; LIST, W.; OTTERMANN, C.R.
Investigation of the ^{6}Li(π,πd)X reaction at Tsub(π) = 219 MeV.

WISSHAK, K.; KAEPPELER, F.
Der Karlsruher 4π Detektor aus Bariumfluorid.

ZAGROMSKI, S.; GILS, H.J.; REBEL, H.; EYRICH, W.; HOFMANN, A.; SCHLOESSER, H.
Das Detektorsystem fuer 0^0-Messungen mit dem Karlsruher Magnetspektrographen 'Little John'.

4th Internat.Workshop on Trace Element Analytical Chemistry in Medicine and Biology, GSF Neuherberg, April 21-23, 1986

HECK, D.; OCHS, A.; KLEMPNOW, A.; KRATT, C.; MAIER, K.P.
Trace element distributions in human liver lobules determined with micro-PIXE.

Internat.Symp.on the Three Body Force in the Three Nucleon System, Washington, D.C., April 24-26, 1986

CIERJACKS, S.; FURIC, M.; LJUNGFELT, S.; MANKIN, U.; PETKOVIC, T.; SIMICEVIC, N.; ULLRICH, H.; BACKENSTOSS, G.; IZICKI, M.; SALVISBERG, P.; STEINACHER, M.; WEBER, P.; WEYER, H.J.
Direct three-nucleon pion-absorption processes in 3 He.

KLAGES, H.O.
ND elastic scattering, breakup reactions and the search for three-nucleon forces.

KLAGES, H.O.; HOFMANN, K.; NITZ, W.; VOELKER, G.; DOLL, P.; FINK, G.; GARRETT, R.; HEERINGA, W.; KOIKE, Y.
Neutron-deuteron elastic scattering in the energy range up to 50 MeV.

KLAGES, H.O.; HOFMANN, K.; NITZ, W.; DOLL, P.; GARRETT, R.; HEERINGA, W.; KRUPP, H.
Analyzing power of the ^{2}H(n,n)d^+ (FSI) breakup reaction from 20 to 50 MeV.

High Energy Physics Discussion Group Annual Meeting, Brookhaven National Laboratory, Upton Li, N.Y., May 8-9, 1986

POTH, H.
Antiproton potential at the AGS.

23rd European Cyclotron Progress Meeting, Debrecen, H, May 15-16, 1986

BECHTOLD, V.; FEHSENFLED, P.; HANSER, A.; MOELLENBECK, J.; SCHWEICKERT, H.
The Karlsruhe Compact Cyclotron an accelerator for medical and technical applications.

Seminar, American Gastroenterological Association, San Francisco, Calif., May 18-21, 1986

OCHS, A.; KLEMPNOW, A.; HECK, D.; KRATT, C.; MAIER, K.P.
Heterogeneous trace-element-distribution in human liver lobules detected by protoninduced X-ray emission (PIXE).

7th Workshop on ECR Ion Sources, Juelich, May 22-23, 1986

BECHTOLD, V.; DOHRMANN, H.; SHEIKH, S.A.
A highly efficient ECR ion source for radioactive beams.

2. Conf.on the Intersections between Particle and Nuclear Physics, Lake Louise, Alberta, CDN, May 26-31, 1986

Koch, H.
Antiprotonic atoms.

POTH, H.
Antihydrogen.

GOERING, K.; KLEIN, U.; KLUGE, W.; MATTHAEY, H.; METZLER, M.; WIEDNER, U.; PEDRONI, E.; FETSCHER, W.; GERBER, H.J.
Determination of the real part of the isospin-even forward scattering amplitude of

low energy pion-nucleon scattering as a test of low energy quantumchromodynamics.

Workshop on Secondary Beams at Kaon Factories, Vancouver, CDN, June 2-5, 1986

BLUEM, P.
The experimental facilities of the European hadron facility.

3rd Pisa Meeting on Advanced Detectors, Castiglione della Pescata, I, June 2-7, 1986

ENGLER, J.
Betrieb eines TMS Kalorimeters.

GEMMEKE, H.
Status of KARMEN-project.

6th Internat.Conf.on High Power Particle Beams, Kobe, J, June 9-12, 1986

BAUER, W.; BRANDELIK, A.; CITRON, A.; EHLERS H.; MELCHIOR, G.; MITTAG, K.; SCHULTHEISS, C.
Pseudofunken-Ionendiode.
Pseudospark - ion diodes.

CITRON, A.; KUEHN, W.; ROGNER, A.; SCHIMASSEK, W.; STOLTZ, O.
Untersuchungen an einer selbstmagnetisch Bsub(Theta)-isolierten Diode.
Investigation of a self-magnetically insulated Bsub(Theta) diode.

4th Internat.Conf.on Particle Induced X-Ray Emission and its Analytical Applications, Tallahassee, Fla., June 9-13, 1986

CICHOCKI, T.; HECK, D.; JARCZYK, L.; ROKITA, E.; STRZALKOWSKI, A.; SYCH, M.
Proton microprobe study of calcium-phosphate complexes in human arteries.

HECK, D.; OCHS, A.; KLEMPNOW, A.; KRATT, C.; MAIER, K.P.
Localized changes of trace element concentrations within deseased human liver lobules.

Internat.Meeting on Nuclear Analytical Methods, Orleans, F, June 19-20, 1986

HECK, D.; OCHS, A.; KLEMPNOW, A.; KRATT, C.; MAIER, K.P.
Trace element distributions within healthy and diseased human livers determined with micro-PIXE.

27th Annual Meeting of the Institute of Nuclear Material Management (INMM), New Orleans, La., June 22-25, 1986

OTTMAR, H.; EBERLE, H.; KOCH, L.
Demonstration of NDA technology for reprocessing input analytical measurements.

8. PERSONNEL

Head of the Institute IK I: Prof.Dr. B. Zeitnitz

Scientific and Technical staff:

Apel. W.-D., Dr.
Böhrer, A.
Deutsch, G.
Dittmann, R.
Doll., P., Dr.
Drexlin, G., DP
Eberhard, V.
Engler, J., Dr.
Fink, G.
Flügge, G., Prof.Dr.
Fries, D.C., Prof.Dr.
Gamerdinger, K., DP
Gemmeke, H., Dr.
Giorginis, G., Dr.
Grandegger, W.
Grimm, A.
Gumbsheimer, R., DI(FH)
Hagert, H.
Hansmeyer, J., DP
Haupenthal, M.
Henkes, Th., DP
Heeringa. W., Dr.
Hesselbarth, J.
Hofmann, K., DP
Hopp, G., Dr.
Hoss, A.
Hucker, H.
Husson, L., Ing.
Jany, P., DP
Jung, J., DP
Keim, H.
Klages, H.O., Dr.
Kleinfeller, J., Dr.
Knapp, J. DP
Krüger, M., Dr.
Krupp, H., DP
Küster, H., DP
Lutz, R., Ing.
Mann, D.
Maschuw, R., Dr.
Mayer, P.
Momayezi, M.
Müller, C.
Müller, H., Prof.Dr.
Nitz, W.
Ottmann, K.H.
Panter, M. Dr.
Plischke, P., Dr.
Ranitzsch, K.H., Dr.
Raupp, F., DP
Reppenhagen, D.
Reuscher, M., Dr.
Schmalz, G., DI
Schmidt, F.K., Dr.
Schneider, H., Dr.
Schnell, R.
Skacel, H.
Spohrer, G.
Strobelt, T.
Völker, G
Vollmer, A.
Wild, B.
Wild, P.
Wochele, J., DP
Wölfle, S.
Wölfl, Chr., DP.
Wolf, J.
Ziegler, P.

Guest scientists:

Ford, T.D., Univ. of Calif., Davis
Finlay, R.W., Ohio Univ., Athens

Head of the Section IK II: Prof. Dr. Anselm Citron

Scientific and Technical Staff:

Aker, E., DP
Bacher, R., DP
Barth, H.
Blüm, P., Dr.
Boschitz, E., Prof. Dr.
Büche, G., Dr.
Bürcker, L.
Cierjacks, S., Dr.
Engelhardt, D., Prof. Dr.
Garcilazo, H., Prof. Dr.
Göring, K. P.
Gotta, D., Dr.
Gyles, W., Dr.
Habfast, C., DP
Heitlinger, K., DP
Henkes, Th., DP
Höhne, A.
Hoffart, A.
Jaki, J., DP
Jödicke, B.
Kärcher, K.
Klein, U., DP
Kluge, W., Prof. Dr.
Koch, H., Prof. Dr.
Kröner, F.
Kunze, M., DP
List, W., DP
Matthäy, H., Dr.
Metzler, M., DP
Ottermann, C.R., Dr.
Poth, H., Dr.
Rohmann, D., Dr.
Rohrbach, W., Dr.
Rzehorz, B.
Schneider, M., DP
Schott, W., DP
Schwertel, J.
Seligmann, B., DP
Simons, L.M., Dr.
Stoll, M.
Tacik, R., Dr.
Ullrich, H., Prof. Dr.
Walther, D., DP
Weddigen, Ch., Prof. Dr.
Wiedner, U., DP
Zach, G.

Guest scientists:

Furić, M., Prof. Dr., U. of Zagreb, YU
Petković, T., Dr., U. of Zagreb, YU
Powers, R., Dr., Arete Assoc., Pasadena, USA
Šimičević, N., DP, U. of Zagreb, YU

Head of the Section IK III: Prof. Dr. Gerhard Schatz

Scientific and Technical staff:

Beer, H., Dr.
Bekk, K., Dr.
Buschmann, J., Dr.
Dennerlein, H.-D.
Eberle, H., Ing.
Feurer, B.
Friederich, H.M.
Gils, H.J., Dr.
Göring, S., DP
Hanser, A., Dr.
Heck, D., Dr.
Heide, N., DP
Jelitto, H., DP
Kälber, W. DP
Käppeler, F., Dr.
Kiener, J., DP
Klay, N., DP
Köhler, A.
Liewehr, W., DP
Lingenfelder, B.
Matussek, P., DP
Meisel, G., Dr.
Michel-Piper, I. DI(FH)
Müller, H.
Oehlschläger, J., D.-Math.
Ottmar, H., Dr.
Rebel, H.G., Prof.Dr.
Rupp, G.
Schmidt, K.A., DP
Voss, F., Dr.
Wisshak, K., Dr.
Zagromski, S., DI(FH)

Guest scientists:

Bao, Z., Dr.
Chongkum, S., DP
Corcalciuc, V., Dr.
Daniels, T.
Dembczyński, J., Prof.Dr.
Grotowski, K., Prof.Dr.
Kozik, T., Dr.
Krivec, R., DP
Kruppa, A., Dr.
Lovas, R., Dr.
Ratynski, W., Dr.
Samanta, S., Dr.
Srivastava, D.K., Dr.

Head of the Cyclotron Laboratory: Dr. Hermann Schweickert

Scientific and Technical Staff:

Acharya, H.
Assmus, K.
Augstein, S.
Baßler, U.
Bauer, G.
Bechtold, V.,Dr.
Bialy, J., DP
Biber,J.
Blank, R.
Bollmann, E., DP
Dohrmann, H.,Ing.
Dressel, M.
Dressen, R.
Ehret, H.-P.
Erbe, D.
Erdel, E.
Ernst, R.
Fehsenfeld, P.,Dr.
Feuerstein,P.
Foßhag, E., Dr.
Franz, J.
Friedrich, L., Dr.
Gegenheimer, B.
Günther,O.
Haushahn, G., DP
Heger, V.
Heidenreich, K.
Heinzmann, H., DI
Heitz, E.
Herrmann, P.
Hirth, W.
Holler, H.
Hünfer, R., Dr.
Huttel, E., Dr.
Jänsch, M.
Kaltenbaek, J.
Kappel,W.-R., Ing.
Kauther, P.
Kernert, N., Dr.
Kessel, M.
Kirste, E.
Kleinrahm, J., Dr.
Klinger, G.
Kögel, B.
Konrad, J.
Krieg, U.
Lang, R.
Maier, W.
Mangold, D.
Mayl, R.
Mirasch,U.
Möck, W.
Möllenbeck, I., Ing.
Peters,J., DP
Pfeifer, R.
Rämer, Ch., Ing.
Ripp, H.
Roth, H.
Sahm,U., Dr.
Seidel, H.
Seidler, M.
Seitz, J.
Seufert, H.
Sheikh, S.
Schimpf,P.
Schmitt, M.
Schönstein, E.
Schüssler,B.
Schütz, R.
Schulz, F., Ing.
Schweickert, H., Dr.
Schwindt, E.
Stöbener, E., Ing.
Thouw, T., Dr.
Uchatius, R.
Uhlemann, S.
Wild, H.
Wiss, L.
Ziegler, P.
Zimmermann, H.
Zimmermann, U.